Preparation and structural studies of halogen bonded co-crystals

Ahmed Salim Mahmood Mahmood

Doctor of Philosophy

Keele University

March 2021

Abstract

The project investigates the reactions of selected aromatic nitrogen compounds with selected di- and interhalogens in order to obtain crystalline N···I halogen-bonded complexes according to the equation:

$$A + B \rightarrow AB$$

where reactant A is a pyridine derivative (3,5-difluoropyridine, 3,5-dichloropyridine, 2,6-dichloropyridine, 2,6-dimethoxypyridine, 4-methoxypyridine, 3-fluoropyridine, 2-fluoro-3-iodopyridine, 2-fluoro-4-iodopyridine, 2-fluoro-5-iodopyridine, 2-cyanopyridine) or a heterocyclic compound (quinoxaline, 2-chloroquinoline, 1,10-phenanthroline). Reactant B represents iodine monochloride, iodine monobromide or iodine, while AB is the product. All the reactions were carried out in 1:1 molar ratio in ethanol as a solvent, starting at room temperature and subsequently cooling the reaction mixture down to 0 °C.

Products can be classified into two groups, the first one (the majority of samples) consists of N···I halogen-bonded complexes with the crystals that form almost instantaneously after the reagents are mixed. These crystals are stable at the room temperature and have a relatively high melting point.

The second group includes pyridinium ion-polyhalogen ion complexes and reactant polymorphs. The formation of these crystals requires placing the reaction mixture in the freezer for more than 12 hours or cooling the reaction mixture down to -45 °C or -75 °C.

All the crystalline products were characterised by ATR-FTIR spectroscopy, UV-Visible spectroscopy and where possible due to crystal size, by single-crystal X-ray diffraction.

Table of Contents

Table of Contents

List of Figures.

List of Tables

CHAPTER (1)

Introduction

1.1 Introduction

The halogen bond (XB), which is analogous to a hydrogen bond (HB), is a highly directional non-covalent interaction between an electrophilic area of a covalently bonded halogen atom X, in a molecule designated as R-X, and another electronegative atom, or electron donor, signified by Y. Hence, the halogen bond formed by this interaction is commonly seen as RX···Y. [1] (Figure 1.1) It is important to note that X can also have multiple covalent bonds or even non-covalent interactions which can create a multitude of different chemical compounds with different states.

Due to their high electronegativity, halogen atoms in halo-organics are classically considered as sites of high electron density. Bearing in mind such consideration, it is generally accepted that halogen atoms can interact by functioning as electron donor sites (i.e., nucleophiles). The ability of halogen atoms to serve as hydrogen bond acceptors was documented as early as the 1920's.[2] Halogen molecules (frequently iodine, bromine, chlorine and even fluorine) or alkyl and aryl halides tend to form complexes with Lewis bases. This tendency had already been noted as early as two hundred years ago[3] and more recently an enormous number of stable intermolecular complexes formed by means of this non-covalent interaction have been recognized.[4]

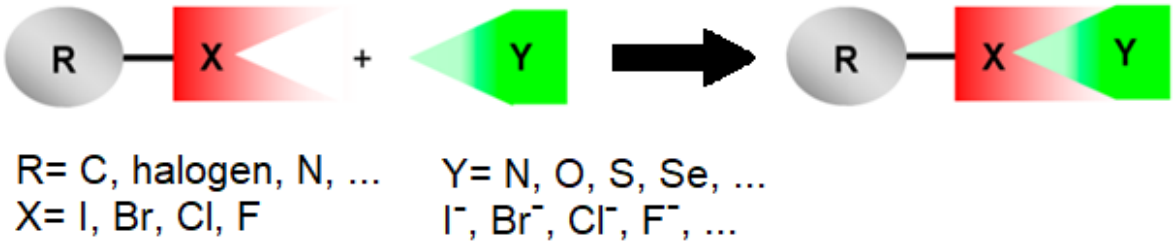

Figure (1.1) - General Scheme for the formation of Halogen bonds[1]

1.1.1 Historical Perspective

The first historical account of halogen bonding was seen in J.L. Gay-Lussac's laboratory in France. In 1813 J.J. Colin [5] had synthesized $H_3N\cdots I_2$ and made several reports of his findings, including one which formed a liquid due to the combination of dry iodine and ammonia in gas form.[1] However, the actual molecular composition was not formalized until the work of Guthrie in 1863, when he obtained the same product as Colin by adding dry iodine to concentrated ammonium nitrate.[6] In addition, Rhoussopoulos prepared quinoline-iodoform adduct in 1883,[3] thus demonstrating that the halocarbons behave like dihalogens when forming Lewis base adducts. All the mentioned adducts contained iodine, which is not surprising since iodine is the best halogen bond donor, so only near to the end of the 19th century, I. Remsen and J.F. Norris were the first to report comparable adducts with bromine and chlorine.[7] However, the first halogen bonding adduct for fluorine was not documented until many years later due to the conditions required for forming such adducts (very low temperature and pressure).[8]

Within the 20th century, the development of characterisation techniques contributed to a better understanding of the nature of XB. In the early 1950s, Benesi and Hildebrand confirmed the existence of I_2-aromatic adducts using UV-Vis spectroscopy.[9] Following that discovery, Mulliken reported formation of analogous complexes with ethers, thioethers and carbonyl derivates.[10] In late 1950s Hassel and his co-workers at the University of Oslo pioneered the study of crystalline complexes of dihalogen molecules with Lewis bases by X-ray diffraction. Specifically, the structure of the bromine-1,4-dioxane and bromine-benzene adducts were found to have a chain of "halogen molecule bridges".[11] (Figure 1.2) In 1968, Bent[12] published a comprehensive review of the structural chemistry of donor-acceptor adducts-the most notable details being how in all complexes, distances between the halogen atom and the electron donor were smaller than the sum of their van der Waals radii; as well as

how both the atoms lay nearly at 180 degrees, which both are unique features of XB. His claims were confirmed by Parthasarathy and Desiraju who made a statistical analysis of Cambridge structural database (CSD) deposited structures.[13]

In 1992 Politzer and Murray[14] showed that the electron density of covalently bound halogen atoms is anisotropic by calculating the surface electrostatic potential, which led to an introduction of a σ-hole concept.[4,8,15-21] Even though a variety of properties for this phenomenon were well known, the scientific community had to agree on a unified name for this type of interaction.

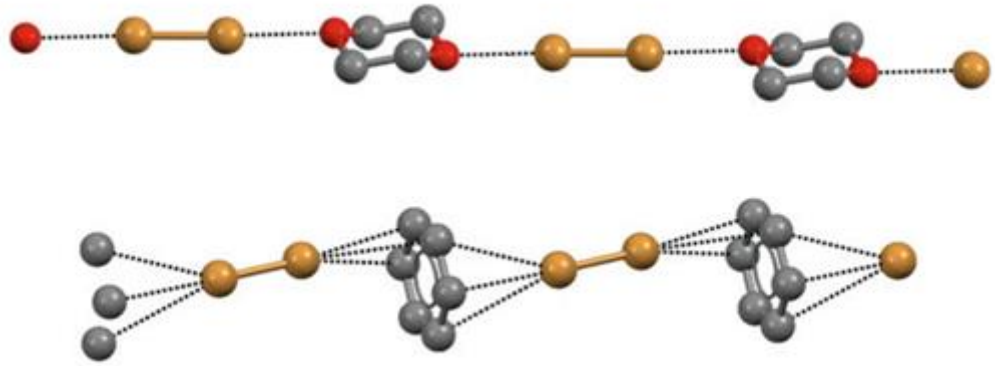

Figure (1.2) Ball-stick representation of $Br_2\cdots$dioxane (top)

and $Br_2\cdots$benzene (bottom) adducts[1,8]

1.1.2 Halogen bond nomenclature

The hydrogen bond was used as a role model for naming the halogen bond interactions. The problem of a variety of names for the same electrophilic interaction of covalently bonded halogen atoms was also discussed in a review by Bent in 1968. The term halogen bond was possibly coined by Zingaro and Hedges[22] to describe the obtained solution complexes of halogens or interhalogens and phosphine oxides and sulphides. It was further used by Martire et al.[23] in 1976 and in a review by Dumas, Gomel and Guerin in 1986.[24] On the contrary, during the same period of time, Klemperer et al. used the term “anti-hydrogen bonding” to

describe interactions in F-Cl···F-H complex, while Desiraju, Steiner[25] and Alkorta[26] classified the interactions of covalently bonded halogen atoms and hydrides as "inverse hydrogen bonding". To avoid any further disputes, leading researchers in the field decided to unify the name and undoubtedly define the features of this interaction in a IUPAC meeting in 2009. [4, 15-21,]

1.2 Definition of the Halogen Bond

A symposium dedicated to the XB was organized in the context of the 238th National Meeting of the American Chemical Society (Washington, DC, Aug 16, 2009), and had the influential role to allow for the emerging consensus on some features of the interaction to be acknowledged. At the edge of a two centuries long process, the IUPAC definition of the XB finally registered the agreement reached by the scientific community.[16] The IUPAC project 2009-032-1-100 was initiated in 2009 with the mission to provide a unified theoretical frame to interactions involving halogens as electrophilic species and to finally classify them in a distinct system. The definition of the halogen bond by the IUPAC recommendation in 2013 is:

"A halogen bond occurs when there is evidence of a net attractive interaction between an electrophilic region associated with a halogen atom in a molecular entity and a nucleophilic region in another, or the same, molecular entity".[16]

1.3 List of Features (as proposed by the IUPAC)

Metrangolo et al.[15] proposed that: "The existence of a halogen bond may be evident by experimental or theoretical, or even both." Some features that are useful as signs for the

halogen bond are mentioned below. The more the number of features met, the more consistent the description of an interaction as a halogen bond is.

In a typical halogen-bonded complex R–X···Y:

• "The interatomic distance between X and the appropriate nucleophilic atom of Y tends to be less than the sum of the van der Waals radii."

• "The length of the R–X covalent bond usually increases relative to the unbounded R–X."

• "The angle R–X···Y tends to be close to 180°, i.e., the halogen bond acceptor Y approaches X along the extension of the R–X bond."

• "The halogen bond strength decreases as the electronegativity of X increases, and the electron withdrawing ability of R decreases."

• "The forces involved in the formation of the halogen bond are primarily electrostatic, but polarization, charge transfer, and dispersion contributions all play an important role. The relative roles of the different forces may vary from one case to the other."

• "The analysis of the electron density topology usually shows a bond path (a "bond path" and a "bond critical point" are defined as "Within the *topological electron distribution theory,* the line resulting from the addition of two gradient paths of the *electron density function* emanating from the *bond critical point* located between each two neighbouring atomic basins" and "Within the *topological electron distribution theory*, a (3, –1) critical point (the point of the gradient field of the electron density within a given neutral configuration in which $\nabla\rho(r,q) = 0$) which is a local maximum in two directions and is a local minimum in the third, i.e. a *saddle point* in the three directions") connecting X and Y and a bond critical point between X and Y."

• "The infrared absorption and Raman scattering observables of both R–X and Y are influenced by halogen bond formation; new vibrational modes associated with the formation of the X…Y bond are also observed."

• “The UV–vis absorption bands of the halogen bond donor usually transform to shorter wavelengths.”

• “The X···Y halogen bond usually affects the nuclear magnetic resonance (NMR) observables (e.g., chemical shift values) of nuclei in both R–X and Y, both in solution and in the solid state.”

• “The peaks have binding energies related to X with the X-ray photoelectron spectrum (XPS) of the compound moving to energies that are lowered in comparison with un-bonded X.”

1.5 General Aspects and Nature of Halogen Bonding

1.5.1 Halogen bond donors

Halogen bond donors are halogen atoms iodine, bromine, chlorine and fluorine. XB donor ability increases in order F<Cl<Br<I. Even though following this trend astatine (At) should have the best properties as XB donor, it is omitted from the list because it is a rare and radioactive element with isotopes of a short half-life (the longest-living isotope ^{210}At has a half-life of 8.1 hours)[27], therefore very little is known about its chemistry and no halogen bond complexes are recorded so far.[15]

When halogen atoms are covalently bonded, their electron density redistribution occurs, and the electrostatic potential becomes anisotropic; a similar behaviour is shown by any other element. This was suggested theoretically and confirmed later by the experimental studies. In covalently bonded halogen atoms, the atomic radius of the halogen atom along the R−X bond axis is shortened, while the radius perpendicular to this axis is prolonged. The expanse of positively charged electrostatic potential occurs at the terminus of the R−X covalent bond. Halogen atom shape becomes more ellipsoidal with the shorter radius always along the covalent bond. (Figure 1.3) In order to describe the phenomenon, the term “polar flattening”

was introduced,[29] which was further proven experimentally through a detailed analysis of the Cambridge Structural Database [30] and computational electron density studies. [31-33]

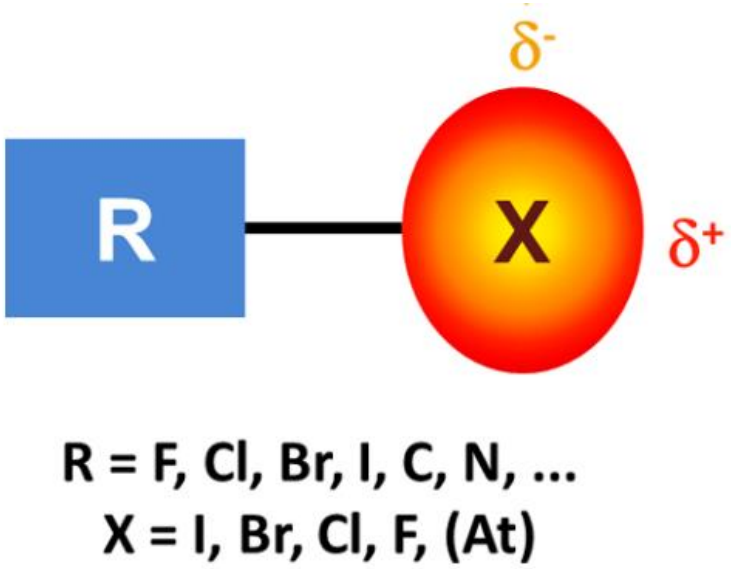

Figure (1.3) Schematic representation of "polar flattening" on a covalently bonded halogen atom[18]

1.5.2 The concept of "σ-hole"

Bearing in mind that the anisotropic nature of the electrostatic potential in the Cl, Br, and I systems, together with the electronegative nature of these halogens, can result in amphilic behaviour, accordingly, the halogen atoms serve as electron-deficient areas when they interact at the pole (electrophilic end), and still again can also serve as electron-rich sites when interacting at the equator (nucleophilic segment).[34,35] As a result, a region of partially negative electrostatic potential (δ^-) emerges perpendicular to R−X axis and a region of a partially positive electrostatic potential (δ^+) develops along the R−X covalent bond on the outermost portion of the halogen surface. This positive region has been denoted by Politzer et al.[28] as a "σ-hole" because it can be seen as a local deficit of electron charge opposite a σ-bond. The σ-hole is surrounded by a belt which has a negative electrostatic potential and is orthogonal to the bond responsible for σ-hole formation. This model elegantly explains the

interaction pattern of covalently bonded halogen atoms, and their directional preferences, i.e., linear interactions with nucleophiles and lateral interactions with electrophiles. The presence of a positive σ-hole accounts for the electrophilic behaviour of halogen atoms, while the focused nature of the σ-hole accounts for the direction of interaction with the lone pair on the XB acceptor atoms thus determining its orientation. [36-40] Practically, the positive potential on the R-X axis increases moving from F to I, i.e. proportional to the polarizability of the halogen atom. (Figure 1.4) The σ-hole concept,[28] offers a sophisticated explanation of the electrophilic behaviour of the halogen atoms. Although this concept is still widely used, there are evident examples of halogen-bonded complexes whose features cannot be rationalized based merely on the concept of the σ-hole, and the outline of the behaviour of the XB bonding is still a point of controversy between computational chemists. [28,36,41-51]

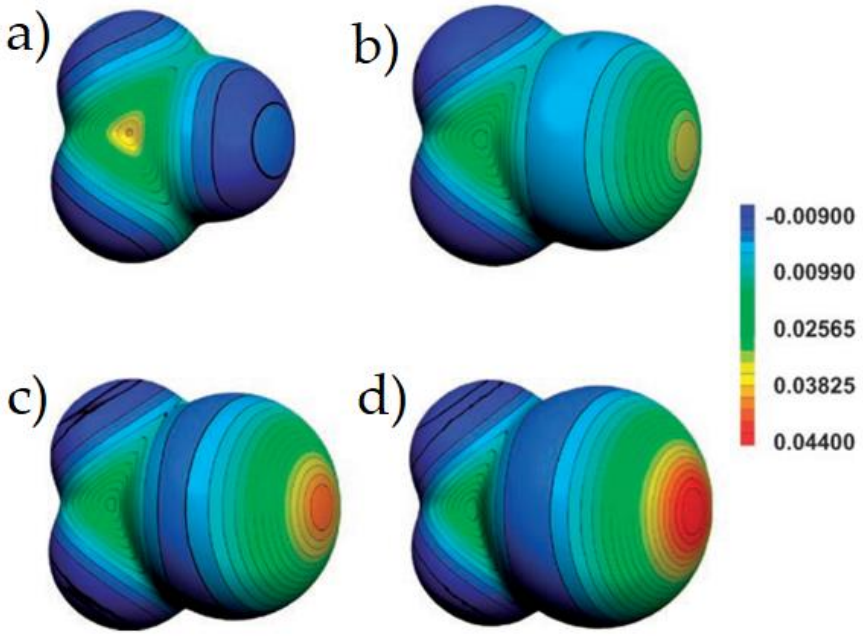

Figure 1.4 The molecular electrostatic potential (in Hartrees) at the isodensity surface with 0.001 electrons $Bohr^{-3}$, (a) CF_4, (b) CF_3Cl, (c) CF_3Br, (d) CF_3I.[52]

1.5.2 Halogen bond acceptors

Amines and pyridine derivatives are two examples of typical nitrogen-atoms-containing organic compounds, which show a more powerful halogen bond formation than do typical oxygen and sulphur complexes. [53,] The efficiency of the sulphur and oxygen atoms as halogen bond acceptors characteristically depend on the behaviour of the halogen bond donors.

Halogen bond acceptors that are sterically inhibited are of lower efficacy. In addition, if there is an increase in the electron density on the electron-pair donor this encourages its Lewis basicity and favours halogen bond creation. A good example of this is the formation of XBs on iodoperfluoroalkylsulfonic salts in the solid state.[55],[56] Furthermore, the halogen bond acceptor aptitude of sp^2-hybridized oxygen atoms increases in solution from acetone, to dimethyl sulfoxide, to hexamethylphosphortriamide.[57,58] Oxygen atoms show lesser affinity as XB acceptors in comparison to nitrogen atoms, nevertheless the opposite is true when pyridine derivatives and the corresponding N-oxides are considered.[53,54]

Another example is seen when neutral species are compared to anions, as the latter show a better XB acceptor activity hence signifying the potential of anions in structural chemistry directed by halogen bonds.[1,8] The strength of the XB with an anion is directly correlated to how much dissociated an ion pair is, i.e. the more charge is transferred from the anion to the antibonding orbital (σ*) of the XB donor, the stronger will be the anion XB. Halide anions form most of the common halogen-bonded adducts. Polyhalide anions can work as XB acceptors.[15] The association course is largely determined by the solvation energies of the starting anions and their adducts in addition to the strength of the resultant halogen bond.[59,60]

Compared to hydrogen bonds, XB is a more directional interaction, and long interactions are less directional than short ones because the σ hole is localized exactly on the elongation of the covalent bond(s) the halogen atom is involved in.[1] This anisotropic spreading of electron density over the halogen atom results in the angle of the covalent and halogen bond over the

halogen atom in R-X···Y to be about 180°. Moreover, n-electron donors (for example ethers and amines) also function as halogen bond acceptors with the interaction favourably manifesting itself along the axis of the donated lone pair of electrons.[15,16] In XBs involving pyridine fragments, the C-X bond is practically on the same plane as the pyridine ring. The precise nature of the halogen-bonding interaction is still debated. Transfer of electron density from the Lewis basic site (electron donor, halogen-bond acceptor) to a Lewis acidic site (electron acceptor, halogen-bond donor) does occur, however, the bonding contributions of the XB interaction depend significantly upon the individual interacting species.[15,16, 61]

1.5.3 Halogen Bond Characteristics: Energy and Geometry

The binding mode of XBs causes the X···Y distances to be smaller than the sum of the van der Waals radii of the atoms involved, thus, the stronger the halogen bond, the shorter the X···Y distance. When the assumption is made the halogen bond is formed as the result of electron donation from Y to the σ-antibonding R-X moiety, the formation of a halogen bond should slightly elongate the covalent R-X bond. [62,63]

Halogen bond strength is comparable to the more well-known intermolecular interactions such as the hydrogen bond. [8,15] HB and XB interactions show analogous drifts in energetic and geometric properties. This common property of XB and HB stems from the fact that halogens serve as electrophiles XB just as the hydrogen atoms do in HB. The main similarity between the two non-covalent interactions is the role of the electrophilic site on the halogen and hydrogen atoms, respectively; the inherent difference is that atoms of groups 17 and 1 are involved.

Yet, XB interactions can be more sensitive to secondary interactions. Broadly speaking, the term halogen bonding generally covers a huge variety of noncovalent interactions whose strengths lie in the range of 10– 200 kJ mol^{-1}.[37,64] The significant strength of some halogen

bonds enables them to prevail over hydrogen bonding when interacting with other molecules. For instance, the construction of intermolecular hydrogen bonds between dissolved species are noticeably repressed if a relatively strong halogen bond donor is supplemented as a co-solute.[65] Several hydrocarbon complexes comprising two nitrogen atoms show more affinity to co-crystallize with halogen bond donors rather than with hydrogen bond donors on competitive co-crystal formation, as seen experimentally.[18] This capacity of XBs to be an alternative for HBs permits the preparation of water-free models of hydroscopic complexes.[66-68]

In comparison to hydrogen atoms, halogen atoms are much bigger and more polarizable; accordingly, XBs are more affected by steric effects than are HBs.[69-79]

Strength of a halogen bond can be controlled in several ways. The simplest is to change the halogen atom used as a donor. One system that this has been particularly well documented is that involving 3-halocyanoacetylene role, when the N···X distances (2.932 Å for iodo-, 2.978 Å for bromo-, and 2.984 Å for chloro- complexes) are considered as the halogen bonds strength indicators in the adducts.[53,54,80]

Moreover, the strength of halogen bonds can be finely-adjusted by altering the halogen atom and the motif to which it is covalently bound; increased halogen-bond donor strength can be achieved by increasing the electron-withdrawing ability of the substituent.

This results in a positive charge for Cl, Br, and I while the electrostatic potential stays negative for the F atom. The extent of the positive field increases in response to the presence of electron-withdrawing neighbouring groups. Experimental outcomes verify that it is conceivable to fine-adjust the strength of the halogen bond in any halocarbon by altering the substituents on the carbon frame.[40,81] (Figure 1.5)

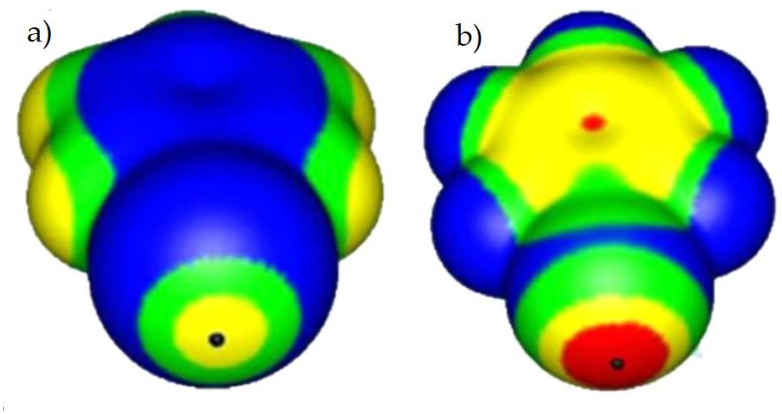

Figure (1.5) Computed electrostatic potentials on 0.001 au molecular surfaces of (a) iodobenzene, and (b) pentafluoroiodobenzene. Colour range (kcal/mol): red, >20; yellow, 20-10; green, 10-0; blue, negative.

Black hemispheres denote the positions of the halogen $V_{S,max}$.[82]

Haloheteroarenes and haloarenes (e.g. mono- or poly- halo substituted pyridine and benzene) are characteristically good XB donors. The halogen atom shows an even better donor nature whenever the heteroaromatic ring gains a positive charge. This effect has been effectively used to regulate the packing of bromo- and iodo-substituted tetrathiafulvalene by-products, which are also molecular conductors. [83,84]

In polyhaloalkanes, both steric as well as electronic effects result in the n-electron donors approaching from the front-side of the C-X covalent bond rather than the back-side attack; accordingly, these complexes commonly form halogen bonds. Tetrabromo-, triiodo-, and tribromomethane have been used broadly to produce halogen-bonded adducts,[85] whereas iodoperfluoroalkanes are also efficient tectons for crystal engineering based on XBs.[86]

Furthermore, the strength of the XB increases as the electron-withdrawing nature of the atom (or complex), attached to a certain halogen increases. The sequence of C(sp)-X>C(sp^2)-X>C(sp^3)-X is commonly used, with halo-alkynes forming the strongest halogen bonds.[11,83,87,88]

Strength and directionality of the halogen bonding is determined by the summation of charge-transfer, electrostatic, dispersion, and polarization interactions following the Pauli exclusion principle. A diversity of theoretical approaches have been advocated for the breakdown of the binding energy into the different contributions.[37,44,48-50,89] On the other hand, there is no universal agreement on this approach. In fact, some other studies, take the view that "the total binding energy is a physical observable while the various proposed components have just a conceptual significance, are not uniquely defined, and are not independent from each other".[15,90-92]

Another important application of halogen bonding is in crystal engineering. This encompasses forming cocrystals with detailed preferred characteristics, such as the spatial orientations and/or component separation. Such implications open the door to limitless future possibilities in material design and development.[4,15,93-96]

1.7 Applications of halogen bonds in crystal engineering

An XB interaction is symbolized by an X···Y interaction between a halogen-bond donor (X) and an acceptor (Y), in which the internuclear distance is less than the sum of their van der Waals radii. The XB interaction is typically co-linear with the R−X covalent bond, as a matter of fact, the angle between constituents is usually at least 175° in the gas phase.[61] This directionality of the interaction, as well as easily tuneable strength properties make XB a very useful tool in crystal engineering.

A tecton is defined as "a molecular building block that possesses the structure and molecular recognition features to predictably self-assemble into crystalline networks".[8] Halogen atoms when their σ hole is amplified by the presence of electron-withdrawing adjacent species can effectively behave as the "sticky sites" that dictate the association of the molecules. This is

shown better with the behaviour of polyhalocarbons, which regularly act as XB tectons. The directionality of halogen bonds permits the supramolecular construction to be predicted from the assembly of the preliminary molecules.

Another important term used in crystal engineering is denticity. IUPAC defined it as: "the number of donor groups in a single ligand that bind to a central atom in a coordination complex".[97] In supramolecular chemistry it refers to the number of donor or acceptor groups in a single tecton that are interacting via HB or XB. A tecton could be monodentate or polydentate (sometimes also referred as multidentate). Most commonly, the number of binding on polydentate tectons ranges from two (bidentate, e.g. ethylenediamine) to six (hexadentate, e.g. ethylenediaminetetraacetic acid (EDTA)), although even the cases of greater denticity are well known (diethylenetriaminepentaacetate, used in complexing lanthanide group metals).[97]

1.7.1 One-dimensional architectures

Halogen bonds tend to be linear, based upon the R-X bond axis of the halogen bond donor and the axis of the lone pair of electrons of the heteroatom in the halogen bond donor. When a pyramidal tridentate halogen bond donor interacts with a monodentate halogen bond acceptor, pyramidal units with four building blocks are created, whereas linear units with three building blocks are formed when a linear bidentate halogen donor interacts with a monodentate halogen acceptor.

If both the halogen bond donor and acceptor are bidentate, formation of one dimensional chains will be the result. Linear endless self-assembled chains are formed by donors and acceptors with parallel and coaxial sites(e.g. 1,4-dihalobenzenes for the former and 4,4'-bipyridine(4,4'-bipy) for the latter).[15] (Figure 1.6a) On the other hand, a stepped chain pattern can be observed if the binding sites are not collinear even though they are parallel (e.g. α,ω-diiodoperfluoroalkanes and 4,4'-bipy).[15](Figure 1.6b) The self-formed chains adopt a "herringbone" structure if the binding sites axes in the elements are not parallel (Figure 1.6c) the angles of the axes in the binding sites strongly dictate the angles along the chain. Angled geometry structuring of the halogen bond donor, the halogen bond receptor or both is manifested in many models. Probably the simplest examples of tuning the angle of the "herringbone" structure is varying the positions of XB donor sites, for example, 1,2- and 1,3-dihaloperfluorobenzenes, 60° and 120°, respectively. Halide anions often perform as bidentate halogen bond acceptors and adopt angled or linear geometrical structuring.[15]

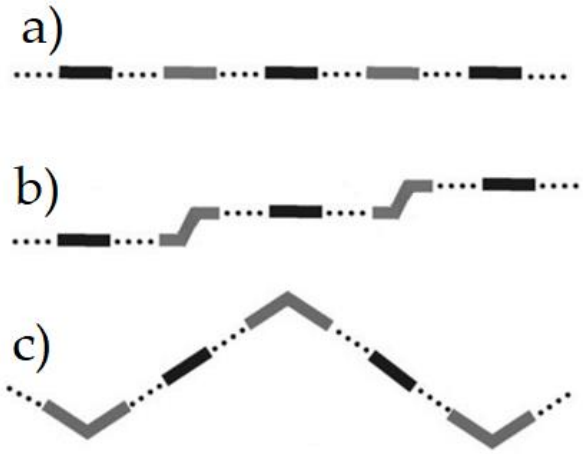

Figure (1.6) One-dimensional halogen bond architecture types,

linear- (a), stepped (b) and herringbone infinite chain (c) pattern;

XB donors (grey), XB acceptors (black), adapted from[8]

1.7.2 Two-dimensional architectures

The two-dimensional architectures are manifested when one or both of the interacting components have three or more XBs. A commonly observed design is the system (honeycomb assembly),[1,8] which is the result of self-assembling of halide anions with dihalocarbons. (Figure 1.7a) Halides behave as tridentate halogen bond acceptors that inhabit the nodes whereas the dihalocarbon components work as bidentate halogen bond donors that join the nodes. A ridged 2D honeycomb design is created as planar geometrical layout over the nodes.

On the other hand, the design can be produced from the self-assembly of tridentate halogen bond donors-acceptors complexes.[1,8] (Figure 1.7b)

Tridentate components self-assemble with other (bi and tri) dentate complexes to produce two dimensional architectures. For example, ribbons are created when a tri dentate halide anions join a bidentate dihalocarbons.[15] (Figure 1.7c)

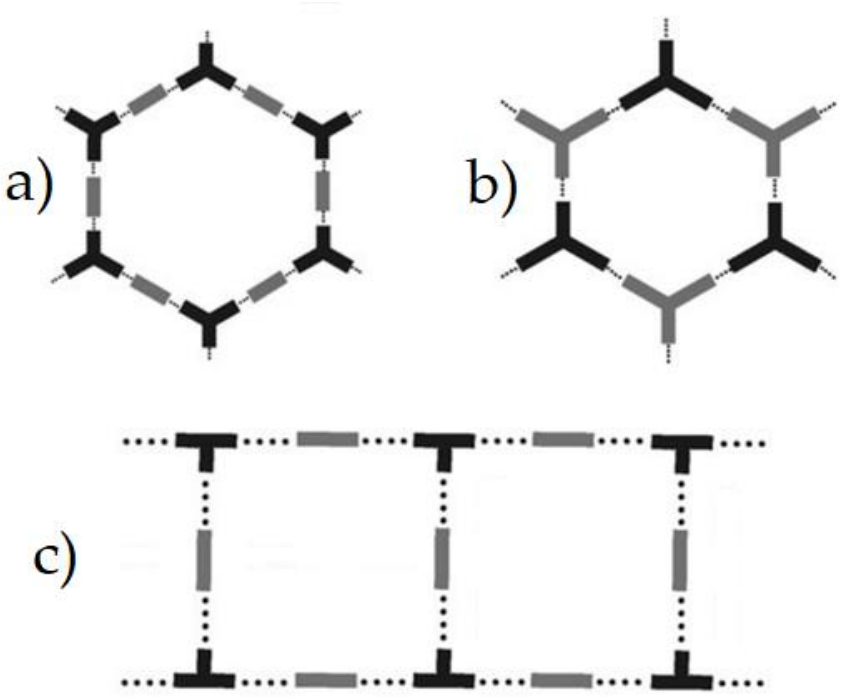

Figure (1.7) Two-dimensional halogen bond architecture types,

honey comb (a, b) and ribbon (c) pattern; XB donors (grey), XB acceptors (black),

adapted from[8]

1.7.3 Three-dimensional architectures

Interaction of a tetradentate module will result in the formation of either two dimensional or three-dimensional architectures. An example of two dimensional architectures are systems resulting from a tetradentate halogen bond acceptor self-assembled at the nodes and linking linear bidentate halogen bond donors.

On the other hand, an example of three-dimensional architecture is the adamantoid networks. They are produced by the self-assembly of dissimilar constituents. An example of such a network is the homocrystal of a self-complementary tetradentate structural block that comprises 2 halogen bond donor sites as well as 2 halogen bond acceptor sites.(Figure 1.8a) Another pattern for the formation of three dimensional architectures is the self-assembly of tetradentate halogen bond acceptors, which are situated at the nodes, with bidentate halogen

bond donors (Figure 1.8b), that manifest a “spacing” role and by the interchange of tetradentate halogen bond donors and acceptors at the nodes of the network.(Figure 1.8c) The aforementioned XB two and three-dimensional systems described above are porous structures frequently contain big holes that are filled by solvent molecules or interpenetration.[8,15]

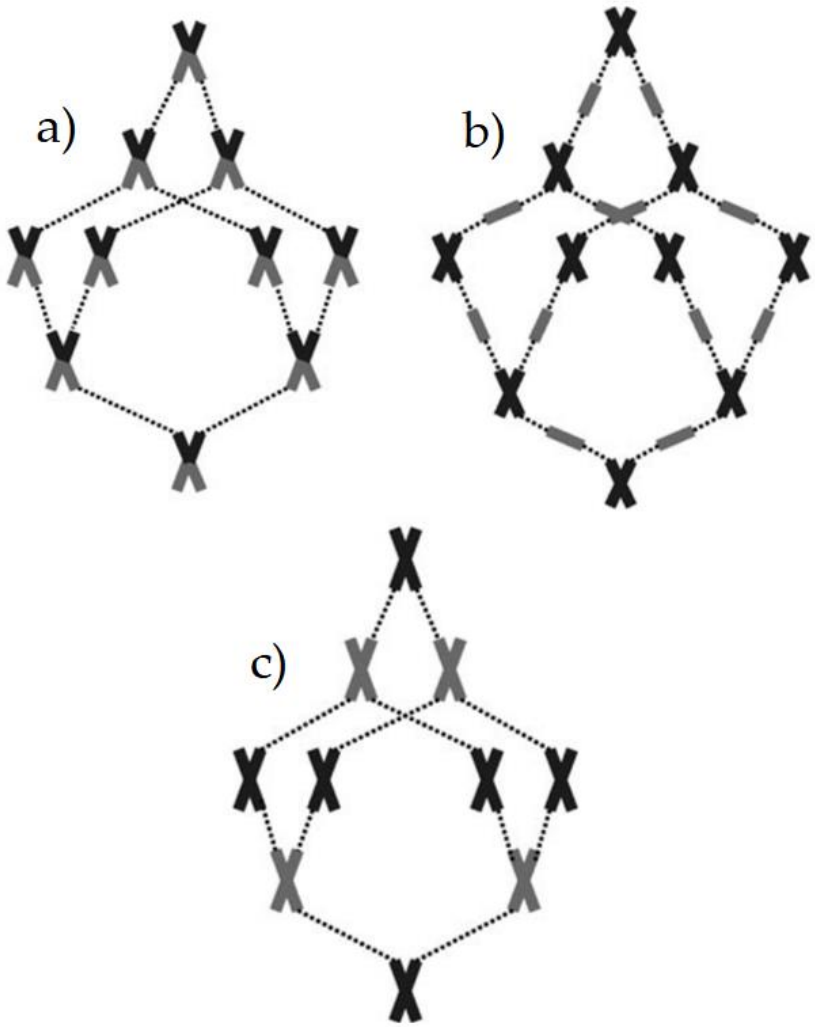

Figure (1.8) Three-dimensional adamantoid halogen bond architecture types, self-assembled (a), tetradentate XB donors and bidentate XB acceptors (b) and), tetradentate XB donors and acceptors; XB donors (grey), XB acceptors (black), adapted from[8]

1.8 Graph-set motif nomenclature

Even though this thesis is focused on preparation and structural studies of halogen bonded complexes, hydrogen bonds have also been observed in several systems. Hydrogen bonds can form a variety of motifs, which could be unequivocally described by graph-set motif nomenclature. Therefore, it is necessary to define and clarify this terminology. Graph-set motif nomenclature consists of a letter which represents the type of motif (R refers to the ring, C stands for a chain, while S is used for an intramolecular and D for a discreet hydrogen bond) and a set of numbers that describe the number of hydrogen bond donors (subscript), acceptors (superscript) and a number in brackets which corresponds to a total number of atoms in a motif. (Figure 1.9) Several examples are shown in Figure 1.10.[98]

$$R_2^2(10)$$

Figure (1.9): Example of Graph-set motif nomenclature

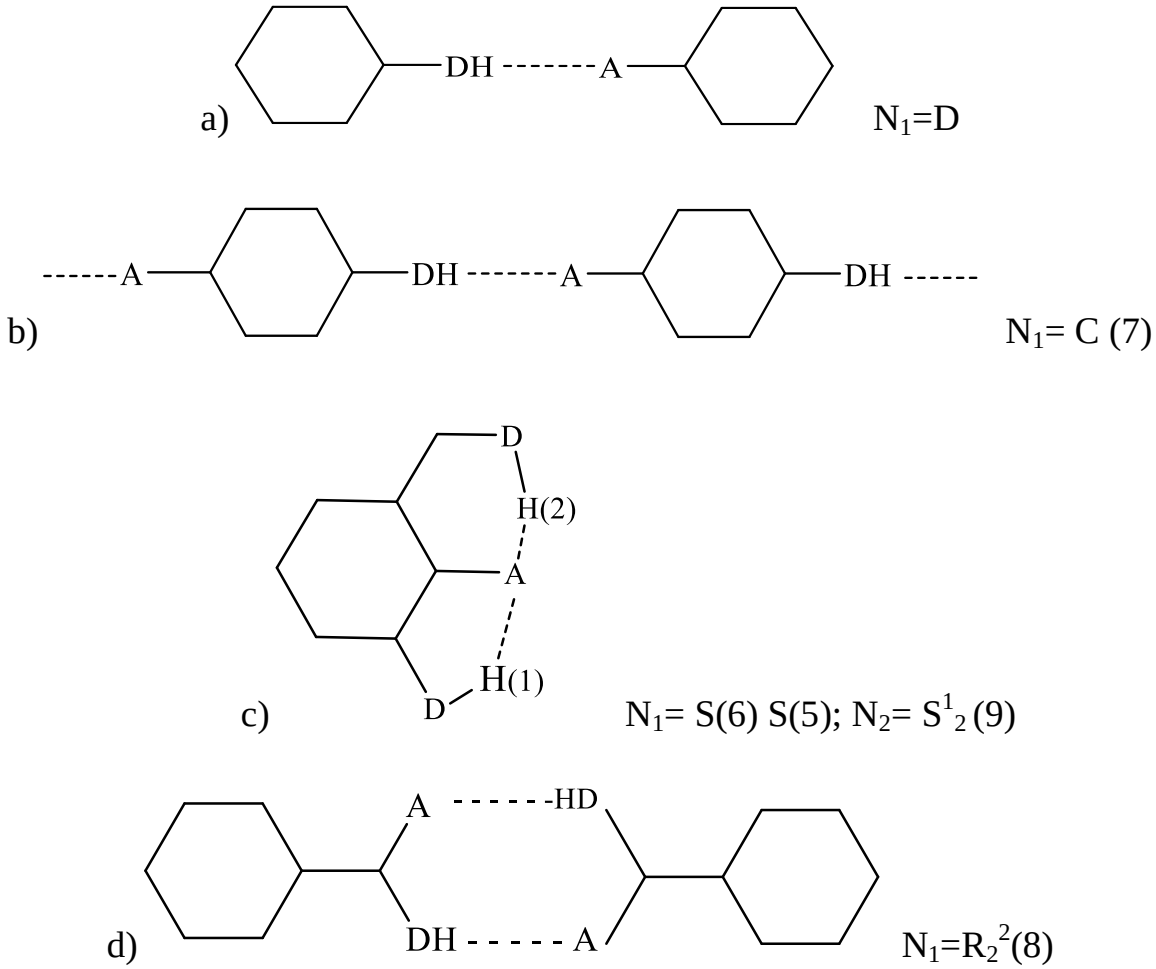

Figure(1.10): Examples of graph-set motifs, a) discreet-, b) chain-,

c) intramolecular-, d) ring hydrogen bond motif, adapted from[98]

1.9 Characterisation techniques

The electromagnetic (EM) spectrum consists of the whole range of frequencies of electromagnetic radiation, each of which can be considered as a wave or particle (photon) travelling at the speed of light. The frequency and wavelength of electromagnetic radiation vary over many orders of magnitude, so the EM spectrum could be divided according to the type of atomic or molecular transition that causes the emission or absorption of photons (e.g. X-ray, UV, IR, microwave) (Table 1.1). Every molecule is capable of absorbing characteristic frequencies of EM radiation. During this process, energy is transferred to the molecule and the intensity of the incident EM radiation is decreased. The difference in

intensities at specific wavelengths offers a possibility to study a variety of aspects of molecular structure. (Table 1.1) Those differences in the beam attenuation occur following the absorption law. The scientific field that studies the interaction of matter and light is called spectroscopy.[99] It is divided by the range of EM spectrum that is utilised, in this work ultraviolet-visible (UV-VIS) and infrared (IR) spectroscopy, X-ray diffraction characterisation techniques are used.

Table 1.1 The electromagnetic spectrum and the corresponding transitions[100]

Transition type	Nuclear	Core electrons	Valence electrons	Molecular vibrations	Molecular rotations, electron spin	Nuclear spin
Radiation type	γ-ray	X-ray	UV	IR	Microwave	Radio wave
Frequency (Hz)	10^{19}	10^{17}	10^{15}	10^{13}	10^{10}	10^{5}

1.9.1 Ultraviolet-visible (UV-VIS) spectroscopy

UV-VIS spectroscopy utilises the wavelengths from 200 to 1500 nm. In this range, electron excitation from low-energy molecular or atomic orbital to a higher-energy orbital occurs. The energy of the incoming photon must be the same as the energy difference of the orbital energies, for excitation to happen. Moreover, except the electronic transitions that are observed in UV-VIS range of the EM spectrum, molecules exhibit two other radiation-induced types of transitions (vibrational and rotational) that occur alongside the electron excitation. Vibrational transitions occur because a molecule has a multitude of quantised energy levels or vibrational states.[99,100]

The absorption law, more familiar as the Beer-Lambert law ($A= \varepsilon lc$), is used to quantitatively determine the amount of light attenuation. Absorption of light is specific for each wavelength and it depends on the path length (l) over which absorption occurs, the concentration (c) and type of the absorbing molecules. Dependence on the type of the molecules is defined through the molar absorptivity constant of the compound (ε). This constant is unique for each compound and the wavelength at which the molecule is observed. The transmittance (T) of the solution is the fraction of the incoming radiation (P_0) transmitted by the absorbing solution ($T=P/P_0$). Transmittance is expressed as a percentage. The absorbance (A) of a solution is related to the transmittance in a logarithmic manner ($A= -\log T$).[99,100]

UV-VIS spectrometer

A spectrometer is a spectroscopic instrument that converts the radiant intensities into electrical signals. UV-VIS spectrometers exist in two main design types, single and double-beam instruments. Double-beam instruments offer an advantage when compared to the single-beam spectrometers because reflection and scattering could occur at the sample holder walls, which cause the loss in the light intensity. To compensate for these effects, in the double-beam instruments the intensity of the beam transmitted through a cell containing the analyte solution is compared with one that traverses an identical cell containing a "blank" sample, which is just a solvent in a majority of the cases. However, due to the compact design, lower cost and maintenance, single-beam instruments are widely used. The reflection and scattering problems in a single beam are addressed by collecting the blank spectrum first, and then deducting it computationally from the sample spectrum. The main components of a single-beam UV-VIS instrument are the source, monochromator, beam splitter, sample holder, detector and a signal amplifier.[100] (Figure 1.11)

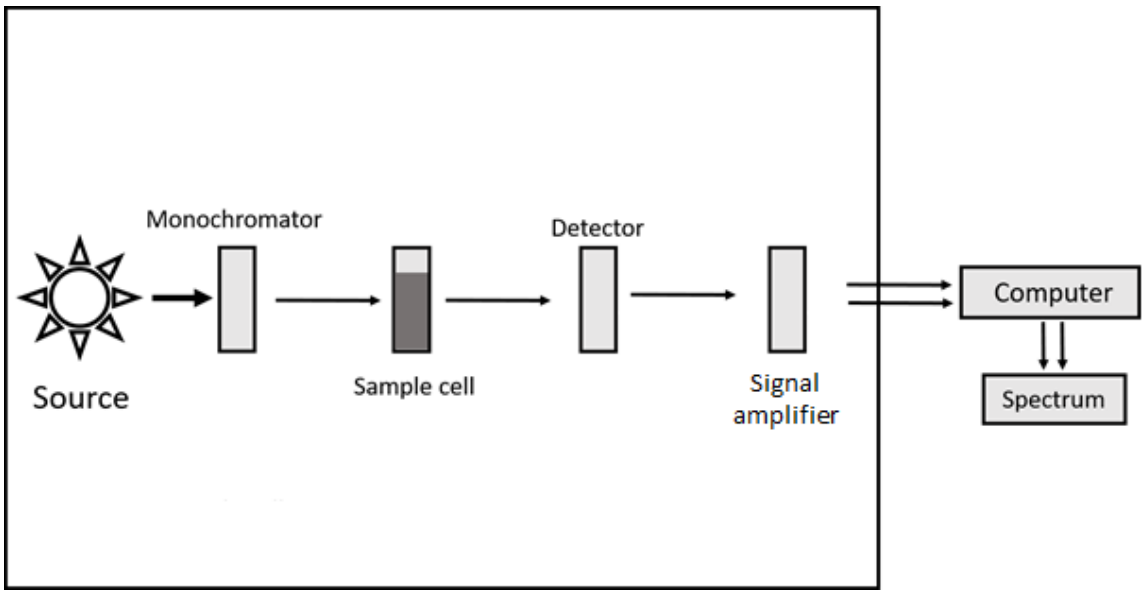

Figure (1.11): Scheme of a double-beam UV-VIS spectrometer,

adapted according to the ref[100]

As a light source usually a deuterium and tungsten lamps are used. Deuterium lamp produces a continuum spectre in a range from 160 to 380 nm, while the tungsten lamp produces light in the range from 240 to 2500 nm. This limited range of EM spectrum is then passed through a monochromator which filters the incident continuous spectra to a single wavelength. The beam with the filtered wavelength passes through the solution of interest and then a detector. The output from the detector is amplified, and the logarithm of the blank-sample ratio is computed and displayed on the computer as a spectrum.[99,100]

1.9.2 Infrared (IR) Spectroscopy

The range of the electromagnetic radiation from 33 to 12000 cm^{-1} is called the infrared region and it is utilised in spectroscopy mainly for the qualitative identification of molecular structure by observing various vibrating properties. This part of the spectrum could be divided into well-defined regions based on the types of vibrations that could be observed:

- Far-Infrared (400-33 cm^{-1}): molecular skeleton and crystal lattice vibrations, molecules containing heavy atoms,
- Mid-Infrared (4000-400 cm^{-1}): the most utilised for organic compounds analysis
- Near Infrared (12820-4000 cm^{-1}): overtones; mainly for quantitative analysis

The simplest modes of vibration that are infrared active are stretching and bending modes. (Figure 1.12) Stretching modes can be divided into symmetric and asymmetric while bending modes can be separated into four different types. Scissoring and rocking are in-plane modes while wagging and twisting are out-of-plane modes.

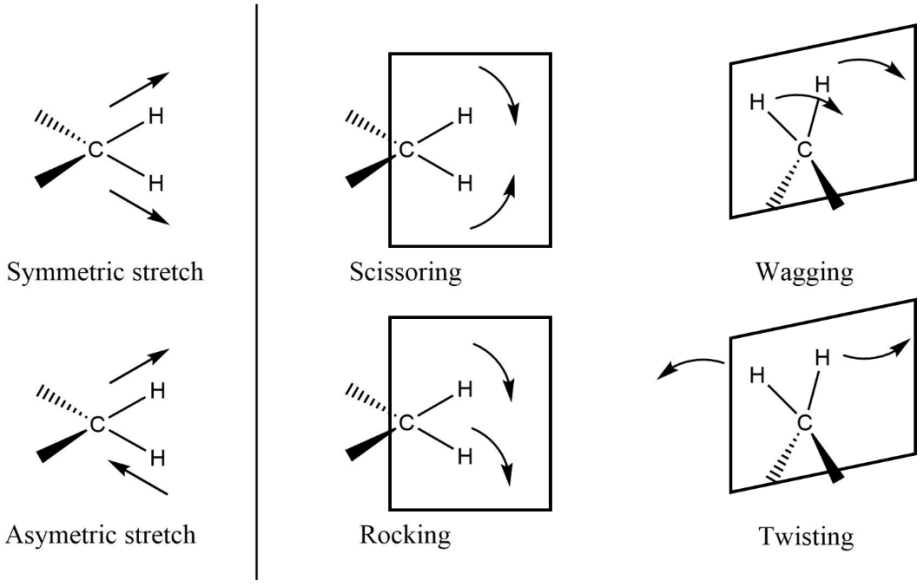

Figure (1.12): Molecular vibration modes,

adapted according to the ref[99]

To perform the structural analysis by IR spectroscopy the molecule under investigation must be infrared active, (i.e. it must absorb IR radiation). When the radiant energy matches the energy of a specific molecular vibration, absorption occurs. A compound that is infrared active must change its dipole moment when vibrating. Molecules with a permanent dipole moment (H_2O and CO) are infrared active, while molecules like Cl_2 and N_2 molecule do not possess a permanent dipole moment, so they are not infrared active. In the case of alkenes (C=C) and alkynes (C≡C) if the bond is symmetrically substituted then no band would be observed in the IR spectrum. In the other hand, if the bond is asymmetrically substituted, a corresponding stretching frequency will be present. Samples in all phases (solid, liquid and gas) could be characterised, but for each phase, a specific sample holder is required.

Fourier Transform Infrared (FTIR) instrument components:

Infrared spectrometers use optical devices for dispersing and focusing electromagnetic radiation of IR frequency which is passed through the sample and any changes in absorbance measured against a reference beam. FTIR spectrometers consist of an IR source, interferometer, sample cell or chamber and a detector. A scheme of an FTIR instrument is shown below (Figure 1.13).

IR source

Common IR sources are silicon carbide rods which are heated by the electric current to approximately 1300 K. IR radiation passes through an aperture which controls the amount of radiation that reaches the sample, and therefore, the detector.

Interferometer

The interferometer is the essential piece of optical equipment, without which the contemporary FTIR system would not exist. The interferometer consists of a beam splitter, a fixed mirror, and a moving mirror. The beam splitter is made of a material which transmits half of the incident radiation and reflects the other half. IR radiation from the source is

separated by the beam splitter and into two beams. One part is transmitted through the beam splitter to the fixed mirror while the other one is reflected in the moving mirror. Both fixed and moving mirror reflect the radiation to the beam splitter where the two beams interfere and produce an interferogram. Both, the moving and the fixed mirror are flat highly reflective surfaces, but the moving mirror is moved by a special mechanism several millimetres once every millisecond.[100]

Detector

There are two classes of infrared detectors; thermal and photonic detectors. Photonic detector exhibits faster response times and higher sensitivity in comparison to their thermal counterparts. The materials used in these detectors are semiconductors with narrow band gaps. The incident IR radiation causes electronic excitations between the ground and first excited states, which in photoconductive detectors result in a change in resistivity which is monitored.[99]

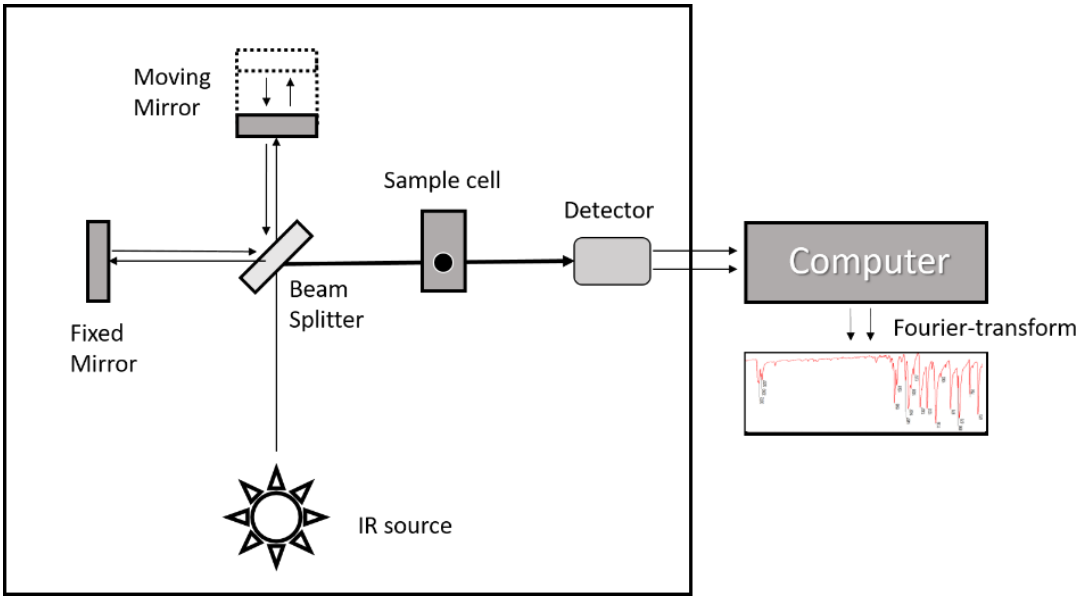

Figure (1.13): FTIR instrument scheme,

adapted according to the ref[100]

Attenuated Total Reflectance (ATR)

IR instruments that utilise an ATR stage simplify the procedure and shorten the time required the sample preparation, while still resulting in a good quality spectrum. The IR radiation in the classic IR spectrometer is passed through the sample and the radiation which is transmitted is measured. ATR measures the changes which occur in an internally totally reflected IR beam that it is in direct contact with a sample (Figure 1.14). The IR beam enters the crystal (at a particular angle of incidence) that is made of a material with a high refractive index. The crystal has to be made of a material with a higher refractive index than the sample. The IR beam is internally reflected and it results in the production of an evanescent wave which can extend beyond the crystal surface and into the sample. Depending on the angle, type of the crystal and the sample, evanescent wave penetrates the sample to a depth from 0.5 to 2 µm. When the IR radiation is absorbed by the sample a change in the evanescent wave occurs, i.e. the wave is attenuated. The attenuated energy is then transferred back to the IR beam in the crystal and is measured by the detector. The most common materials to be used as ATR crystals are zinc selenide (ZnSe) and Germanium (Ge) and diamond. Instruments which use diamond as the ATR crystal material exhibit greater durability and robustness, than ZnSe and Ge. [100]

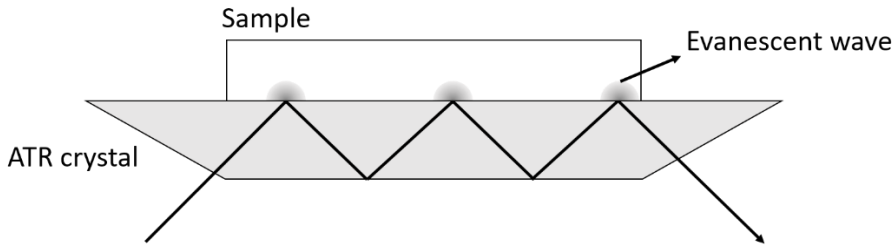

Figure (1.14): ATR crystal scheme adapted according to the ref[100]

1.9.3 X-ray diffraction

In spectroscopic characterisation techniques, the difference in absorption or emission of radiation is measured while the wavelength of the incident light is varied. On the other hand, by using diffraction techniques, characterisation is based on the scattering of EM radiation on the sample. For the crystalline materials, X-ray part of the spectrum is ideal for the diffraction since its wavelengths (0.1-10 nm) coincide with the scale of chemical bonds and atom sizes. Apart from X-ray, diffraction of electrons and neutrons on crystals is observed, as well. Single-crystal X-ray diffraction is a non-destructive characterisation technique that provides detailed information about the internal lattice of crystalline substances (unit cell dimensions, bond-lengths and angles, details of site-ordering). The interaction of the incident rays with the sample produces constructive interference by the Bragg's Law ($n\lambda=2d\sin\theta$), where θ is the glancing angle of X-rays of a specific wavelength (λ), d is the interplanar spacing of the crystal and n (integer number) represents the order of reflection. (Figure 1.15) Bragg's law relates the EM wavelength to the diffraction angle and the lattice spacing in a crystalline sample. Diffracted X-rays are then counted by the detector and further processed. By changing the geometry of the incident rays, the orientation of the central crystal and the detector, all possible diffraction directions of the lattice should be attained.[101,102]

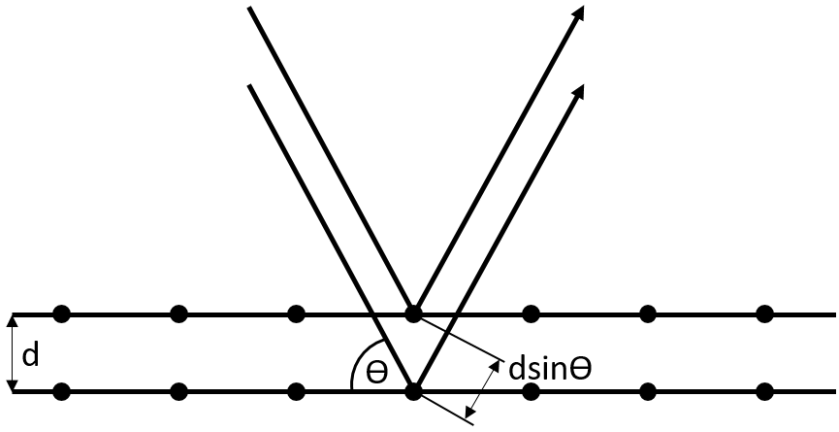

Figure (1.15): Scheme of the Bragg's diffraction law[101]

Samples should be optically clear and unfractured crystals ideally from 200-550 μm in any direction. If no suitable specimen could be found, crystals can be broken off a larger sample and the best fragment selected. During a standard characterisation experiment, the crystal is mounted using a small drop of oil on a nylon loop, which is then cooled so the oil solidifies. The loop is attached to a metal pin, which is further mounted onto a goniometer head. The goniometer head containing the sample is then attached to the diffractometer. Samples are then centred by all three (X, Y and Z) directions. Subsequently, a preliminary set of frames is collected to determine the unit cell. This set of data is then used to select the reduced primitive cell, the appropriate crystal system and corresponding Bravias lattice, and to calculate and refine the orientation matrix.[101-103]

After the refined cell and orientation matrix have been determined, intensity data is collected. Generally, the data is collected from 4 to 55 2θ degrees for Mo-anode. A complete data collection requires from 2-24 hours, based on the specimen (collection could be constrained depending on the symmetry of the material to shorten the collection time) and the type of the diffractometer.

The collected data from the X-ray analysis needs interpretation and refinement to obtain the sample crystal structure. Miller indices (*hkl*) are assigned to collected reflections, to indicate its position in the collected diffraction pattern. The pattern is related to lattice and the unit cell in real space as a reciprocal Fourier transform. After the data collection step, the phase problem has to be solved to determine the set of phases, which needs to be further combined with the structure factors to calculate the electron density of the analysed material from which the crystal structure obtained. There are several procedures present to solve the phase problem. The usual method currently is to use direct methods, where phases are assigned initially to strong reflections and then iterated until a refined fit is produced. The obtained data is further refined by least-squares. The final solution of the crystal structure contains a

corresponding *R*-value that represents a difference between the calculated and observed structures in percentage.[103]

Single-crystal X-ray diffractometer

The principal components of a single-crystal X-ray diffractometer are an X-ray source, a goniometer with a sample holder and a detector. (Figure 1.16)

X-ray sources

X-rays could be generated in a cathode ray tube or by a synchrotron. For the laboratory use X-rays are generated in a cathode ray tube by heating a filament to produce electrons, which are then accelerated towards a target by applying a voltage. When accelerated electrons are of sufficient energy to displace inner shell electrons of the target material, X-ray spectra characteristic of the target (usually copper or molybdenum) is produced. These spectra consist of several specific wavelengths, usually K_α and K_β. To be more specific, K_α further has $K_{\alpha1}$ and $K_{\alpha2}$. $K_{\alpha1}$ is of a shorter wavelength and twice as intense as $K_{\alpha2}$. Filtering or crystal monochromators are required to produce monochromatic radiation necessary for diffraction. $K_{\alpha1}$and $K_{\alpha2}$ are very close in wavelength, therefore a weighted average is used. Molybdenum is generally used as anode material for single-crystal diffraction, MoK_α = 0.7107Å. These X-rays are then collimated to make a more concentrated beam and directed to the crystal sample mounted on a goniometer.[101-103]

Goniometer-sample holder

Goniometers are instruments that allow objects to be rotated into precise angular positions. Modern single-crystal diffractometers use 4-circle goniometers. They are noted as 2θ, χ, φ, and Ω. These notations define the relationship of the incident monochromatic X-rays, the crystal lattice and a detector. Incident radiation could be either, transmitted reflected of scattered. A beam stop is located directly opposite the collimator to block transmitted rays

and prevent the detector damage. Diffracted rays at the correct orientation for the configuration of the crystal are then collected by the detector.[102]

Detector

When the geometry of the incident X-rays impinging the sample satisfies the Bragg Equation, constructive interference occurs. A detector records and processes this X-ray signal and converts it to a count rate which is then processed by a computer. Previously photographic films and pixel detectors were used, but in contemporary single-crystal diffractometers, CCD (charge-coupled device) technology is used to transform the intensity of X-ray photons into a corresponding electrical signal.[101-103]

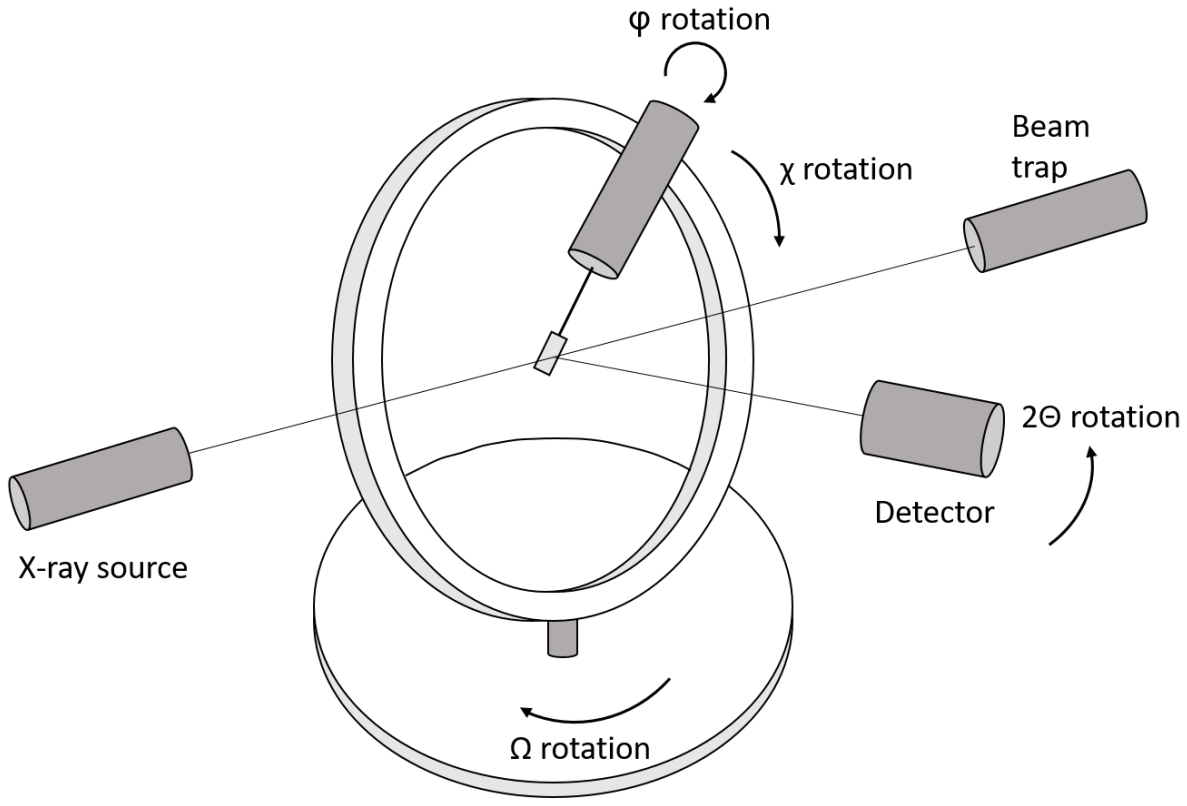

Figure (1.16) Scheme of an X-ray single-crystal diffractometer,

adapted from ref[102]

CHAPTER (2)
Experimental

2. Methodology

2.1- Materials

Table 2.1 List of starting materials and corresponding suppliers

Material	**Supplier**
3,5-difluoropyridine	Fluorochem
3,5-dichloropyridine	Fluorochem
2,6-dichloropyridine	Acros Organics
2,6-dimethoxypyridine	ALDRICH
3-fluoropyridine	Fluorochem
2-fluoro-3-iodopyridine	Fluorochem
2-fluoro-4-iodopyridine	Fluorochem
2-fluoro-5-iodopyridine	Apollo Scientific
2-cyanopyridine	Acros Organics
4-methoxypyridine	T C I
2-chloroquinoline	Alfa Aesar
1,10-phenanthroline	Alfa Aesar
Quinoxaline	Apollo Scientific
Iodine monochloride	Acros Organics
Iodine	Fisher Chemical
Iodine monobromide	Acros Organics
Methanol	Fisher Chemical
Ethanol	Fisher Chemical
Dichloromethane	Fisher Chemical

2.2- Procedure

For solid starting materials the aromatic nitrogen compounds (0.007 mol) A were dissolved in ethanol (3 mL) and added to a round-bottomed flask. If the starting material was a liquid, it was placed directly in a round-bottomed flask. ICl, IBr, I_2 1.20 g (0.007 mol), 1.55 g (0.007 mol), 1.90g (0.007 mol) respectively B was dissolved in 4 mL of ethanol and cooled to 0 °C for 30 min and added dropwise to compound A. Crystals were formed immediately for some products while for the other products it was necessary to place the samples in a freezer at -20 °C for at least 12 hours before a precipitate was formed. If no crystals were formed on cooling the samples were left in a fume hood for the solvent to evaporate. If no suitable crystalline material was obtained using these procedures the fine product powder was dissolved in the minimum amount (2 mL) of solvent (dichloromethane, methanol) and cooled to -75 °C to obtain samples of required size and quality.

2.3 -Instrumentation

2.3.1 IR analysis

ATR FT-IR spectra were recorded on the crystalline samples using Thermo-Scientific NICOLET iS 10 FT-IR Spectrometer with a diamond crystal. Background spectra were recorded in 16 scans from 600-4000 cm^{-1} and then the crystalline sample was loaded onto the IR sample stage crystalline sample was added until the transmittance of key signals was lower than 90 percentages and 16 scans were collected from 600-4000 cm^{-1} with the spectral resolution of 4 cm^{-1}.

2.3.2 UV-Visible analysis

UV-Visible spectra were recorded on the solutions of the samples using a Thermo-Scientific, EVOLUTION 220- UV-Visible spectrophotometer and were recorded from 300-800 nm.

The liquid samples were placed in 1 cm pathlength quartz cell.

2.3.3 XRD analysis

X-ray intensity data for all crystals were collected and analysed by Drs R. H. Jones and C Hawes at -150 °C (123 K) using a Bruker D8 QUEST diffractometer equipped with a PHOTON 50 CMOS area detector using Mo Kα radiation, λ = 0.71073 Å. The raw area detector data frames were reduced and corrected for absorption effects using the Bruker APEX3 and SADABS programs. Structures were solved using a variety of methods (programs SIR92, SUPERFLIP)[104, 105] and refined by least-squares procedures.

2.4 –Experimental data

2.4.1 Experimental conditions

3,5-difluoropyridine-ICl

3,5-difluoropyridine (0.862 g) (0.007 mol) was placed in a round bottom flask. ICl (1.210 g) (0.007 mol) was dissolved in 4 mL of ethanol and cooled to 0 ℃ for 30 min. The ICl solution was then added dropwise to the 3,5-difluoropyridine solution. Yellow crystals were formed immediately. The precipitate was filtered using a Hirsh funnel and stored in a freezer. Weight (1.58 g) Yield (76%); m.p. 107-109 ℃.

3,5-dichloropyridine-ICl

3,5-dichloropyridine (1.125) g (0.007 mol) was mixed with ethanol (3 mL). ICl (1.210 g) (0.007 mol) was dissolved in 4 mL of ethanol and cooled to 0 ℃ for 30 min. The ICl solution was then added dropwise to the 3,5-dichloropyridine solution. Dark yellow crystals were formed immediately. The precipitate was filtered using a Hirsh funnel and stored in a freezer. Weight 1.17g Yield (50%) m.p. 140-143 ℃.

2,6-dichloropyridine-ICl

2,6-dichloropyridine (1.125) g (0.007 mol) was mixed with ethanol (3 mL). ICl (1.210 g) (0.007 mol) was dissolved in 4 mL of ethanol and cooled to 0 ℃ for 30 min. The ICl solution was then added dropwise to the 2,6-dichloropyridine solution. Orange crystals were formed immediately. The precipitate was filtered using a Hirsh funnel and stored in a freezer. Weight (1.52 g), Yield (65%); m.p. 91-93 ℃.

2,6-dimethoxypyridinium-ICl_2^-

2,6-dimethoxypyridine (1.042 g) (0.007 mol) was placed in a round bottom flask. ICl (1.210 g) (0.007 mol) was dissolved in 4 mL of ethanol and cooled to 0 ℃ for 30 min. The ICl solution was then added dropwise to the 2,6-dimethoxypyridine solution. Yellow crystals were formed immediately. The precipitate was filtered using a Hirsh funnel and stored in a freezer. Weight (1.33 g) Yield (59%); m.p. 136-138 ℃.

4-methoxypyridine-ICl

4-methoxypyridine (0.818 g) (0.007 mol) was placed in a round bottom flask. ICl (1.210 g) (0.007 mol) was dissolved in 4 mL of ethanol and cooled to 0 ℃ for 30 min. The ICl solution was then added dropwise to the 4-methoxypyridine solution. Dark orange crystals were formed immediately. The precipitate was filtered using a Hirsh funnel and stored in a freezer. Weight (1.52 g) Yield (74%); m.p. 165-168 ℃.

3-fluoropyridine-ICl

3-fluoropyridine (0.727 g) (0.007 mol) was placed in a round bottom flask. ICl (1.210 g) (0.007 mol) was dissolved in 4 mL of ethanol and cooled to 0 ℃ for 30 min and added dropwise to the 3-fluoropyridine, which had also been cooled. Yellow crystals were formed immediately. The precipitate was filtered using Hirsh funnel and placed in a freezer. Weight (1.15 g). Yield (59%); m.p. 106-109 ℃.

2-fluoro-3-iodopyridine-ICl

2-fluoro-3-iodopyridine (1.672 g) (0.007 mol) was mixed with ethanol (3 mL). ICl (1.210 g) was dissolved in 4 mL of ethanol and cooled to 0 ℃ for 30 min. The ICl solution was then added dropwise to the 2-fluoro-3-iodopyridine solution. No precipitate was formed immediately; the solution was placed in a freezer overnight. Brown crystals were formed and were filtered using a Hirsh funnel and stored in a freezer. Weight (1.90 g) Yield (66%); m.p. 105-107 ℃.

2-fluoro-4-iodopyridine-ICl

2-fluoro-4-iodopyridine (1.672 g) (0.007 mol) was mixed with ethanol (3 mL). ICl (1.210 g) (0.007 mol) was dissolved in 4 mL of ethanol and cooled to 0 °C for 30 min. The ICl solution was then added dropwise to the 2-fluoro-4-iodopyridine solution. No precipitate was formed The solution was placed in the freezer overnight. However, no precipitate was formed. The solution was placed in a fume hood for a few days until orange crystals were formed. These were filtered using a Hirsh funnel and stored in a freezer. Weight (1.23 g) Yield (42%); m.p. 136-138 °C.

2-fluoro-5-iodopyridine-ICl

2-fluoro-5-iodopyridine (1.672 g) (0.007 mol) of was mixed with ethanol (3 mL). ICl (1.210 g) (0.007 mol) was dissolved in 4 mL of ethanol and cooled to 0 °C for 30 min. The ICl solution was then added dropwise to the 2-fluoro-5-iodopyridine solution. Light orange crystals were formed immediately. These were filtered using Hirsh funnel and stored in a freezer. Weight 1.78 g Yield (62%); m.p. 133-135 °C.

2-cyanopyridinium-ICl_2^-

2-cyanopyridine (0.780 g) (0.007 mol) was mixed with ethanol (3 mL). ICl (1.210 g) (0.007 mol) was dissolved in 4 mL of ethanol and cooled to 0 °C for 30 min. The ICl solution was then added dropwise to the 2-cyanopyridine solution. Brown crystals were formed immediately. These were filtered using a Hirsh funnel and stored in a freezer. Weight (1.31 g) Yield (66%); m.p. 94-96 °C.

1,10-phenanthroline-ICl

1,10-phenanthroline **(**1.351 g) (0.007 mol) was mixed with ethanol (3 mL). ICl (1.210 g) (0.007 mol) was dissolved in 4 mL of ethanol and cooled to 0 °C for 30 min. The ICl solution

was then added dropwise to the 1,10-phenanthroline solution. Yellow crystals were formed immediately. These were filtered using a Hirsh funnel and stored in a freezer. Weight (0.96 g) Yield (37%); m.p. 214-217 °C.

Quinoxaline-ICl

Quinoxaline (0.976 g) (0.007 mol) was mixed with ethanol (3 mL). ICl (1.210 g) (0.007 mol) was dissolved in 4 mL of ethanol and cooled to 0 °C for 30 min. The ICl solution was then added dropwise to the quinoxaline solution. No precipitate formed immediately, the solution was allowed to warm to room temp. and stirred more than half an hour. To this solution, 5 mL of hexane was added. Light Brown crystals were formed, and were filtered using a Hirsh funnel and subsequently stored in a freezer. Weight (1.35 g) Yield (61%); m.p. 109-111 °C.

2-chloroquinoline-ICl

2-chloroquinoline (1.227 g) (0.007 mol) was mixed with dichloromethane (5 mL). ICl (1.210 g) (0.007 mol) was dissolved in 4 mL of dichloromethane and cooled to 0 °C for 30 min. The ICl solution was then added dropwise to the 2-chloroquinoline solution. Brown crystals were formed immediately. The precipitate was filtered using a Hirsh funnel and stored in a freezer. Weight (1.65 g) Yield (67%); m.p. 117-120°C.

3,5-difluoropyridine-IBr

3,5-difluoropyridine (0.862 g) (0.007 mol) was placed in a round bottom flask. IBr (1.551 g) (0.007 mol) was dissolved in 4 ml of ethanol and cooled to 0 °C for 30 min. The IBr solution was then added dropwise to the 3,5-difluoropyridine solution. No precipitate was formed immediately; the solution was placed in a freezer overnight. Brown crystals were formed. The precipitate was filtered using Hirsh funnel and stored in a freezer Weight (1.55 g) Yield (64%); m.p. (No melting point could be recorded as this was below room temperature).

3,5-dichloropyridine-IBr

3,5- dichloropyridine (1.125 g) (0.007 mol) was mixed with ethanol (3 mL). IBr (1.551 g) (0.007 mol) was dissolved in 4 ml of ethanol and cooled to 0 °C for 30 min. The IBr solution was then added dropwise to the 3,5-dichloropyridine solution No precipitate was formed immediately; the solution was placed in a freezer overnight. Dark brown crystals were formed. The precipitate was filtered using Hirsh funnel and stored in a freezer. Weight (1.21 g) Yield (45%), m. p(No melting point could be recorded as this was below room temperature).

2,6-dichloropyridine-IBr

2,6-dichloropyridine (1.125 g) (0.007 mol) was mixed with ethanol (3 ml). IBr (1.551 g) (0.007 mol) was dissolved in 4 ml of ethanol and cooled to 0 °C for 30 min. The IBr solution was then added dropwise to the 2,6-dichloropyridine solution. Brown crystals were formed immediately. The precipitate was filtered using Hirsh funnel and stored in a freezer. Weight (1.57 g), Yield (58%); m.p. 77-80 °C.

2,6-dimethoxypyridine-IBr

2,6-dimethoxypyridine (1.042 g) (0.007 mol) was placed in a round bottom flask. IBr (1.551 g) (0.007 mol) was dissolved in 4 ml of ethanol and cooled to 0 ℃ for 30 min. The IBr solution was then added dropwise to the 2,6-dimethoxypyridine solution. Brown crystals were formed immediately. The precipitate was filtered using Hirsh funnel and stored in a freezer. Weight (0.44 g) Yield (20%); m.p. 52-55℃.

4-methoxypyridine-IBr

4-methoxypyridine (0.818 g) (0.007 mol) was mixed with ethanol (3 ml). IBr (1.551 g) (0.007 mol) was dissolved in 4 ml of ethanol and cooled to 0 ℃ for 30 min. The IBr solution was then added dropwise to the 4-methoxypyridine solution. Brown crystals were formed immediately. The precipitate was filtered using Hirsh funnel and stored in a freezer. Weight (1.31 g) Yield (55%); m.p. 38-40℃.

3-fluoropyridine-IBr

3-fluoropyridine (0.727 g) (0.007 mol) was placed in a round bottom flask. IBr (1.551 g) (0.007 mol) was dissolved in 4 mL of ethanol and cooling to 0 ℃ for 30 min and dropwise to 3-fluoropyridine. Brown crystals was formed immediately. The precipitate was filtered using Hirsh funnel and placed in a freezer. Yield (30%); m.p. 58-61℃.

2-fluoro-3-iodopyridine- IBr

2-fluoro-3-iodopyridine (1.675 g) (0.007 mol) was mixed with ethanol (3 mL). IBr (1.551 g) (0.007 mol) was dissolved in 4 mL of ethanol and cooled to 0 ℃ for 30 min. The IBr solution was then added dropwise to the2-fluoro-3-iodopyridine solution. Dark brown needle crystals were formed immediately. The precipitate was filtered using Hirsh funnel and stored in a freezer. Yield (52%); m.p. 76-79 ℃.

2-fluoro-4-iodopyridine-IBr

2-fluoro-4-iodopyridine (1.67g) (0.007mol) was mixed with ethanol (3 mL). IBr 1.551 g (0.007 mol) was dissolved in 4 mL of ethanol and cooled to 0 ℃ for 30 min. The IBr solution was then added dropwise to the 2-fluoro-4-iodopyridine solution. Brown needle crystals were formed immediately. The precipitate was filtered using Hirsh funnel and stored in a freezer. Yield (52%); m.p. 88-91 ℃.

2-fluoro-5-iodopyridine- IBr

2-fluoro-5-iodopyridine (1.67g) (0.007mol) was mixed with ethanol (3 mL). IBr 1.551g (0.007 mol) was dissolved in 4 mL of ethanol and cooled to 0 ℃ for 30 min. The IBr solution was then added dropwise to the2-fluoro-5-iodopyridine solution. Brown needle crystals were formed immediately. The precipitate was filtered using Hirsh funnel and stored in a freezer. Yield (52%); m.p. 96-99 ℃.

2-Cyanopyridine- IBr

2-cyanopyridine (0.787g) (0.007mol) was mixed with ethanol (3 mL). IBr 1.551g (0.007 mol) was dissolved in 4 mL of ethanol and cooled to 0 ℃ for 30 min. The IBr solution was then added dropwise to the2-cyanopyridine solution. Brown crystals were formed immediately. The precipitate was filtered using Hirsh funnel and stored in a freezer. Yield (42%); m.p. 94-96 ℃.

1,10-Phenanthroline- IBr

1,10-Phenanthroline (1.351 g) (0.007mol) was mixed with ethanol (3 mL). IBr (1.551 g) (0.007mol) was dissolved in 4 mL of ethanol and cooled to 0 ℃ for 30 min. The IBr solution was then added dropwise to the1,10-Phenanthroline solution. Light brown crystals were

formed immediately. The precipitate was filtered using Hirsh funnel and stored in a freezer. Weight (1.44 g)Yield (49%); m.p.191-194°C.

Quinoxaline-IBr (yellow)

Quinoxaline (0.976 g) (0.007 mol) was mixed with ethanol (3 mL). IBr (1.551 g) (0.007 mol) was dissolved in 4 mL of ethanol and cooled to 0 °C for 30 min. The IBr solution was then added dropwise to the Quinoxaline solution. No precipitate was formed immediately; the solution was placed in the freezer for in excess of 12 hours. Brown crystals were formed. The precipitate was filtered using a Hirsh funnel and stored in a freezer. Weight (1.14 g) Yield (45%); m.p. 56-59°C.

2-ethoxyquinolinium-IBr_2^-

2-chloroquinoline (1.227 g) (0.007 mol) was mixed with ethanol (3 mL). IBr (1.551 g) (0.007 mol) was dissolved in 4 mL of ethanol and cooled to 0 °C for 30 min. The IBr solution was then added dropwise to the2-chloroquinoline solution. No precipitate was formed immediately, the solution was placed in a freezer overnight, with brown crystals being formed. The precipitate was filtered using Hirsh funnel and stored in a freezer Weight (1.04 g) Yield (37%); m.p. 131-133 °C.

3,5-difluoropyridine-I_2

3,5-difluoropyridine (0.862 g) (0.007 mol) was placed in a round bottom flask. I_2 (1.905 g) (0.007 mol) was dissolved in 4 ml of ethanol and cooled to 0 °C for 30 min. The I_2 solution was then added dropwise to the 3,5-difluoropyridine solution. Brown crystals were formed immediately. The precipitate was filtered using Hirsh funnel and stored in a freezer. Weight (1.04g) Yield (37%); m.p. 125-128°C.

3,5-dichloropyridine-I_2

1.125 g (0.007 mol) of 3,5- dichloropyridine was mixed with ethanol (3 ml). I_2 (1.905 g) (0.007 mol was dissolved in 4 ml of ethanol and cooled to 0 °C for 30 min. The I_2 solution was then added dropwise to the 3,5-dichloropyridine solution. Dark brown crystals were formed immediately. The precipitate was filtered using Hirsh funnel and stored in a freezer. Weight (0.85) Yield (28%); m.p. 130-133°C.

2,6-dichloropyridine-I_2

1.125 g (0.007 mol) of 2,6 - dichloropyridine was mixed with ethanol (3 ml). I_2 (1.905 g) (0.007 mol) was dissolved in 4 ml of ethanol and cooled to 0 °C for 30 min. The I_2 solution was then added dropwise to the 2,6-dichloropyridine solution. Orange crystals were formed immediately. The precipitate was filtered using Hirsh funnel and stored in a freezer. Weight (1.57 g), Yield (68%); m.p. 95-97 °C.

2,6-dimethoxypyridine-I_2

1.042 (0.007 mol) of 2,6-dimethoxypyridine was placed in a round bottom flask I_2 (1.905 g) (0.007 mol) was dissolved in 4 ml of ethanol and cooled to 0 °C for 30 min. The I_2 solution was then added dropwise to the 2,6-dimethoxypyridine. Yellow crystals were formed

immediately. The precipitate was filtered using Hirsh funnel and stored in a freezer. Weight (0.63 g) Yield (21%); m.p. 68-70°C.

4-methoxypyridine-I_2

0.818 g (0.007 mol) of 4-methoxypyridine was mixed with ethanol (3 ml). I_2 (1.905 g) (0.007 mol) was dissolved in 4 ml of ethanol and cooled to 0 °C for 30 min. The I_2 solution was then added dropwise to the 4-methoxypyridine solution. No precipitate was formed immediately, the solution was placed in the freezer for more than 12 hours. Dark orange crystals were then formed, the precipitate was filtered using Hirsh funnel and stored in a freezer. Weight (0.49) Yield (24%); m.p. 91-93°C.

3-fluoropyridine-I_2

0.727 g (0.007 mol) of 3-fluoropyridine was placed in a round bottom flask. I_2 (1.905 g) (0.007 mol) was dissolved in 4 mL of ethanol and cooling to 0 °C for 30 min and dropwise to 3-fluoropyridine. No precipitate was formed immediately. The solution was placed in the freezer more than 12 hours. Brown crystals were then formed, the precipitate was filtered using a Hirsh funnel and stored in a freezer. Weight (0.80 g), Yield (30%); m.p. (No melting point could be recorded as this was below room temperature).

2-fluoro-3-iodopyridine-I_2

2-fluoro-3-iodopyridine (1.672 g) (0.007 mol) was mixed with ethanol (3 mL). I_2 (1.905 g) (0.007 mol) was dissolved in 4 mL of ethanol and cooled to 0 °C for 30 min. The I_2 solution was then added dropwise to the 2-fluoro-3-iodopyridine solution. No precipitate was formed immediately, the solution was placed in the freezer for more than 12 hours. However, no precipitate was formed, the solution was placed in a fume hood for a few days until brown crystals were formed. These were filtered using Hirsh funnel and stored in a freezer. Weight (0.8 g) Yield (22%); m.p. 125-128 °C.

2-fluoro-4-iodopyridine-I_2

2-fluoro-4-iodopyridine (1.672 g) (0.007 mol) was mixed with ethanol (3 mL). I_2 (1.905 g) was dissolved in 4 mL of ethanol and cooled to 0 °C for 30 min. The I_2 solution was then added dropwise to the 2-fluoro-4-iodopyridine solution No precipitate was formed immediately, the solution was placed in the freezer more than 12 hours. Brown crystals were then formed, the precipitate was filtered using a Hirsh funnel and stored in a freezer. Weight (1.90 g) Yield (66%); m.p. 62-65 °C.

2-fluoro-5-iodopyridine-I_2

2-fluoro-5-iodopyridine (1.672 g) (0.007 mol) was mixed with ethanol (3 mL). I_2 (1.905 g) was dissolved in 4 mL of ethanol and cooled to 0 °C for 30 min. The I_2 solution was then added dropwise to the2-fluoro-5-iodopyridine solution. No precipitate was formed immediately, the solution was placed in the freezer more than 12 hours. Brown crystals were then formed, the precipitate was filtered using Hirsh funnel and stored in a freezer. Weight (1.90 g) Yield (66%); m.p. 32-35 °C.

2-cyanopyridine-I_2

0.787g (0.007 mol) of 2-cyanopyridine was mixed with ethanol (3 mL). I_2 (1.905 g) (0.007 mol was dissolved in 4 mL of ethanol and cooled to 0 °C for 30 min. The I_2 solution was then added dropwise to the 2-cyanopyridine solution. No precipitate was formed immediately the solution was placed in the freezer for more than 12 hours. However, no precipitate was formed, the solution was placed in a fume hood for a few days until a brown non-crystalline precipitate was formed. This was dissolved in 3 mL of dichloromethane and cooled to -75°C. Brown crystals were then formed, these were filtered using a Hirsh funnel and stored in a freezer. Weight (0.75 g), Yield (27%); m.p. (No melting point could be recorded as this was below room temperature).

1,10-phenanthroline-I_2

1,10-phenanthroline (1.351 g) (0.007 mol) was mixed with ethanol (3 mL). I_2 (1.905 g) (0.007 mol) was dissolved in 4 mL of ethanol and cooled to 0 ℃ for 30 min. The I_2 solution was then added dropwise to the1,10-phenanthroline solution. No precipitate was formed immediately, the solution was placed in the freezer for more than 12 hours. Dark grey crystals were then formed, the precipitate was filtered using Hirsh funnel and stored in a freezer. Weight (1.06 g) Yield (32%); m.p. 137-139℃.

Quinoxaline-I_2

Quinoxaline (0.976 g) (0.007 mol) was mixed with ethanol (3 mL). I_2 (1.905 g) (0.007 mol) was dissolved in 4 mL of ethanol and cooled to 0 ℃ for 30 min. The I_2 solution was then added dropwise to the Quinoxaline solution No precipitate was formed immediately, the solution was placed in the freezer for more than 12 hours. However, no precipitate was formed, the solution was then placed in a fume hood for a few days until reddish brown crystals were formed. These were filtered using a Hirsh funnel and stored in a freezer. Weight (1.02 g) Yield (35%); m.p. 126-129℃.

2-chloroquinoline-I_2

2-chloroquinoline (1.227 g) (0.007 mol) was mixed with dichloromethane (5 mL). I_2 (1.905 g) (0.007 mol) was dissolved in (4 mL) of dichloromethane and cooled to 0 ℃ for 30 min. The I_2 solution was then added dropwise to the2-chloroquinoline solution. No precipitate was formed immediately, the solution was placed in the freezer for more than 12 hours. Brown crystals were then formed, the precipitate was filtered using a Hirsh funnel and stored in a freezer. Weight (1.26 g) Yield (40%); m.p. 118-121 ℃.

2.5 ATR-FTIR data.

ATR-FTIR spectrum band positions for starting material are shown in Table 2.2 and for the ICl, IBr and I_2 halogen bond complexes are shown in Table 2.3, while ATR-FTIR Spectra of both the starting material and for all products in is each of the corresponding chapters.

Table 2.2 ATR-FTIR spectrum band positions of starting materials expressed in cm^{-1}.

Starting material	C-Cl	C-F	C-N	C=C	C-H
3,5-difluoropyridine		1042	1577	1476	3101
3,5-dichloropyridine	728		1423	1555	3070
2,6-dichloropyridine	737		1584	1654	3039
2,6-dimethoxypyridine			1530	1545	3102
4-methoxypyridine			1547	1616	3097
3-fluoropyridine		1074	1576	1645	3054
2-fluoro-3-iodopyridine		1109	1556	1579	3024
2-fluoro-4-iodopyridine		1073	1578	1645	3056
2-fluoro-5-iodopyridine		1075	1557	1579	3055
2-cyanopyridine			1462	1578	3060
1,10-phenanthroline			1502	1586	
Quinoxaline			1530	1630	3038
2-chloroquinoline	751		1493	1585	3097

Table 2.3 ATR-FTIR spectrum band positions of ICl-halogen bonded complexes expressed in cm^{-1}.

Product	C - Cl	C-F	C-N	C=C	C-H
3,5-difluoropyridine-ICl		1082	1561	1437	3072
3,5-dichloropyridine-ICl	700		1407	1535	3039
2,6-dimethoxypyridine-ICl			1483	1548	3011
4-methoxypyridine-ICl			1500	1604	3098
3-fluoropyridine-ICl		1099	1557	1605	3036
2-fluoro-3-iodopyridine-ICl		1036	1511	1585	3083
2-fluoro-4-iodopyridine-ICl		1072	1540	1583	3082
2-fluoro-5-iodopyridine-ICl		1041	1568	1592	3045
2-cyanopyridine-ICl			1552	1587	3093
1,10-phenanthroline-ICl			1496	1545	3052
Quinoxaline-ICl			1494	1608	
2-chloroquinoline-ICl	747		1510	1614	3058

Table 2.4 ATR-FTIR spectrum band positions of IBr-halogen bonded complexes expressed in cm^{-1}.

Product	C-Cl	C-F	C-N	C=C	C-H
3,5-difluoropyridine-IBr		1152	1538	1610	3065
3,5-dichloropyridine-IBr	1099		1551	1462	3054
2,6-dichloropyridine-IBr			1556	1609	3050
2,6-dimethoxypyridine-IBr			1544	1609	3003
4-methoxypyridine-IBr			1560	1604	3015
3-fluoropyridine – IBr		1114	1584	1603	3100
2-cyanopyridine-IBr			1581	1604	3090
1,10-phenanthroline-IBr			1563	1615	
Quinoxaline-IBr				1612	3038
2-chloroquinoline-IBr			1539	1608	3097

Table 2.5 ATR-FTIR spectrum band positions of I_2-halogen bonded complexes expressed in cm^{-1}.

Product	C-Cl	C-F	C-N	C=C	C-H
3,5-difluoropyridine-I_2		1382	1549	1437	3024
3,5-dichloropyridine-I_2			1407	1535	3039
2,6-dimethoxypyridine-I_2			1534	1608	3000
4-methoxypyridine-I_2			1560	1604	3090
3-fluoropyridine-I_2		1115	1585	1605	3086
2-cyanopyridine-I_2			1577	1600	3084
1,10-phenanthroline-I_2			1561	1612	3052
Quinoxaline-I_2			1557	1672	
2-chloroquinoline-I_2			1562	1615	3059

Chapter (3)
Iodine monochloride

3.1. Introduction.

The pioneering work on halogen bonding was performed on systems including dihalogens,[6,10] but the majority of the current halogen bond research involves organohalogen or inorganic halide XB donors. However, the dihalogens continue to attract interest.[106] The majority of investigations are related to studying the interactions of iodine (I_2) in biological systems with antithyroid drugs.[107,108]

Dihalogens can be divided into two groups, homoatomic (X_2), and heteroatomic (XY) which are also called interhalogens. As it was mentioned in the general introduction, due to the size and polarizability of the atoms, the XB donor ability for homoatomic dihalogens increases in order $F_2 < Cl_2 < Br_2 < I_2$. In systems where homonuclear dihalogens approach the nucleophilic region of XB acceptor, charge separation occurs. For simplicity, the X atom interacting with XB acceptor will be labelled as X_I, while the X atom not included in interaction will be labelled as X_{II}. On the X_I end, there is an accumulation of positive charge, while the negative charge accumulates on the X_{II} end. After the formation of an XB with a Lewis base, the negative charge on the X_{II} makes it more likely to act as an acceptor of a different XB or HB, than as the XB donor. In addition to that, the initial X─X bond is elongated due to the mixing of the Lewis base HOMO orbital with the empty σ* orbital of a dihalogen.[109, 110]

Heteroatomic dihalogens (XY) are polar because of different atoms present in the molecule and this property impacts the XB donor features. The negative charge is located on the more electronegative halogen atom (Y) thus making the less electronegative halogen (X) the XB donor atom. For the iodine-containing heteronuclear dihalogens the XB donor ability is

stronger, the more difference in the electronegativity there is, causing the better charge separation.

Iodine monochloride is a heteronuclear dihalogen that is observed as a solid in two polymorph forms that melt near room temperature, dark-red needles (α-form, m.p. 27.2 °C) and brown-red platelets (β-form, m.p. 13.9 °C). It is soluble in methanol, ethanol, ether, pyridine, acetone, and acetic acid, but hydrolyses when in contact with water.[111] Iodine monochloride is prepared by reaction of gaseous iodine and chlorine in 1:1 ratio, the bond length of ICl in the gas phase was determined by microwave spectroscopy (2.3210 Å).[27]

In a study by Ouvrard et al. 141 halogen bond complexes based on homo- and heteronuclear dihalogens were studied[112]. These authors report that in these systems N, O, S, P, As and Se are observed to act as XB acceptors, while Cl, Br and I as XB donors. They concluded that for the studied systems, the mean R-X···Y bond angle is 176°, which is more linear by 11-38° [112] than the corresponding O-H···Y HBs. Moreover, for the sp^2- hybridized N bases the XB direction is very close to the axis of the nonbonding electron pair and the Y···X halogen bond length and the elongation of the dihalogen bond are significantly related to the donation strength of the Lewis base, but the Lewis acid strength ($Br_2 < I_2 < IBr < ICl$) does not rely on the softness of the base. In this introduction, only the complexes containing N···ICl will be presented in Table (3.0.1).

Table 3.0.1 Geometric parameters of literature reported N···I-Cl halogen bonded complexes, adapted from ref.[106,112]

REFCODE	Complex name	N···I (Å)	I-Cl (Å)	N···I-Cl (°)
CLQUIC[113]	2-Chloroquinoline iodomonochloride	2.432	2.446	179.93
GANXAV[114]	3-Bromo-1-chloroiodopyridine	2.344	2.473	178.43
GANXOJ[114]	1-Chloroiodo-4-(dimethylamino)pyridine	2.246	2.562	179.24
PMTTIC[115]	Pentamethylenetetrazole iodine monochloride	2.347	2.437	176.11
PYRIIC10[116]	Pyridine iodomonochloride	2.290	2.510	178.72
REWWUL[117]	Triphenylphosphane(trimethylsilyl)imide iodochloride	2.327	2.554	178.64
TAGNEV[118]	trans-N,N-bis(Chloroiodo)-2,2-bipyridine	2.343 2.336	2.478 2.459	176.16 179.32
TAGNEV01[114]	N,N-bis(Chloroiodo)-2,2-bipyridine	2.321 2.337	2.488 2.497	175.33 179.40
TMEICL[119]	Trimethylamine iodomonochloride	2.303	2.524	176.88
ZAVDAB[120]	(Chloro-iodo)-trimethylsilyl-trimethylphosphoranimine	2.228	2.651	177.39
ZAVDEF[120]	(Chloro-iodo)-N-chloro-triphenylphosphoranimine	2.294	2.512	176.49

It can be observed that 11 complexes containing N···I-Cl have been reported. The average N···I distance is 2.319 Å, while the value for I-Cl bond is 2.507 Å. A complex with refcode ZAVDAB[120120] has the shortest N···I value (2.228 Å) that indicates the strongest XB, and the most elongated I-Cl bond (2.651 Å) is observed in the same system, as well. All the N···I-Cl angles are very close to the ideal value of 180°, with an average value of 177.85°.

3.2. Aim

This chapter aims to prepare and characterise crystalline N···I halogen-bonded complexes formed by a reaction between the selected aromatic nitrogen compounds with iodine monochloride. The starting materials were chosen because of the large variety in their base strength. All the crystalline complexes are characterised by ATR-FTIR spectroscopy, UV-Vis spectroscopy and single-crystal X-ray diffraction. From the structures obtained by X-ray diffraction the halogen bond lengths and angles within the N···I unit are determined and correlated with the electronic spectra.

3.3 Investigation of halogen bonded complexes

3.3.1 3,5-difluoropyridine- ICl

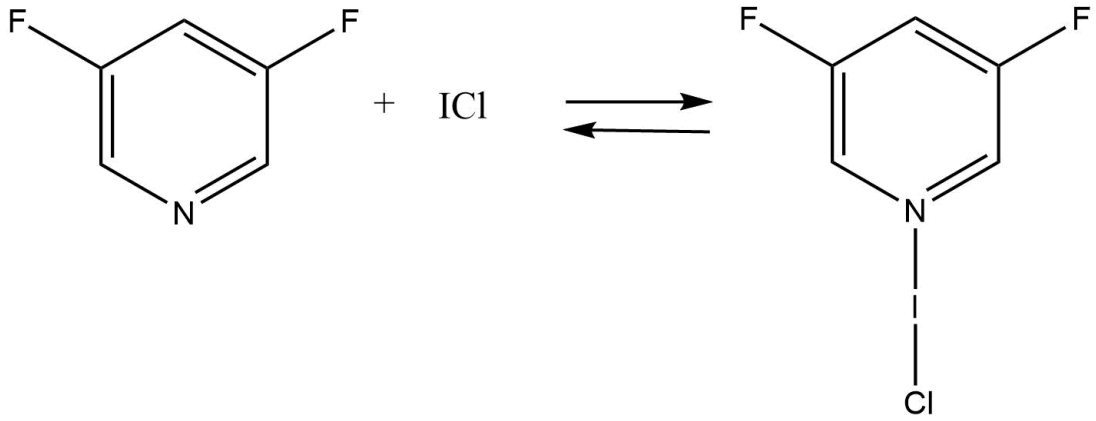

UV-Visible spectra for 3,5-difluoropyridine- ICl solution

All the spectra were collected using methanol as the solvent, the concentration of the samples was 10^{-3} M. The base 3,5-difluoropyridine absorbed at 303 nm and ICl absorbed at 341 nm. A new band appeared at 443 nm when the two above starting materials were mixed, which is not attributed to the 3,5-difluoropyridine or ICl. This new band supports the argument that the formation of the halogen bonded complex occurs. That means λ_{max} for 3,5-difluoropyridine is shifted 140 nm toward higher wavelengths, which is called bathochromic shift or redshift, Figure (3.1.1). The starting material and the resulting complex are also characterised by ATR-FTIR, Figures (3.1.2, 3.1.3).

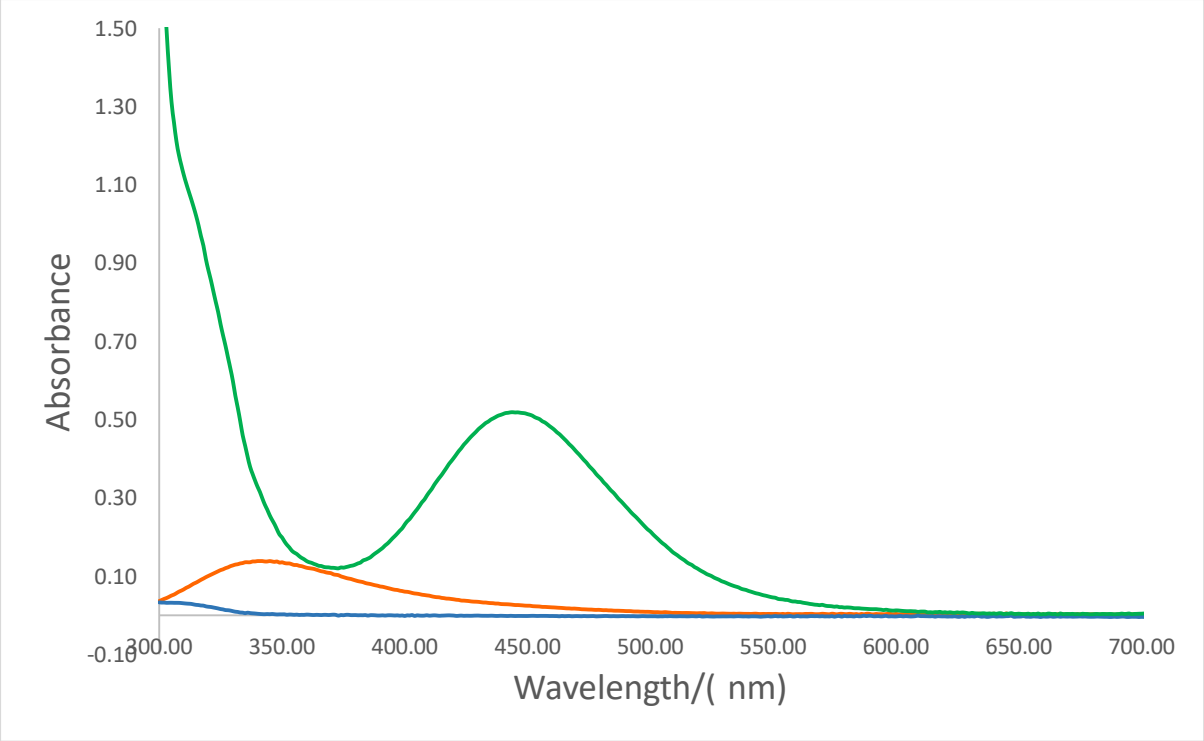

Figure (3.1.1): UV-Visible spectra for the 3,5-difluoropyridine-ICl system: 3,5-difluoropyridine (Blue), ICl (Orange) and 3,5-difluoropyridine-ICl (Green), the spectra were collected using methanol as the solvent, the concentration of the samples was 10^{-3} M.

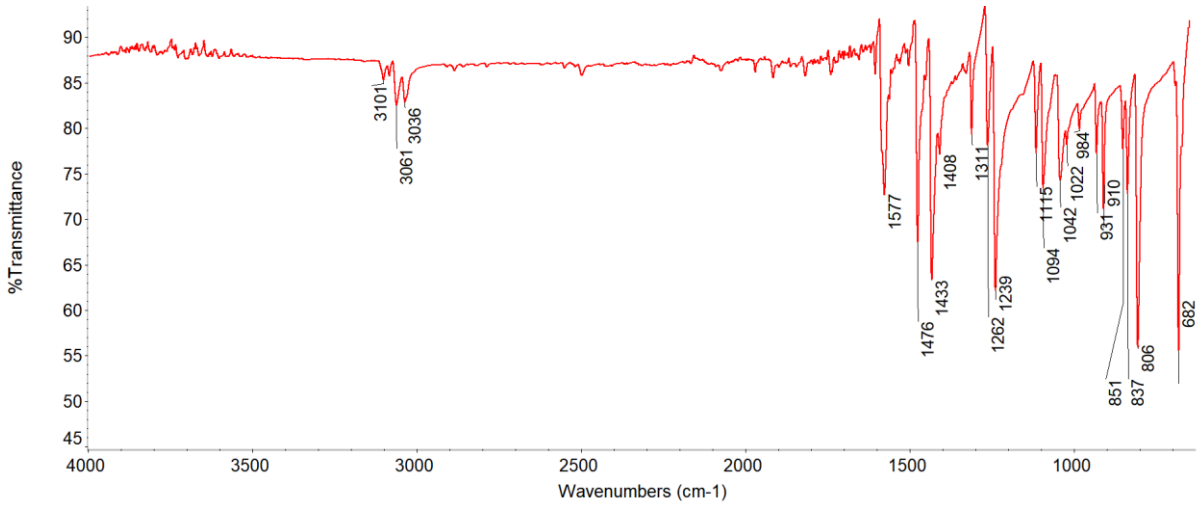

Figure (3.1.2): IR spectrum of 3,5-difluoropyridine.

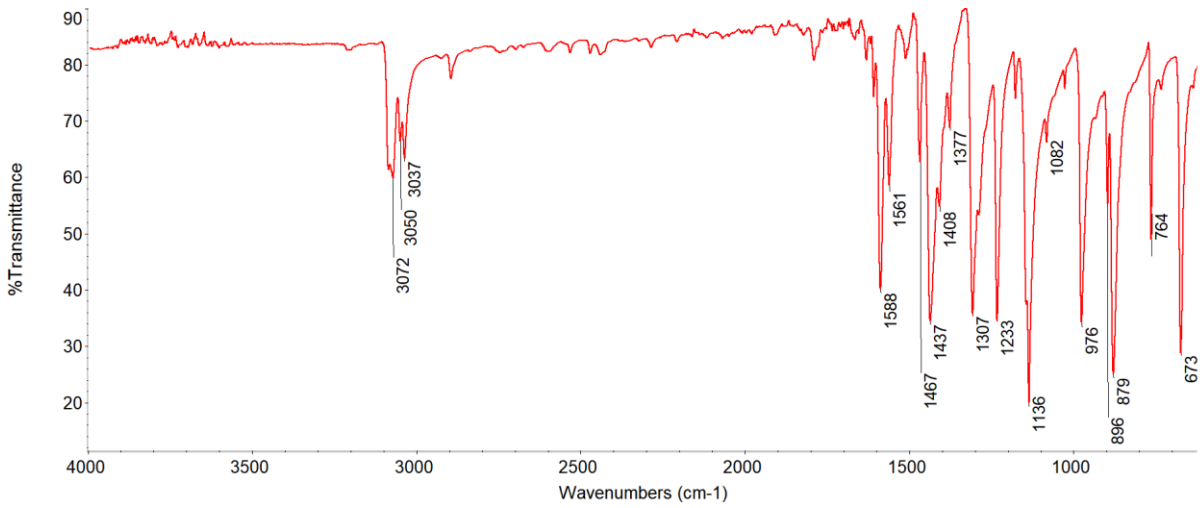

Figure (3.1.3): IR spectrum of 3,5-difluoropyridine-ICl.

XRD measurements:

1.Crystal Structure of 3,5-difluoropyridine-ICl

Crystallographic data for 3,5-difluoropyridine are given in Table (3.1), and selected bond lengths and angles in Table (3.2). A Thermal ellipsoid plot of the structure together with the numbering scheme used is given in Figure (3.1.4)

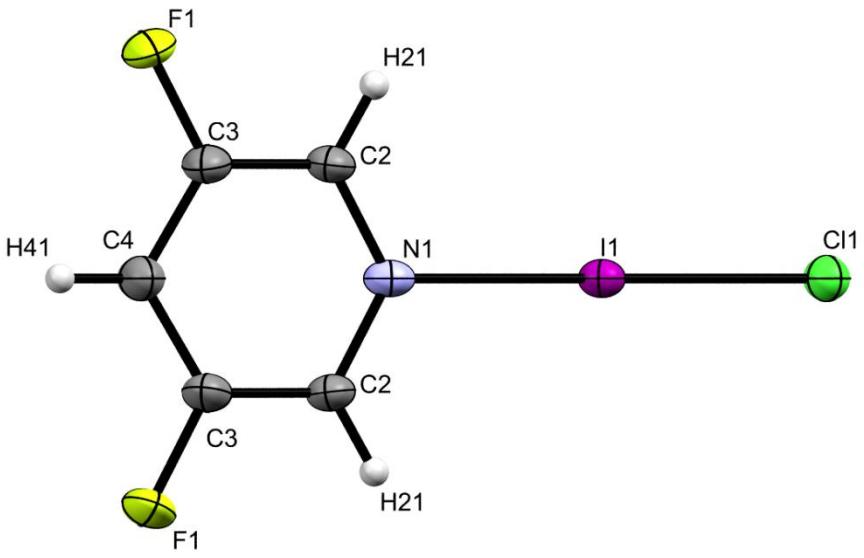

Figure (3.1.4): Thermal ellipsoid plot of 3,5-difluoropyridine-ICl.

3,5-difluoropyridine crystallises in the monoclinic space group $P2_1/m$. The molecule thus possesses crystallographic mirror symmetry with I1, Cl1, N1, C4 and H41 lying in the mirror plane, Figure (3.1.5).

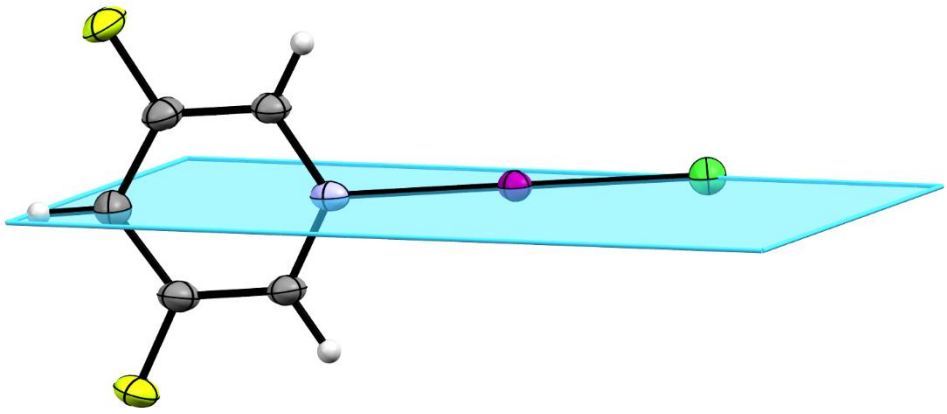

Figure (3.1.5): Thermal ellipsoid plot of 3,5-difluoropyridine showing relationship to crystallographic mirror plane possessed by molecule.

The halogen bond distance between N and I is 2.358(6) Å (N···I-Cl angle is 178.60(1)), which is less than the sum of van der Waals radii of N and I (3.51 Å).[121] The distance between I and Cl for the product is 2.470(2) Å, while the same distance for the iodine monochloride is 2.3210 Å.[27]

Complexes are further interconnected via series of C-H···F and C-H···Cl hydrogen bonds, Figures (3.1.6, 3.1.7). In the C–H···Cl hydrogen bond, H···Cl distance is (2.789 Å) and the C–H···Cl angle is (143.13°). The hydrogen bonding motif can be described by the graph set motif $R_2^2(10)$ shown in Figure (3.1.8). There is also C–H···F hydrogen bond present (2.641 Å). This distance is within the literature reported values for C-H···F hydrogen bonds containing sp^2 hybridised carbon.[122] The distance between C and F is 0.029 Å less than the summation of van der Waals radii and C–H···F angle is (129.67°). Graph motif present in this type of hydrogen bond is $R_2^2(8)$, while both hydrogen bonds are a part of $R_3^3(10)$ motif, Figure (3.1.8). In this figure, the orange contact refers to the halogen bond between N and I, while the red contacts refer to the hydrogen bonds between H and F, H and Cl.

All the analogous complexes are in the single plane and they are linked via C-H···F HBs to complexes in the plane above and via C-H···Cl hydrogen bonds to complexes in the plane below, Figures (3.1.6, 3.1.7). The vertical distance between the two planes where complexes are linked via C-H···F HBs is 1.163 Å, while the distance between centroids of two adjacent molecules in these planes is 6.751 Å, Figure (3.1.9). The vertical distance between the planes where complexes are linked via C-H···Cl HBs is 1.580 Å, while the distance between centroids of two adjacent molecules in these planes is 9.451 Å, Figure (3.1.10).

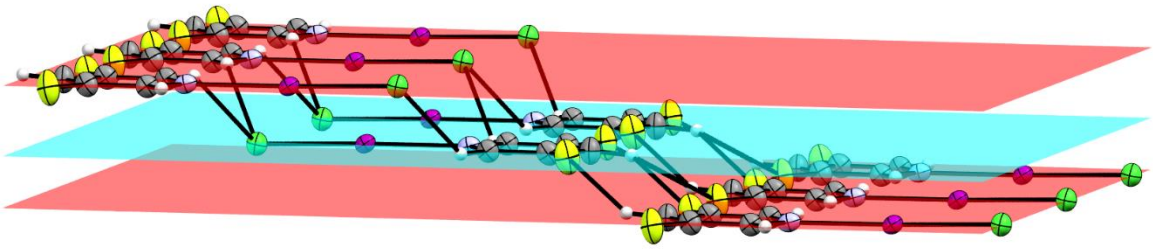

Figure (3.1.6): View showing planes consisting of 3,5-difluoropyridine –ICl complexes linked by C-H···F and C-H···Cl hydrogen bonds

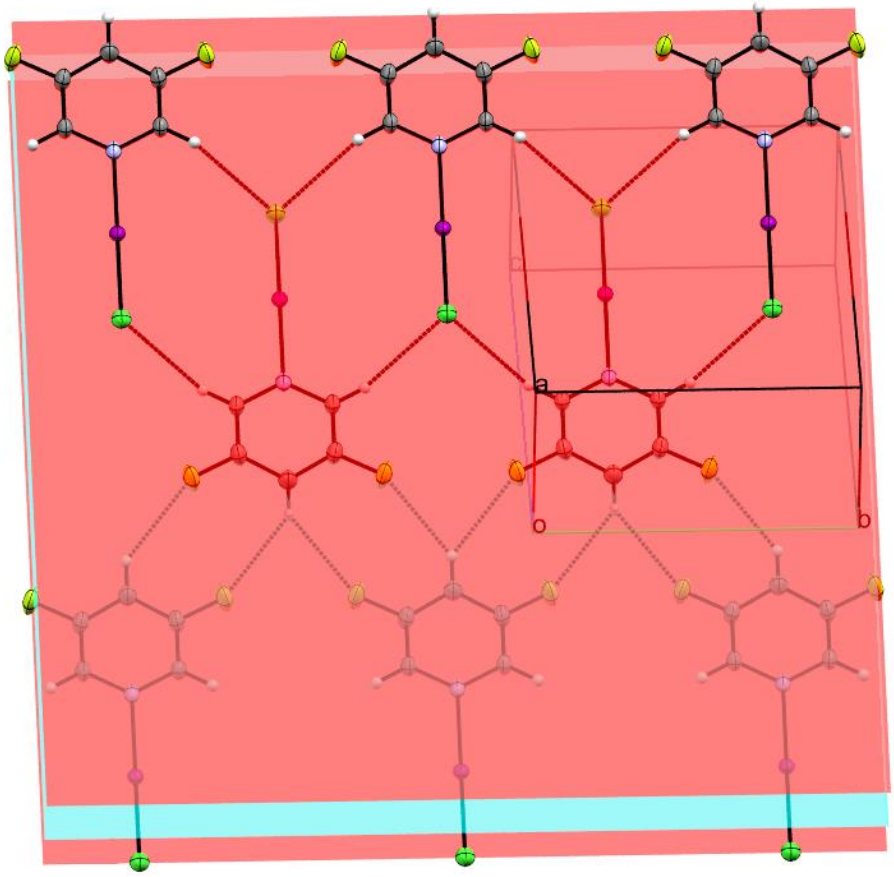

Figure (3.1.7) View showing vertical view on the planes consisting of 3,5-difluoropyridine – ICl complexes linked by C-H···F and C-H···Cl hydrogen bonds

.

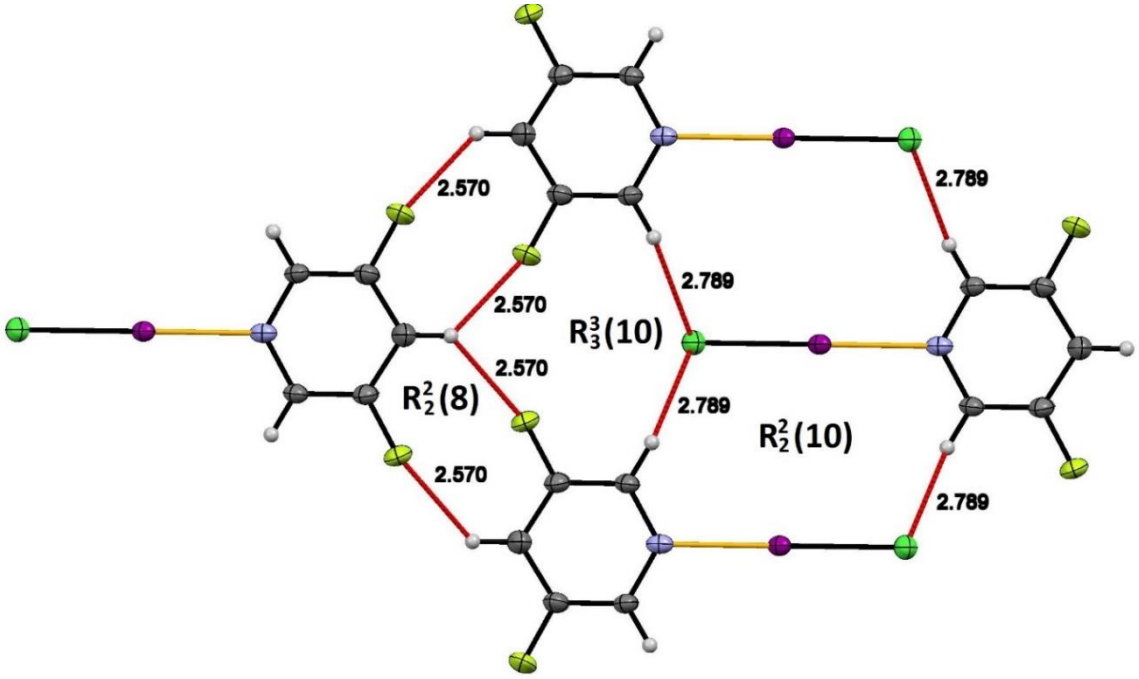

Figure (3.1.8) View showing 3,5-difluoropyridine–ICl approximately along a-axis with the corresponding hydrogen bonding patterns labelled according to graph set motif nomenclature.

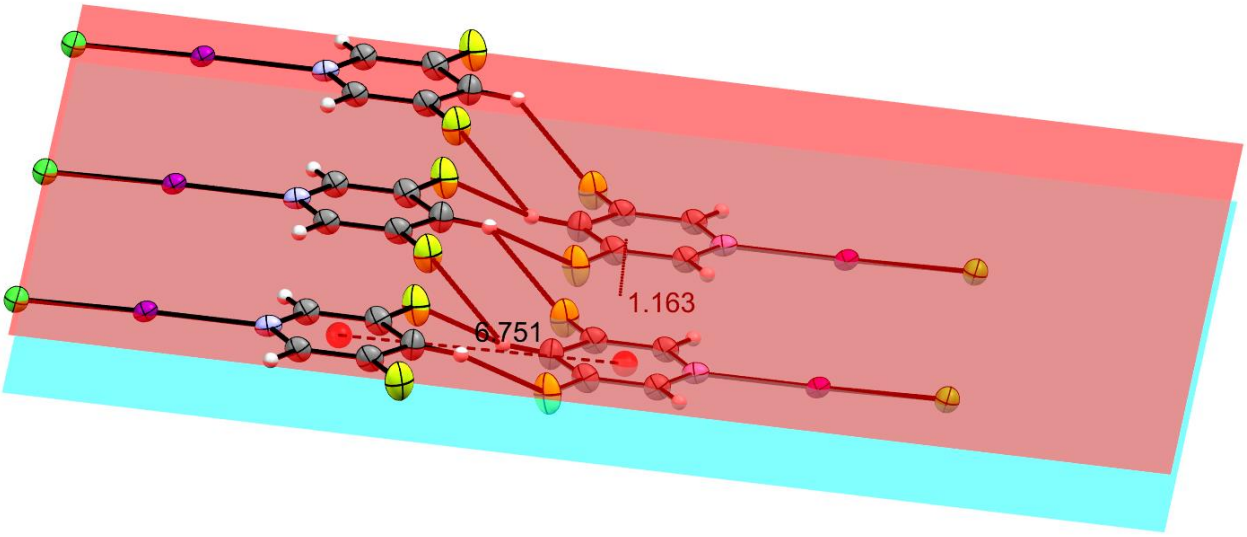

Figure (3.1.9) View showing the distance between the centroids of two 3,5- difluoropyridine –ICl molecules and the vertical distance between two adjacent planes where complexes are linked via C-H···F hydrogen bonds

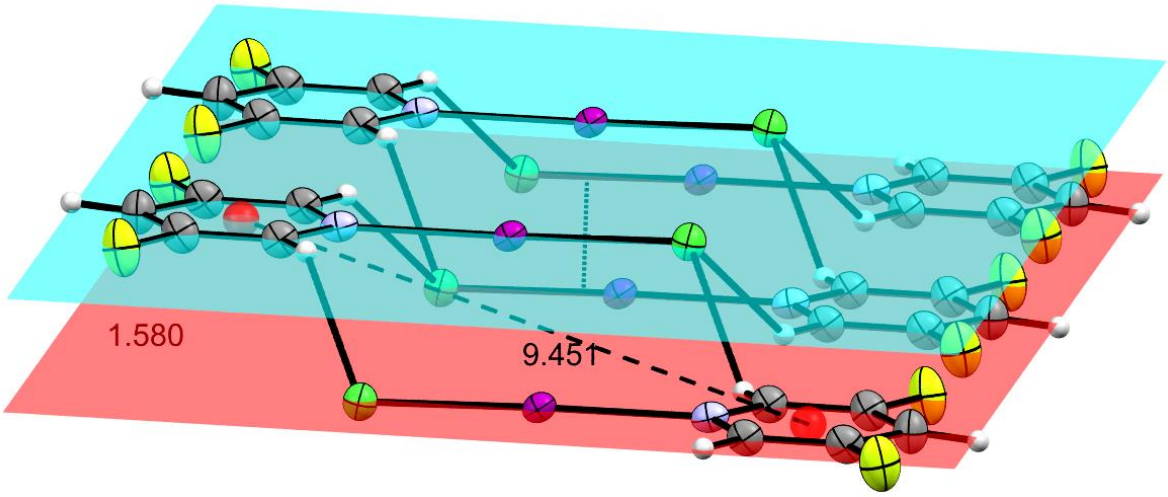

Figure (3.1.10) View showing the distance between the centroids of two 3,5- difluoropyridine –ICl molecules and the vertical distance between two adjacent planes where complexes are linked via C-H···Cl hydrogen bonds

Table (3.1) Crystallographic data for 3,5-difluoropyridine -ICl complex.

Crystal data	
Chemical formula	$C_5H_3ClF_2IN$
M_r	277.44
Crystal system, space group	Monoclinic, $P2_1/m$
T/K	123
a, b, c (Å)	4.1747 (1), 7.9188 (3), 11.5313 (4)
β (°)	91.5981 (17)
V/ ($Å^3$)	381.06 (2)
Z	2
Radiation type	Mo Kα
μ / (mm^{-1})	4.51
Crystal size / (mm)	0.33 × 0.12 × 0.06
Data collection	
Diffractometer	Bruker Kappa Apex2
Absorption correction	Multi-scan SADABS (Siemens, 1996)
T_{min}, T_{max}	0.58, 0.76
No. of measured, independent and observed [$I > 2.0\sigma(I)$] reflections	16270, 1046, 962
R_{int}	0.049
$(\sin \theta/\lambda)_{max}$ /($Å^{-1}$)	0.674

Refinement	
$R[F^2 > 2\sigma(F^2)]$, $wR(F^2)$, S	0.029, 0.073, 1.08
No. of reflections	1044
No. of parameters	54
No. of restraints	2
H-atom treatment	H-atom parameters constrained
$\Delta\rho_{max}$, $\Delta\rho_{min}$ (e Å^{-3})	1.70, −1.17

Table (3.2): Selected interatomic contacts/ Å and /^{o} for the complex 3,5-difluoropyridine – ICl.

Atom1	Atom2	Length	Atom1	Atom2	Atom3	Angle
I1	Cl1	2.470(2)	Cl1	I1	N1	178.691)
I1	N1	2.358(6)	I1	N1	C2	119.3(3)
N1	C2	1.336(5)	I1	N1	C2	119.3(3)
N1	C2	1.336(5)	C2	N1	C2	121.4(6)
C2	C3	1.376(7)	N1	C2	C3	119.4(5)
C3	C4	1.381(6)	C2	C3	C4	122.3(5)
C3	F1	1.344(5)	C2	C3	F1	118.7(4)
C4	C3	1.381(6)	C4	C3	F1	118.9(4)
C2	C3	1.376(7)	C3	C4	C3	115.2(4)
C3	F1	1.344(5)	H41	C4	C3	122.3(5)
			N1	C2	C3	119.4(5)
			C4	C3	C2	122.3(4)

3.3.2 3,5-dichloropyridine- ICl

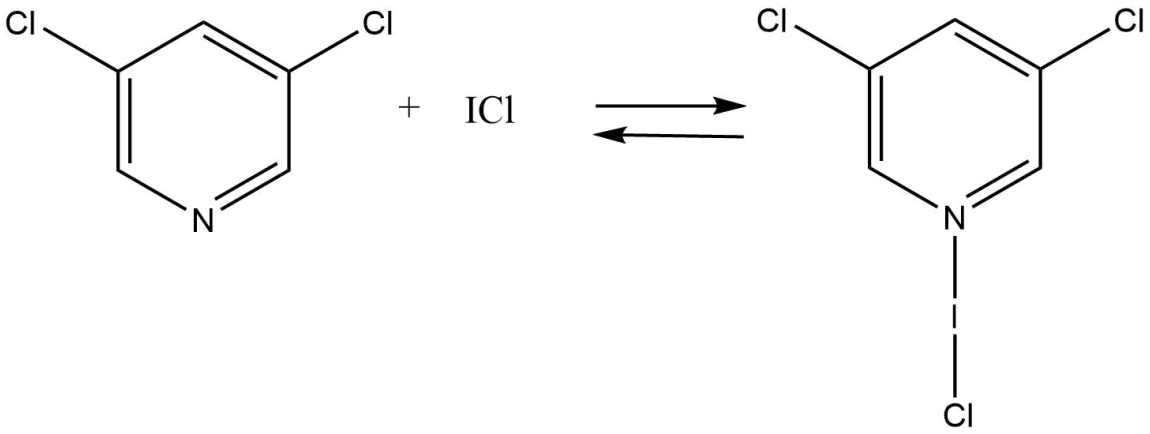

UV-Visible spectra of 3,5-dichloropyridine- ICl solution.

All the spectra were collected using methanol as the solvent, the concentration of the samples was 10^{-3} M. The base 3,5-dichloropyridine absorbed at 335 nm and ICl absorbed at 341 nm. When the two above starting materials were mixed a new band appeared at 444 nm, which is not attributed to starting materials. This new band confirms the formation of the halogen bonded complex. That means λ_{max} for 3,5-dichloropyridine is shifted 109 nm toward higher wavelengths, Figure (3.2.1). Starting material and the resulting complex are also characterised by ATR-FTIR, Figures (3.2.2, 3.2.3).

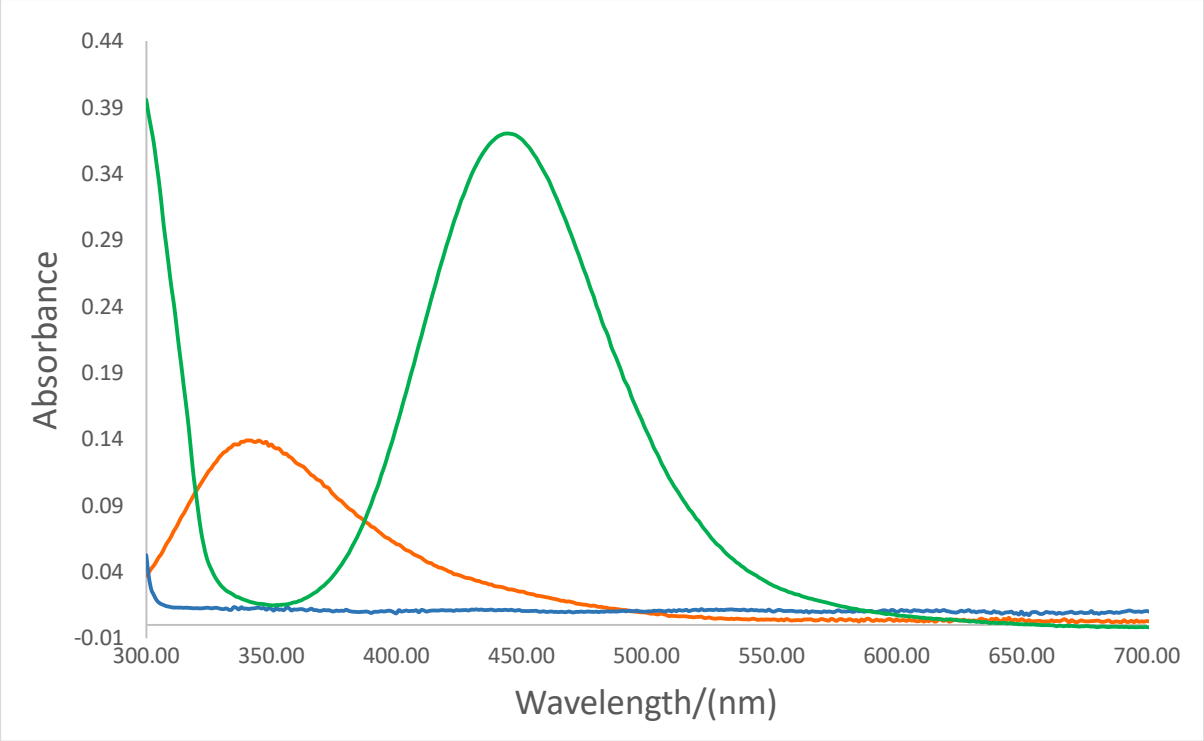

Figure (3.2.1): UV-Visible spectra of 3,5-dichloropyridine-ICl: 3,5-dichloropyridine (Blue), ICl (Orange), 3,5-dichloropyridine-ICl (Green), the spectra were collected using methanol as the solvent, the concentration of the samples was 10^{-3} M.

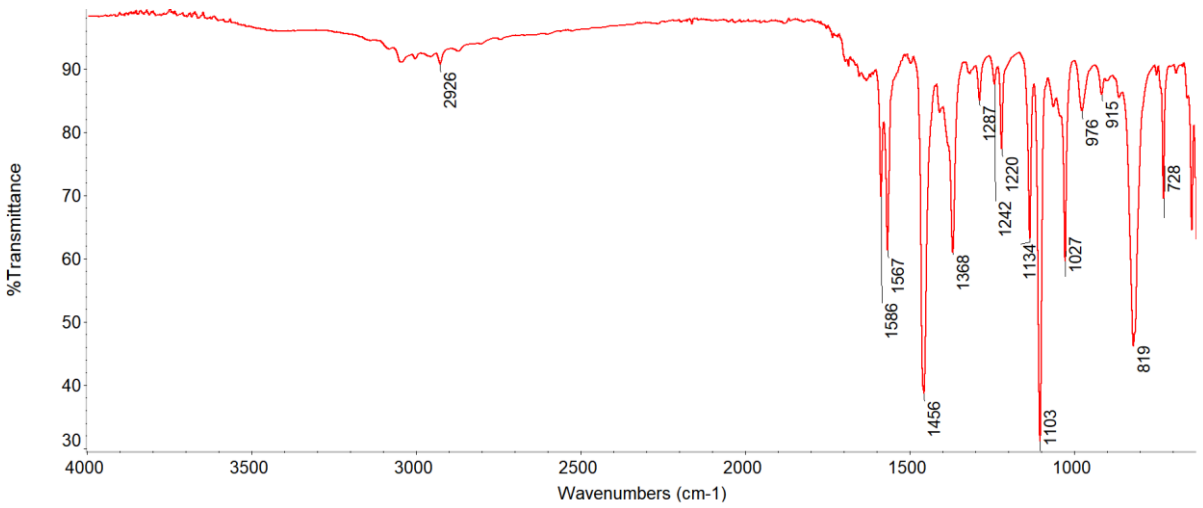

Figure (3.2.2): IR spectrum of 3,5-dichloropyridine.

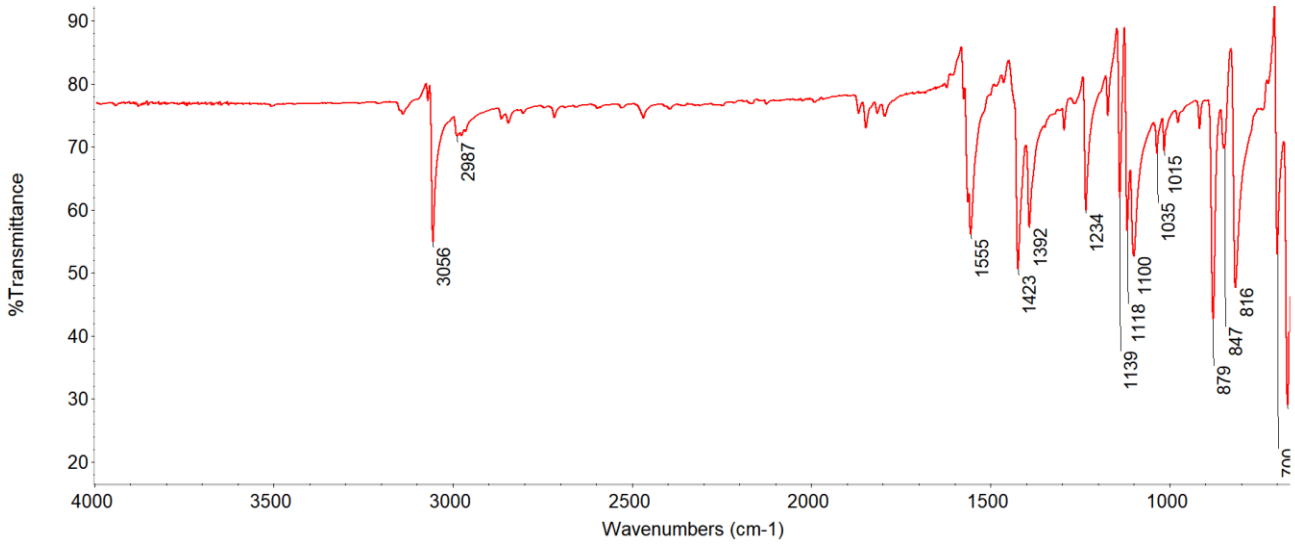

Figure (3.2.3): IR spectrum of 3,5-dichloropyridine-ICl

XRD measurements for 3,5-dichloropyridine -ICl

Crystal Structure of 3,5-dichloropyridine-ICl

Crystallographic data for 3,5-dichloropyridine are given in Table (3.3), and selected bond lengths and angles in Table (3.4). A Thermal ellipsoid plot of the structure together with the numbering scheme used is given in Figure (3.2.4).

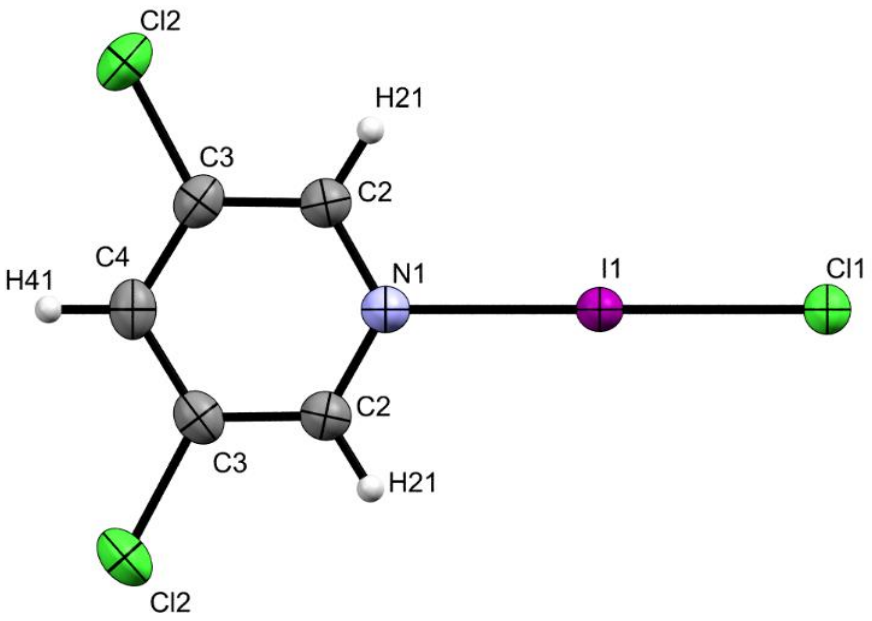

Figure (3.2.4): Thermal ellipsoid plot of 3,5-dichloropyridine-ICl.

3,5-dichloropyridine-ICl crystallises in the orthorhombic space group Cmcm. The molecule possesses exact mm crystallographic symmetry. One mirror plane contains Cl1, I1, N1, C4 and H41, whilst the mirror plane which is perpendicular to it comprises in addition to these atoms C2, C3, Cl2 and H21. Due to the presence of the two mirror planes at right angles to each other, there is only $^{1}/_{4}$ of a molecule in the asymmetric unit, Figure (3.2.5).

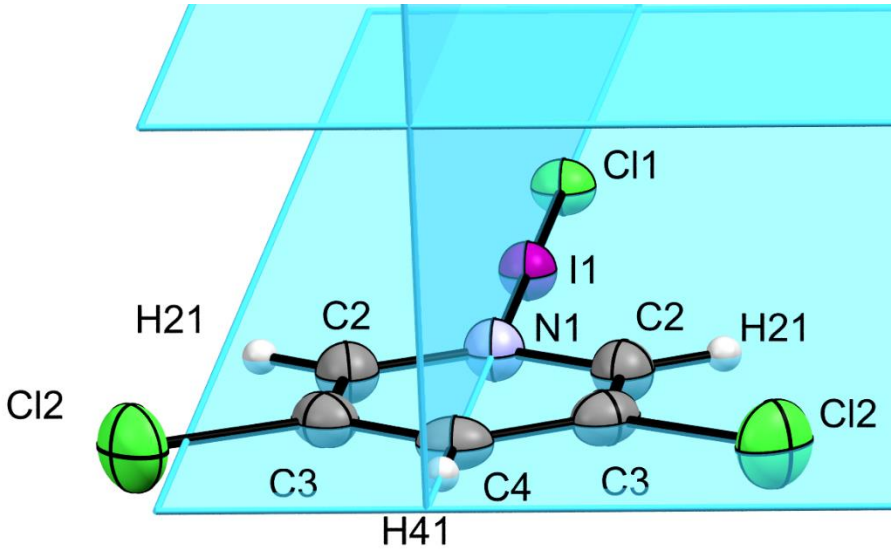

Figure (3.2.5): Thermal ellipsoid plot of 3,5-dichloropyridine-ICl showing relationship to crystallographic mirror plane possessed by the complex.

Table (3.3) Crystallographic data for 3,5-dichloropyridine -ICl complex.

Crystal data	
Chemical formula	$C_5H_3Cl_3IN$
M_r	310.35
Crystal system, space group	Orthorhombic, Cmcm
T/K	123
a, b, c/ (Å)	6.6920 (3), 14.8401 (6), 9.1150 (4)
V/ ($Å^3$)	905.21 (7)
Z	4
Radiation type	Mo Kα
μ/ (mm^{-1})	4.35
Crystal size/ (mm)	0.30 × 0.22 × 0.15
Data collection	
Diffractometer	Bruker Kappa Apex3
Absorption correction	Multi-scan SADABS (Siemens, 1996)
T_{min}, T_{max}	0.38, 0.51
No. of measured, independent and observed [$I > 2.0\sigma(I)$] reflections	18747, 989, 773
R_{int}	0.028
$(\sin \theta/\lambda)_{max}$ /($Å^{-1}$)	0.786
Refinement	
$R[F^2 > 2\sigma(F^2)]$, $wR(F^2)$, S	0.018, 0.046, 1.11
No. of reflections	803

No. of parameters	39
No. of restraints	6
H-atom treatment	H-atom parameters constrained
$\Delta\rho_{max}$, $\Delta\rho_{min}$ (e Å^{-3})	0.74, −0.79

Table (3.4): Selected interatomic contacts/ Å and /^{o} for the complex 3,5-dichloropyridine–ICl.

Atom1	Atom2	Length	Atom1	Atom2	Atom3	Angle
I1	Cl1	2.4872(9)	Cl1	I1	N1	180
I1	N1	2.341(3)	I1	N1	C2	119.4(2)
N1	C2	1.336(3)	I1	N1	C2	119.4(2)
N1	C2	1.336(3)	C2	N1	C2	121.1(4)
C2	C3	1.386(4)	N1	C2	C3	120.1(3)
C3	C4	1.384(4)	C2	C3	C4	120.8(3)
C3	Cl2	1.729(3)	C2	C3	Cl2	118.7(2)
C4	C3	1.384(4)	C4	C3	Cl2	120.5(2)
C2	C3	1.386(4)	C3	C4	C3	117.1(4)
C3	Cl2	1.729(3)	N1	C2	C3	120.1(3)
			C4	C3	C2	120.8(3)
			C4	C3	Cl2	120.5(2)
			C2	C3	Cl2	118.7(2)

3,5-dichloropyridine and ICl are connected via halogen bond between N atom of the pyridine ring and I atom of ICl. The distance of N···I interaction is 2.342 Å, which is less than the sum of van der Waals radii for N and I (3.51 Å).[121] The second indication of halogen bond is the distance between I and Cl (2.487 Å) which is elongated compared to the bond distance of ICl in the gas phase (2.3210 Å).[27] The 3,5-dichloropyridine-ICl molecular complex forms a chain running parallel with c-axis, Figure (3.2.6). These chains are connected by C-H···Cl hydrogen bonds, where chlorine from I-Cl moiety acts as a bifurcated acceptor. The distance between H and Cl atom in C-H···Cl hydrogen bond is 2.695 Å, which is shorter than the sum

of van der Waals radii of H and Cl (2.96 Å),[121] and the C-H···Cl angle is 165.4(2)°. Moreover, the $R_2^2(10)$ graph set motif can be assigned to this hydrogen bond, Figure (3.2.7). Because a chlorine atom is larger than a fluorine atom and due to the lack of the equivalent of the C-H···F hydrogen bonds between the layers of chains on the side of the pyridine ring opposite to the N···I-Cl XB, the complexes are linked by C-H···Cl hydrogen bonds that are within the same plane, (Figures (3.2.8), (3.2.9)). This is the opposite to the 3,5-difluoropyridine-ICl, where both types of hydrogen bonds linked the complexes in different planes. The lack of the equivavlent of C-H···F hydrogen bonds could also be observed by the increase in distance between the centroids of two adjacent pyridine rings within the plane (8.143 Å), which is significantly longer than the corresponding one in the 3,5-difluoropyridine-ICl (6.751 Å), while the distance between two centroids of complexes linked via C-H···Cl is similar, 9.451 Å and 9.287 Å, respectively. (Figures 3.1.9, 3.1.10, 3.2.9) The distance between two planes in 3,5-dichloropyridine-ICl is 3.346 Å, the distance between two centroids of the adjacent 3,5-dichloropyridine molecules between the planes is 5.694 Å (Figure (3.2.9)).

Also, it is observed that the distance of H···Cl interaction (2.789 Å) in the 3,5-difluoropyridine-ICl complex is longer than the distance of H···Cl (2.695 Å) in 3,5-dichloropyridine-ICl. This is supported by shorter elongation of I-Cl bond in 3,5-difluoropyridine-ICl (2.470 Å) than in 3,5-dichloropyridine-ICl (2.487 Å). The effect can be explained by a more charge transfer in the dichloropyridine complex leading to a greater negative charge on the chlorine, which leads to a stronger hydrogen bond. Additionally, only one type of hydrogen bonds present in dichloropyridine complex indicates that the electron density of the organic molecule is not split between two interactions, rather than just one.

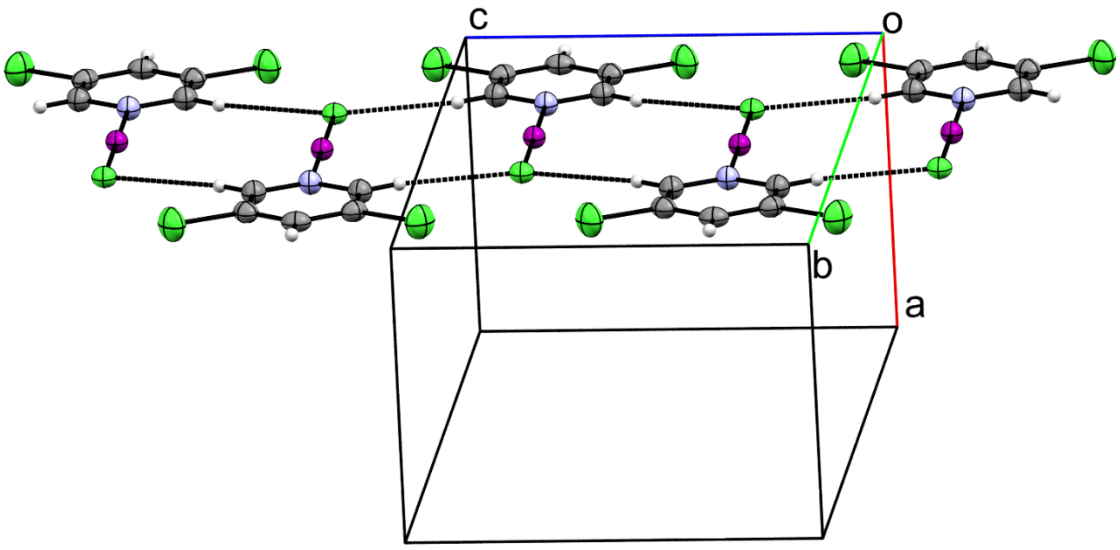

Figure (3.2.6): Packing diagram of 3,5-dichloropyridine -ICl

viewed parallel to the c-axis.

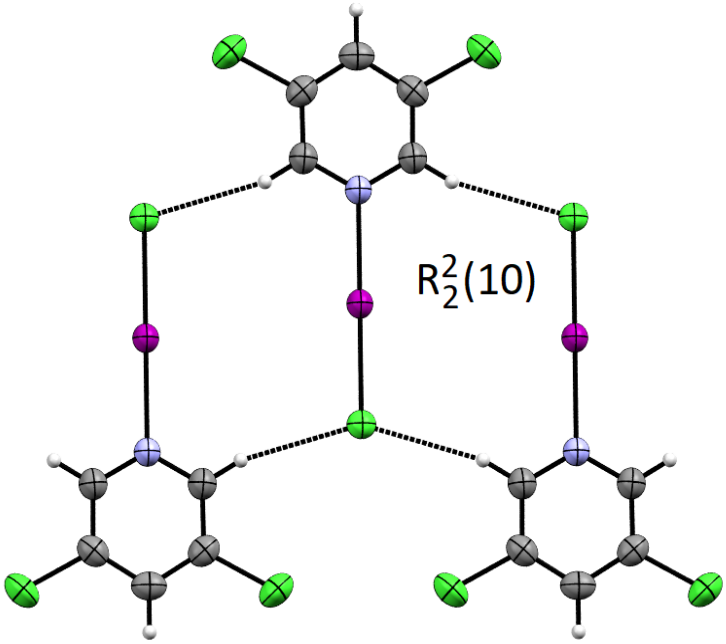

Figure (3.2.7): Thermal ellipsoid plot of 3,5-dichloropyridine-ICl showing

the graph set motif of the C-H···Cl hydrogen bond

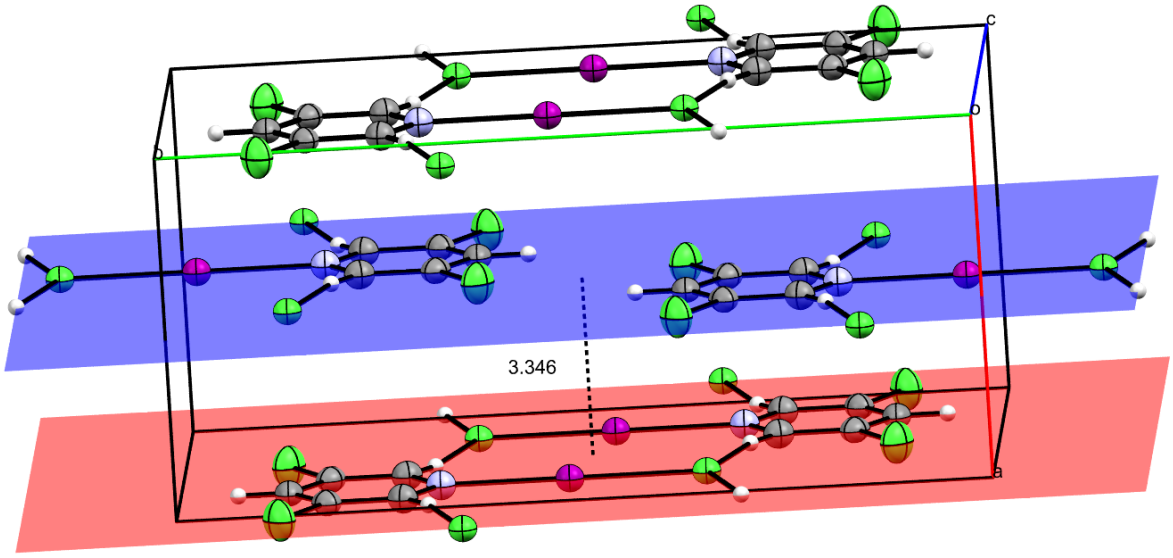

Figure (3.2.8): Stacking of two adjacent planes containing 3,5-dichloropyridine –ICl complexes.

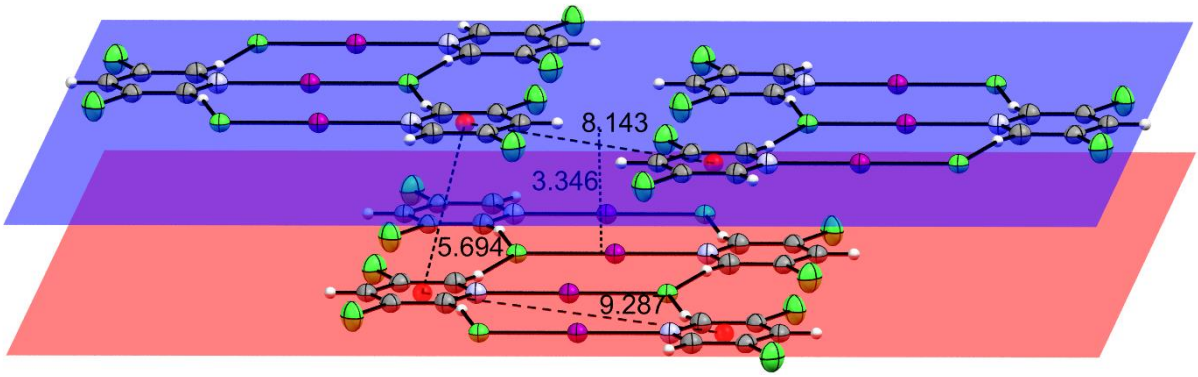

Figure (3.2.9): Stacking of two adjacent planes containing 3,5-dichloropyridine –ICl complexes.

3.3.3 2,6-dichloropyridine- ICl

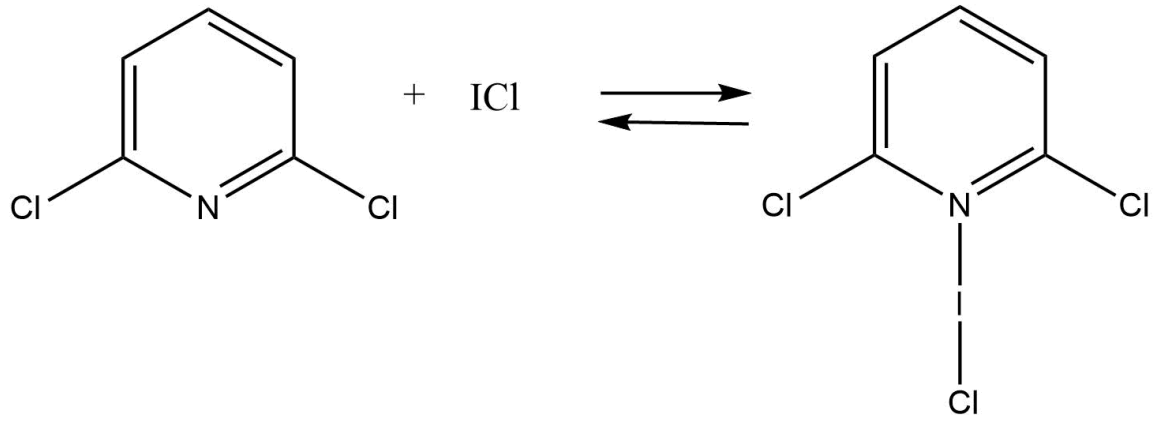

Crystal Structure of 2,6-dichloropyridine

Unfortunately, the crystals obtained are not of the halogen bonded complex but rather that of the starting material 2,6-dichloropyridine. ATR-FTIR spectrum is given in Figure 3.3.1 and crystallographic data for 2,6-dichloropyridine in Table (3.5), and selected bond lengths and angles in Table (3.6). A thermal ellipsoid plot of the structure together with the numbering scheme used is given in Figure (3.3.2)

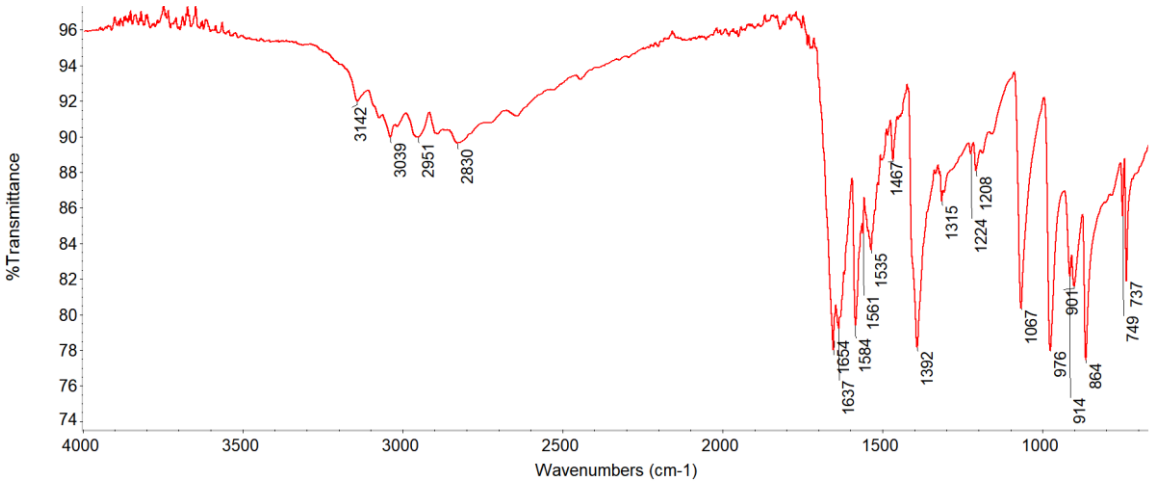

Figure (3.3.1) ATR-FTIR spectrum of 2,6-dichloropyridine

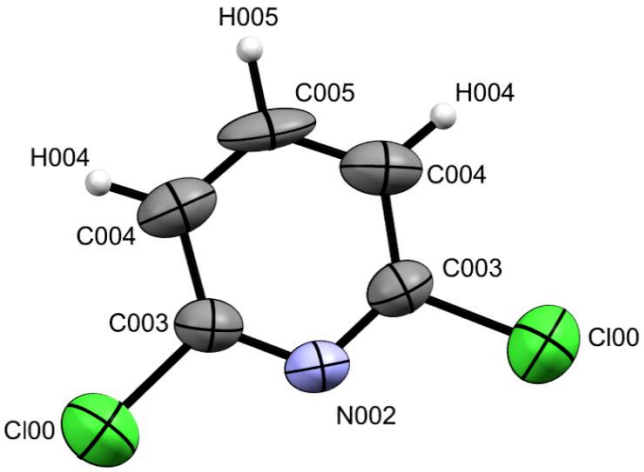

Figure (3.3.2): Thermal ellipsoid plot of 2,6-dichloropyridine.

2,6-dichloropyridine crystallises in the monoclinic space group $P2_1/m$ with Z=2. The molecule thus possesses exact crystallographic mirror symmetry with atoms N1, C4 and H41 lying in mirror plane Figure (3.3.3). The individual bond lengths agree well with the values reported in the Cambridge Crystallographic Database.[123-127]

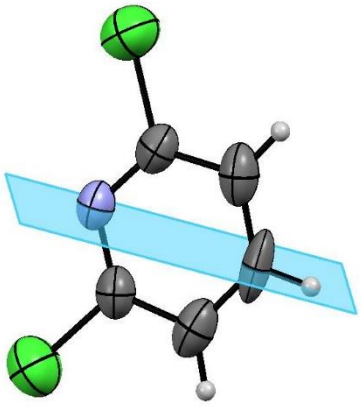

Figure (3.3.3): Thermal ellipsoid plot of 2,6-dichloropyridine showing relationship to crystallographic mirror plane possessed by molecule.

Table (3.5) Crystallographic data for 2,6-dichloropyridine.

Crystal data	
Chemical formula	($C_5H_3Cl_2N$)
M_r	495.76
Crystal system, space group	Monoclinic, $P2_1/m$
T/K	298
a, b, c (Å)	3.870 (3), 14.845 (11), 5.441 (4)
β (°)	97.49 (3)
V/ ($Å^3$)	309.9 (4)
Z	2
Radiation type	Mo Kα
μ /(mm^{-1})	3.59
Crystal size /(mm)	× ×
Data collection	
Diffractometer	Bruker Kappa Apex3
Absorption correction	–
No. of measured, independent and observed [$I > 2\sigma(I)$] reflections	844, 320, 231
R_{int}	0.062
θ_{max} /(°)	20.9

$(\sin \theta/\lambda)_{max}$ /($Å^{-1}$)	0.502
Refinement	
$R[F^2 > 2\sigma(F^2)]$, $wR(F^2)$, S	0.063, 0.156, 1.11
No. of reflections	320
No. of parameters	40
H-atom treatment	H-atom parameters constrained
$\Delta\rho_{max}$, $\Delta\rho_{min}$ (e $Å^{-3}$)	0.25, −0.28

Table (3.6): Selected interatomic contacts/ Å and /^{o} for the complex 2,6-dichloropyridine

Atom1	Atom2	Length	Atom1	Atom2	Atom3	Angle
Cl1	C1	1.738 (6)	C2	N1	C2	115.4(2)
N1	C2	1.323(7)	N1	C2	C3	125.3(1)
C2	C3	1.382(9)	C2	C3	C4	116.8(1)
C3	C4	1.383(7)	C3	C4	C3	120.0(1)
			Cl1	C2	N1	115.0(1)
			Cl1	C2	C3	119.7(1)

Of the 2,6-dihalo- substituted pyridines only that of 2,6-difluoropyridine has been reported.[123] The ipso angle N1-C2-C3 angle 125.3°) is slightly smaller to the average seen than in the case of the difluoro- compound (126°), which is presumably the result of the greater electronegativity of fluorine.[124] The observed ipso C2-N1-C2 angle 115.4° is identical to that

seen compared in the fluoro compound,115.4(7)°. Both of these angles at N do not differ significantly from that observed in pyridine itself 116.5°.[125]

In the structure of 2,6-dichloropyridine, two different intermolecular interactions appear to be present. In the first of these, there are C-H···N hydrogen bonds, with C-N Å and C-H···N 172.8° which are aligned in the 101 direction to form linear chains, Figure (3.3.4).

The main reason for obtaining starting material 2,6-dichloropyridine instead of the halogen bond complex could be due to the starting material 2,6-dichloropyridine containing two chlorine groups which cause an effect from two sides:

Firstly, the two chlorine atoms that are moderately good electron-withdrawing groups thus act to decrease the electron density on N atom for pyridine ring. Secondly, the position of these two groups (ortho- position) acts to prevent ICl from attacking the N atom of the pyridine ring by the steric hindrance.

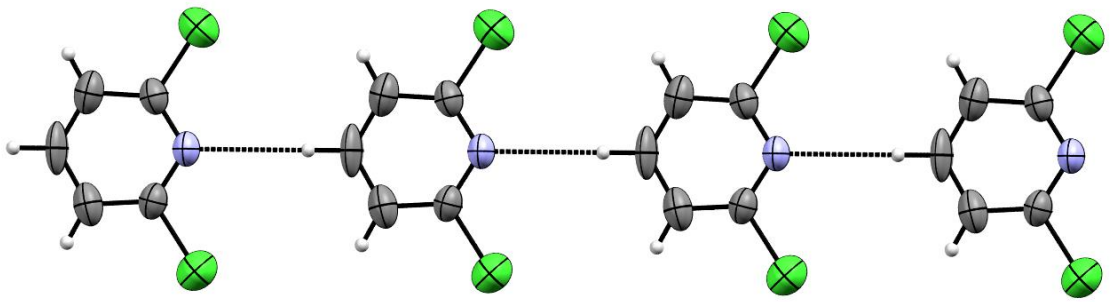

Figure (3.3.4) View normal to the chain direction

The other interactions are Cl···Cl halogen bonds 3.362 Å which are approximately in the 121 direction, Figure (3.3.5). These are type I halogen bonds[125] as the difference between the 2 the C-Cl···Cl angle in the bond is 0° which is less than 15° and thus defines a type I interaction.

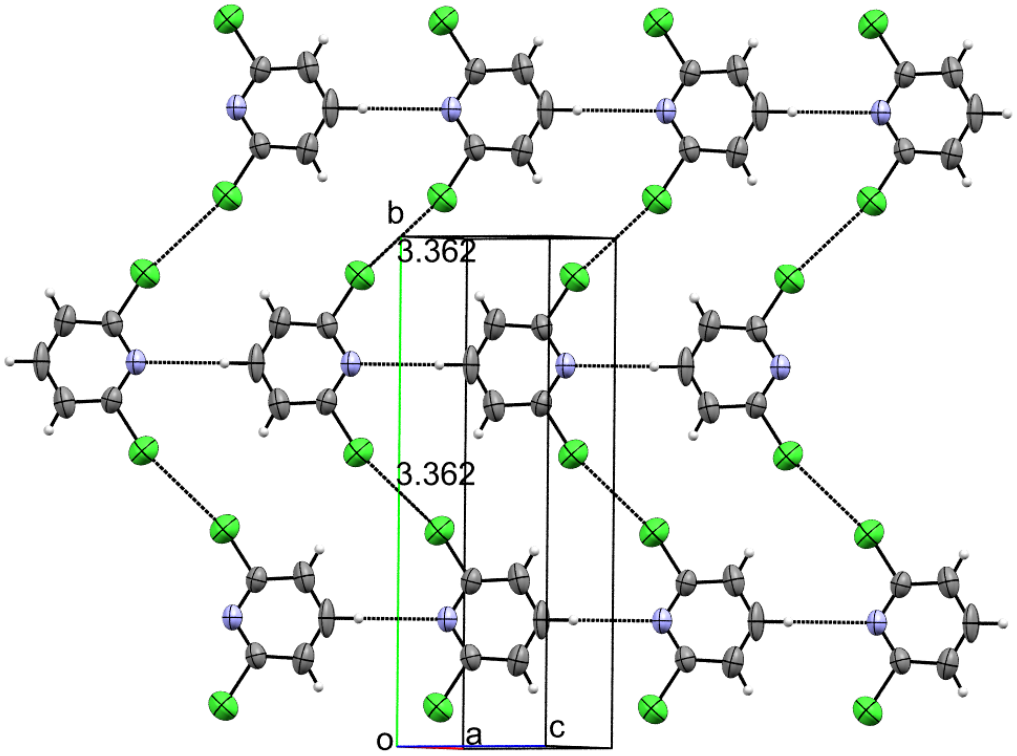

Figure (3.3.5) interactions are Cl···Cl halogen bonds which are approximately in the 121 direction.

The overall effect of these interactions is to produce layers in approximately the 101 plane, Figure (3.3.6)

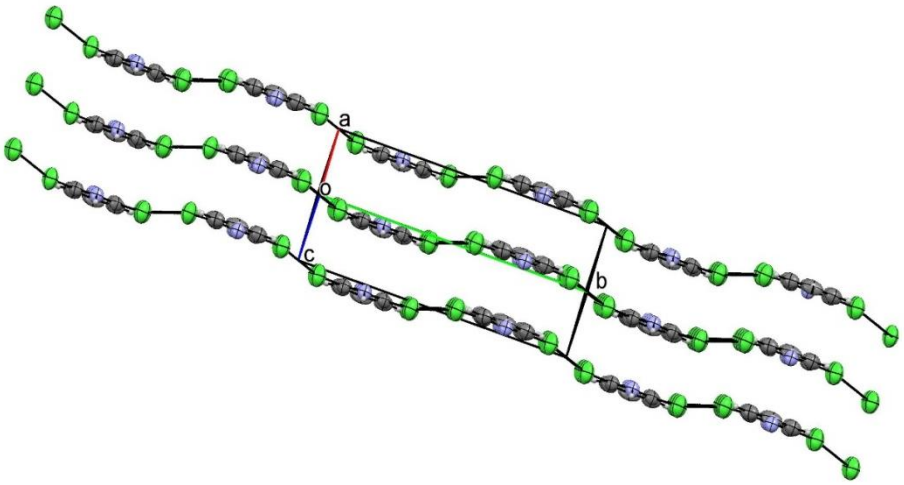

Figure (3.3.6) layers in approximately the 101 plane.

The closest distance of approach between an atom and that of atom in the layer above is typically 3.4-3.41 Å, Figure (3.3.6) whilst the centroid to centroid distance is 3.870 Å, Figure 3.3.7

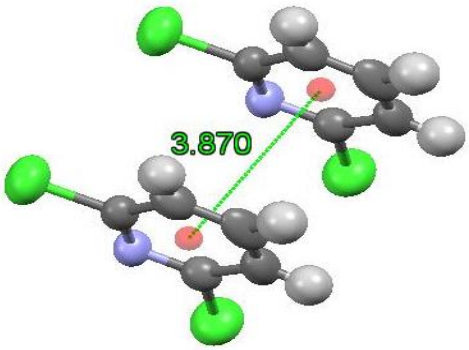

Figure (3.3.7) View showing the distance between the centroids

of two 2,6- dichloropyridine –ICl molecules

3.3.4 2,6-dimethoxypyridine- ICl

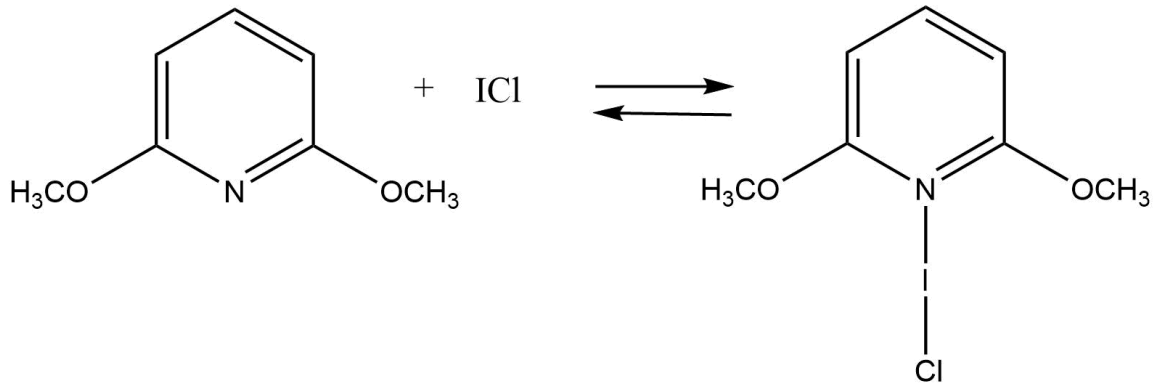

UV-Visible spectra of the 2,6-dimethoxypyridine-ICl solution

All the spectra were collected using methanol as the solvent, the concentration of the samples was 10^{-3} M. The base 2,6-dimethoxypyridine absorbed at 316 nm and iodine monochloride ICl at 341 nm. A new band appeared at 446 nm when the two above starting materials were mixed which cannot be attributed to the 2,6-dimethoxypyridine or ICl. That means λ_{max} for 2,6-dimethoxypyridine is shifted 130 nm toward higher wavelengths. Figure (3.4.1) Starting material and the resulting complex are also characterised by ATR-FTIR, Figures (3.4.2, 3.4.3).

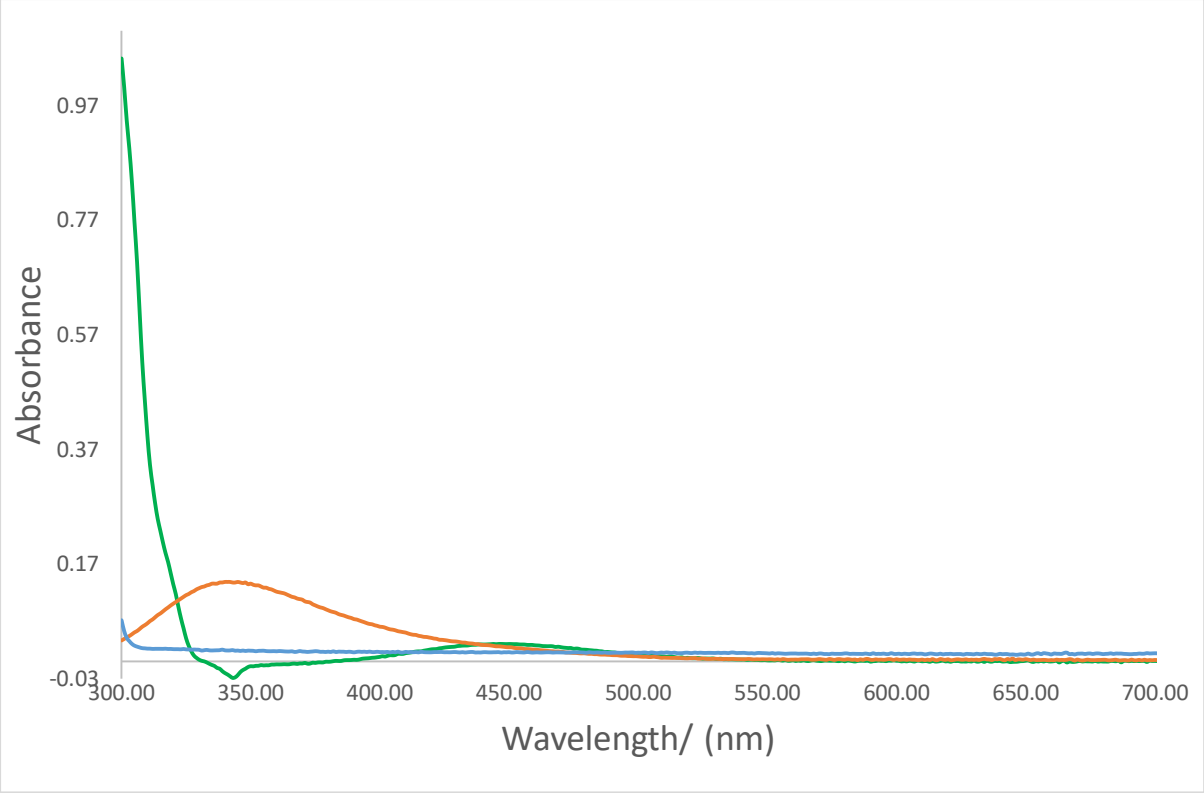

Figure (3.4.1): UV-Visible spectra of 2,6-dimethoxypyridine –ICl system: 2,6-dimethoxypyridine (Blue), ICl (Orange), 2,6-dimethoxypyridinium- ICl_2^- (Green),the spectra were collected using methanol as the solvent, the concentration of the samples was 10^{-3} M.

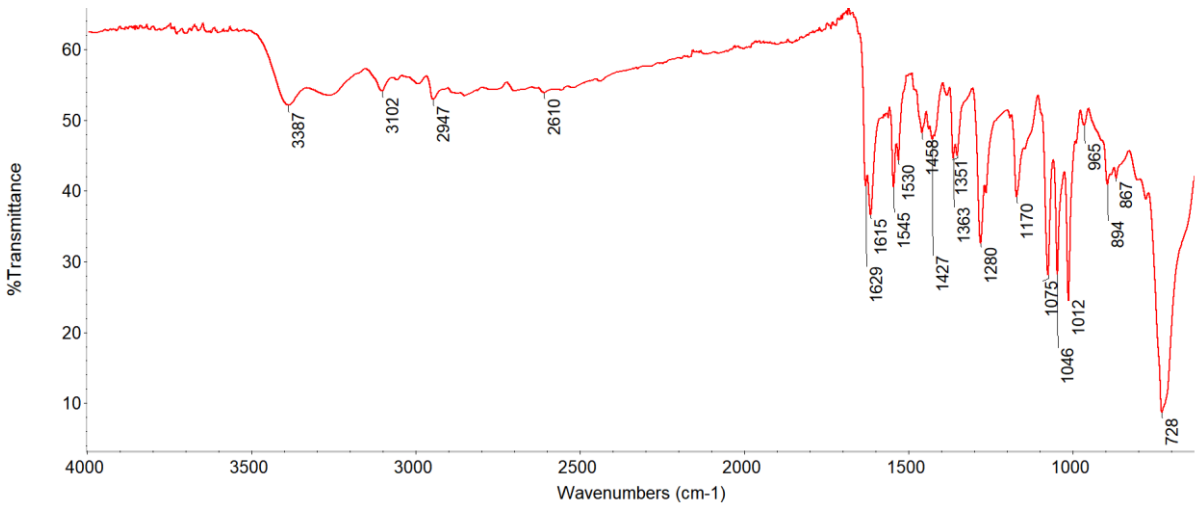

Figure (3.4.2): ATR-FTIR spectrum of 2,6-dimethoxypyridine

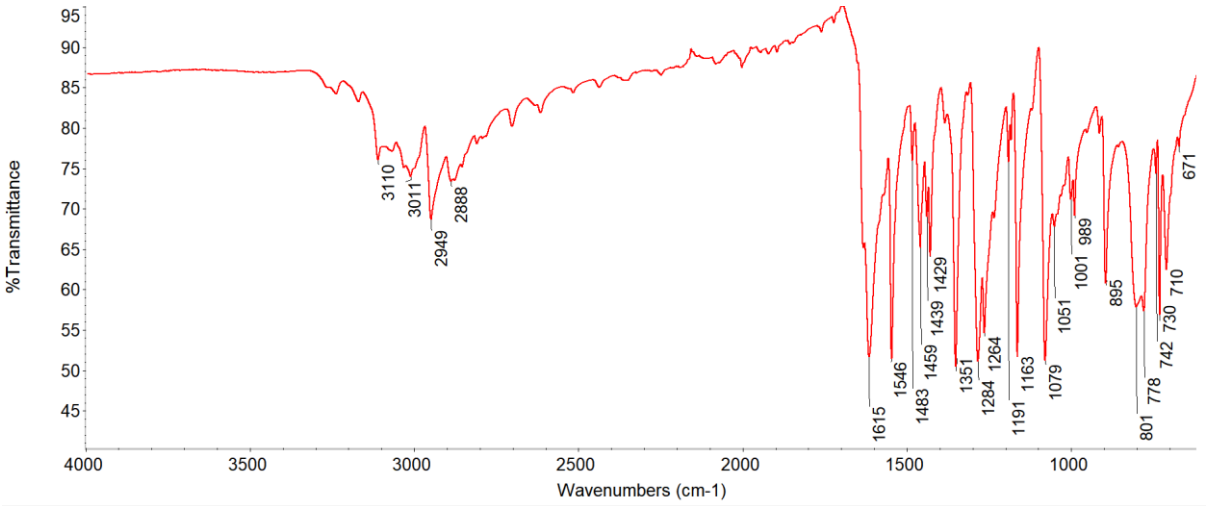

Figure (3.4.3): ATR-FTIR spectrum of 2,6-dimethoxypyridinium- ICl_2^-

XRD measurements for 2,6-dimethoxypyridinium - ICl_2^-

Crystal Structure of 2,6-dimethoxypyridinium- ICl_2^-

Instead of the expected 2,6-dimethoxypyridine-ICl complex linked via the Cl-I···N halogen bond, the 2,6-dimethoxypyridinium- ICl_2^- complex is observed. Crystallographic data for 2,6-dimethoxypyridinium- ICl_2^- are given in Table (3.7), and selected bond lengths and angles in Table (3.8) A Thermal ellipsoid plot of the structure together with the numbering scheme used is given in Figure (3.4.4)

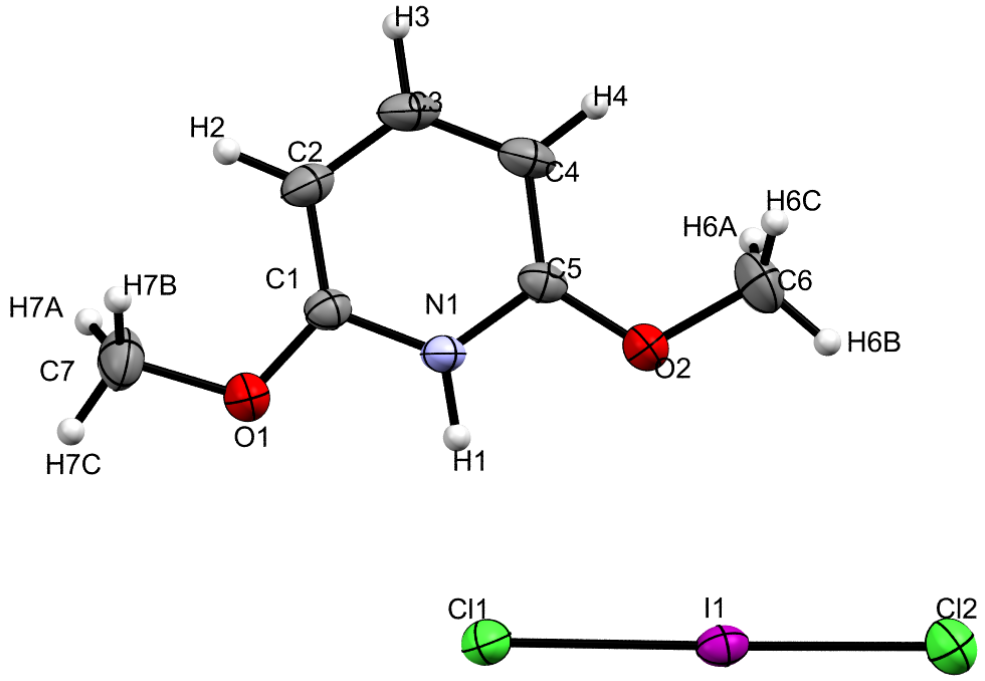

Figure (3.4.4): Thermal ellipsoid plot of 2,6-dimethoxypyridinium – ICl_2^-

2,6-dimethoxypyridinium- ICl_2^- crystallises in the monoclinic space group $P2_1/n$. The structure unlike many of the other compounds studied possesses no exact crystallographic symmetry, and thus the asymmetric unit comprises of just a pyridinium cation and ICl_2^- anion with a hydrogen bond between the pyridine ring and the ICl_2^-. The distance between the centroids of pyridine rings of two adjacent molecules of 2,6-dimethoxypyridinium is 5.942 Å, Figures (3.4.5,3.4.6).

Table (3.7): Crystallographic data for 2,6-dimethoxypyridinium – ICl_2^- complex.

Crystal data	
Chemical formula	$Cl_2I \cdot C_7H_{10}NO_2$
M_r	337.96
Crystal system, space group	Monoclinic, $P2_1/n$
T/K	190
a, b, c (Å)	7.2986 (3), 12.6919 (6), 12.6654 (6)
β (°)	102.413 (2)
V/ ($Å^3$)	1145.81 (9)
Z	4
Radiation type	Mo Kα
μ / (mm^{-1})	3.23
Crystal size / (mm)	0.29 × 0.23 × 0.19
Data collection	
Diffractometer	Bruker APEX-II CCD
Absorption correction	Multi-scan
T_{min}, T_{max}	0.643, 0.747
No. of measured, independent and observed [$I > 2\sigma(I)$] reflections	23883, 5626, 4529

R_{int}	0.029
$(\sin \theta/\lambda)_{max}$ /($Å^{-1}$)	0.838
Refinement	
$R[F^2 > 2\sigma(F^2)]$, $wR(F^2)$, S	0.028, 0.055, 1.08
No. of reflections	5626
No. of parameters	123
No. of restraints	1
H-atom treatment	H atoms treated by a mixture of independent and constrained refinement
$\Delta\rho_{max}$, $\Delta\rho_{min}$ (e $Å^{-3}$)	0.74, −0.91

Table (3.8): Selected interatomic contacts/ Å and /^{o} for the complex 2,6-dimethoxypyridinium –ICl_2^-.

Atom1	Atom2	Length	Atom1	Atom2	Atom3	Angle
I1	Cl1	2.6041(5)	Cl1	I1	Cl2	178.99(2)
I1	Cl2	2.5176(5)	C1	O1	C7	117.2(1)
O1	C1	1.325(2)	C5	O2	C6	117.7(1)
O1	C7	1.440(2)	C1	N1	C5	123.4(1)
O2	C5	1.318(2)	O1	C1	N1	112.0(1)
O2	C6	1.443(2)	O1	C1	C2	128.5(1)
N1	C1	1.344(2)	N1	C1	C2	119.5(1)
N1	C5	1.350(2)	C1	C2	C3	117.5(2)
C1	C2	1.380(2)	H2	C2	C3	121.3
C2	C3	1.387(3)	C2	C3	C4	122.7(2)
C3	C4	1.376(3)	H3	C3	C4	118.7
C4	C5	1.383(2)	C3	C4	C5	117.7(2)
			H4	C4	C5	121.2
			O2	C5	N1	111.8(1)
			O2	C5	C4	128.9(1)
			N1	C5	C4	119.2(1)

Instead of a complex linked by a Cl-I···N halogen bond, this system crystallised as an ionic complex 2,6-dimethoxypyridinium- ICl_2^- linked through the N-H···Cl hydrogen bond. The formation of polyhalogen ions is discussed below. Based on mechanisms described in section (3.4 Discussion) that suggest the formation of polyhalogen ions occurs due to the hydrolysis,

it can be observed that hydrogen ions are formed as a byproduct of that reaction. These hydrogen ions can further protonate the nitrogen atom of the pyridine ring, thus enabling the formation of the crystalline halogen-bonded complex by balancing the charge in the crystal, as well. The distance between the iodine atom and the two chlorine atoms within the ion is different, with the distance between the iodine atom and Cl1 being 2.6041(5) Å and the distance between the iodine atom and Cl2 2.5177(6) Å. The difference in bond lengths is observed because of the N1-H1···Cl1 hydrogen bond, where the N1···Cl1 distance is 3.224(1) Å, and the N1-H1···Cl1 angle is 166.90(2) °. This hydrogen bond causes the elongation of the bond between I1 and Cl1, while the I1-Cl2 bond is shorter because Cl2 is not included in any of the non-covalent interactions.

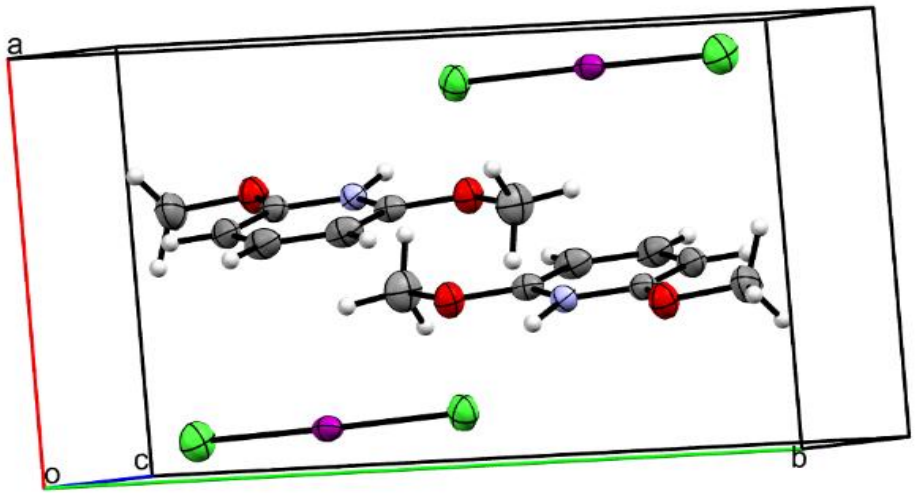

Figure (3.4.5): Stacking of two adjacent molecules of 2,6-dimethoxypyridinium -ICl_2^-.

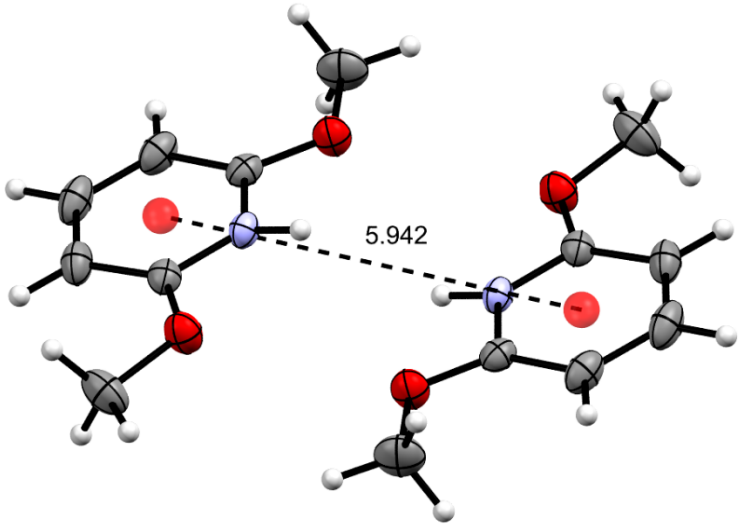

Figure (3.4.6): View showing the distance between the centroids of two of 2,6-dimethoxypyridinium -ICl_2^-.

3.3.5 4-methoxypyridine- ICl

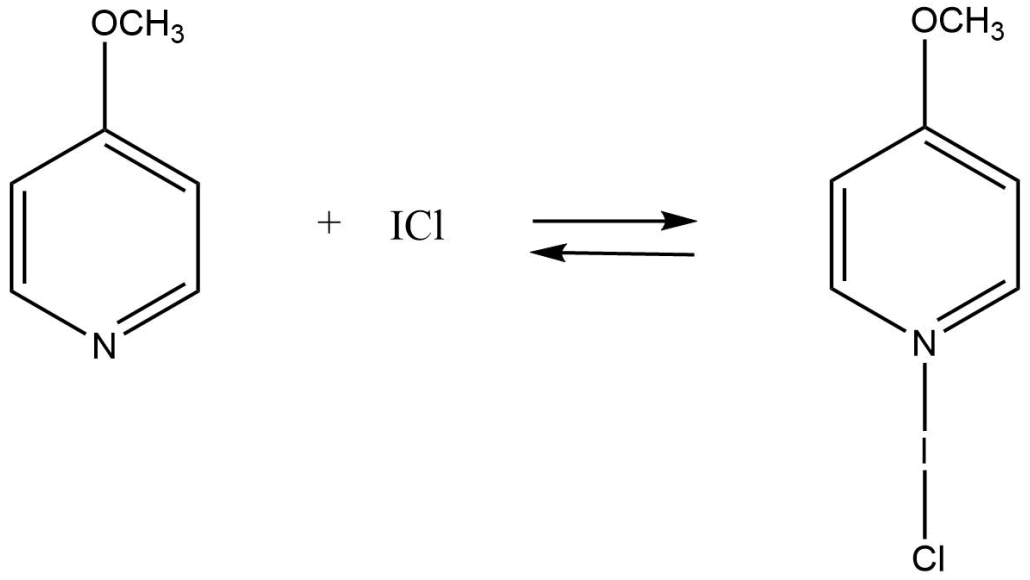

UV-Visible spectra for 4-methoxypyridine-ICl solution

All the spectra were collected using methanol as the solvent, the concentration of the samples was 10^{-3} M. The base 4-methoxypyridine absorbed at 328 nm and iodine monochloride absorbed at 341 nm. A new band appeared at 359 nm when the two above starting materials were mixed which is not attributed to the 4-methoxypyridine or ICl. λ_{max} for 4-methoxypyridine was shifted 31 nm toward higher wavelengths (Figure 3.5.1). Starting material and the resulting complex are also characterised by ATR-FTIR, Figures (3.5.2, 3.5.3).

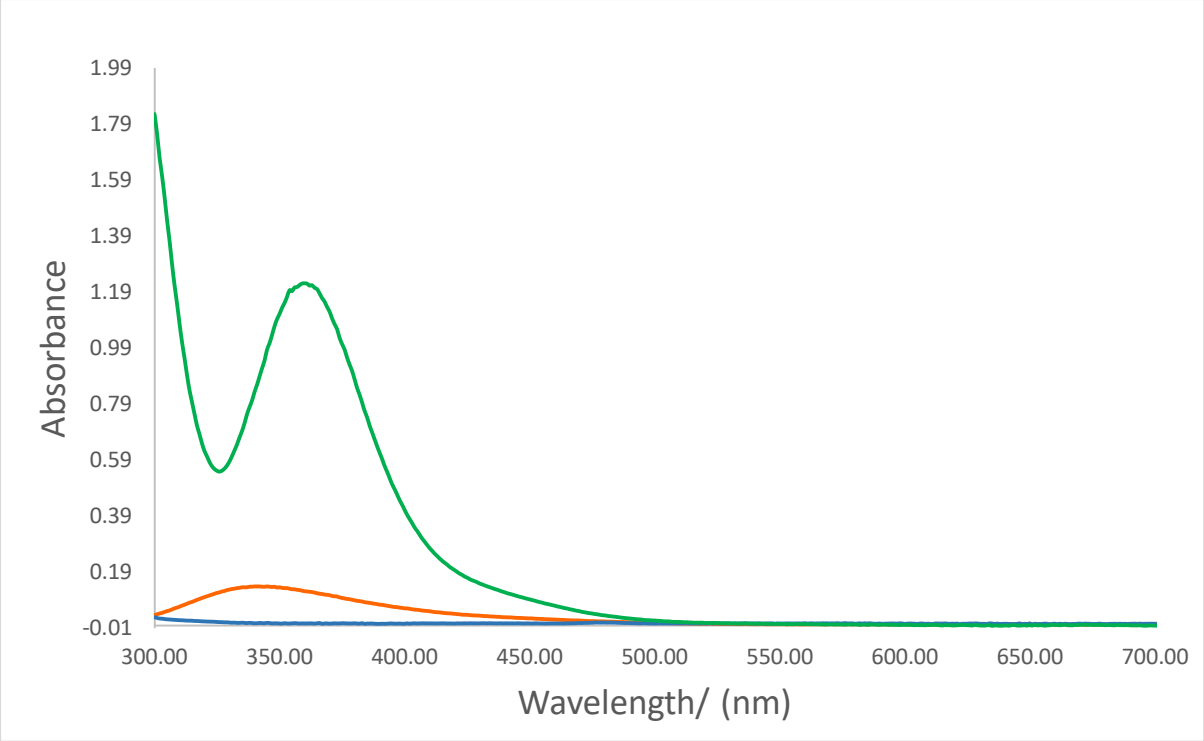

Figure (3.5.1): UV-Visible spectra of 4-methoxypyridine -ICl: 4-methoxypyridine (Blue), ICl (Orange), 4- methoxypyridine -ICl (Green), the spectra were collected using methanol as the solvent, the concentration of the samples was 10^{-3} M.

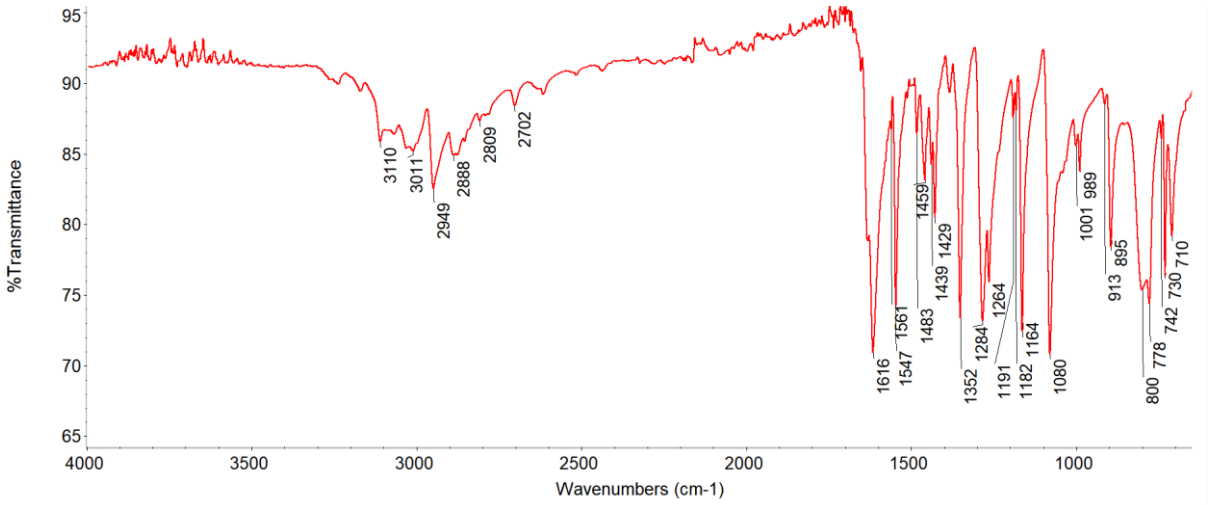

Figure (3.5.2): ATR-FTIR spectrum of 4-methoxypyiridine

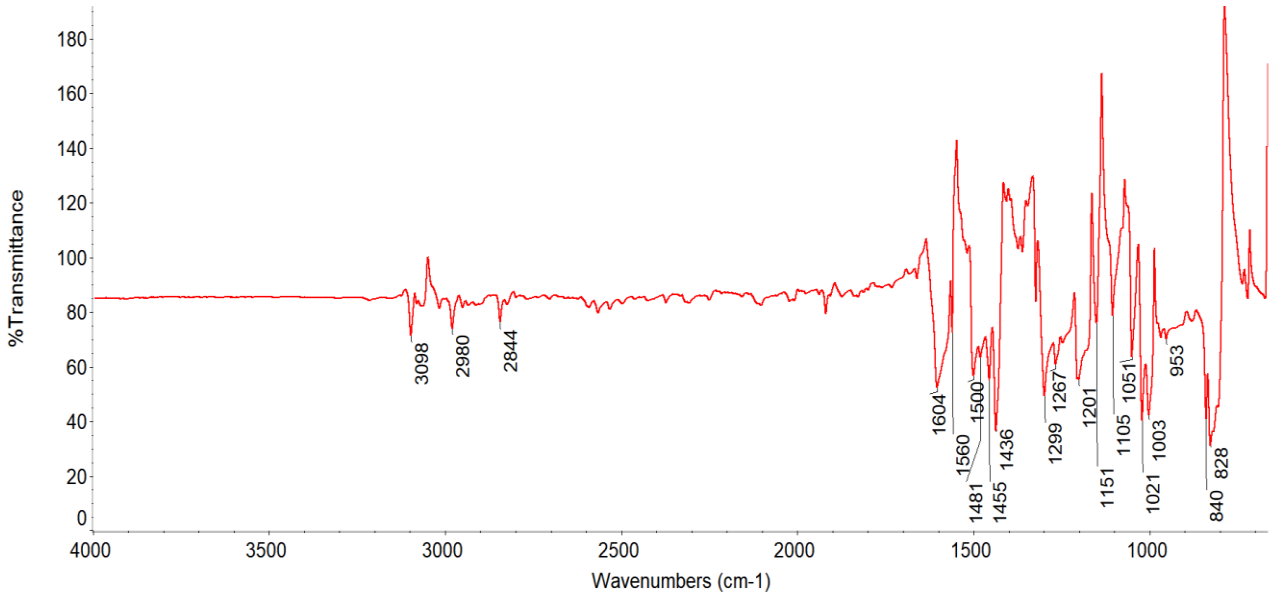

Figure (3.5.3): ATR-FTIR spectrum of 4-methoxypyiridine-ICl

(Spectrum should be collected again prior to further publication of the data)

XRD measurements for 4-methoxypyridine –ICl

Crystal Structure of 4-methoxypyridine-ICl

Crystallographic data for 4-methoxypyridine- ICl are given in Table (3.9), and selected bond lengths and angles in Table (3.10) A Thermal ellipsoid plot of the structure together with the numbering scheme used is given in Figure (3.5.4)

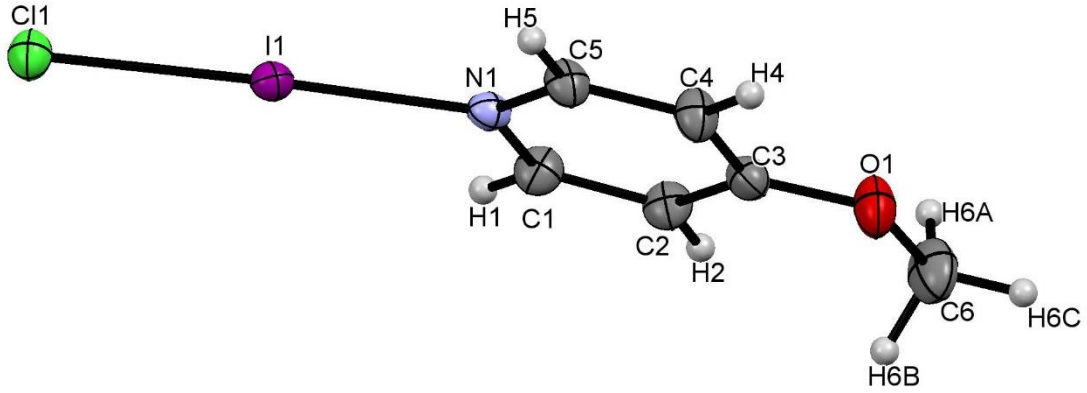

Figure (3.5.4): Thermal ellipsoid plot of 4-methoxypyridine-ICl.

4-methoxypyridine-ICl crystallises in the monoclinic space group $P2_1/n$. The molecular complex possesses no exact crystallographic symmetry. Moreover, the unit cell consists of four complexes (Figure 3.5.5) and the asymmetric unit of one 4-methoxypyridine and one ICl molecule. They are connected through the N atom of the pyridine ring and I atom of the ICl moiety. The selected distances between the following atoms are atoms: N1 and I1 2.272(3) Å, I1 and Cl1 2.528(1) Å, N1 and C1, and C5 are 1.331(4) Å, 1.347(3) Å respectively, and of C3-O, and C6-O was 1.344(4) Å, 1.440(4) Å, respectively.

Measured angles: N-I-Cl was 177.87(7) °, I-N-C1 and I-N-C5 was121.1(2º), 118.0(2) º respectively C3-O-C6 was 118.0(3) °. Table (3.10).

4-methoxypyridine and ICl are connected by Cl–I···N halogen bond. The distance of N···I interaction is 2.272(3) Å, which is shorter than the sum of N and I van der Waals radii (3.51 Å).[121] Moreover, the distance between I and Cl (2.528(1) Å) which is an elongation compared to the ICl bond length in the gas phase (2.3210 Å).[27] Also, I-Cl elongation and the N···I distance in this complex indicate that the halogen bond interaction is the strongest amongst the comparable complexes within this work (3,5-dichloropyridine-ICl, 3,5-difluoropyridine). The central distance between two molecules with 4-methoxy groups facing

in opposite directions in 4.191 Å, while the distance between two adjacent molecules through the inversion centre is 6.551 Å, Figure (3.5.5) The complex units are not interconnected by hydrogen bonds like in the cases of 3,5-difluoro- and 3,5-dichloropyridine-ICl samples. Even though the ether oxygen atom could act as a hydrogen bond acceptor, there are no strongly polarised bonds (N-H, O-H) in the system that are necessary for such interactions. [128] Additionally, the C-H···Cl hydrogen bonds, that linked mentioned complexes in chains, are not observed as well. Since the elongation of the I-Cl bond (2.528 Å) is more significant than in the previously mentioned complexes (2.470 Å and 2.487 Å, respectively), the large amount of electron density is transferred into XB interaction. Therefore, the additional hydrogen bond would require even more electron density redistribution, which could ultimately lead to I-Cl bond cleavage.

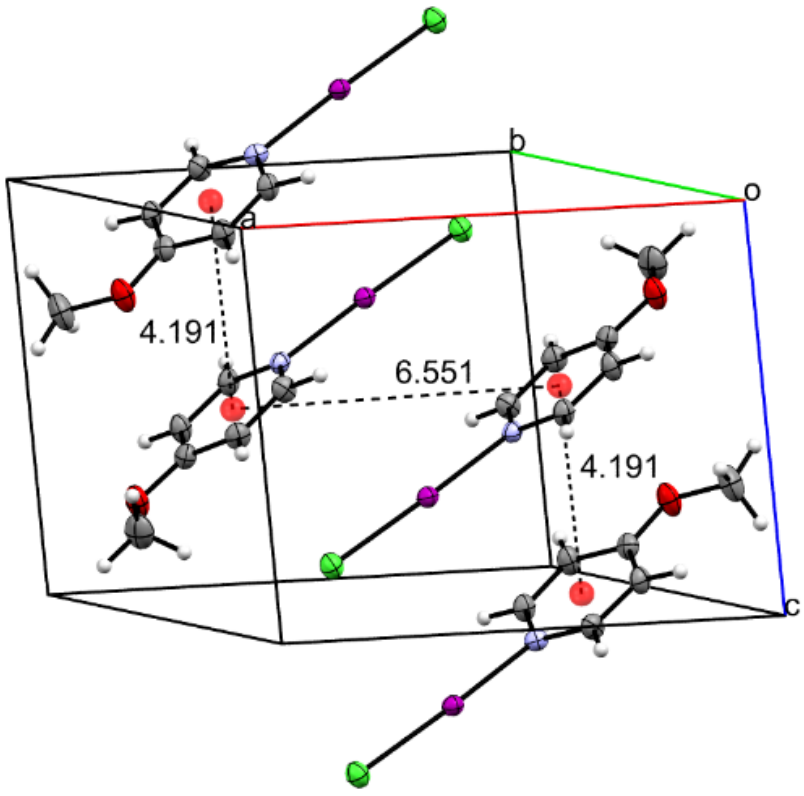

Figure (3.5.5) View showing the distance between the centroids of two 4-methoxypyridine -ICl molecules.

Table (3.9) Crystallographic data for 4-methoxypyridine –ICl.

Crystal data	
Chemical formula	$Cl_2I{\cdot}C_7H_{10}NO_2$
M_r	337.96
Crystal system, space group	Monoclinic, $P2_1/n$
T/K	190
a, *b*, *c* (Å)	7.2986 (3), 12.6919 (6), 12.6654 (6)
β (°)	102.413 (2)
V/ (Å^3)	1145.81 (9)
Z	4
Radiation type	Mo *K*α
μ/ (mm^{-1})	3.23
Crystal size/ (mm)	0.29 × 0.23 × 0.19
Data collection	
Diffractometer	Bruker *APEX*-II CCD
Absorption correction	Multi-scan
T_{min}, T_{max}	0.643, 0.747
No. of measured, independent and observed [$I > 2\sigma(I)$] reflections	23883, 5626, 4529

R_{int}	0.029
$(\sin \theta/\lambda)_{max}$ /(Å^{-1})	0.838
Refinement	
$R[F^2 > 2\sigma(F^2)]$, $wR(F^2)$, S	0.028, 0.055, 1.08
No. of reflections	5626
No. of parameters	123
No. of restraints	1
H-atom treatment	H atoms treated by a mixture of independent and constrained refinement
$\Delta\rho_{max}$, $\Delta\rho_{min}$ (e Å^{-3})	0.74, −0.91

Table (3.10): Selected interatomic contacts/ Å and /^{o} for the complex 4-methoxypyridine -ICl

I1—Cl1	2.5305 (4)	C3—C4	1.3935 (19)
I1—N1	2.2717 (12)	C4—C5	1.3993 (18)
N1—C2	1.3376 (17)	C4—O7	1.3395 (19)
N1—C6	1.3476 (17)	C5—C6	1.371 (2)
C2—C3	1.381 (2)	C8—O7	1.4416 (19)
Cl1—I1—N1	177.76 (3)	C3—C4—C5	118.88 (13)
I1—N1—C2	121.03 (9)	C3—C4—O7	125.05 (12)
I1—N1—C6	119.47 (9)	C5—C4—O7	116.06 (12)
C2—N1—C6	119.00 (13)	C4—C5—C6	118.93 (13)
N1—C2—C3	122.63 (13)	C5—C6—N1	122.16 (12)
C2—C3—C4	118.38 (12)	C8—O7—C4	117.82 (12)

3.3.6 3-fluoropyridine- ICl

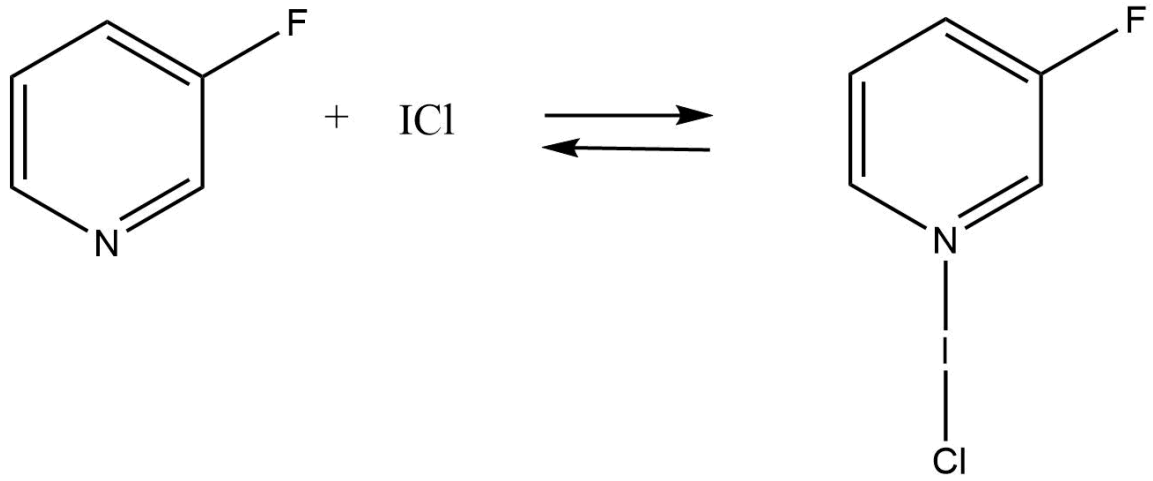

UV-Visible spectra for 3-fluoropyridine- ICl solution

All the spectra were collected using methanol as the solvent, the concentration of the samples was 10^{-3} M. The base 3-fluoropyridine absorbed at 303 nm and iodine monochloride (ICl) absorbed at 341 nm. Two new bands appeared at 358 nm and 444 nm when the above-mentioned starting materials were mixed. These bands are not attributed to the 3-fluoropyridine or ICl. λ_{max} for 3-fluoropyridine is shifted 55 nm and 141 nm, while for ICl. λ_{max} was shifted 17 nm toward higher wavelengths (Figure 3.6.1). Starting material and the resulting complex are also characterised by ATR-FTIR, Figures (3.6.2, 3.6.3).

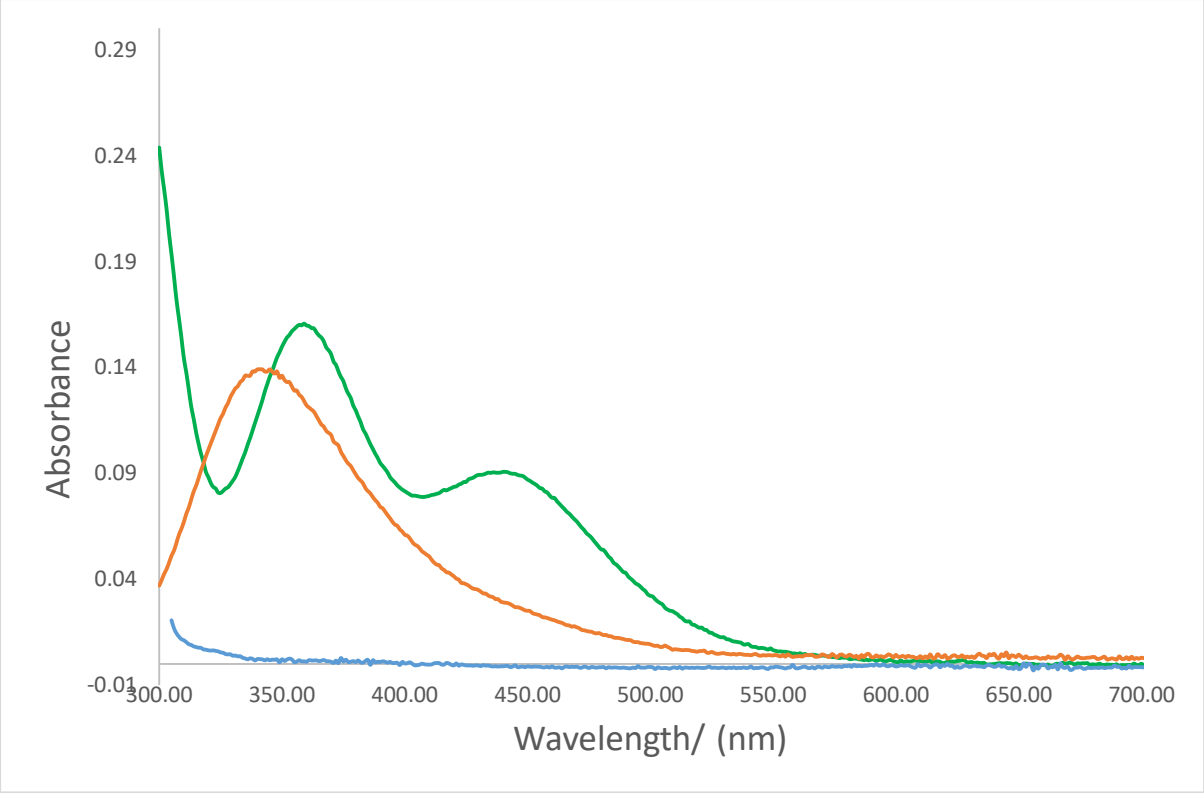

Figure (3.6.1): UV-Visible spectra of 3-fluoropyridine -ICl: 3-fluoropyridine (Blue), ICl (Orange), 3-fluoropyridine -ICl (Green), the spectra were collected using methanol as the solvent, the concentration of the samples was 10^{-3} M.

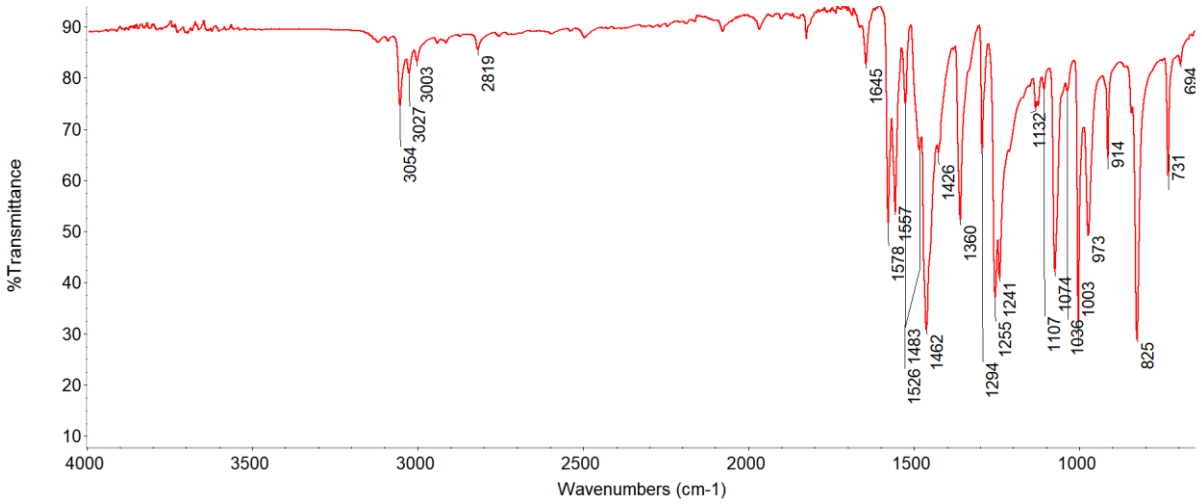

Figure 3.6.2 ATR-FTIR spectrum of 3-fluoropyridine

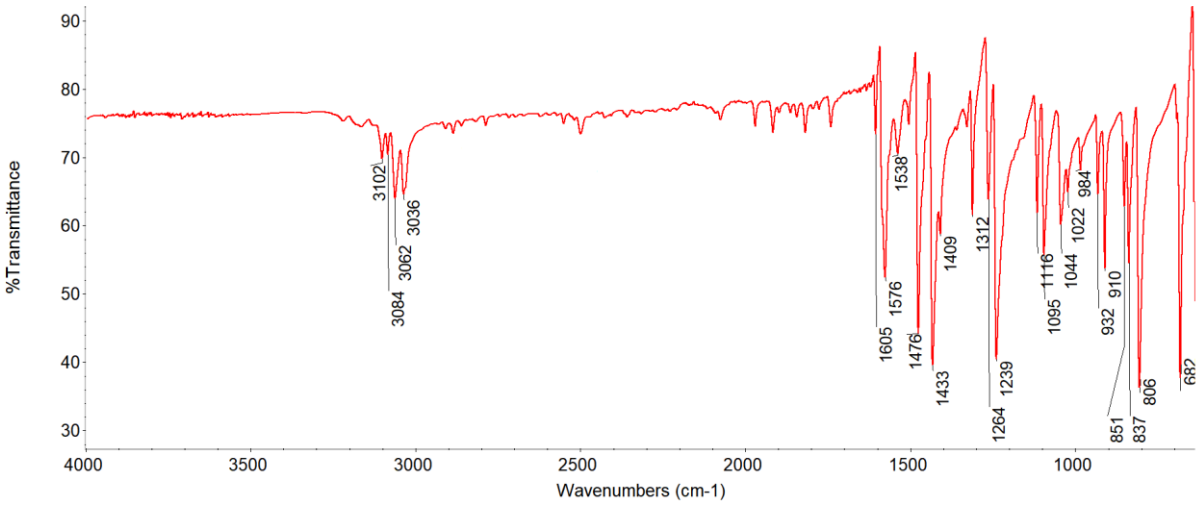

Figure 3.6.3 ATR-FTIR spectrum of 3-fluoropyridine –ICl

3.3.7 2-Fluoro-3-iodopyridine-ICl:

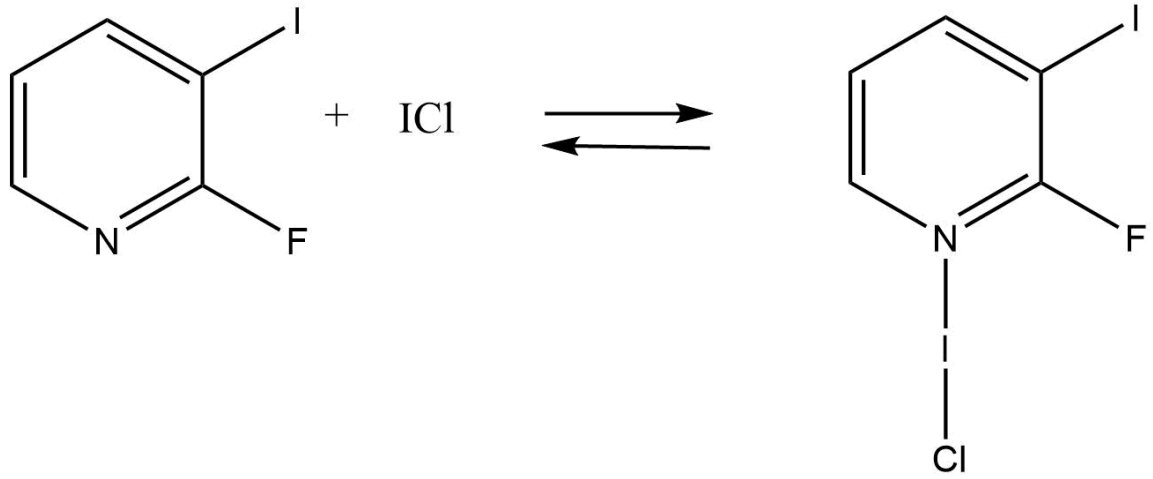

UV-Visible spectra for 2-fluoro-3-iodopyridine ICl solution

All the spectra were collected using methanol as the solvent, the concentration of the samples was 10^{-3} M. The base 2-fluoro-3-iodopyridine displays two main absorption bands at 316 nm and 445 nm, while ICl absorbed at 341 nm. The new band appeared at 450 nm when the above-mentioned starting materials were mixed. That band is not attributed to the 2-fluoro-3-iodopyridine or ICl. λ_{max} for 2-fluoro-3-iodopyridine is shifted 134 nm toward higher wavelengths (Figure 3.7.1). Starting material and the resulting complex are also characterised by ATR-FTIR, Figures (3.7.2, 3.7.3).

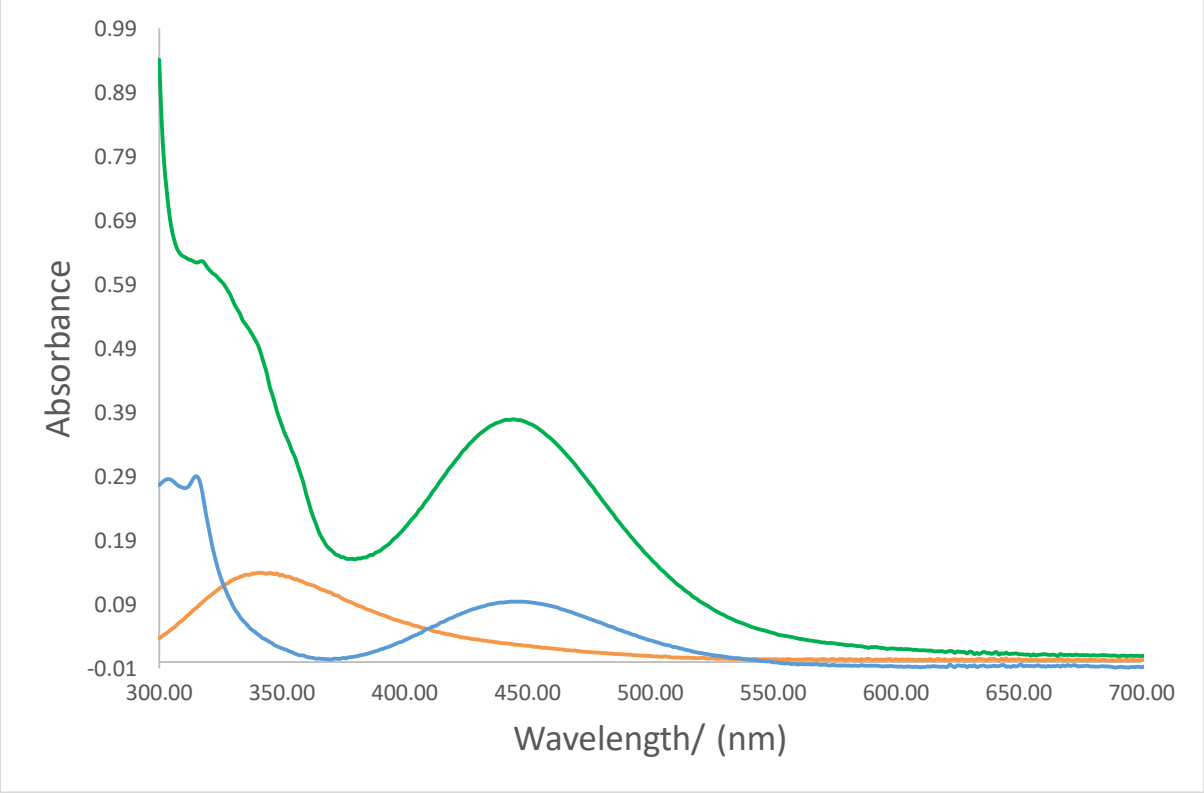

Figure (3.7.1): UV-Visible spectra of 2-fluoro-3-iodopyridine -ICl: 2-fluoro-3-iodopyridine (Blue), ICl (Orange), 2-fluoro-3-iodopyridine –ICl (Green), the spectra were collected using methanol as the solvent, the concentration of the samples was 10^{-3} M.

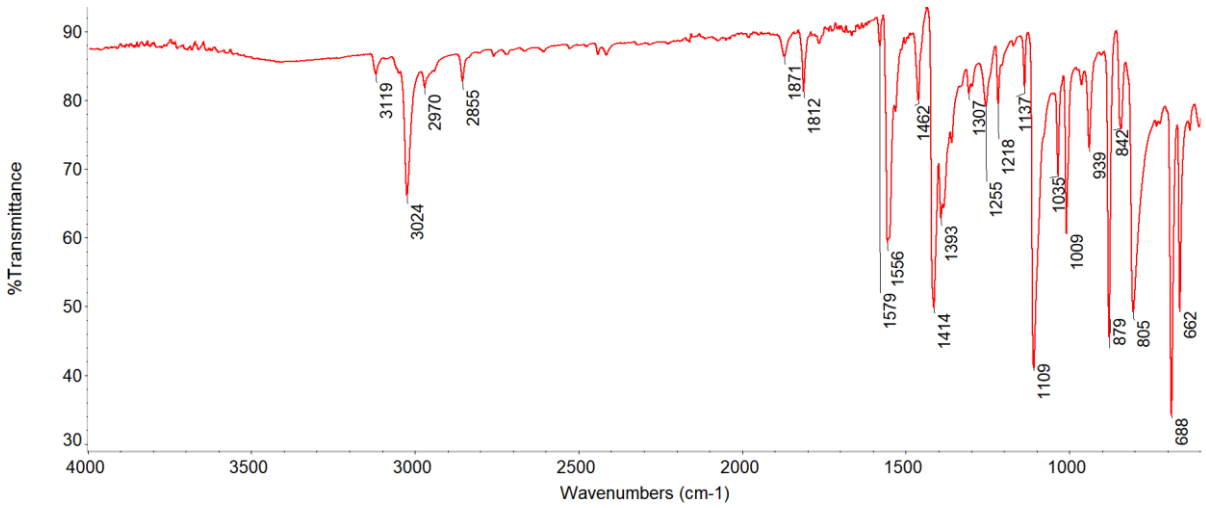

Figure (3.7.2) ATR-FTIR spectrum of 2-fluoro-3-iodopyridine

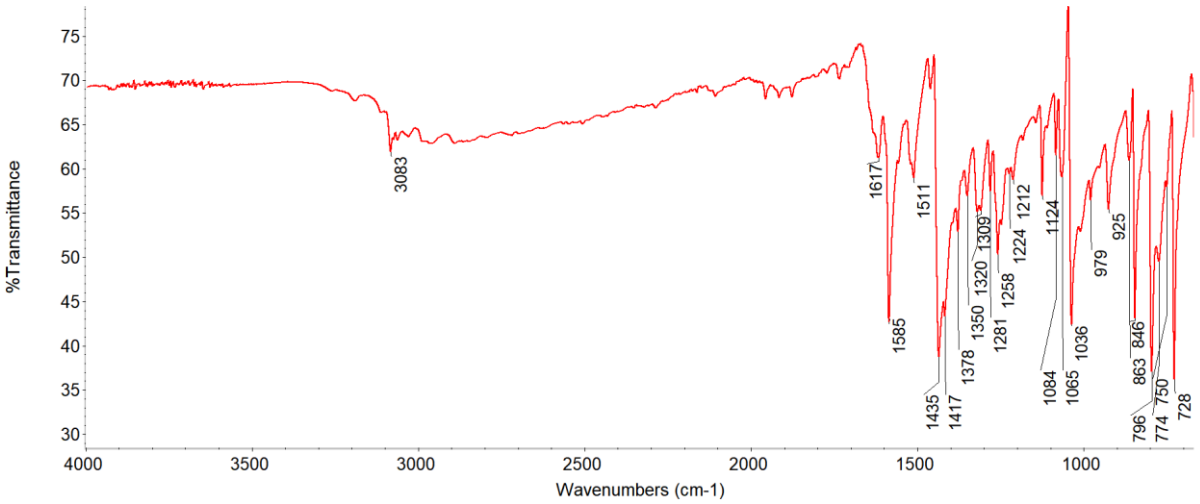

Figure (3.7.3) ATR-FTIR spectrum of 2-fluoro-3-iodopyridine – ICl

3.3.8 2-fluoro-4-iodopyridine-ICl:

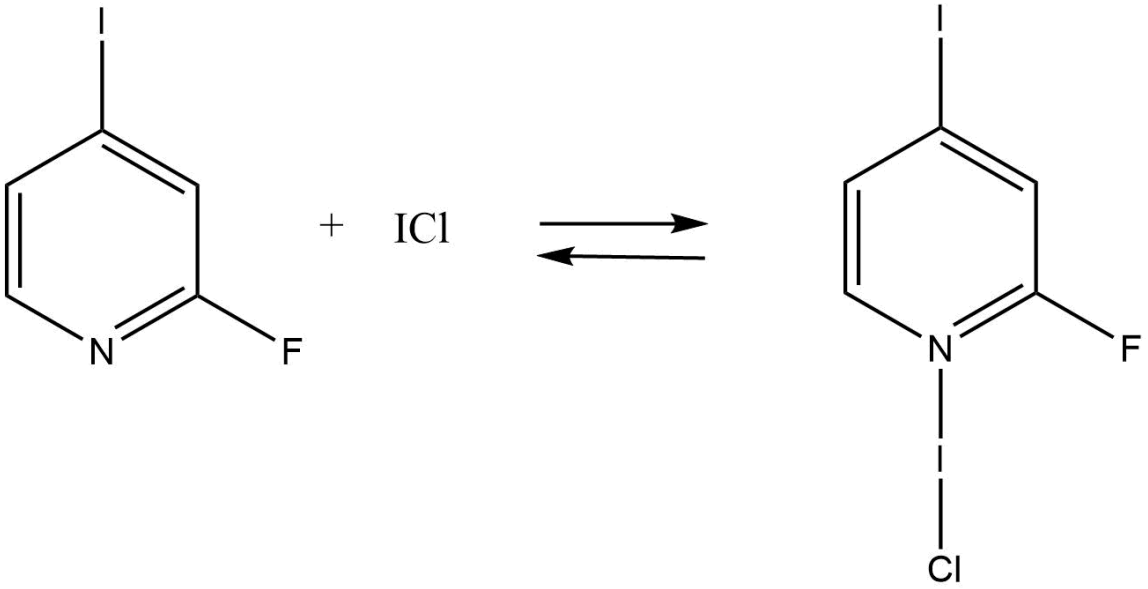

UV-Visible spectra for 2-fluoro-4-iodopyridine-ICl solution

All the spectra were collected using methanol as the solvent, the concentration of the samples was 10^{-3} M. The base 2-fluoro-4-iodopyridine displays the main absorption band at 351 nm, while ICl absorbed at 341 nm. The new band appeared at 446 nm when the above-mentioned starting materials were mixed. That band is not attributed to the 2-fluoro-4-iodopyridine or ICl. λ_{max} for 2-fluoro-4-iodopyridine was shifted 95 nm toward higher wavelengths (Figure 3.8.1). Starting material and the resulting complex are also characterised by ATR-FTIR, Figures (3.8.2, 3.8.3).

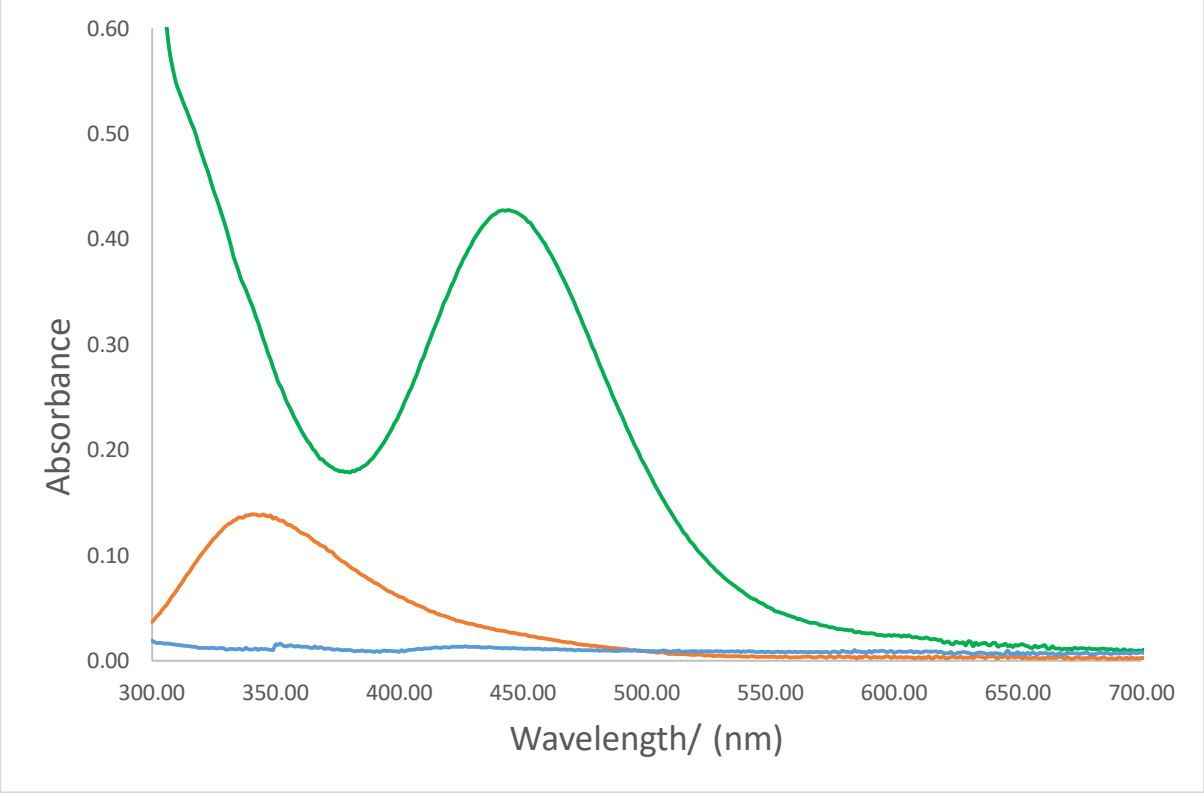

Figure (3.8.1) UV-Visible spectra of 2-fluoro-4-iodopyridine -ICl: 2-fluoro-4-iodopyridine (Blue), ICl (Orange), 2-fluoro-4-iodopyridine -ICl (Green), the spectra were collected using methanol as the solvent, the concentration of the samples was 10^{-3} M..

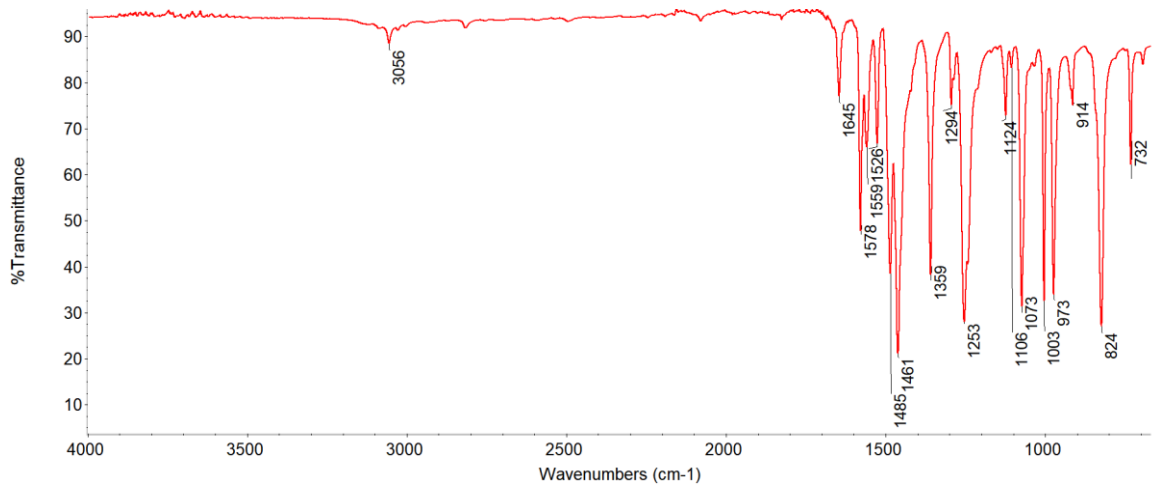

Figure (3.8.2) ATR-FTIR spectrum of 2-fluoro-4-iodopyridine

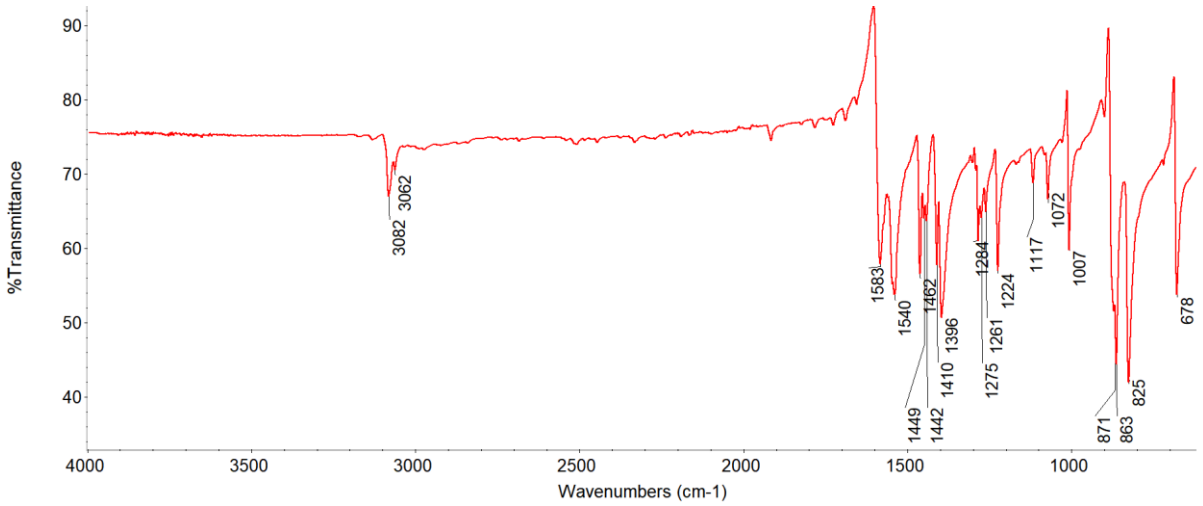

Figure (3.8.3) ATR-FTIR spectrum of 2-fluoro-4-iodopyridine -ICl

3.3.9 2-fluoro-5-iodopyridine-ICl:

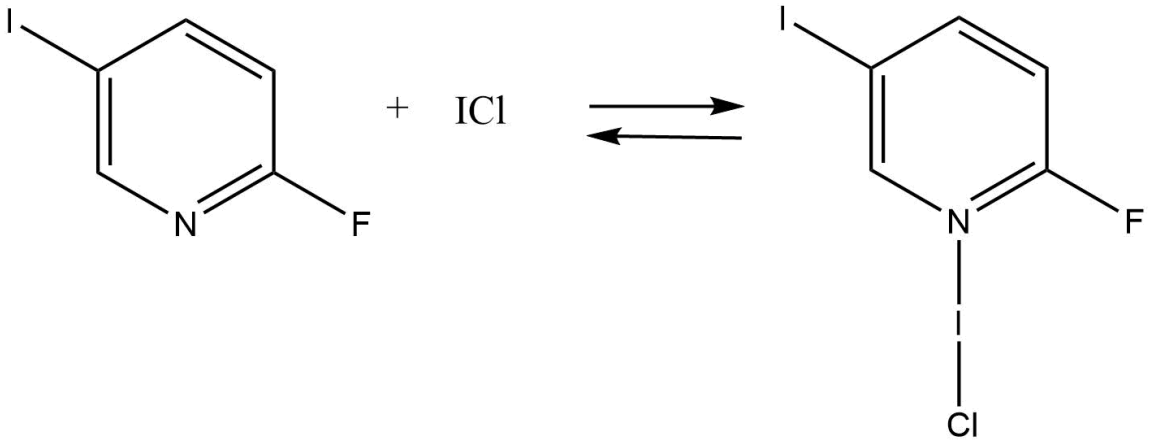

UV-Visible spectra for 2-fluoro-5-iodopyridine- ICl solution

All the spectra were collected using methanol as the solvent, the concentration of the samples was 10^{-3} M. The base 2-fluoro-5-iodopyridine displays two main absorption bands at 317 nm and 448 nm, while ICl absorbed at 341 nm. Two new bands appear at 346 nm and 442 nm when the above-mentioned starting materials were mixed. These bands are not attributed to the 2-fluoro-5-iodopyridine or ICl. λ_{max} at 317 nm for 2-fluoro-5-iodopyridine was shifted 29 nm and the λ_{max} at 448 nm for 2-fluoro-5-iodopyridine was shifted for 6 nm toward lower wavelengths (blue shift) (Figure 3.9.1). Starting material and the resulting complex are also characterised by ATR-FTIR, Figures (3.9.2, 3.9.3).

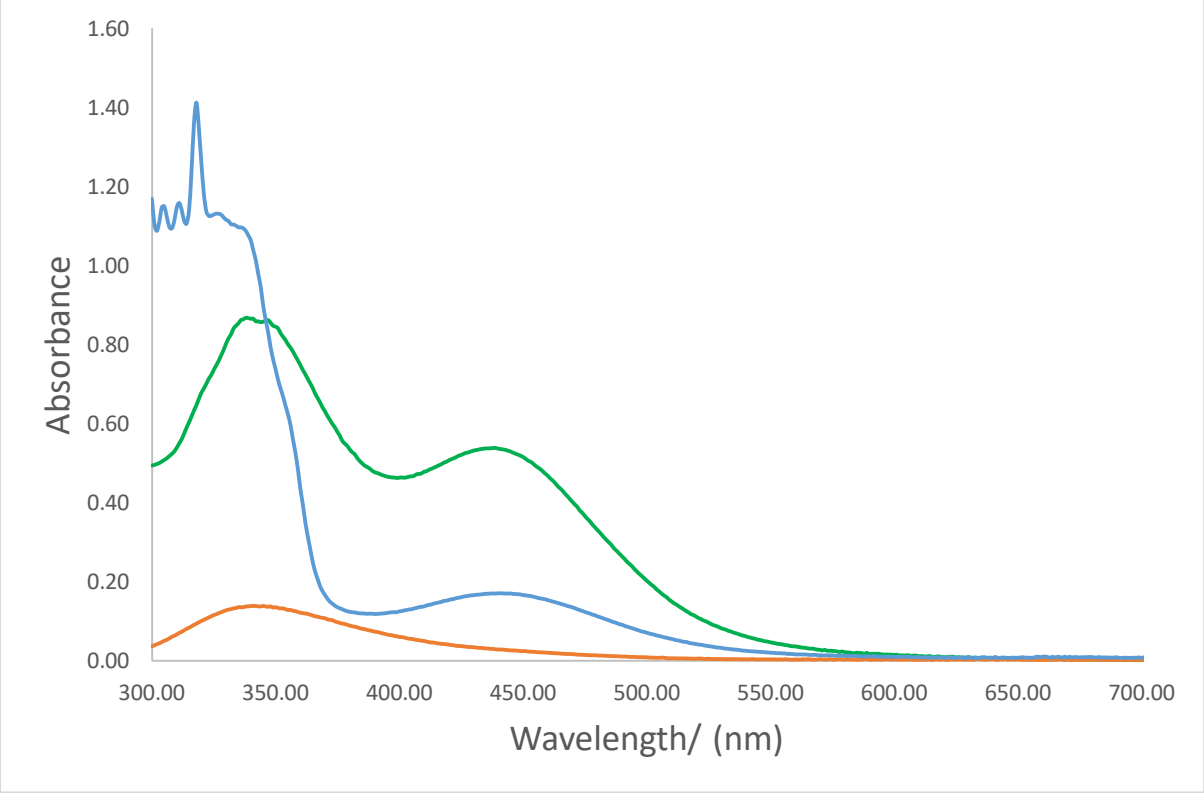

Figure (3.9.1): UV-Visible spectra of 2-fluoro-5-iodopyridine -ICl: 2-fluoro-5-iodopyridine (Blue), ICl (Orange), 2-fluoro-5-iodopyridine –ICl (Green), the spectra were collected using methanol as the solvent, the concentration of the samples was 10^{-3} M.

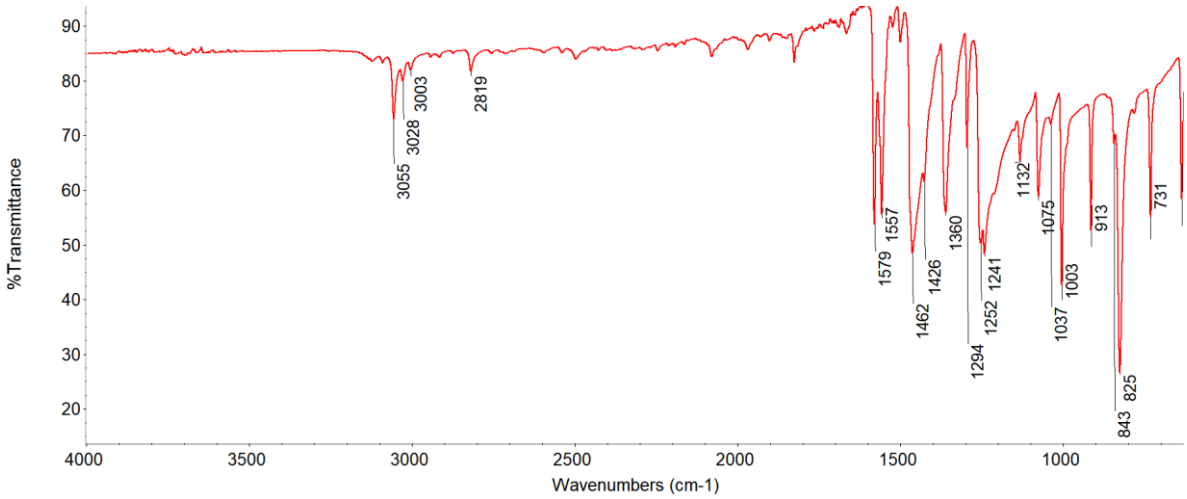

Figure (3.9.2) ATR-FTIR spectrum of 2-fluoro-5-iodopyridine

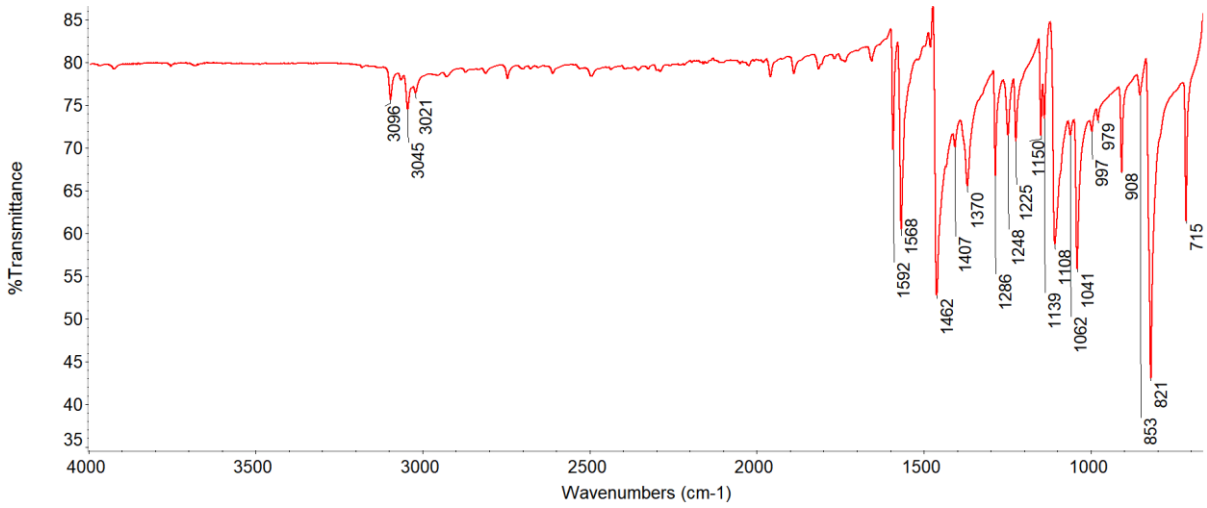

Figure (3.9.3) ATR-FTIR spectrum of 2-fluoro-5-iodopyridine -ICl

3.3.10 2-Cyanopyridine ICl

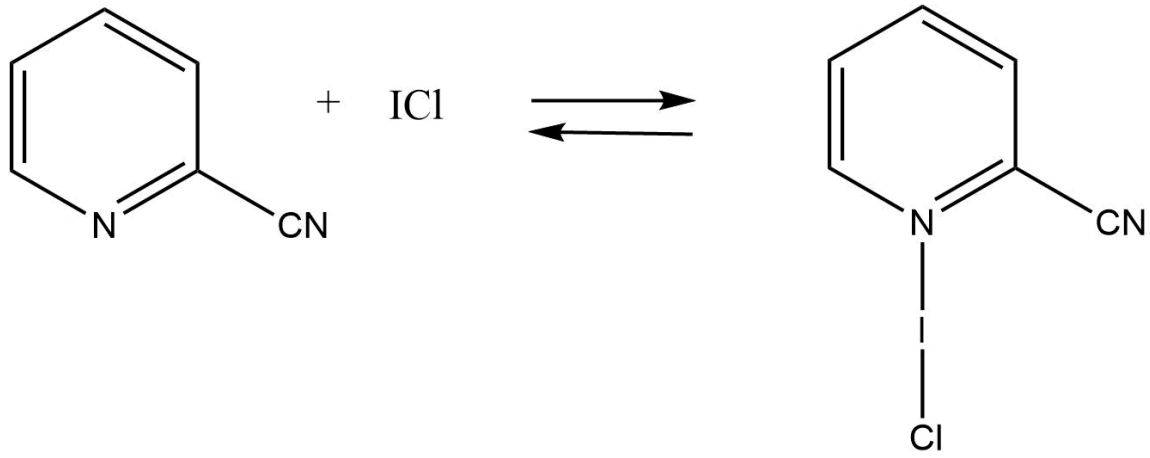

UV-Visible spectra for 2-Cyanopyridine- ICl solution

All the spectra were collected using methanol as the solvent, the concentration of the samples was 10^{-3} M. The base 2-cyanopyridine absorbed at 305 nm and iodine monochloride ICl absorbed at 341 nm. Two new bands appeared at 341 and 442 nm when the two above starting materials were mixed which is not attributed to the 2-cyanopyridine or ICl. λ_{max} for 2-cyanopyridine is shifted 137 nm toward higher wavelengths, Figure (3.10.1). Starting material and the resulting complex are also characterised by ATR-FTIR, Figures (3.10.2, 3.10.3).

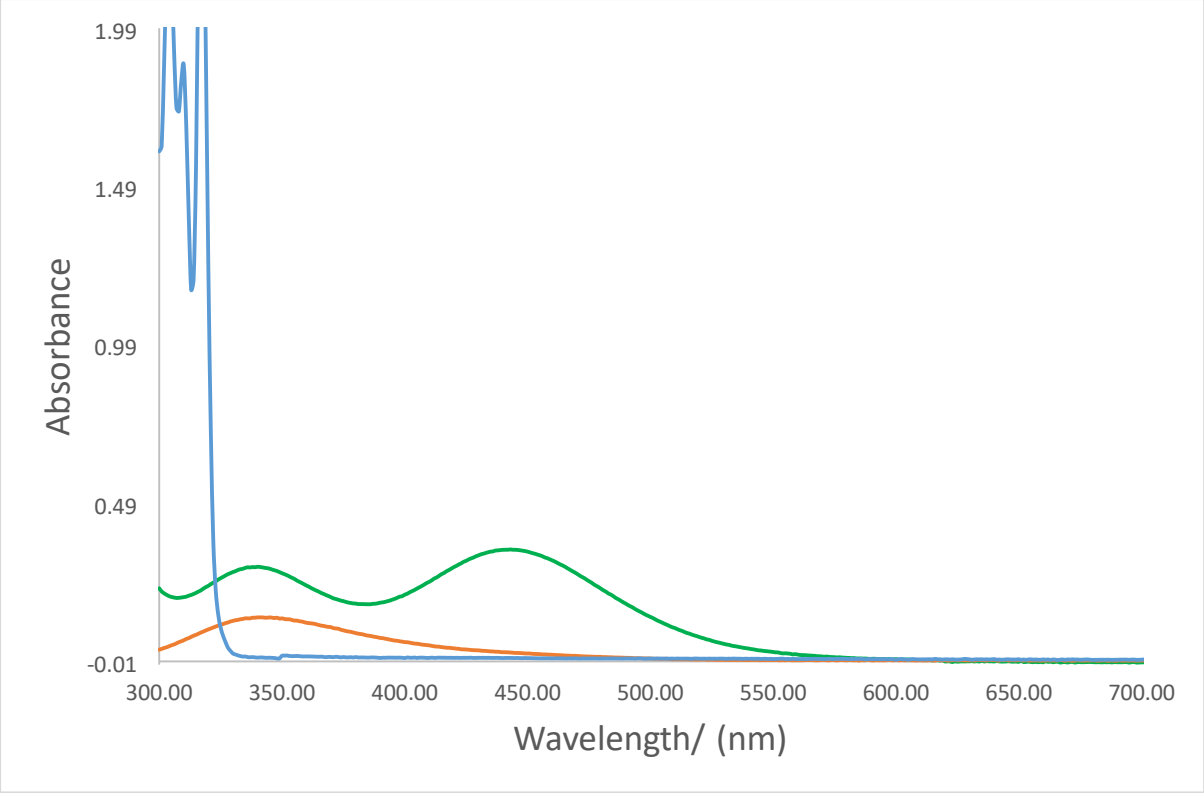

Figure (3.10.1): UV-Visible spectra of 2-cyanopyridine –ICl system: 2-cyanopyridine (Blue), ICl (Orange), 2-cyanopyridinium - ICl_2^- (Green), the spectra were collected using methanol as the solvent, the concentration of the samples was 10^{-3} M.

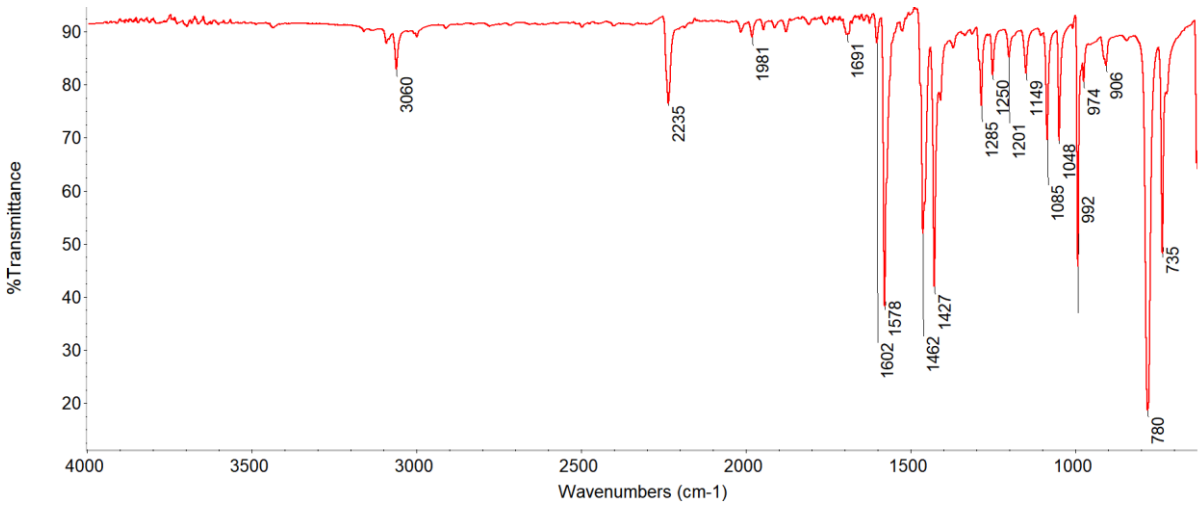

Figure (3.10.2) ATR-FTIR spectrum of 2-cyanopyridine

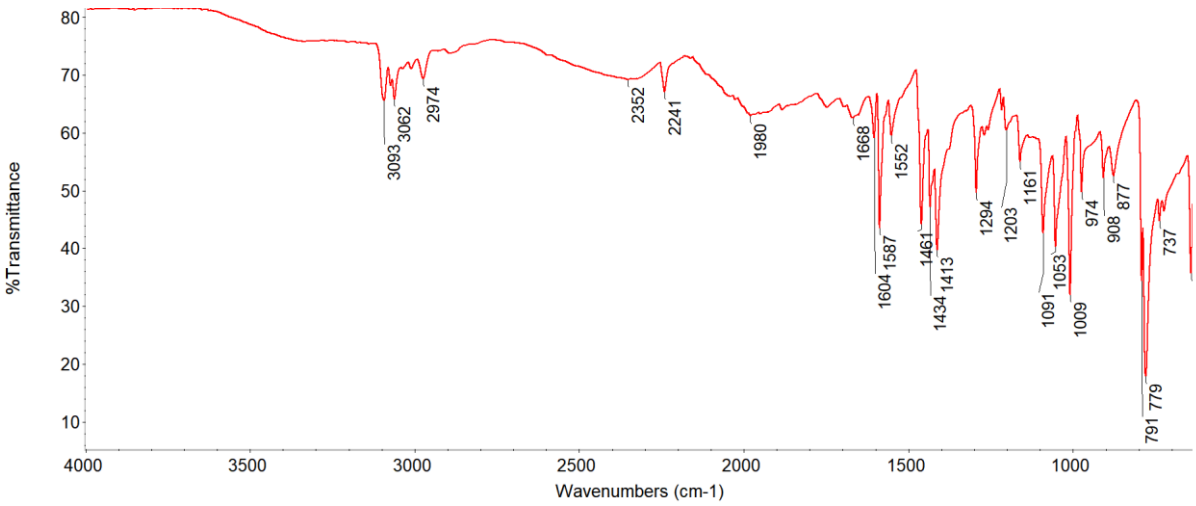

Figure (3.10.3) ATR-FTIR spectrum of 2-cyanopyridinium- ICl_2^-

XRD measurements for 2-cyanopyridinium – ICl_2^-

Crystal Structure of 2-cyanopyridinium - ICl_2^-

Crystallographic data for 2-cyanopyridinium - ICl_2^- are given in Table (3.11), and selected bond lengths and angles in Table (3.12) A Thermal ellipsoid plot of the structure together with the numbering scheme used is given in Figure (3.10.4).

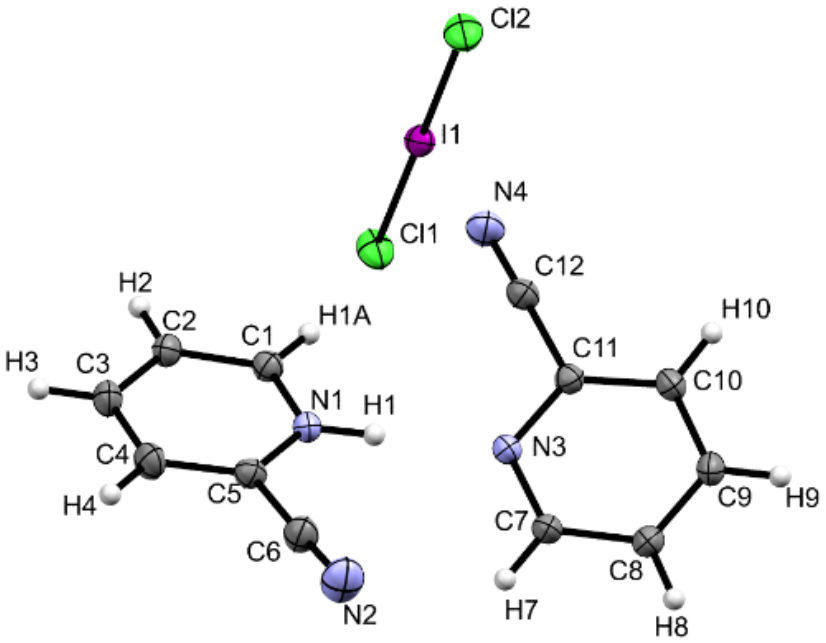

Figure (3.10.4): Thermal ellipsoid plot of 2-cyanopyridinium - ICl_2^-.

The complex crystallises in the monoclinic space group $P2_1/c$, with four complex units within the unit cell, Figure (3.10.5). There is no imposed crystallographic symmetry on this complex. The structure comprises of two 2-cyanopyridine molecules, which are linked by the proton of a hydrogen bond to form a $[H(C_7H_4N_2)_2]^+$ ion, the charge of which is balanced by the ICl_2^- anion. In this sample, instead of co-crystallising the starting materials, forming of pyridinium ions and ICl_2^- could be observed. Hydrolysis of ICl is one of the mechanisms that suggest the formation of these ions, which will be discussed below. The selected distances

between atoms; Cl1-I is 2.5531(6), Cl2-I is 2.5540(6) Å, N1-H1is 0.919 Å, H1-N3 is 1.825 Å, N1-Cl1 is 3.238 Å.

Measured angles; Cl1-I-Cl2 is 179.68(2) °, C5-C6-N2 is 177.7(2) °, C11-C12-N4 is 178.84°, N1-C5-C6 is 116.3(2) °, N3-C11-C12 is 115.2(2) °, N1-H1-N3 is 176.84°, N1-Cl1-I is 165.29°.

There are two molecules of 2-cyanopyridine in the asymmetric unit (the molecule containing N1 atom is a pyridinium ion while the other one is neutral molecule) with an ICl_2^-. Because of the presence of a hydrogen bond N-H···N and lack of any interaction between the ICl_2^- and the four N atoms, the two I-Cl distances in the ion are almost equal 2.5531(6) Å, 2.5541(6) Å. This contrasts with the previous ICl_2^- salt where preferential hydrogen bonding leads to a difference in the ICl distances. In an N1-H1···N3 hydrogen bond, the distance between N1 and N3 is 1.825 Å, (Figure 3.10.6) which less than the sum of Van der Waals radii (2.75 Å),[121] and the N1-H1-N3 angle is 176.84°. A distance of 4.015Å was observed for the centroid distance between two pyridine ring of 2-cyanopyridine – ICl_2^-, Figure (3.10.7).

Table (3.11) Crystallographic data for 2-cyanopyridinium- ICl_2^-.

Crystal data	
Chemical formula	$Cl_2I{\cdot}C_6H_5N_2{\cdot}H\ C_6H_4N_2$
M_r	407.03
Crystal system, space group	Monoclinic, $P2_1/c$
T/K	150
a, *b*, *c* (Å)	9.6982 (18), 13.243 (2), 11.553 (2)
β (°)	93.207 (6)
V/ (Å^3)	1481.5 (5)
Z	4
Radiation type	Mo *K*α
μ / (mm^{-1})	2.51
Crystal size / (mm)	0.25 × 0.2 × 0.14
Data collection	
Diffractometer	Bruker *APEX*-II CCD
Absorption correction	Multi-scan
T_{min}, T_{max}	0.656, 0.747
No. of measured, independent and observed [$I > 2\sigma(I)$] reflections	25524, 4701, 4291

R_{int}	0.028
$(\sin \theta/\lambda)_{max}$ / (Å^{-1})	0.725
Refinement	
$R[F^2 > 2\sigma(F^2)]$, $wR(F^2)$, S	0.022, 0.054, 1.13
No. of reflections	4701
No. of parameters	175
No. of restraints	1
H-atom treatment	H atoms treated by a mixture of independent and constrained refinement
$\Delta\rho_{max}$, $\Delta\rho_{min}$ (e Å^{-3})	0.86, −0.68

Table (3.12): Selected interatomic contacts /Å and /^{o} for the complex 2-cyanopyridinium - ICl_2^-.

Atom1	Atom2	Length	Atom1	Atom2	Atom3	Angle
I1	Cl1	2.5531(6)	Cl1	I1	N1	177.76(3)
I1	Cl2	2.5541(6)	I1	N1	C2	121.03(9)
N1	C1	1.333(2)	I1	N1	C6	119.46(9)
N1	H1	0.92(2)	C2	N1	C6	119.0(1)
N1	C5	1.352(2)	N1	C2	C3	122.6(1)
N2	C6	1.148(3)	N1	C2	H21	117.8
C1	C2	1.388(3)	C2	C3	C4	118.4(1)
C2	H2	0.95	C2	C3	H31	120.4
C2	C3	1.385(3)	C4	C3	H31	121.2
C3	H3	0.95	C3	C4	C5	118.9(1)
C5	C6	1.443(3)	C4	C5	C6	122.4(2)
N3	C7	1.335(2)	N1	C6	C5	122.2(1)
N3	C11	1.357(2)				
N4	C12	1.142(3)				
C7	C8	1.394(3)				
C8	C9	1.386(3)				
C9	H9	0.95				
C9	C10	1.394(3)				
C10	C11	1.387(2)				
C11	C12	1.452(3)				

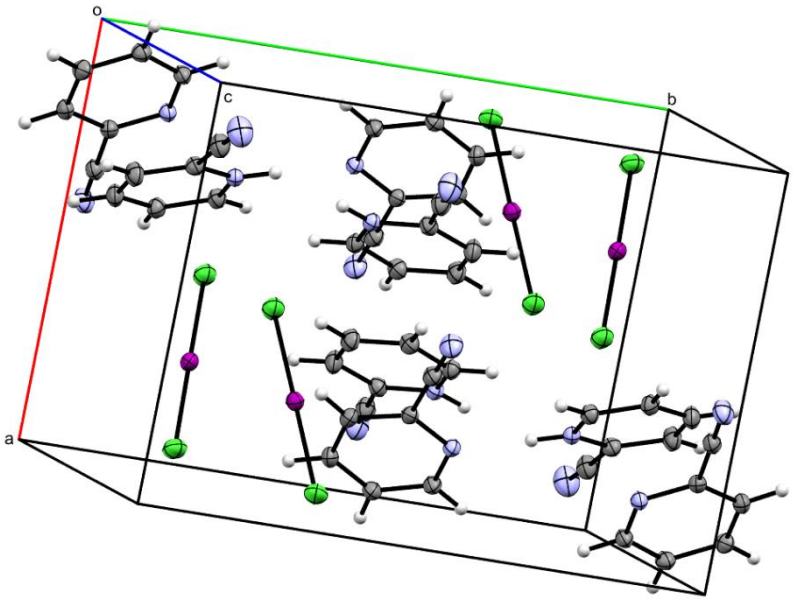

Figure (3.10.5): Packing diagram of 2-cyanopyridinium -ICl_2^-

approximately along to c axis

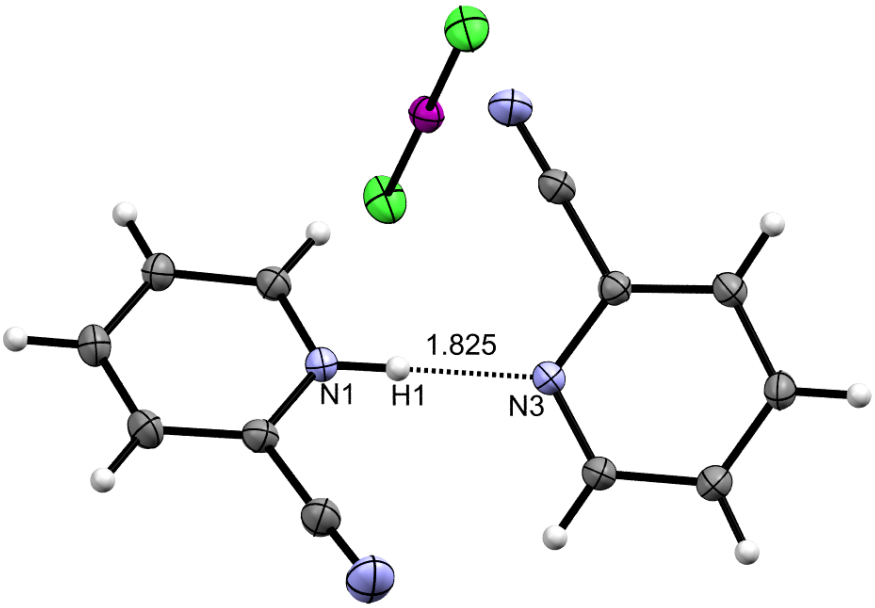

Figure (3.10.6): View showing the N1-H1···N3 hydrogen bond in 2-cyanopyridinium -ICl_2^-

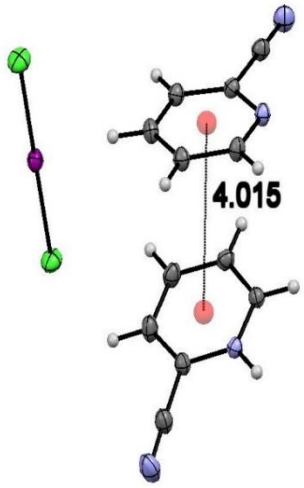

Figure (3.10.7): View showing the distance between the centroids of two 2-cyanopyridinium -ICl_2^-molecules.

3.3.11 1,10-Phenanthroline-ICl

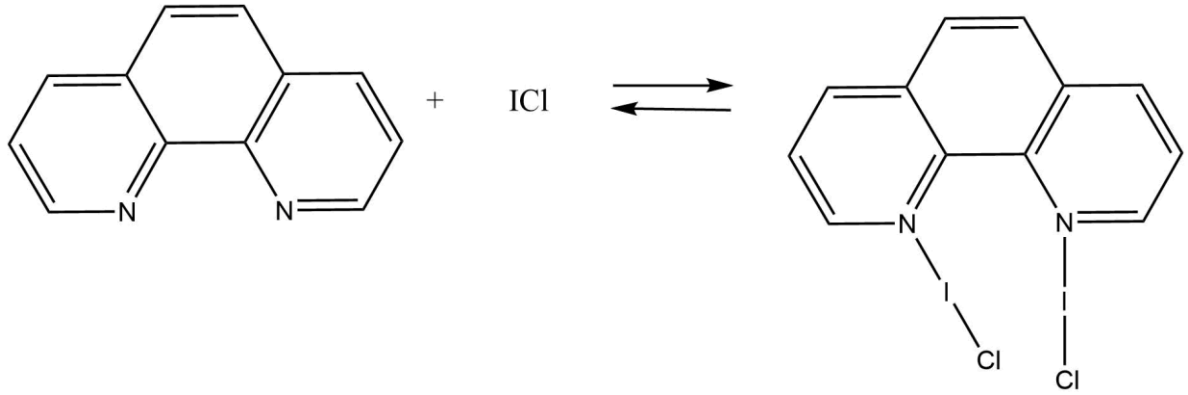

UV-Visible spectra for 1,10-phenanthroline - ICl solution

All the spectra were collected using methanol as the solvent, the concentration of the samples was 10^{-3} M. The base 1,10-phenanthroline absorbed at 308 nm and iodine monochloride ICl absorbed at 341 nm. A new band appeared at 440 nm when the two above starting materials were mixed which is not attributed to the 1,10-phenanthroline or ICl. This new band confirms the formation of the halogen bonded complex. That means λ_{max} for 1,10-phenanthroline is shifted 132 nm toward higher wavelengths, Figure (3.11.1). Starting material and the resulting complex are also characterised by ATR-FTIR, Figures (3.11.2, 3.11.3).

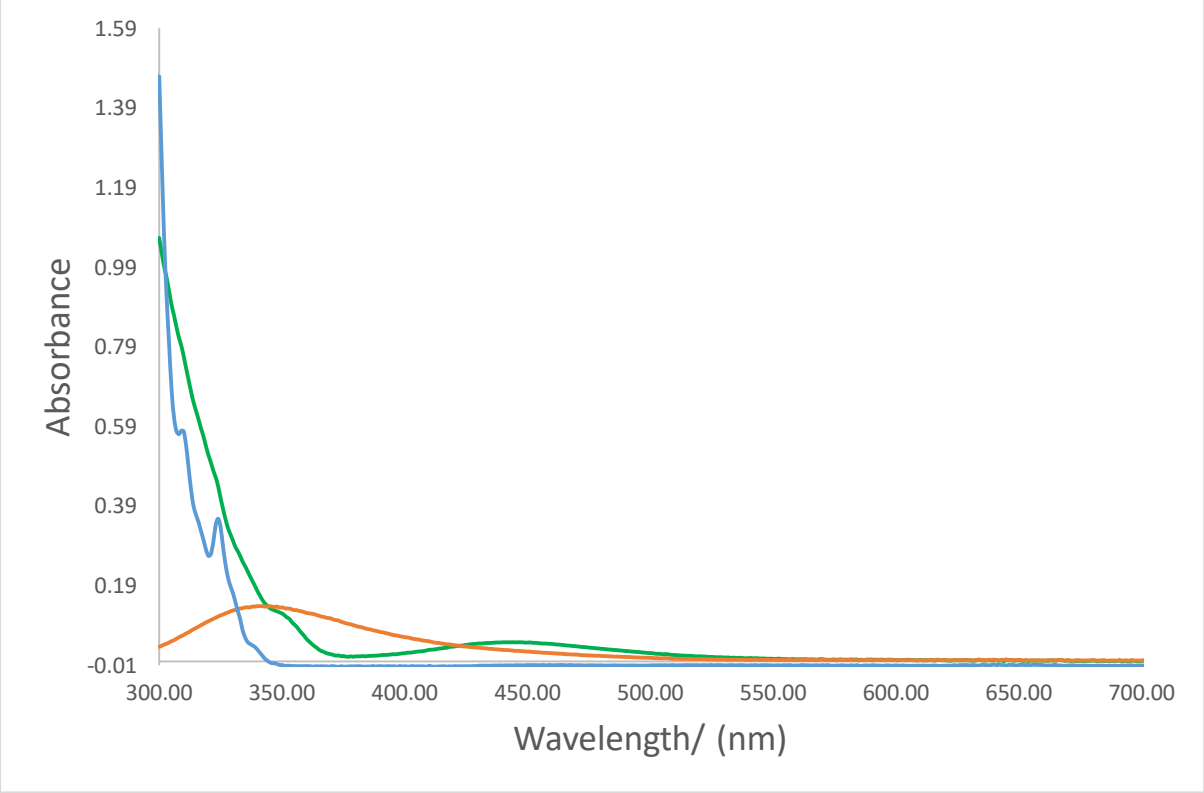

Figure (3.11.1): UV-Visible spectra of 1,10-phenanthroline –ICl system: 1,10-phenanthroline (Blue), ICl (Orange), 1,10-phenanthroline - ICl (Green), the spectra were collected using methanol as the solvent, the concentration of the samples was 10^{-3} M.

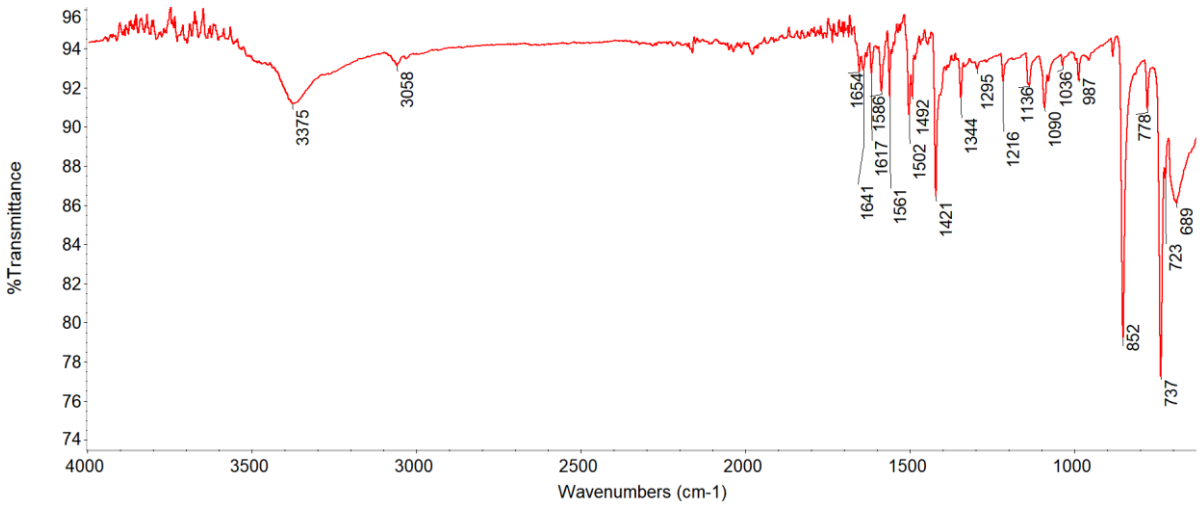

Figure (3.11.2): ATR-FTIR spectrum of 1,10-phenanthroline

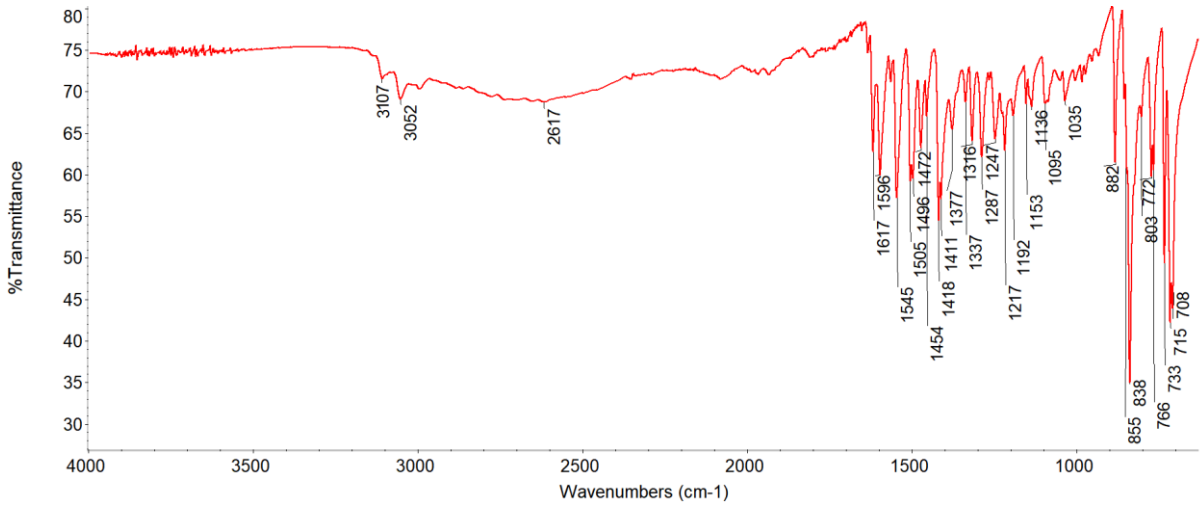

Figure (3.11.3) ATR-FTIR spectrum of 1,10-phenanthroline- ICl

3.3.12 Quinoxaline-ICl:

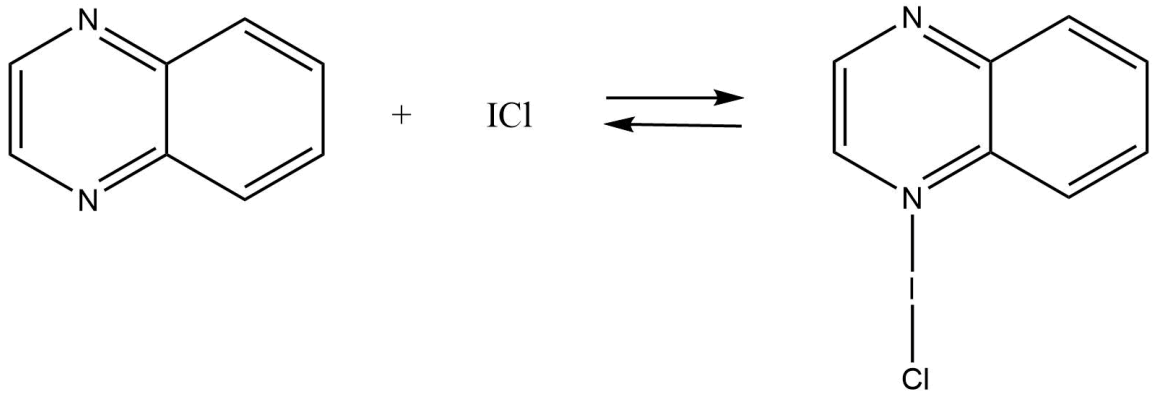

UV-Visible spectra for Quinoxaline - ICl solution

All the spectra were collected using methanol as the solvent, the concentration of the samples was 10^{-3} M. The base quinoxaline displays two main absorption bands at 323 nm and 460 nm, while ICl absorbed at 341 nm. The new band appeared at 444 nm when the above-mentioned starting materials were mixed. That band is not attributed to the quinoxaline or ICl. λ_{max} at 323 nm for quinoxaline was shifted 121 nm toward lower wavelengths (blue shift) (Figure 3.12.1). Starting material and the resulting complex are also characterised by ATR-FTIR, Figures (3.12.2, 3.12.3).

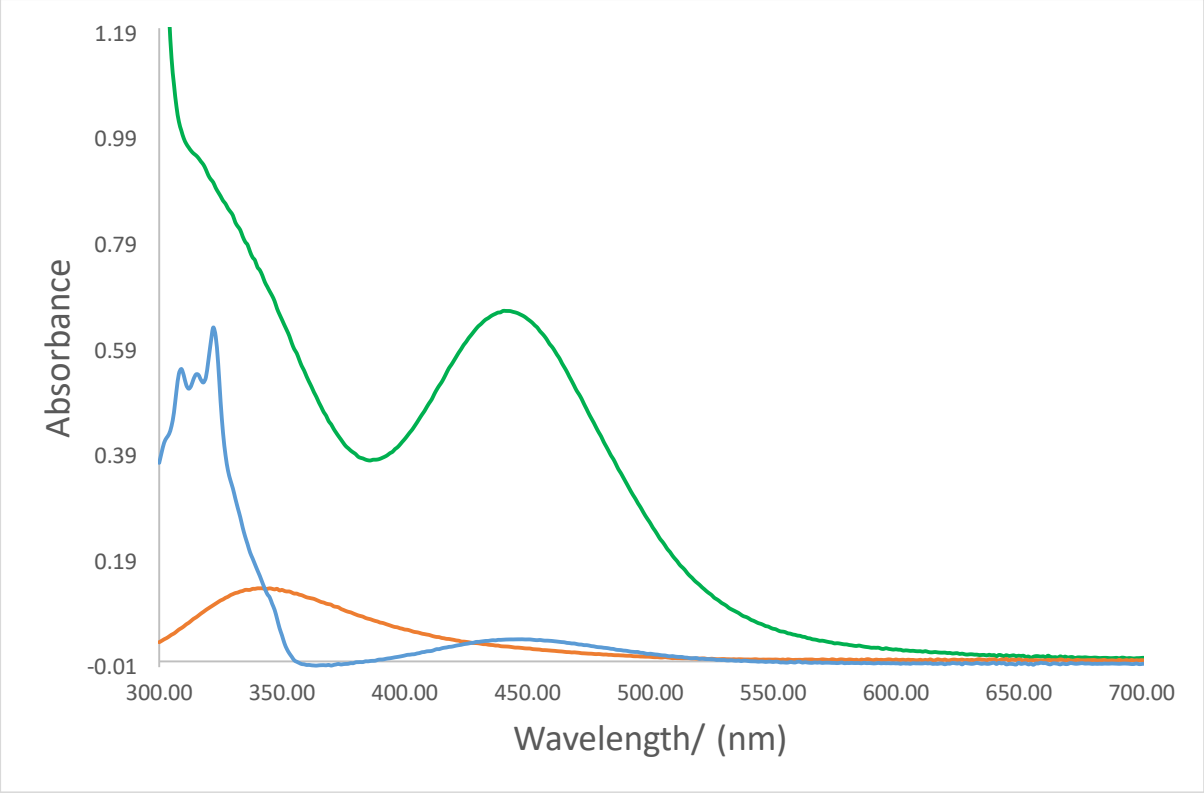

Figure (3.12.1) UV-Visible spectra of quinoxaline –ICl system:

quinoxaline (Blue), ICl (Orange), quinoxaline- ICl (Green), the spectra were collected using methanol as the solvent, the concentration of the samples was 10^{-3} M.

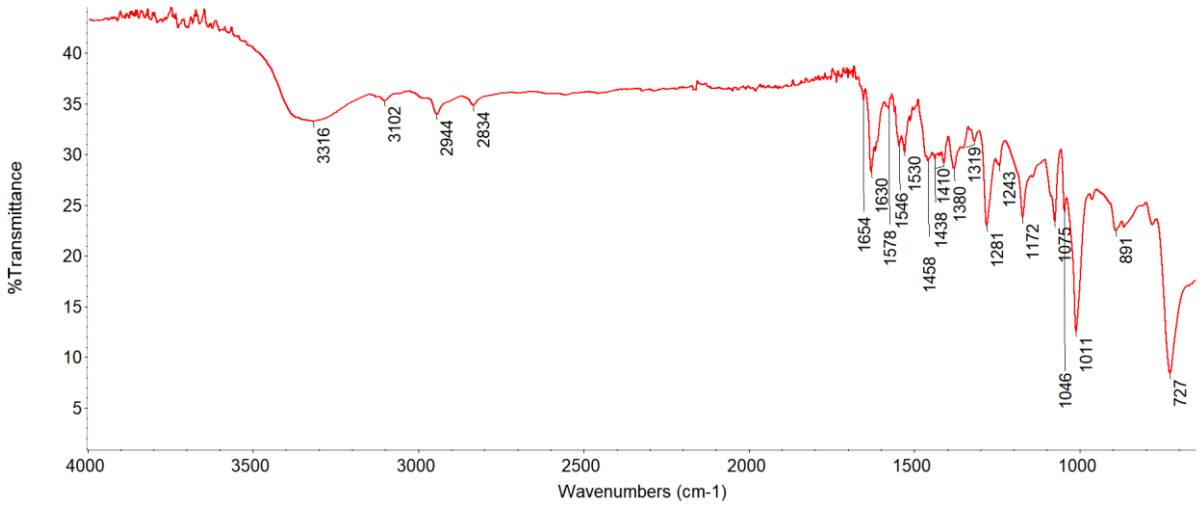

Figure (3.12.2): ATR-FTIR spectrum of quinoxaline

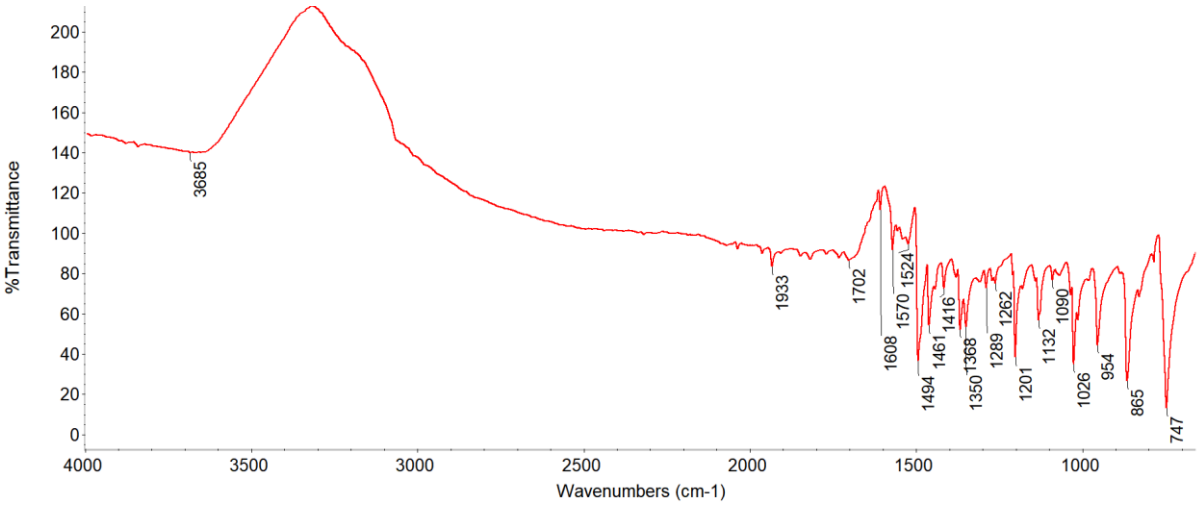

Figure (3.12.3): ATR-FTIR spectrum of quinoxaline-ICl.

(Spectrum should be collected again prior to further publication of the data)

3.3.13 2-chloroquinoline-ICl:

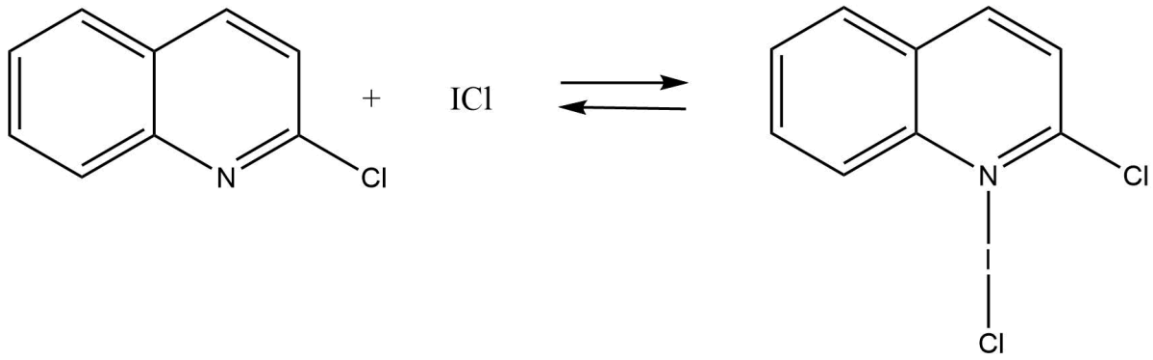

UV-Visible spectra for 2-chloroquinoline - ICl solution

All the spectra were collected using methanol as the solvent, the concentration of the samples was 10^{-3} M. The base 2-chloroquinoline displays two main absorption bands at 319 nm and 460 nm, while ICl absorbed at 341 nm. The new band appeared at 449 nm when the above-mentioned starting materials were mixed. That band is not attributed to the 2-chloroquinoline or ICl. λ_{max} at 319 nm for 2-chloroquinoline was shifted 130 nm toward higher wavelengths (redshift) and the λ_{max} at 460 nm for 2-chloroquinoline is shifted for 11 nm toward lower wavelengths (blue shift) (Figure 3.13.1). Starting material and the resulting complex are also characterised by ATR-FTIR, Figures (3.13.2, 3.13.3).

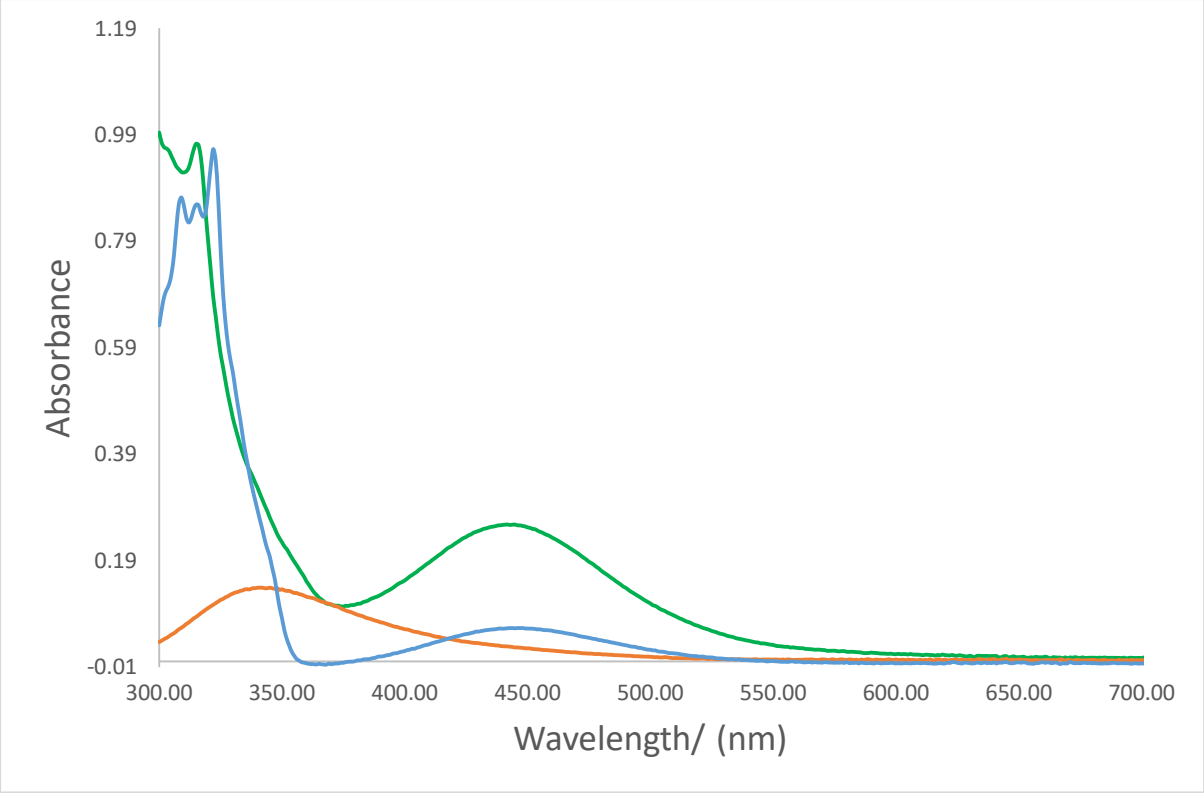

Figure (3.13.1): UV-Visible spectra of 2-chloroquinoline –ICl system: 2-chloroquinoline (Blue), ICl (Orange), 2-chloroquinoline ICl (Green), the spectra were collected using methanol as the solvent, the concentration of the samples was 10^{-3} M.

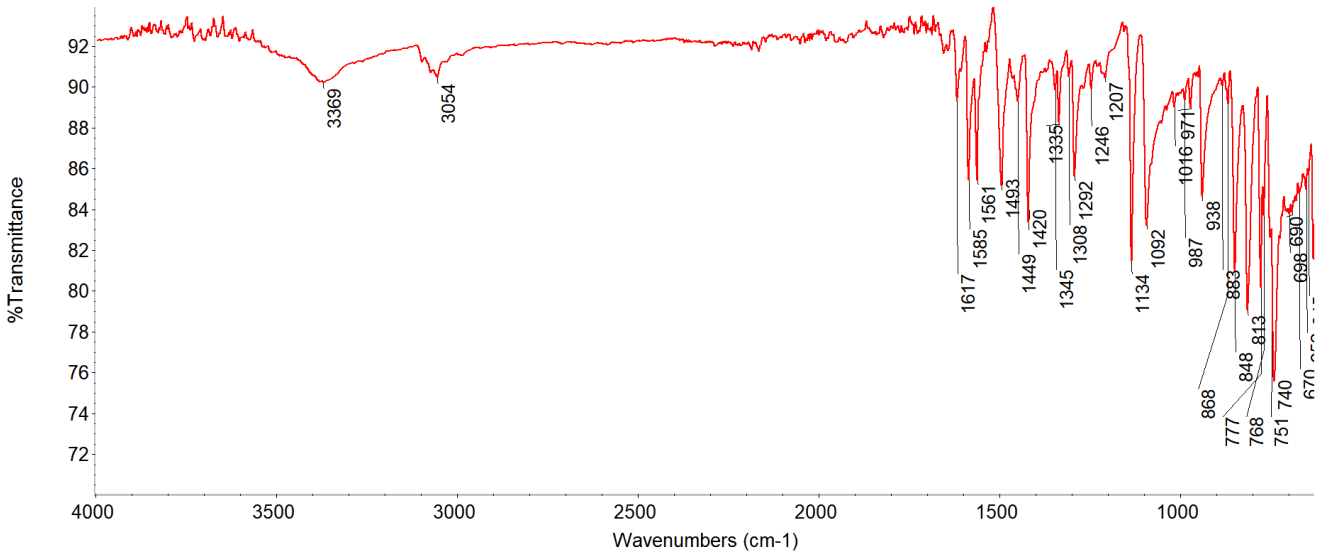

Figure (3.13.2): ATR-FTIR spectrum of 2-chloroquinoline

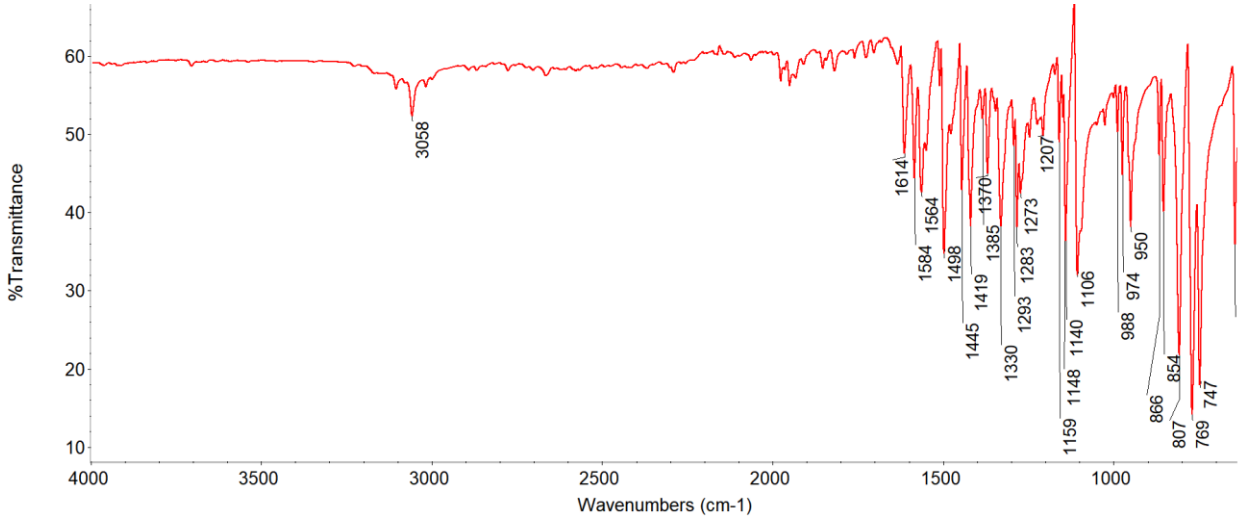

Figure (3.13.3): ATR-FTIR spectrum of 2-chloroquinoline -ICl

Table 3.13: Distance between atoms /Å, measured angles / ^{o}, λ max /nm and melting point/°C for ICl complexes.

Compound	N···I Å	I-Cl Å	N···I-Cl ^{o}	λmax/ nm	m. p. / °C
3,5-difluoropyridine-ICl	2.358(6)	2.470(2)	178.69(1)	443	107-109
3,5-dichloropyridine-ICl	2.341(3)	2.4872(9)	180.00	444	140-143
2,6-dichloropyridine-ICl				442	91-93
2,6-dimethoxypyridine-ICl_2^-		2.6041(5), 2.5176(5)		446	136-138
4-methoxypyridine-ICl	2.2717(12)	2.5305(4)	177.76(3)	359	165-168
3-fluoropyridine-ICl				358	106-109
2-fluoropyridine-3-iodopyridine-ICl				438	135-137
2-fluoropyridine-4-iodopyridine-ICl				445	136-138
2-fluoropyridine-5-iodopyridine-ICl				438	133-135
2-cyanopyridine –ICl_2^-		2.5531(6), 2.5541(6)	177.76(3)	442	94-96
1,10-phenanthroline-ICl				440	214-217
Quinoxaline-ICl				439	109-111
2-chloroquinoline-ICl				443	117-120

3.4 Discussion

Prepared complexes can be separated into two main groups, the ones characterised by single-crystal X-ray diffraction, UV-VIS and ATR-FTIR spectroscopy, and the ones characterised just by the latter two techniques. The former group can further be separated based on the observed structural properties, (A) complexes with N···I-Cl halogen bond, (B) ionic complexes containing polyhalogen ions and (C) crystals of the starting materials. The first group contains three complexes (3,5-difluoropyridine-ICl, 3,5-dichloropyridine-ICl and 4-methoxypyridine-ICl). Halogen bond geometrical properties of these compounds are compared with the selected literature data in Table 3.14. The complexes are chosen because in all of them an sp^2 N atom is halogen bonded to the iodine atom of the ICl moiety. It could be noticed that the nomenclature system in Table 3.0.1 is not uniform, therefore all the literature complexes will be labelled in a consistent way for better clarity. Since in the complexes with refcodes TAGNEV[118] and TAGNEV01[114] two interactions are present, they are labelled as (1) and (2) shown in Figure (3.14.1). In addition, for the pyridine-ICl complex, instead of values reported by Ouvrard et al.[112], the redetermined values from a more recent paper by Jones et al.[129] are chosen. Thermal ellipsoids of the selected complexes are presented in Figure (3.14.1).

Table (3.14.1) Geometric parameters of selected N···I-Cl halogen bonded complexes, adapted from ref.[106,112], data reported in this work is marked bold

Complex name (REFCODE)	**N···I (Å)**	**I-Cl (Å)**	**N···I-Cl (°)**	**C-N-C (°)**
4-(N,N-dimethylamino)pyridine-ICl (GANXOJ)[114]	2.246	2.562	179.24	117.93
4-methoxypyridine-ICl	**2.272**	**2.528**	**177.76**	**119.01**
Pyridine-ICl (PYRIIC11)[116]	2.290	2.510	178.72	119.83
N, N-bis(ICl)-2,2-bipyridine (1) (TAGNEV01)[114]	2.321	2.497	175.33	119.59
trans-N,N-bis(ICl)-2,2-bipyridine (2) (TAGNEV)[118]	2.336	2.459	179.32	119.82
N, N-bis(ICl)-2,2-bipyridine (2) (TAGNEV01)[114]	2.337	2.488	179.40	119.75
3,5-dichloropyridine-ICl	**2.341**	**2.487**	**180.00**	**121.16**
trans-N,N-bis(ICl)-2,2-bipyridine (1) (TAGNEV)[118]	2.343	2.478	176.16	118.73
3-bromopyridine-ICl (GANXAV)[114]	2.344	2.473	178.43	119.99
3,5-difluoropyridine-ICl	**2.358**	**2.470**	**178.60**	**121.35**
2-chloroquinoline-ICl (CLQUIC)[113]	2.432	2.446	179.93	116.83

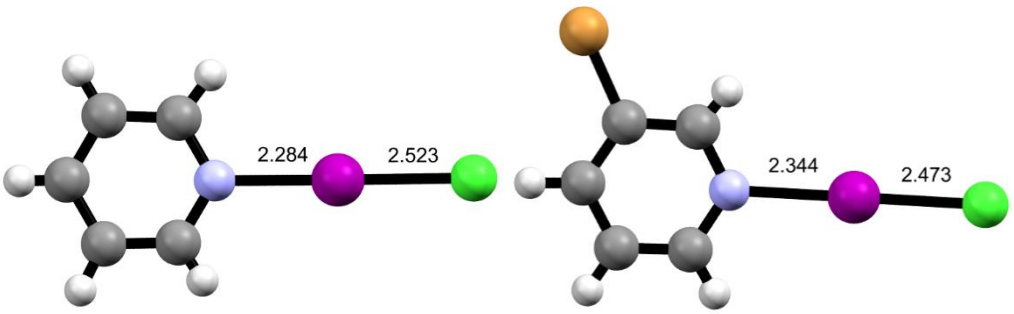

PYRIIC11[116] GANXAV[114]

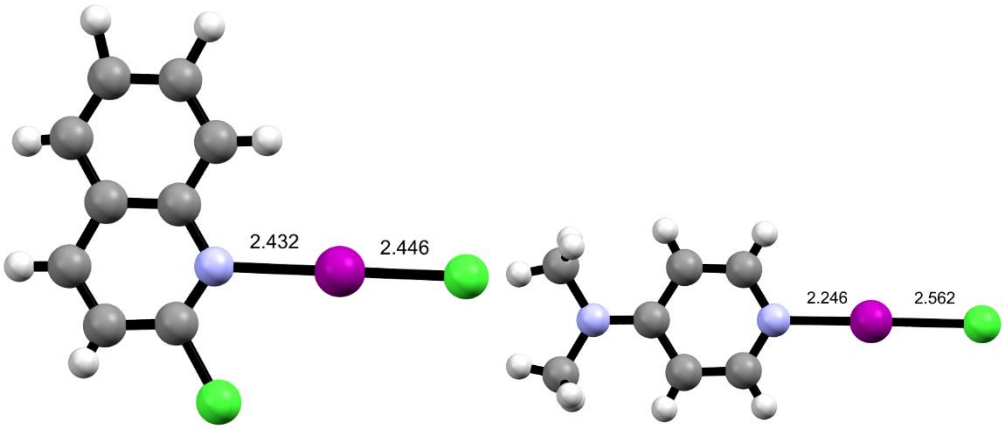

CLQUIC[113] GANXOJ[114]

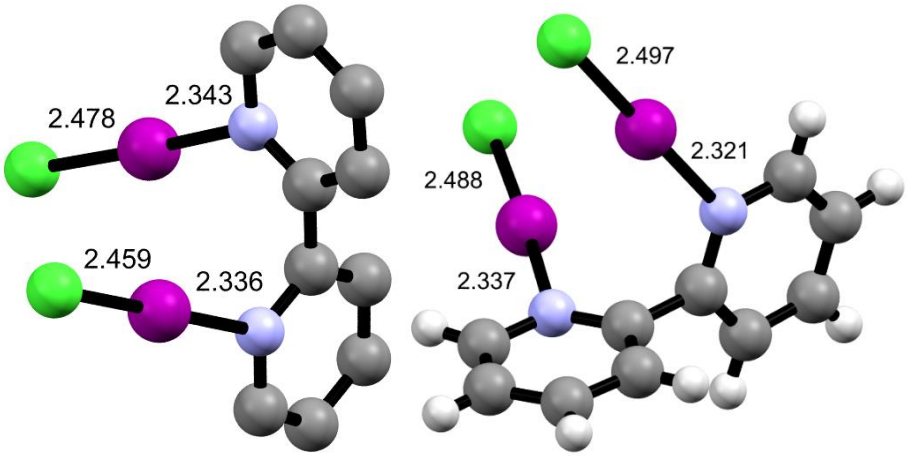

TAGNEV[118] TAGNEV01[114]

Figure (3.14.1) Ball and stick representation plots of selected literature complexes

According to Table (3.14.1), it has been observed that there is a relationship between the base strength and the N···I and I-Cl distances and C-N-C angle. Base strength can be described as

the ability of a base to donate a free electron pair to other species in order to accept a proton. The greater the ability to donate the electrons, the greater the base strength is. Generally, the base strength is known by the pKa values of their conjugate acids (the higher the pKa value of the conjugate acid, the stronger the base is). [128] Conjugate acids are species that form when bases acquire a proton, while a pKa value is a negative logarithm of the acid dissociation constant. Several factors affect the base strength of organic species. The first and the most important one is the electronegativity of an element on which the free electron pair is located. The less the electronegative the element is, the stronger the base because the free electron pair will be more available for the interaction with the protons. Other factors affecting the base strength are the hybridisation of the electronegative element (sp^3>sp^2>sp), the electronegative element being attached to electron-withdrawing or -donating groups (the latter increase the basicity) and stabilisation of an electron pair either by conjugation or being involved in the preservation of aromaticity (the less stabilised the electron pair is, the stronger the base). In the complexes prepared in this work and the literature reported ones, it was observed that as the base strength increases, N···I distance and the C-N-C angle in the pyridine ring decrease (with some exceptions), while the elongation of I-Cl distance increases, too. This trend can be correlated with the electron-donating or electron-withdrawing properties of the groups on the pyridine ring. It is well known that in organic chemistry in electrophilic aromatic substitution these properties are related to so-called activation or deactivation of the ring.[128] The general trend is, if just a hydrogen atom is taken as a reference, groups prone to π-donation (alkoxy-, amino-, amides) are strongly activating and alkyl groups with no electron-withdrawing groups are moderately activating due to the inductive effect. On the other hand, halogens are moderately deactivating due to their high electronegativity, while groups like cyano-, nitro-, carbonyl-, haloalkyl- and ammonium are highly deactivating because of their π-acceptor properties.[128] For the selected N···I-Cl

halogen bond systems, this trend could be observed through the N···I interaction distance, because the more electrons are donated to the pyridine ring, the higher the electron density could be expected on the ring N atom, which can further interact with the σ-hole of the iodine atom from ICl. Subsequently, the more electron density on the nitrogen atom, the stronger the N···I interaction should be. This is manifested by the shortening of the N···I distance, while at the same time by elongation of the I-Cl bond, as well. For the prepared and literature-based complexes, the mentioned trend is observed. If the pyridine-ICl complex is taken as a reference point, then electron-donating methoxy- and dimethylamino- groups expectedly have shorter N···I distance, while the halo- groups longer interaction distance. The position of the group on the ring relative to the pyridine N atom should be noted too, methoxy- and dimethylamino- groups are in para-position, bearing in mind that both of them are ortho- and para-activating, this surely contributed to increasing the electron density on the N atom. In contrary, halo- groups are all except the 2-chloroquinoline in meta-positon relative to the pyridine N atom, and since they are meta- activating, all the halo-groups in meta-position have similar N···I distance, while for 2-chloroquinoline, where chlorine atom is in the ortho-position, the distance is noticeably greater. Therefore, it would be reasonable to expect from the complexes where no suitable crystalline material is observed that values for 2,6-dimethoxypyridine halogen bonded complex should be similar to values of 4-methoxypyridine-ICl. Quinoxaline and 1,10-phenanthroline complexes would be similar to the values observed in N, N-bis(ICl)-2,2-bipyridine complexes, while for the halo-complexes (3-fluoropyridine-ICl, 2-fluoro-3-iodopyridine-ICl, 2-fluoro-4-iodopyridine-ICl, 2-fluoro-5-iodopyridine-ICl and 2,6-dichloropyridine) the measured values to be close to the already observed halo-complexes. Due to the strongest π-acceptor properties, the longest N···I interaction should be expected in the 2-cyanopyridine-ICl complex. The other two mentioned parameters follow the same trend, but with some exceptions. For the I-Cl bond length, a

slight exception is observed in trans-*N*, *N*-bis(ICl)-2,2-bipyridine (2) complex, while for the C-N-C angle there are three noticeable outliers, 3,5-difluoropyridine-ICl, trans-*N*, *N*-bis(ICl)-2,2-bipyridine (1) and 2-chloroquinoline-ICl.

The second subgroup consists of ionic complexes containing polyhalogen ions (2,6-dimethoxypyridinium-ICl_2^-, 2-cyanopyridinium- ICl_2^-). Instead of co-crystallising the starting materials, the formation of pyridinium ions and ICl_2^- could be observed. There are several suggested mechanisms which could explain the formation of polyhalogen anions. One of the mechanisms suggests that these ions could be formed due to the presence of water in the reaction system. As reported by Philbrick[130] upon hydrolysis of ICl (equations 1, 2), ICl_2^- anion is present as the main form of iodine in concentrated solution.

$$ICl + H_2O \rightleftharpoons IOH + HCl$$

$$ICl + HCl \rightleftharpoons [ICl_2]^- + H^+$$

The occurrence of polyhalogen anions in the final complexes and therefore in the reaction system is most likely to occur due to the traces of water present in the solvent (ethanol) used in the preparation of the product. To compensate for the negative charge, the corresponding pyridinium complexes are occurring.

Among the complexes in this subgroup, the main difference that can be observed is that for the 2,6-dimethoxypyridinium- ICl_2^- there is a hydrogen bond between the pyridinium cation and the polyhalogen anion, while in the 2-cyanopyridinium complex, there are no hydrogen bonds between the organic cations and the corresponding anion. The variation in the bond distance for I-Cl1, I-Cl2 in 2,6-dimethoxypyridinium- ICl_2^- is due to the presence of N1-H1···Cl1 hydrogen bond. This hydrogen bond causes the elongation of the bond length in I-Cl1, while the I1-Cl2 bond is shorter because Cl2 is not included a hydrogen bond or in any of the non-covalent interactions. (Table 3.14.2)

The bond distance between iodine and both of chlorine atoms in 2-cyanopyridinium- ICl_2^- is approximately equal. This is the result ICl_2^- not involved in any kind of supramolecular interactions, rather an N-H···N hydrogen bond links two organic bases, from which one is positively charged and the other is neutral.

Table (3.14.2) Geometrical parameters of ICl_2^- ions in 2,6-dimethoxypyridinium- ICl_2^- and 2-cyanopyridinium- ICl_2^- complexes

Crystalline complexes	**I-Cl1**	**I-Cl2**
2,6-dimethoxypyridinium- ICl_2^-	2.6041(5)	2.5177(6)
2-cyanopyridinium- ICl_2^-	2.5531(6)	2.5540(6)

The third subgroup (crystalline complexes from the starting material**)** consists of only one sample. Instead of the expected halogen-bonded complex, only the starting material crystallised from the reaction solution. The absence of the complex could be explained by several possible reasons. First of which attributed to two chlorine atoms in 2,6-dichloropyridine, which are considerably strong electron-withdrawing groups and hence they reduce the electron density on N atom of the pyridine ring. Besides, the ortho- positions of chlorine atoms also assist to prevent N atom of the pyridine ring from attacking ICl by the steric hindrance.

Complexes in which no suitable crystalline material was obtained could be characterised by other techniques to determine the presence of the halogen bond in the complex. In this work, UV-VIS and ATR-FTIR spectroscopy were used. Even though the new bond is formed between the iodine from ICl moiety and the nitrogen from pyridine ring, which can be observed using IR spectroscopy below 500 cm^{-1}, the complexes were not studied in such a way because there was no access to the instrument with a suitable detection range.

Therefore, the research has been focused on the influence of addition ICl to the starting material by comparison of the pyridine ring vibrations generally, and N=C bond particularly, to determine whether ICl interacts with the pyridine N atom. If the N atom is involved in a non-covalent or supramolecular interaction then part of its electron density should be transferred into that interaction, thus weakening the bonds already present in the compound. In FTIR spectrum it would mean that wavenumber corresponding to C=N bond should be moved toward lower wavenumbers (Table 3.14.3) and for UV-VIS spectroscopy that band characteristic for an organic base should be shifted towards higher wavelengths because XB acceptors are electron donors (Lewis bases), some of the electron density is redistributed into the halogen bond interaction. (Table 3.14.3 and 3.14.4)

Table (3.14.3) Wavenumbers of selected bands in ATR-FTIR spectra correlated with specific bonds of the starting materials (St. m.) and the corresponding ICl complexes (C.)

Starting material	ν(C=N), cm^{-1}		ν(C=C), cm^{-1}		ν(C-H), cm^{-1}	
	St. m	C.	St. m	C.	St. m.	C.
3,5-difluoropyridine	1577	1561	1476	1437	3101	3072
3,5-dichloropyridine	1423	1407	1555	1535	3070	3039
2,6-dimethoxypyridine	1530	1483	1545	1548	3102	3011
4-methoxypyridine	1547	1500	1616	1604	3110	3098
3-fluoropyridine	1576	1557	1645	1605	3054	3036
2-fluoropyridine-3-iodopyridine	1556	1511	1579	1585	3024	3083
2-fluoropyridine-4-iodopyridine	1578	1540	1645	1583	3056	3082
2-fluoropyridine-5-iodopyridine	1557	1568	1579	1592	3055	3045
2-cyanopyridine	1462	1434	1578	1587	3060	3062
1,10-phenanthroline	1502	1496	1586	1545	3058	3052
Quinoxaline	1530	1494	1630	1608	3038	3021
2-chloroquinoline	1493	1449	1585	1564	3054	3058

As known from the complexes characterised by X-ray diffraction, two different types of interactions were observed, halogen bond and hydrogen bond. In systems like 3,5-fluoropyridine-ICl where the halogen bond is present, the band of the starting material was shifted from 1577 cm^{-1} to 1561 cm^{-1} and this shift confirms the bonding between 3,5-fluoropyridine and ICl. On the other hand, using the starting material such as 2,6-dimethoxypyridine the shift was also observed (from 1530 cm^{-1} to 1483 cm^{-1}) upon the addition of ICl to the starting material, but this was due to the presence of N-H···Cl hydrogen bond. The same shift occurs with C=C band and C-H band, respectively. This shifting

towards lower wavelengths refers to an interaction of the interhalogens (ICl) with N atom of the pyridine ring, which as result of the resonance and the conjugation on the pyridine ring and this leads to a decrease of the double bond feature and due to the presence of the electron-withdrawing group on the ring which caused decreasing the electron density reducing bond order. [131,132]

Table (3.14.4) Wavelengths of selected bands in UV-VIS spectra of the starting materials (St. m.) and the corresponding ICl complexes (C.)

Starting material	$\lambda_{(Starting\ material)}$ /nm	$\lambda_{(Complex)}$ /nm
3,5-difluoropyridine	303	451
3,5-dichloropyridine	335	458
2,6-dimethoxypyridine	316	-
4-methoxypyridine	328	442
3-fluoropyridine	303	386
2-fluoropyridine-3-iodopyridine	316,445	369, 469
2-fluoropyridine-4-iodopyridine	351	326, 438
2-fluoropyridine-5-iodopyridine	317,448	434
2-cyanopyridine	305	346, 440
1,10-phenanthroline	308	343, 435
Quinoxaline	323, 460	440
2-chloroquinoline	319, 460	439

This new band confirms the formation of the halogen bonded complex. Even though in the IUPAC list of features it is listed that the formation of the halogen bonds usually moves the absorption bands to lower wavelengths, for these systems, the opposite effect is noticed. In other words, λ_{max} of the starting material was shifted towards higher wavelengths, which is

called a bathochromic or a red shift. This shift could be observed because of adding the saturated groups such as amine, hydroxyl and halogens to the chromophores. It should be noted that there is a possibility of observing peaks below 300 nm, but since the spectra were collected from 300 to 800 nm, only peaks appearing in this region will be used for interpretation of structural features. Complexes that had the structure characterised by single crystal X-ray diffraction, have distinctive UV-VIS spectra. Samples that contain a N···I-Cl halogen bond (3,5-difluoropyridine-ICl, 3,5-dichloropyridine-ICl and 4-methoxypyridine-ICl) have a single and a more intense peak when compared to complexes containing polyhalogen ions (2,6-dimethoxypyridine-ICl_2^-, 2-cyanopyridine-ICl_2^-). This peak intensity could be correlated with the charge-transfer feature of the halogen bond. When either halogen or a hydrogen bond are present in the sample, the charge transfer component is more significant than just the electrostatic interactions that can be observed in ionic complexes. The position of the peak could also be correlated with observed interaction strength, in case of 4-methoxypyridine complex, the peak is at 386 nm, while for the 3,5-difluoropyridine-ICl and 3,5-dichloropyridine-ICl where the XB interactions are much weaker, the peaks are positioned at 451 and 458 nm, respectively. For the ICl_2^- containing complexes, it has been observed that the peak is of a much lower intensity and positioned from 440-450 nm. These peak positions could be attributed to an equilibrium between ICl_2^- and iodide ions, as reported by Kazantseva et al.[133] The exception to this trend is observed in 2-cyanopyridine-ICl_2^- where two intense peaks can be observed. These peaks could be explained by the presence of hydrogen bonds which have the charge transfer component, as well. Based on peak shapes, positions and intensities in their UV-VIS spectra, it would be reasonable to assume that 3-fluoropyridine-ICl, 2-fluoro-3-iodopyridine-ICl, 2-fluoro-4-iodopyridine-ICl, 2-fluoro-3-iodopyridine-ICl and quinoxaline-ICl complexes are halogen-bonded, Figure

(3.14.2). On the other hand, 1,10-phenantroline should contain ICl_2^- ion in the structure (Figure 3.14.3).

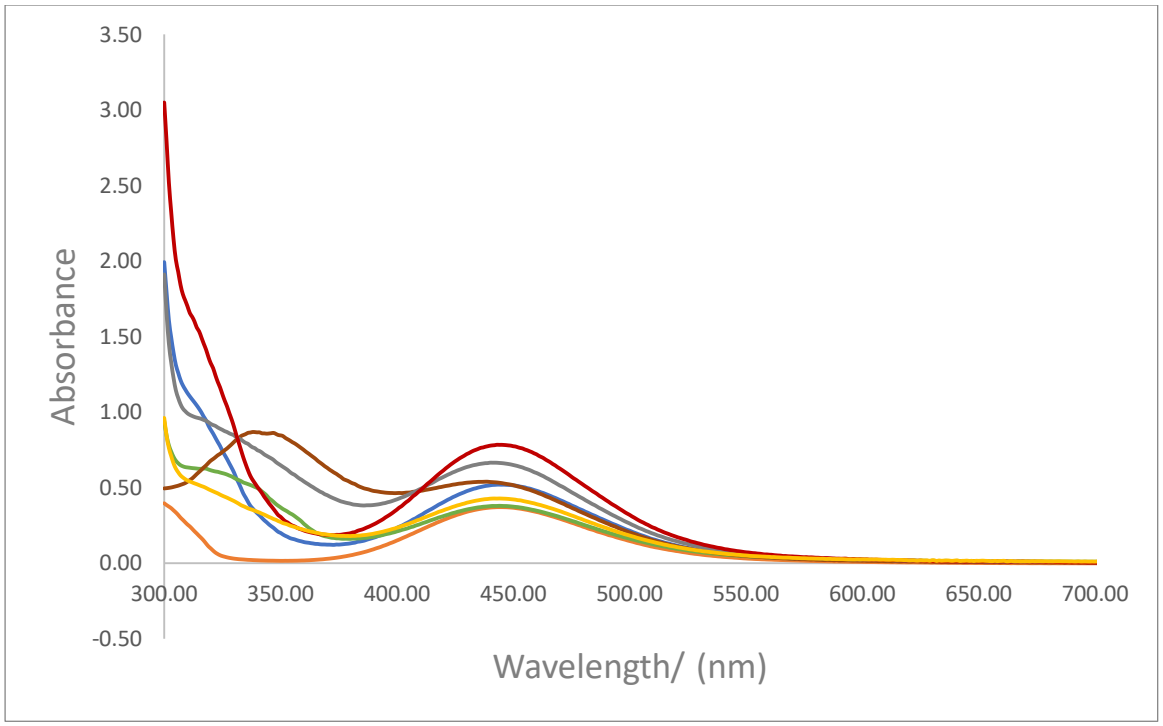

Figure (3.14.2) UV-VIS spectra of 3,5-difluoropyridine-ICl (Blue), 3,5-dichloropyridine-ICl (Orange), 2-fluoro-3-iodopyridine-ICl (Green), 2-fluoro-4-iodopyridine-ICl (Gold), 2-fluoro-5-iodopyridine (Brown), Quinoxaline-ICl (Silver), 2-chloroquinoline-ICl (Red), the spectra were collected using methanol as the solvent, the concentration of the samples was 10^{-3} M.

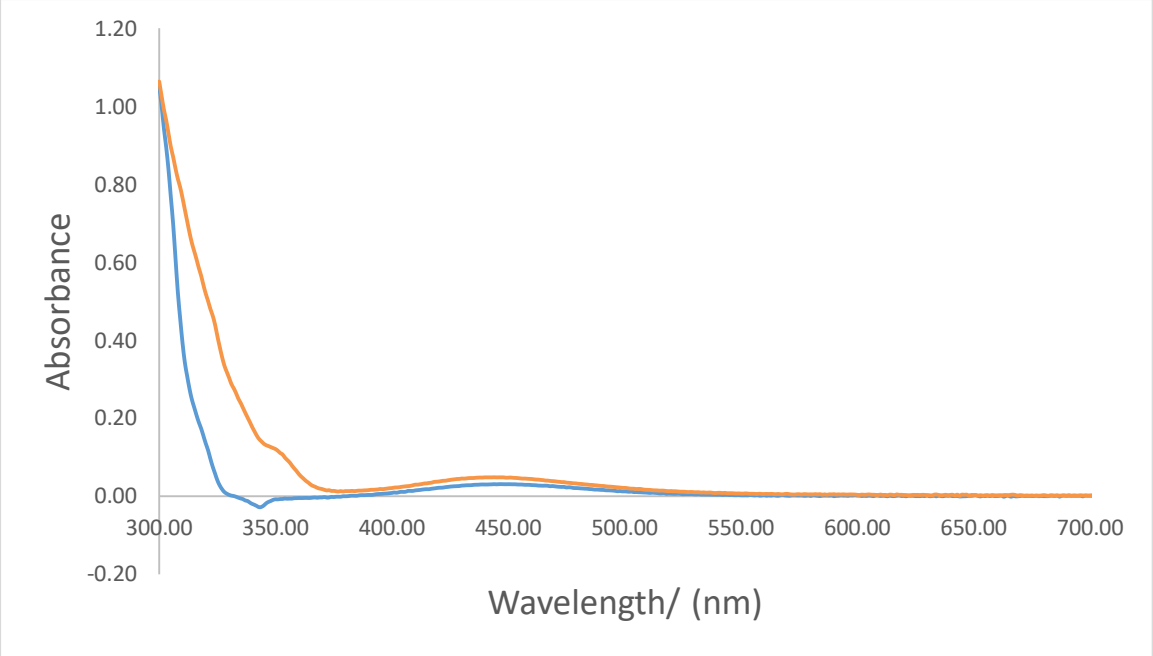

Figure (3.14.3) UV-VIS spectra of 2,6-dimethoxypyridine-ICl_2^- (Blue) and 1,10-phenantroline- ICl_2^- (Orange), the spectra were collected using methanol as the solvent, the concentration of the samples was 10^{-3} M.

Chapter (4)
Iodine monobromide

4.1. Introduction.

Heteronuclear interhalogens can form a variety of compositions (XY, XY_3, XY_5, XY_7). All the dinuclear interhalogens are known, as well as their thermal stabilities. ClF is very stable, IBr and ICl moderately, while BrCl dissociates easily. Compounds with more than one Y atom are fluorides, except for ICl_3.[126,134] Iodine monobromide is formed by the direct combination of the comprising elements. In the gas phase, IBr bond distance determined by microwave spectroscopy is 2.4691 Å.[27] At room temperature, IBr is a black crystalline material with a melting point of 41 °C and boiling point of 116 °C.[126,134]

Recently, Jones et al.[129] reported a rare phenomenon of colossal negative thermal expansion when they redetermined the structure of a pyridine-IBr complex. That system has positive thermal expansion along a and c axes and a negative one along the b axis. Such a phenomenon is observed due to the temperature-induced weakening of C-H···Br hydrogen bond, which then causes the rearrangement in the packing of the complexes.

The IBr containing XB complexes are much less represented in the literature than the corresponding ICl and I_2 ones.[112,106] Some of the reasons for this could be that IBr the charge separation is in between of the I-X (Cl, Br, I) dihalogens, with ICl having the better charge separation because of the higher electronegativity of a chlorine atom and thus higher possibility of forming XB complexes in borderline systems. On the other hand, even if I_2 is a non-polar and has no charge separation at all, it is often used because it is a homonuclear molecule. Moreover, Montis et al.[135] reported that they experienced problems regarding the IBr reactivity, frequently leading to scarce reproducibility and formation of unexpected products, which was observed in this work, as well. Even though XB complexes containing IBr with a variety of XB acceptors (P, S, As, Se) have been reported,[112] only the ones containing N···IBr introduction will be presented in Table 4.0.1.

Table 4.0.1 Geometric parameters of literature reported N···I-Br halogen bonded complexes, adapted from ref.[106,112]

REFCODE	Complex name	N···I (Å)	I-Br (Å)	N···I-Br (°)
TAGNIZ[118]	Cis N, N-bis (Bromoiodo)-2,2-bipyridine	2.461	2.577	175.84
TASPEJ[136]	2,5-bis(2-Pyridiniumyl)-3,6-bis(2-pyridyl) pyrazine bis(iodobromide)	2.405 2.410	2.595 2.588	175.14 173.99
PYIOBR03[129]	Pyridine-IBr	2.304	2.653	178.57
SOWDOZ[137]	[S)-2-(1,8-naphthalimido)-2-quinuclidin-3-y] xCHCl3	2.279	2.678	178.17
ZESSAU[135]	2-arylselanyl pyridine-IBr	2.411	2.623	178.74

It can be observed that five complexes containing N···I-Br have been reported. The average N···I distance is 2.376 Å, while the value for I-Br bond is 2.621 Å. A complex with refcode SOWDOZ[137] has the shortest N···I value (2.279 Å) that indicates the strongest XB, and the most elongated bond (2.678 Å) is observed in the same system, as well. All the N···I-Br angles with an average value of 176.65°.

4.2- Aim

This chapter aims to prepare and characterise crystalline complexes that contain N···I halogen bond. A range of pyridine derivatives is chosen as XB acceptor, while iodine monobromide serves as XB donor. The organic starting materials are chosen because of the wide range of base strength, which is going to be correlated with the strength of the XB interaction. All the crystalline complexes are going to be characterised by ATR-FTIR spectroscopy, UV-Vis spectroscopy and if the crystal of a suitable size is obtained, single-crystal X-ray diffraction. From the structures obtained by X-ray diffraction the halogen bond lengths and angles within the N···I unit will be determined and correlated with the electronic spectra.

4.3 Investigation of halogen bonded complexes

4.3.1 3,5-difluoropyridine- IBr

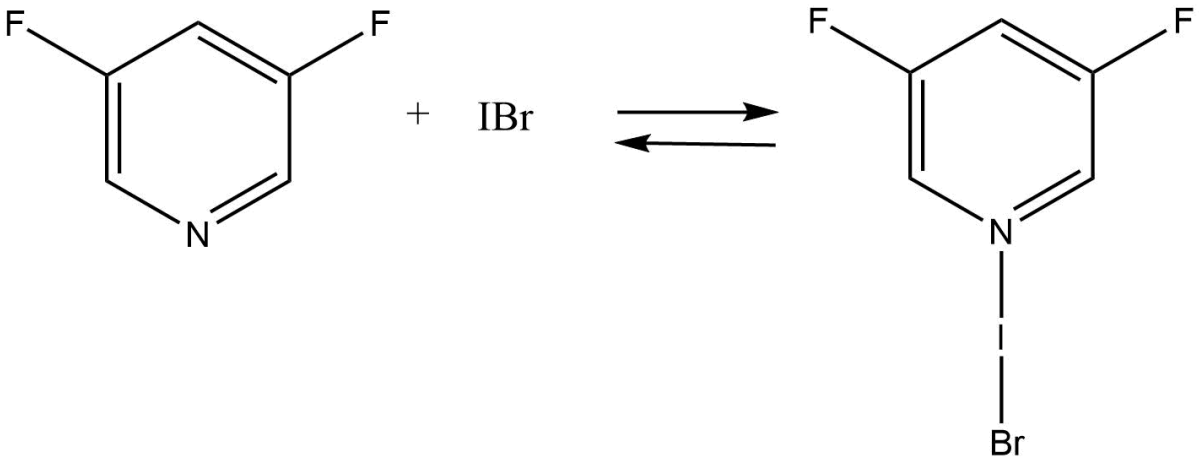

UV-Visible Spectra for 3,5-difluoropyridine-IBr solution

All the spectra were collected using methanol as the solvent, the concentration of the samples was 10^{-3} M. The base 3,5-difluoropyridine absorbs at 303 nm while IBr displays two main absorption bands at 317 nm and 454 nm. When the starting materials are mixed the new band appears at 384 nm. That band is not attributed to the 3,5-difluoropyridine or IBr. Rather, it indicates that the reaction between the starting materials occurred because λ_{max} at 303 nm for 3,5-difluoropyridine was shifted 80 nm toward higher wavelengths (red shift), Figure (4.1.1). Starting material and the resulting complex are also characterised by ATR-FTIR, Figures (3.1.2, 4.1.2).

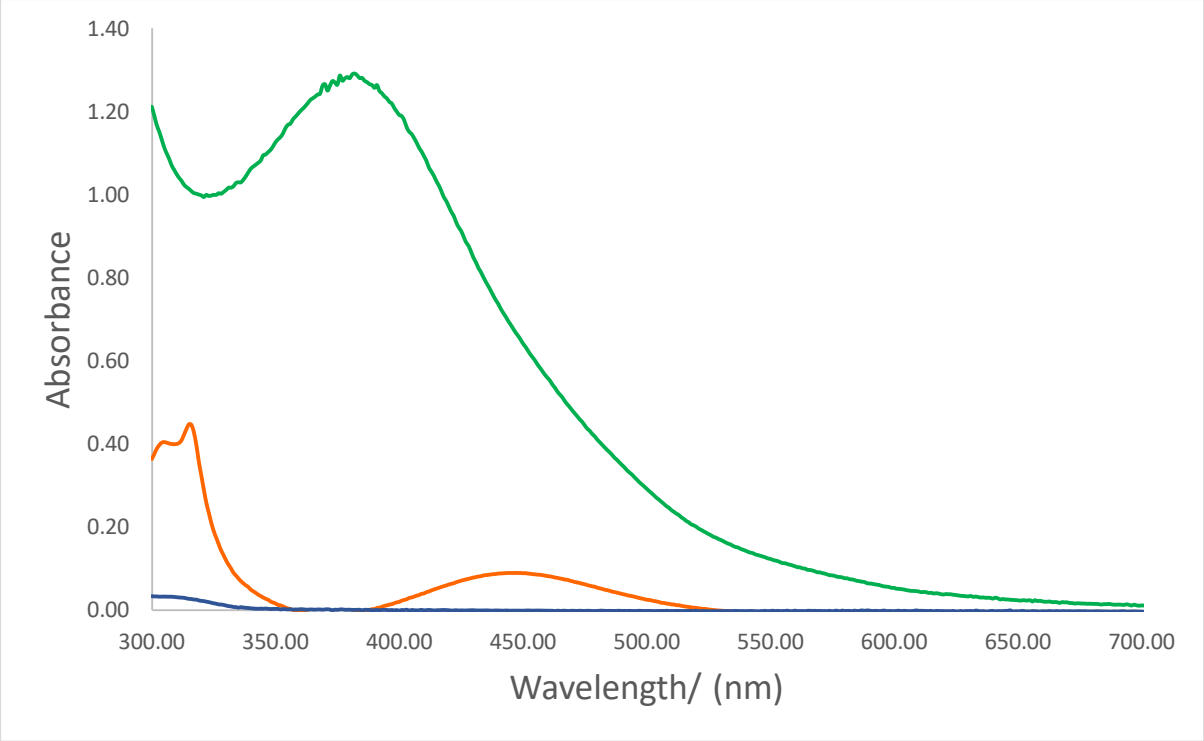

Figure (4.1.1) UV- Visible Spectra of 3,5-difluoropyridine -IBr: 3,5-difluoropyridine (Blue), IBr(Orange), 3,5-difluoropyridine - IBr (Green), the spectra were collected using methanol as the solvent, the concentration of the samples was 10^{-3} M.

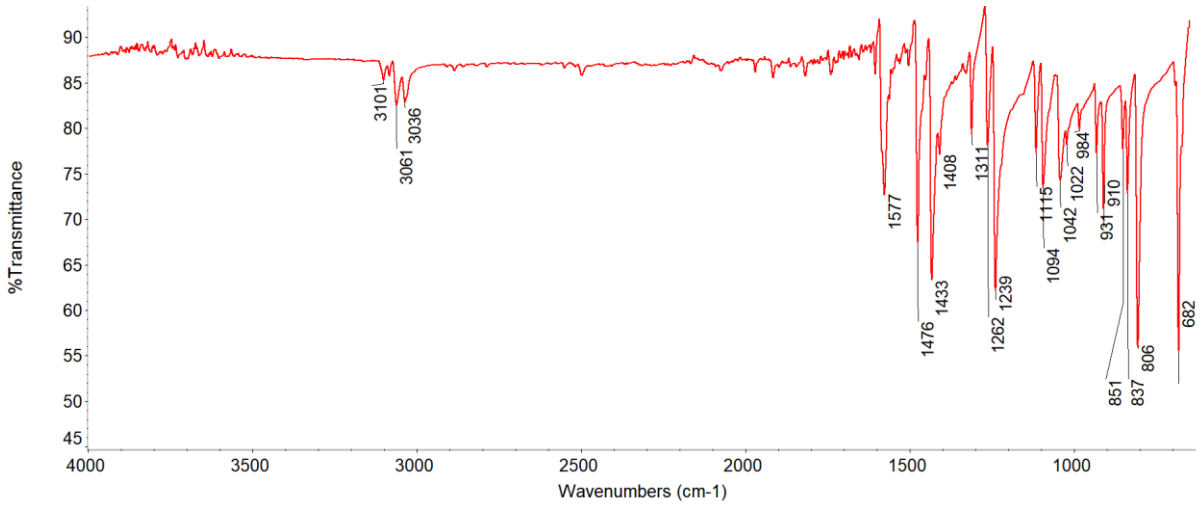

Figure (3.1.2): IR spectrum of 3,5-difluoropyridine.

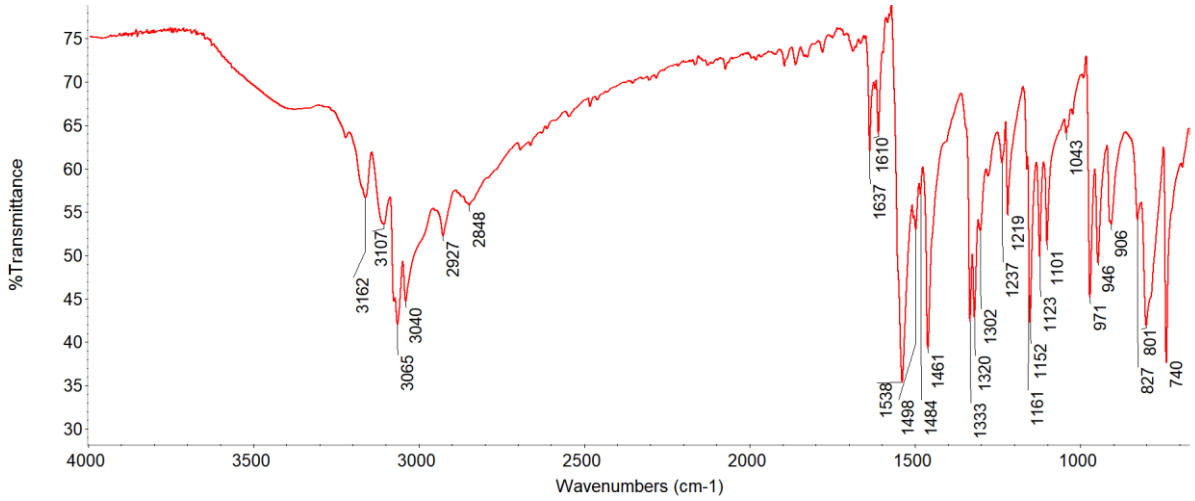

Figure (4.1.2) ATR-FTIR spectrum of 3,5-difluoropyridine-IBr.

4.3.2 3,5-dichloropyridine- IBr

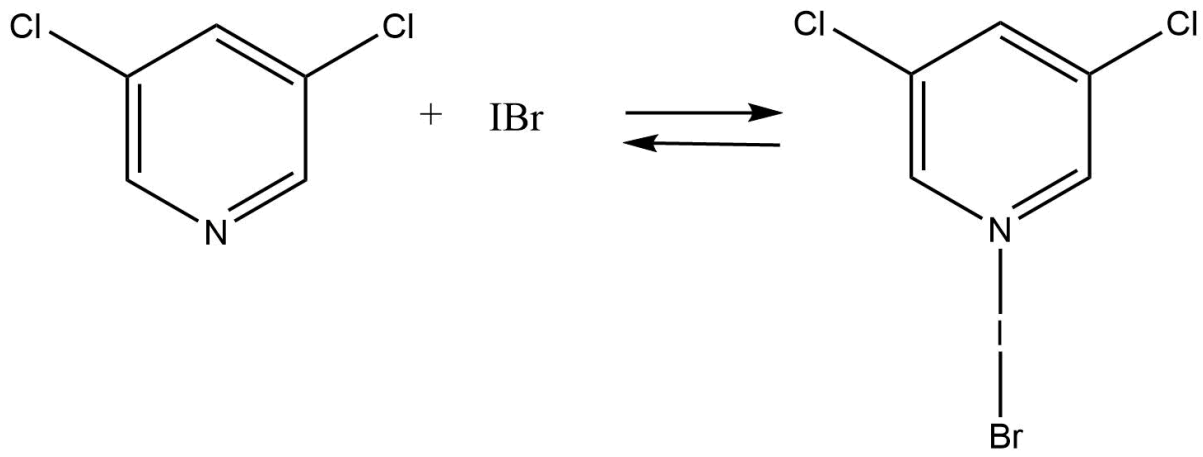

UV-Visible Spectra for 3,5-dichloropyridine-IBr solution

All the spectra were collected using methanol as the solvent, the concentration of the samples was 10^{-3} M. The base 3,5-dichloropyridine absorbs at 335 nm and iodine monobromide IBr at 317 nm and 454 nm. The new band appears at 388 nm when the two above starting materials are mixed. This band, which is not attributed to the 3,5-dichloropyridine or IBr suggests the formation of the halogen bonded complex, λ_{max} for 3,5-dichloropyridine was shifted 53 nm toward higher wavelengths, Figure (4.2.1). Starting material and the resulting complex are also characterised by ATR-FTIR, Figures (3.2.2, 4.2.2).

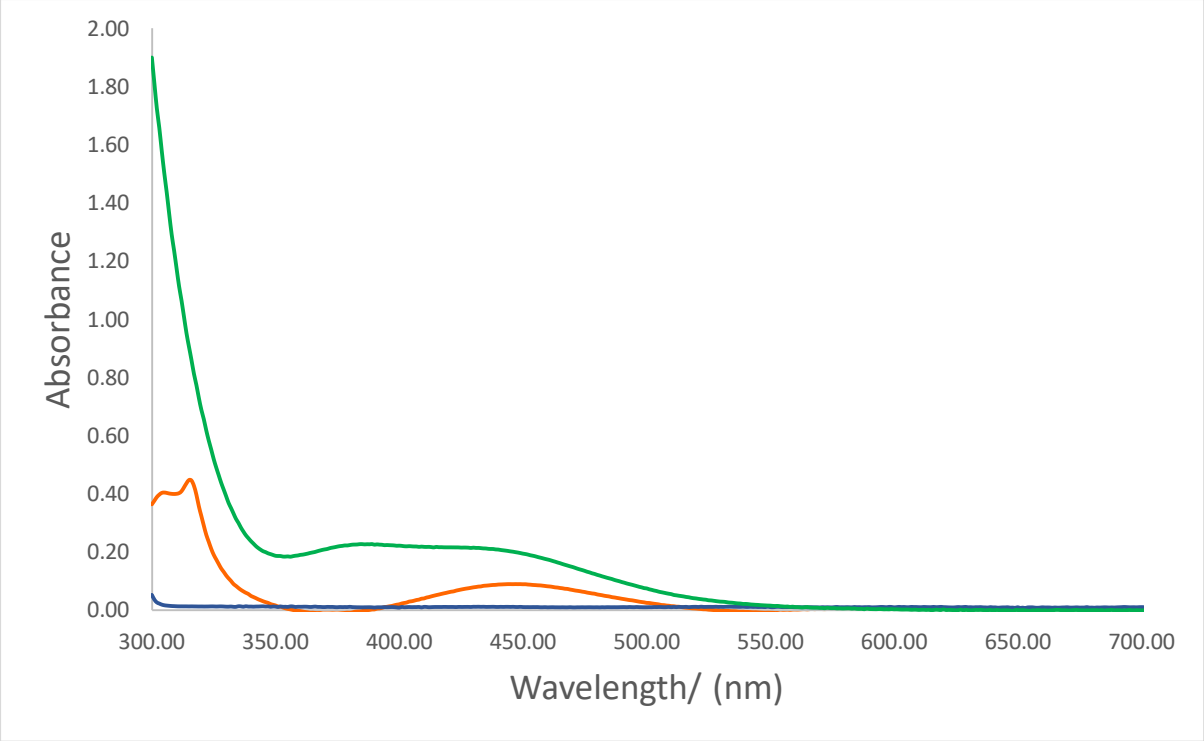

Figure (4.2.1) UV- Visible Spectra of 3,5-dichloropyridine-IBr: 3,5-dichloropyridine (Blue), IBr (Orange), 3,5-dichloropyridine- IBr (Green), the spectra were collected using methanol as the solvent, the concentration of the samples was 10^{-3} M.

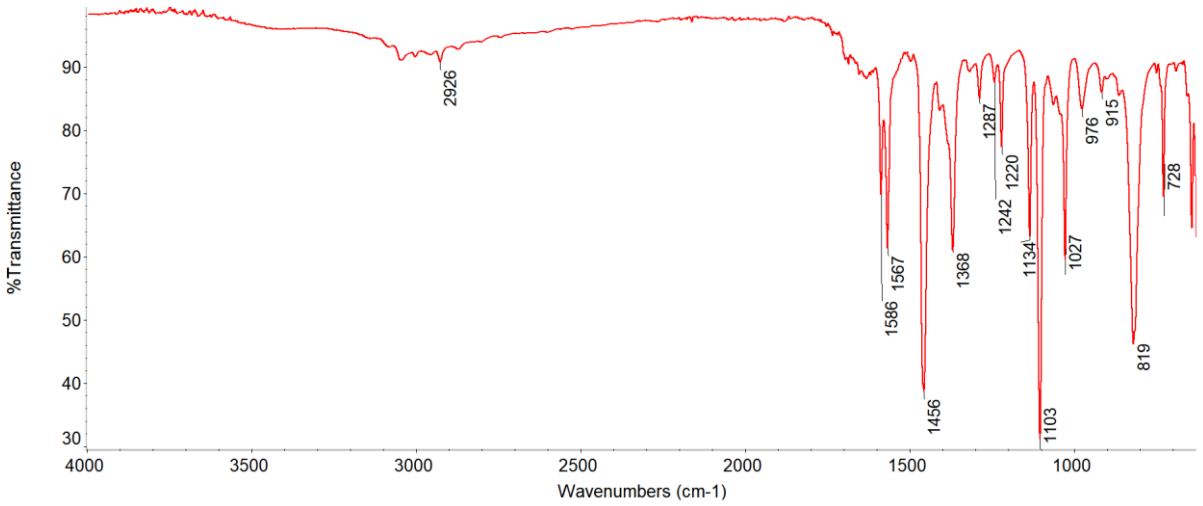

Figure (3.2.2): IR spectrum of 3,5-dichloropyridine.

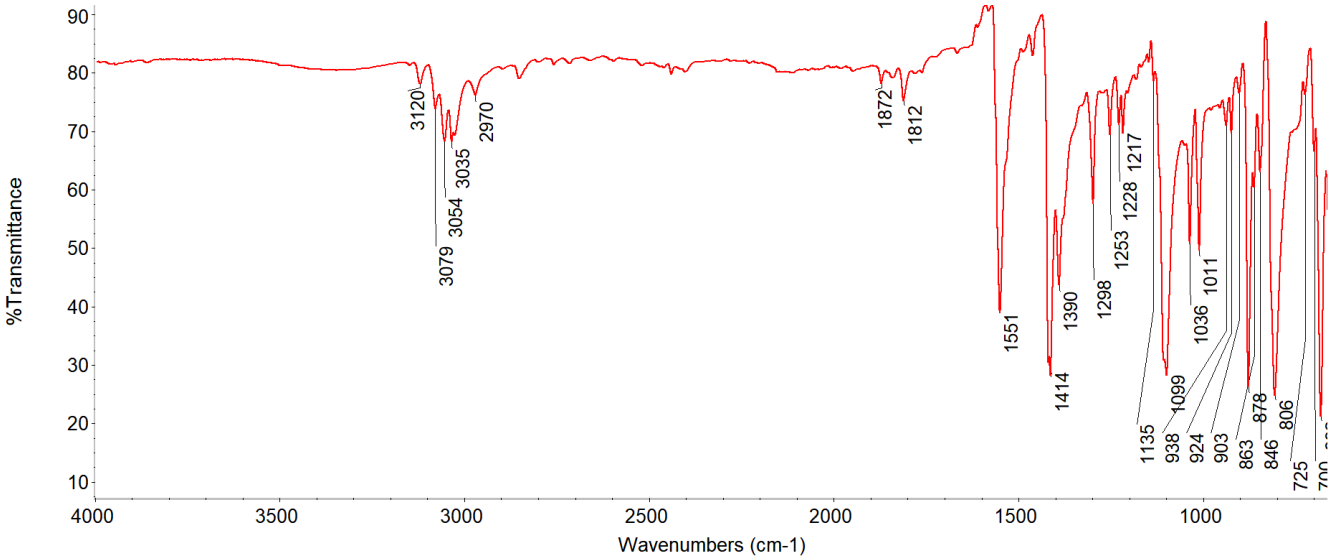

Figure (4.2.2) ATR-FTIR spectrum of 3,5-dichloropyridine-IBr.

4.3.3 2,6-dichloropyridine- IBr

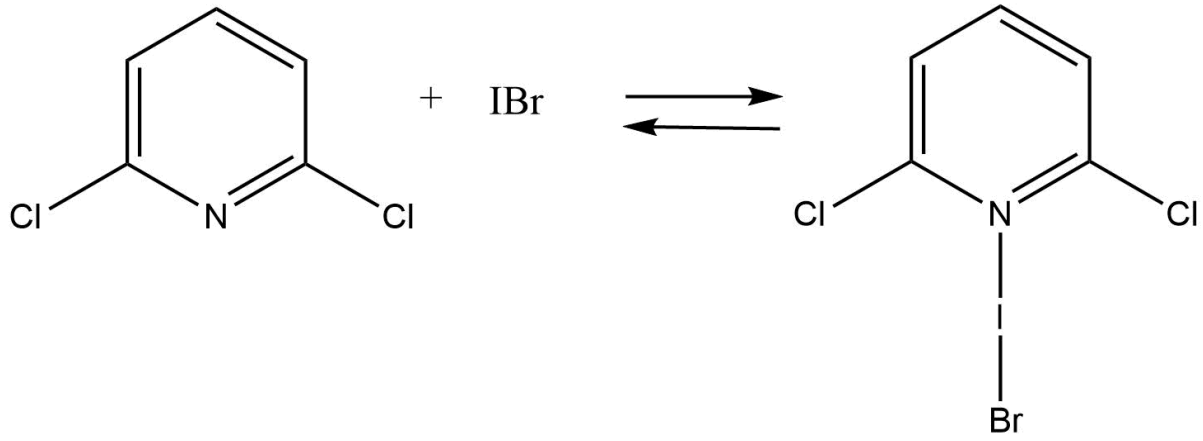

UV-Visible Spectra for 2,6-dichloropyridine-IBr solution

All the spectra were collected using methanol as the solvent, the concentration of the samples was 10^{-3} M. The base 2,6-dichloropyridine absorbs at 335 nm and IBr absorbs at 317 nm and 454 nm. The new band appears at 434 nm when the two above starting materials are mixed which is not attributed to the 2,6-dichloropyridine or IBr. λ_{max} for 2,6-dichloropyridine was shifted 99 nm toward higher wavelength because of XB interaction with IBr Figure (4.3.1).Starting material and the resulting complex are also characterised by ATR-FTIR, Figures (3.3.1, 4.3.2).

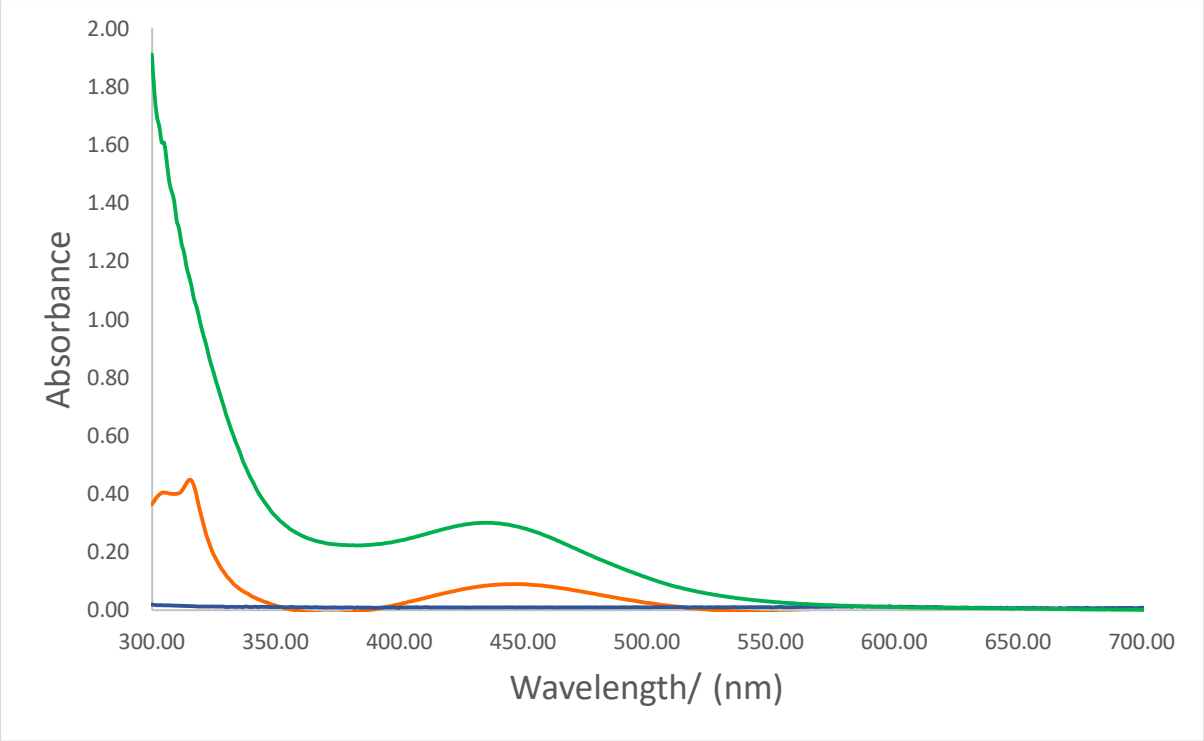

Figur (4.3.1) UV-Visible Spectra of 2,6-dichloropyridine-IBr : 2,6-dichloropyridine (Blue), IBr(Orange), 2,6-dichloropyridine- IBr (Green), the spectra were collected using methanol as the solvent, the concentration of the samples was 10^{-3} M.

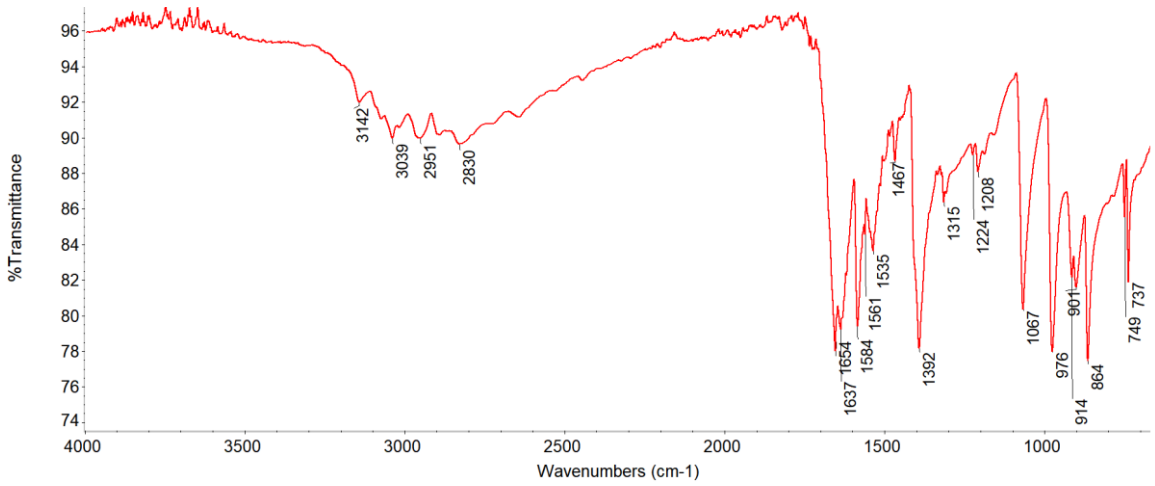

Figure (3.3.1) ATR-FTIR spectrum of 2,6-dichloropyridine

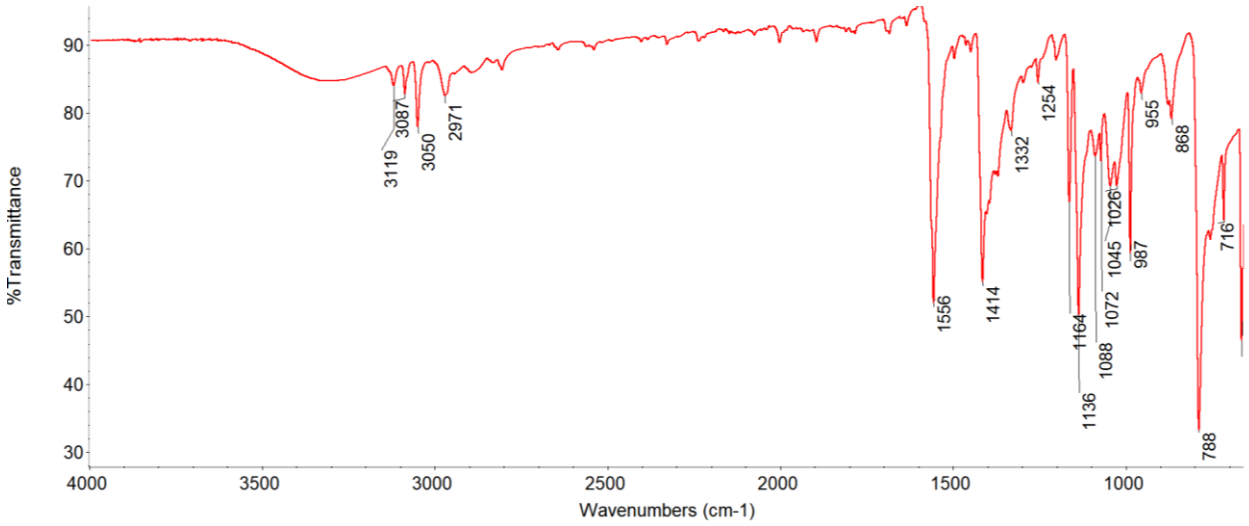

Figure (4.3.2) ATR-FTIR spectrum of 2,6-dichloropyridine-IBr.

4.3.4 2,6-dimethoxypyridine- IBr

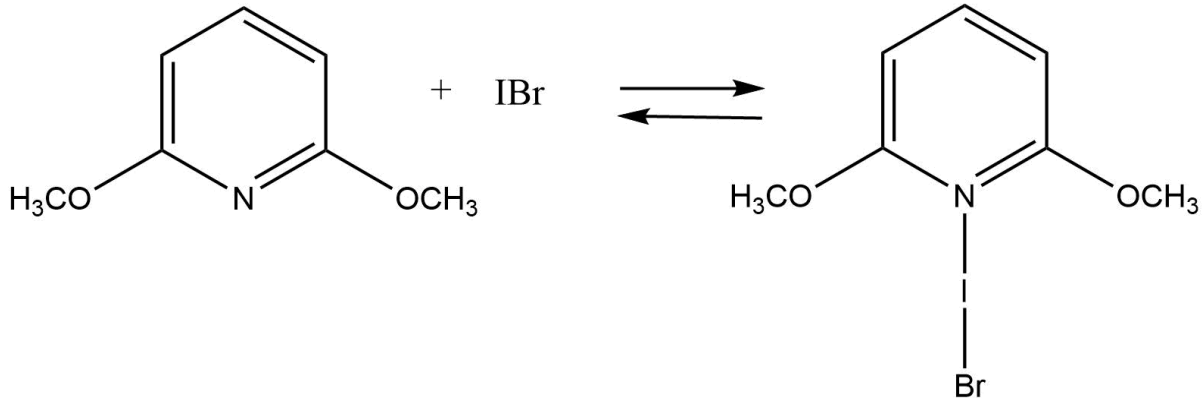

UV-Visible Spectra for 2,6-dimethoxypyridine-IBr solution

All the spectra were collected in methanol, the concentration of all the samples was 10^{-3} M. The base 2,6-dimethoxypyridine absorbs at 316 nm and iodine monobromide absorbs at 317 nm and 454 nm. The new band appears at 440 nm when the two above starting materials are mixed which is not attributed to the 2,6-dimethoxypyridine or IBr. λ_{max} for 2,6-dimethoxypyridine was shifted 124 nm toward higher wavelengths, Figure (4.4.1) Starting material and the resulting complex are also characterised by ATR-FTIR, Figures (3.4.2, 4.4.2).

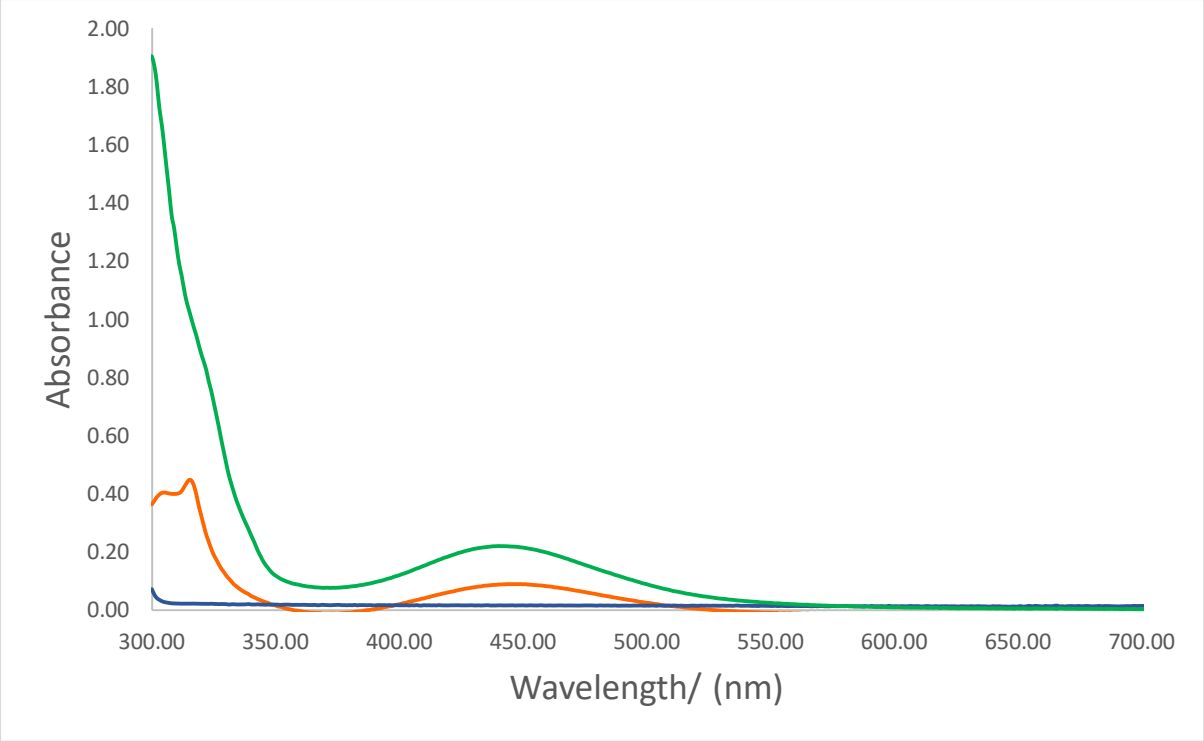

Figure (4.4.1) UV- Visible Spectra of 2,6-dimethoxypyridine -IBr : 2,6-dimethoxypyridine (Blue), IBr (Orange), 2,6-dimethoxypyridine - IBr (Green), the spectra were collected using methanol as the solvent, the concentration of the samples was 10^{-3} M.

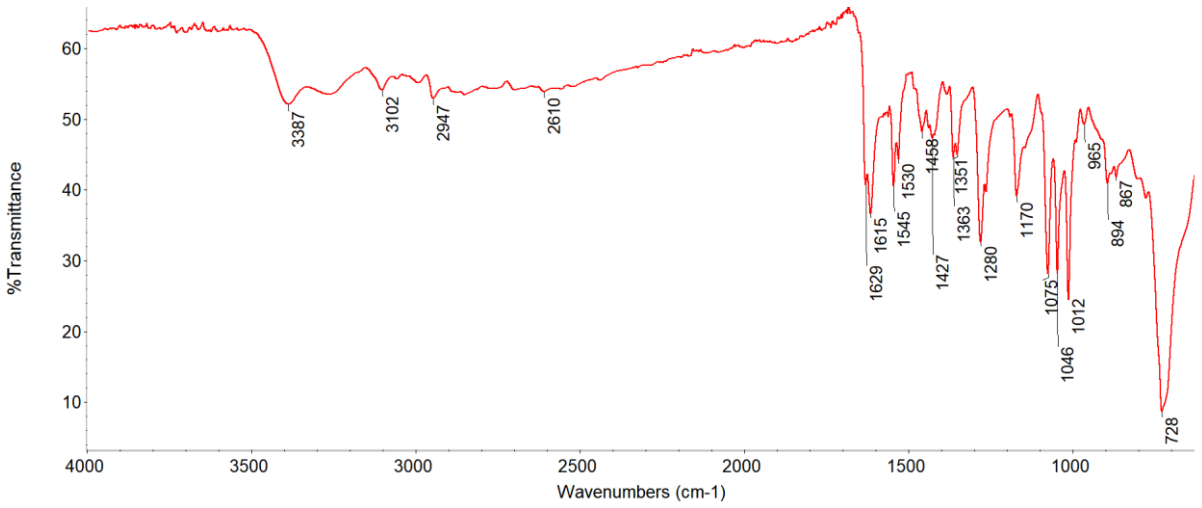

Figure (3.4.2): ATR-FTIR spectrum of 2,6-dimethoxypyridine

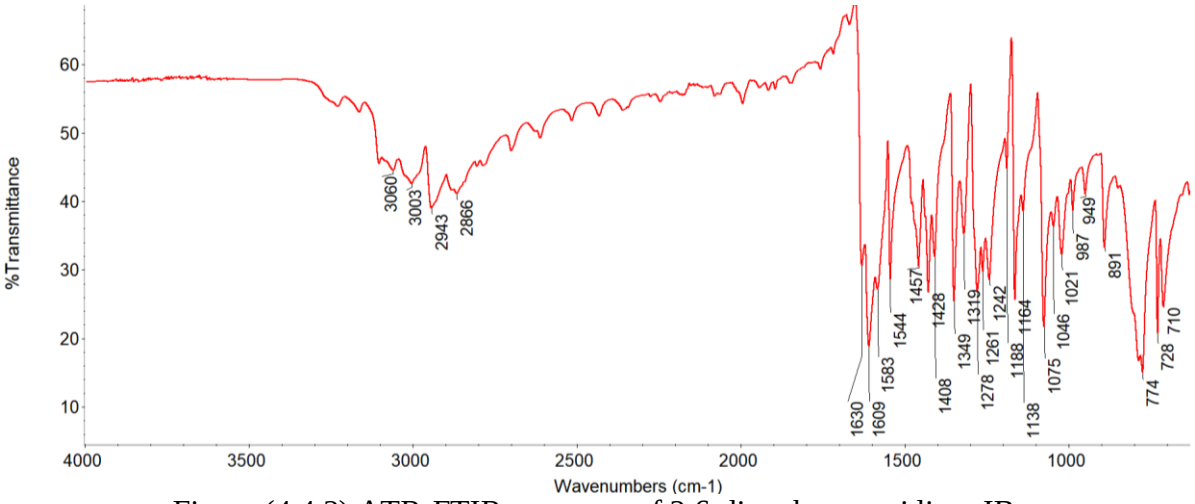

Figure (4.4.2) ATR-FTIR spectrum of 2,6-dimethoxypyridine -IBr

4.3.5 4-methoxypyridine- IBr

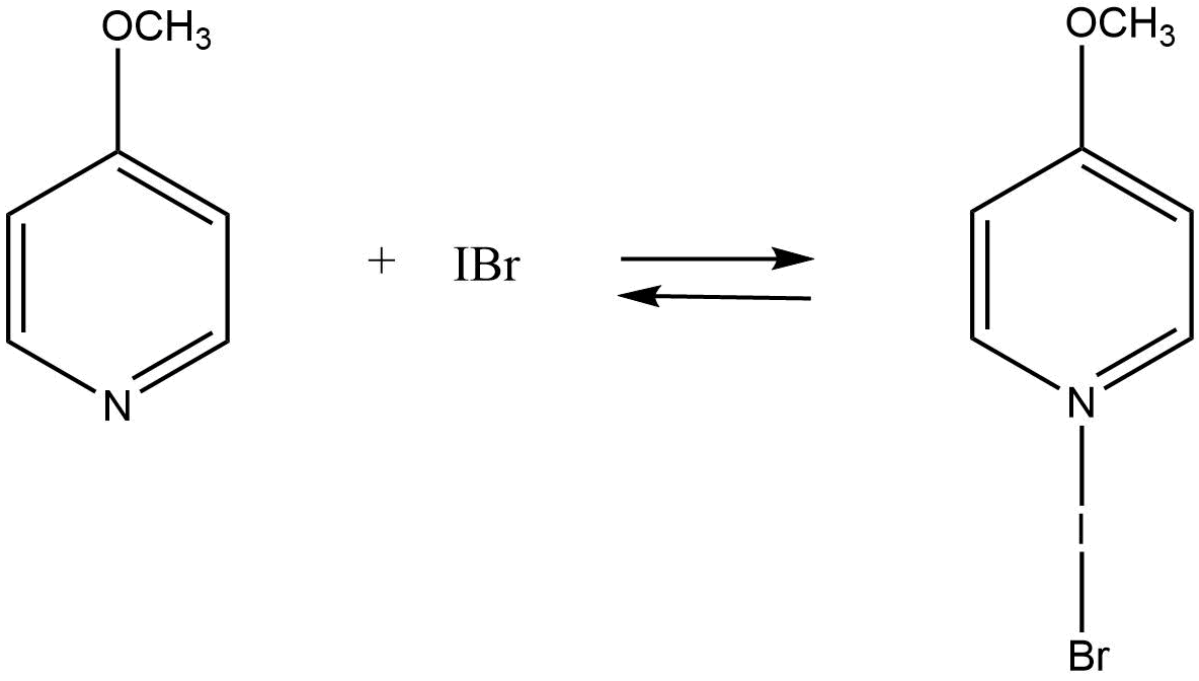

UV-Visible Spectra for 4-methoxypyridine -IBr solution

All the spectra were collected in methanol, the concentration of all the samples was 10^{-3} M. The base 4-methoxypyridine absorbs at 328 nm and iodine monobromide IBr absorbs at 317 nm and 454 nm. A new band appears at 435 nm when the two above starting materials are mixed which is not attributed to the 4-methoxypyridine or IBr. This new band confirms the formation of the halogen bonded complex. That means λ_{max} for 4-methoxypyridine were shifted 107 nm and for IBr were shifted 121 nm toward higher wavelength. Figure (4.5.1). Starting material and the resulting complex are also characterised by ATR-FTIR, Figures (3.5.2, 4.5.2).

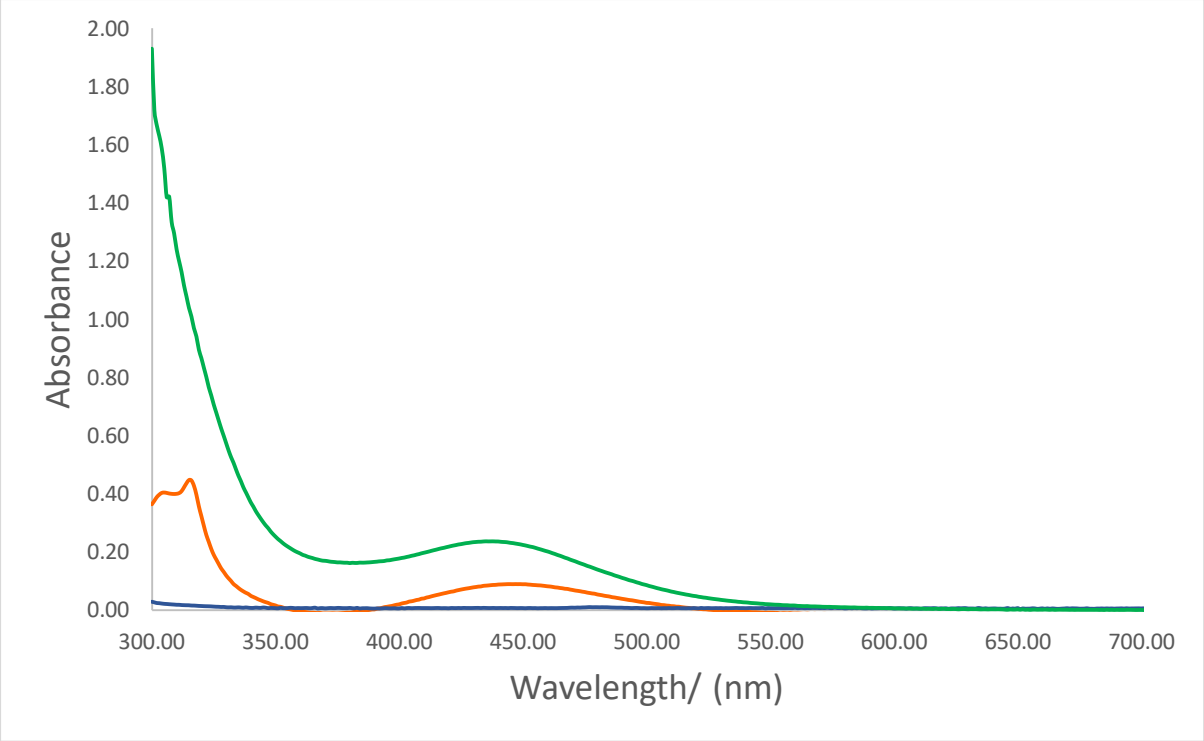

Figure (4.5.1) UV- Visible Spectra of 4-methoxypyridine -IBr : 4-methoxypyridine (Blue), IBr(Orange), 4-methoxypyridine - IBr (Green), the spectra were collected using methanol as the solvent, the concentration of the samples was 10^{-3} M.

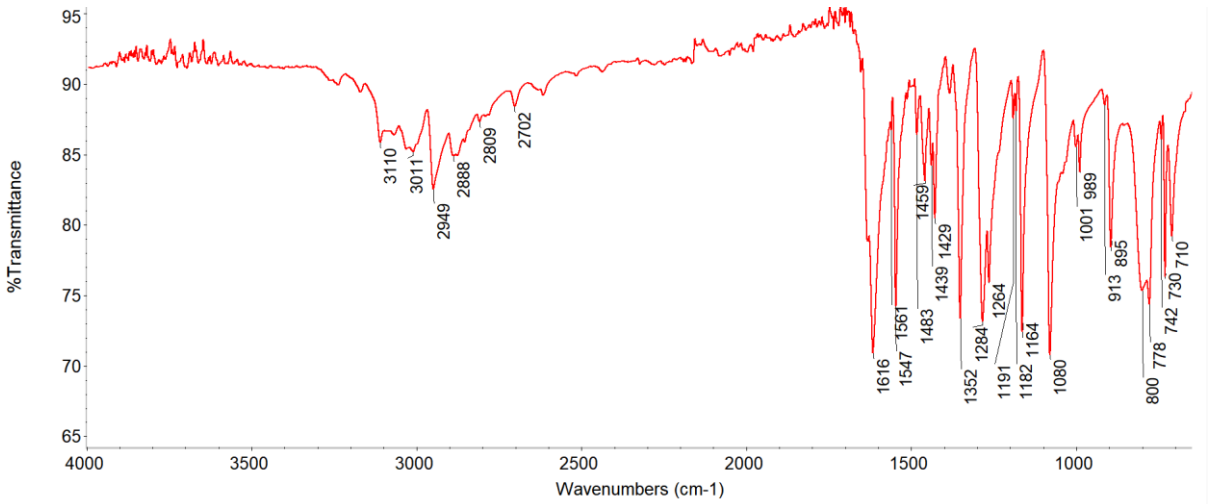

Figure (3.5.2): ATR-FTIR spectrum of 4-methoxypyiridine.

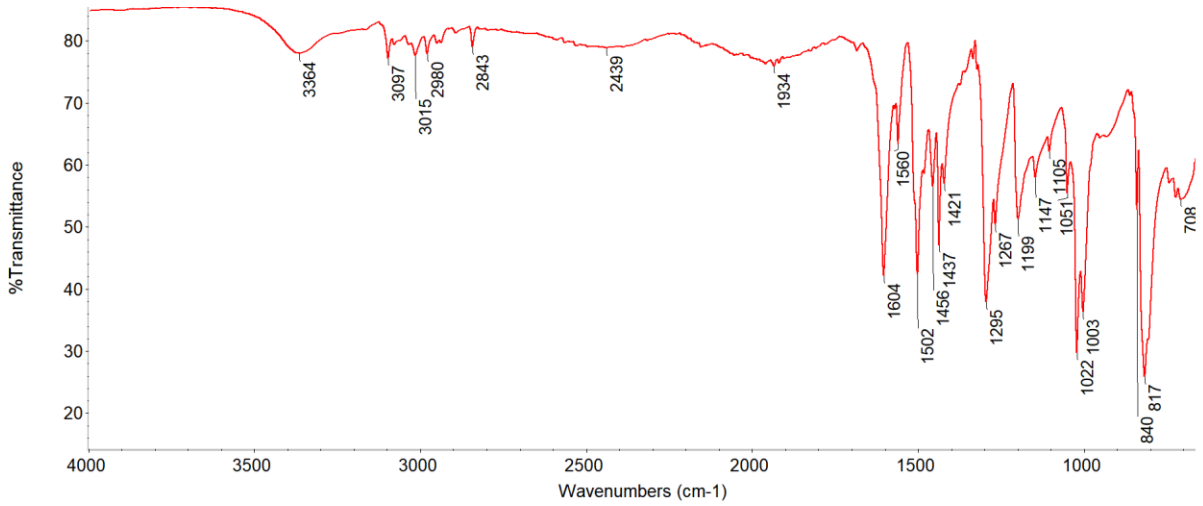

Figure (4.5.2) ATR-FTIR spectrum of 4-methoxypyridine -IBr

4.3.6 3-fluoropyridine- IBr

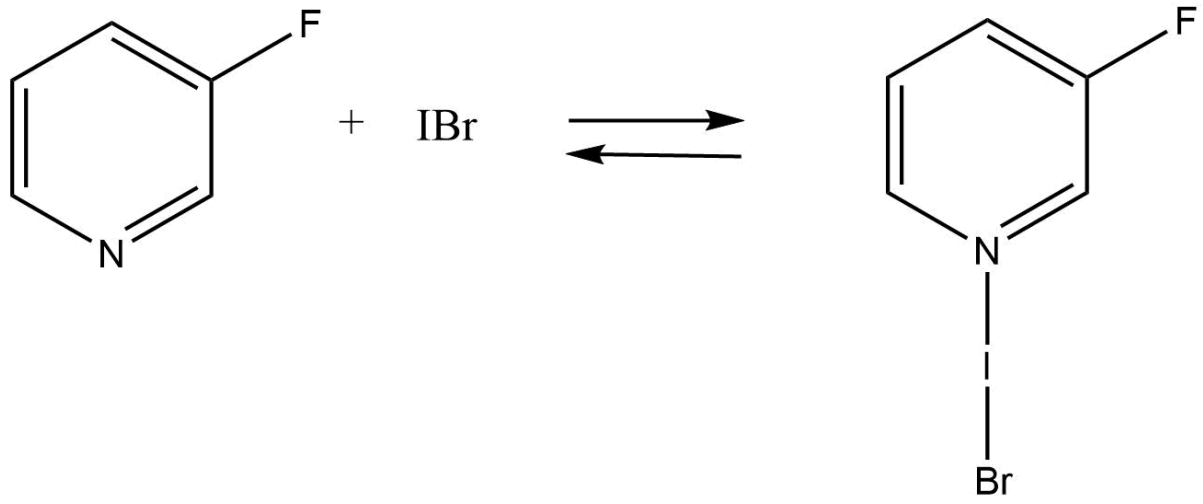

UV-Visible Spectra for 3-fluoropyridine -IBr solution

All the spectra were collected in methanol, the concentration of all the samples was 10^{-3} M. The base 3-fluoropyridine absorbs at 303 nm and iodine monobromide IBr absorbs at 317 nm and 454 nm. A new band appears at 387 nm when the two above starting materials are mixed which is not attributed to the 3-fluoropyridine or IBr. This new band confirms the formation of the halogen bonded complex. That means λ_{max} for 3-fluoropyridine was shifted 73 nm toward higher wavelength which is called bathochromic shift or red shift, Figure (4.6.1.) Starting material and the resulting complex are also characterised by ATR-FTIR, Figures (3.6.2, 4.6.2).

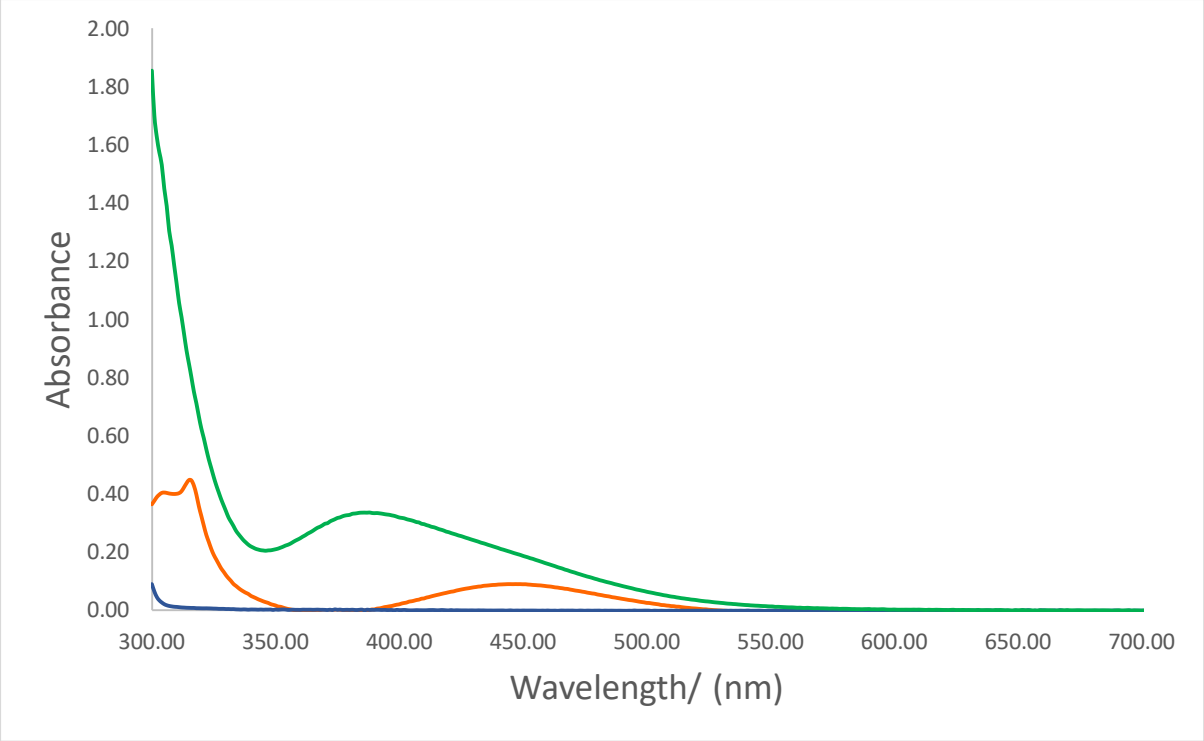

Figure (4.6.1) UV- Visible Spectra of 3-fluoropyridine -IBr : 3-fluoropyridine (Blue), IBr(Orange), 3-fluoropyridine - IBr (Green), the spectra were collected using methanol as the solvent, the concentration of the samples was 10^{-3} M.

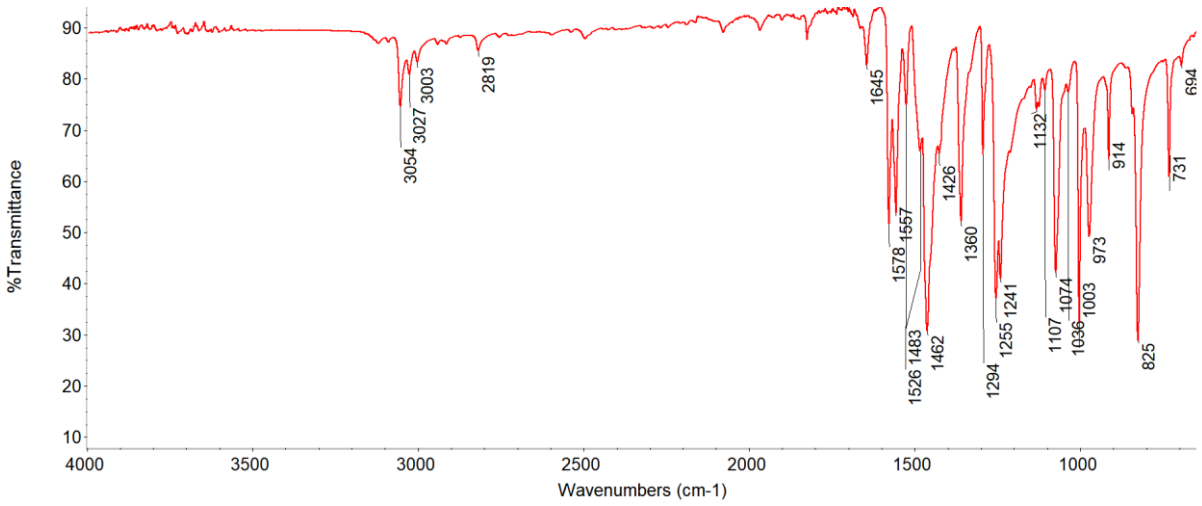

Figure 3.6.2 ATR-FTIR spectrum of 3-fluoropyridine

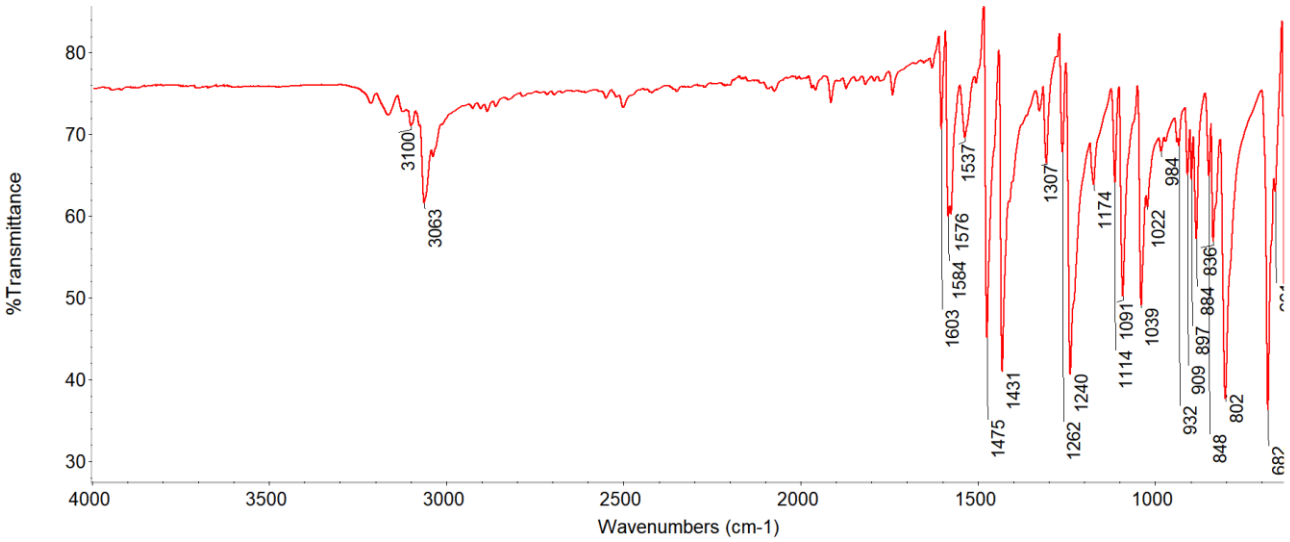

Figure (4.6.2) ATR-FTIR spectrum of 3-fluoropyridine –IBr.

Crystal Structure of 3-fluoropyridine -IBr

Crystallographic data for 3-fluoropyridine are given in Table (4.1), and selected bond lengths and angles in Table (4.2). A thermal ellipsoid plot of the structure together with the numbering scheme used is given in Figure (4.6.3).

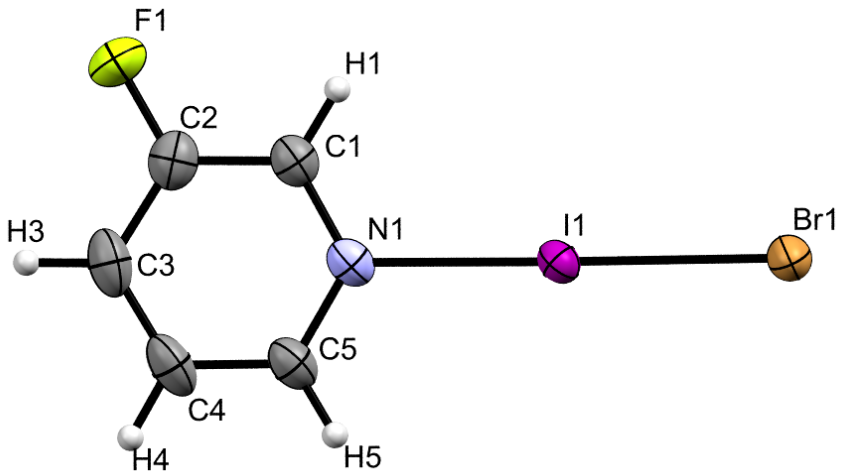

Figure (4.6.3) Thermal ellipsoid plot of 3-fluoropyridine-IBr with atom labelling scheme.

3-fluoropyridine-IBr crystallises in the monoclinic space group $P2_1/c$. The molecule possesses no exact crystallographic symmetry because the pyridine ring shows

crystallographic disorder, with the fluorine atoms being disordered about a pseudo mirror plane, and with refined occupancies of 0.78(1) and 0.22(1).

The 3-fluoropyridine and the IBr moiety interact via N1···I1-Br1 halogen bond. The N1···I1 interaction distance is 2.369(3) Å, which is less than the sum of van der Walls radii of these atoms (3.53 Å).[121] The distance between the iodine atom and bromine atom is 2.6222(5) Å, which is longer than the distance of the starting material (IBr) in gas phase 2.4691 Å[27] and the N1···I1-Br1 angle is 178.93(6). Complexes are packed in pairs, with units within the same pair staying almost in the same plane (Figure 4.6.4), and the adjacent pair in the different plane that intersects the first one at 27.77°. The vertical distance between two parallel planes is 3.456 Å, while the distance between two centroids of pyridine rings is 4.377 Å (Figures 4.6.5 and 4.6.6) No other non-covalent interactions are observed. Even though some (C-H···Br) short contact can be detected (between adjacent pairs C-Br 3.910 Å, and within the pair 3.761 Å) their values are longer than the corresponding ones found in the literature (3.376 Å).[138]

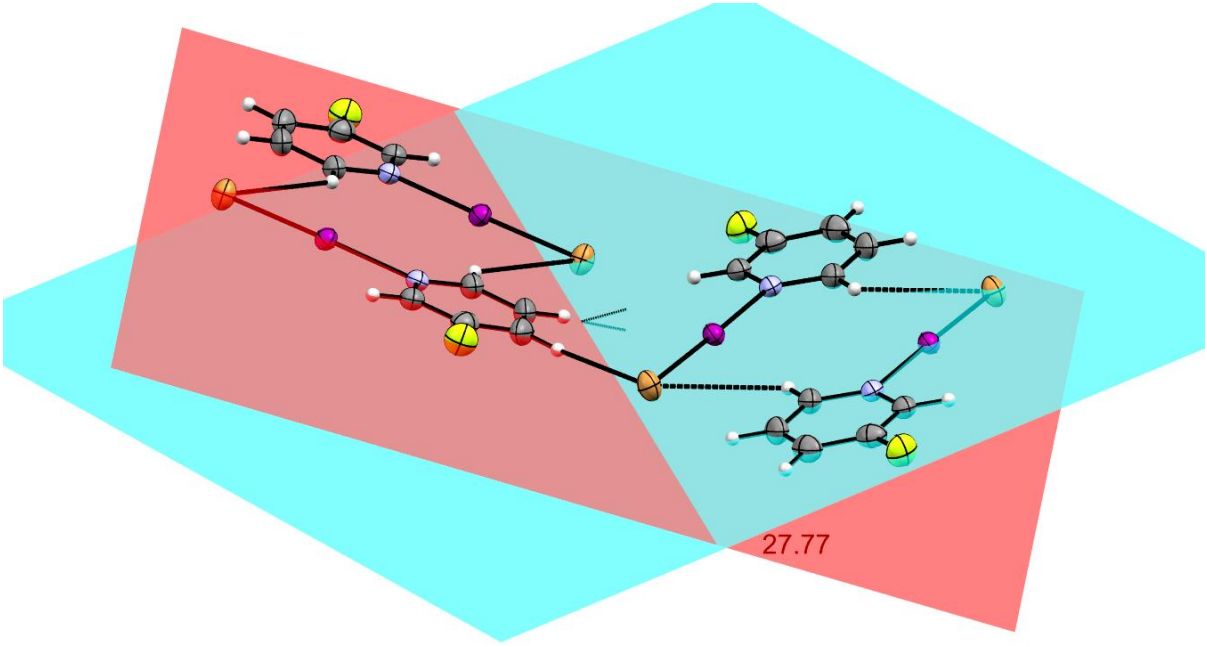

Figure (4.6.4): Packing diagram of 3-fluoropyridine –IBr approximately along to a-axis.

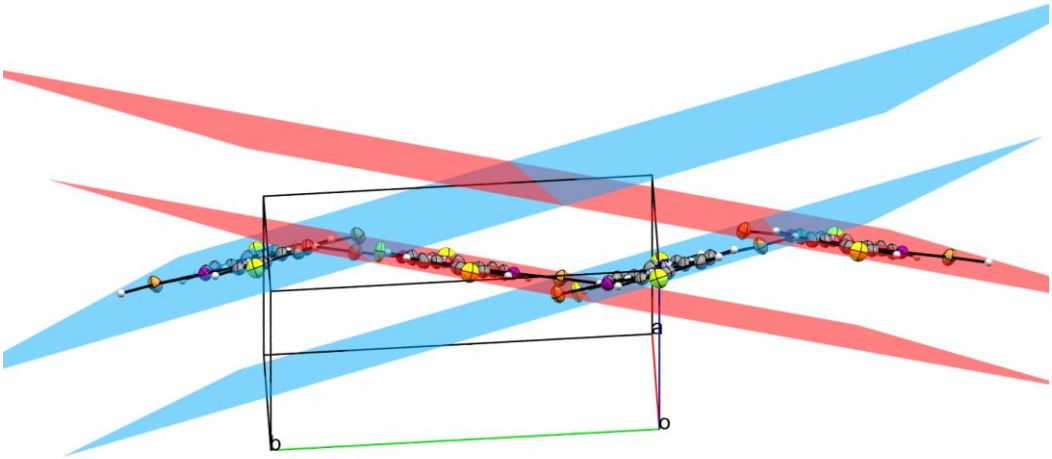

Figure (4.6.5): Packing diagram of 3-fluoropyridine –IBr approximately along to b axis

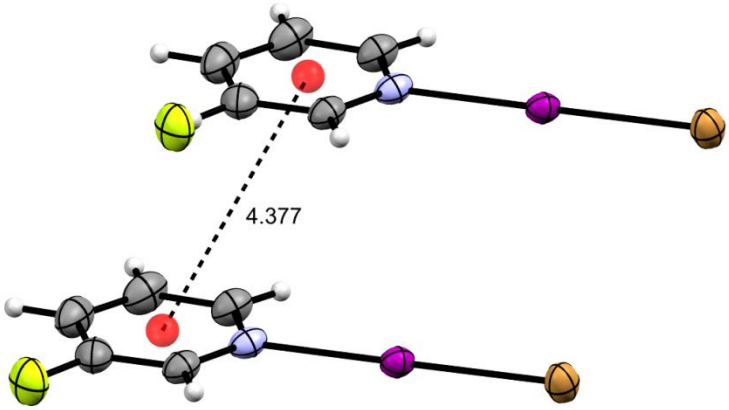

Figure (4.6.6) View showing the distance between the centroids of two 3-fluoropyridine –IBr molecules

Table 4.1: Crystallographic data for the complex 3-fluoropyridine-IBr.

Crystal data	
Chemical formula	C_5H_4BrFIN
M_r	303.90
Crystal system, space group	Monoclinic, $P2_1/c$
T/K	150
a, *b*, *c* (Å)	4.3767 (7), 14.401 (2), 12.2961 (19)
β (°)	97.698 (5)
V/ (Å^3)	768.0 (2)
Z	4
Radiation type	Mo *K*α
μ/ (mm^{-1})	9.30
Crystal size/ (mm)	0.32 × 0.15 × 0.12
Data collection	
Diffractometer	Bruker *APEX*-II CCD
Absorption correction	Multi-scan
T_{min}, T_{max}	0.400, 0.747
No. of measured, independent and observed [$I > 2\sigma(I)$] reflections	16451, 3215, 2721
R_{int}	0.043

$(\sin \theta/\lambda)_{max}$ /($Å^{-1}$)	0.797
Refinement	
$R[F^2 > 2\sigma(F^2)]$, $wR(F^2)$, S	0.033, 0.068, 1.18
No. of reflections	3215
No. of parameters	92
H-atom treatment	H-atom parameters constrained
$\Delta\rho_{max}$, $\Delta\rho_{min}$ /(e $Å^{-3}$)	0.86, −1.20

Table (4.2): Selected interatomic contacts /Å and /^{o} for the complex 3-fluoropyridine-IBr.

Atom1	Atom2	Length	Atom1	Atom2	Atom3	Angle
I1	Br1	2.6222(5)	Br1	I1	N1	178.93(6)
I1	N1	2.369(3)	I1	N1	C5	119.9(2)
N1	C5	1.331(4)	I1	N1	C1	118.5(2)
N1	C1	1.325(4)	C5	N1	C1	121.5(3)
F1	C2	1.289(5)	C4	C3	C2	117.3(4)
C3	C4	1.363(6)	C3	C4	C5	120.3(3)
C3	C2	1.376(6)	N1	C5	C4	120.3(3)
C4	C5	1.382(5)	F1	C2	C3	118.7(4)
C2	C1	1.378(5)	F1	C2	C1	119.7(3)
			C3	C2	C1	121.6(4)
			N1	C1	C2	119.0(3)

4.3.7 2-fluoro- 3-iodopyridine- IBr

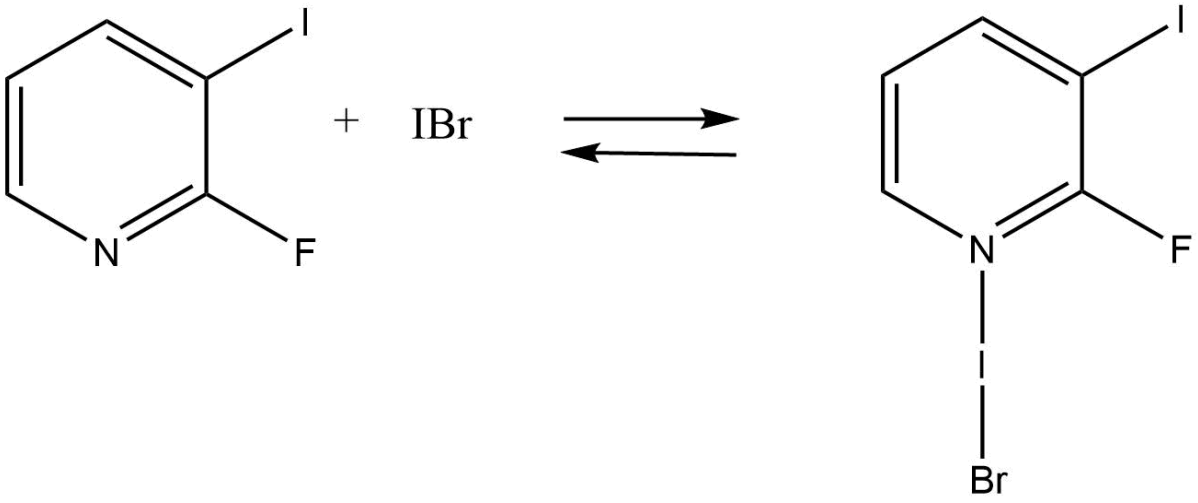

UV-Visible Spectra for 2-fluoro-3-iodopyridine -IBr solution

All the spectra were collected in methanol, the concentration of all the samples was 10^{-3} M. The base 2-fluoro-3-iodopyridine absorbs at 316 nm and iodine monobromide IBr absorbs at 317 nm and 454 nm. A new band appears at 436 nm when the two above starting materials are mixed which is not attributed to the 2-fluoro-3-iodopyridine or IBr. λ_{max} for 2-fluoro-3-iodopyridine was shifted 120 nm higher wavelength, Figure (4.7.1).

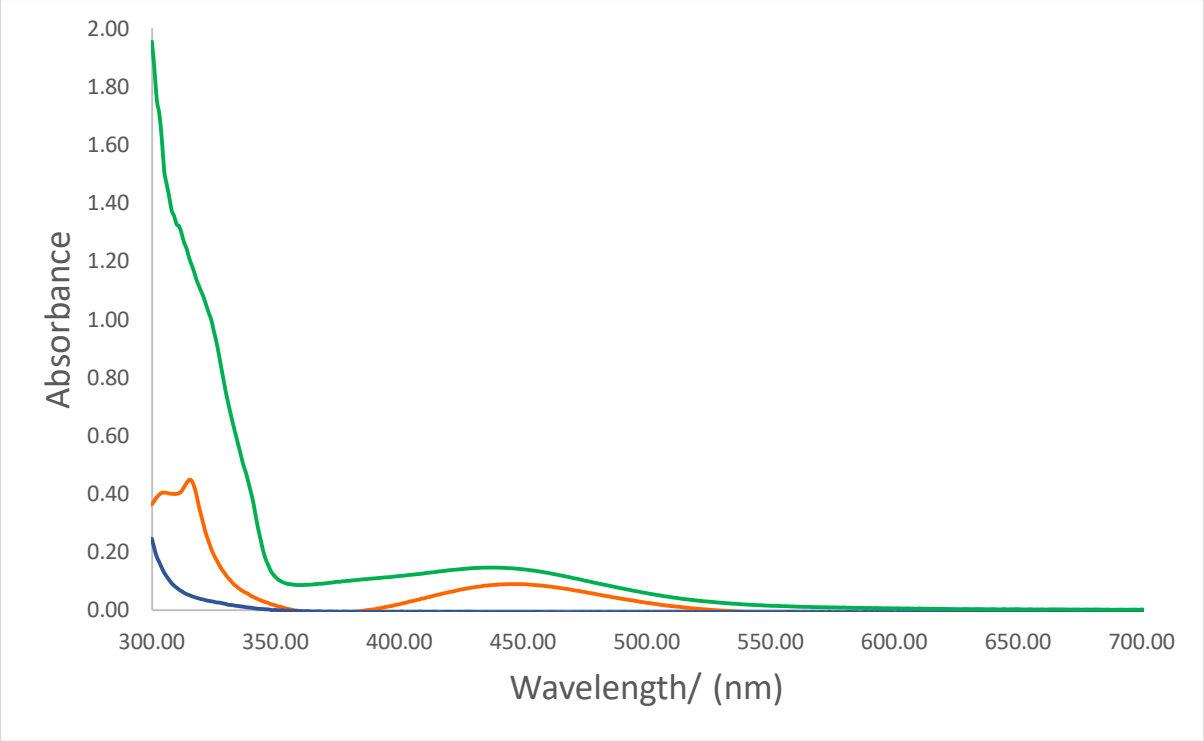

Figure (4.7.1) UV- Visible Spectra of 2-fluoro-3-iodopyridine -IBr : 2-fluoro-3-iodopyridine (Blue), IBr(Orange), 2-fluoro-3-iodopyridine - IBr (Green), the spectra were collected using methanol as the solvent, the concentration of the samples was 10^{-3} M.

4.3.8 2-fluoro- 4-iodopyridine- IBr

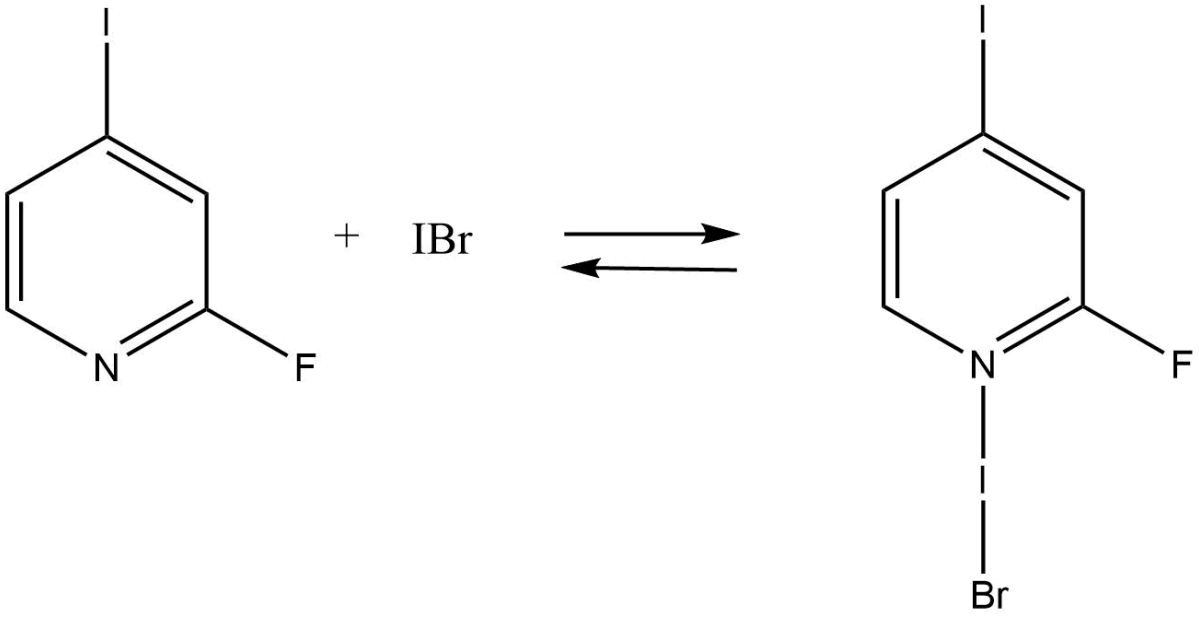

UV-Visible Spectra for 2-fluoro-4-iodopyridine -IBr solution

All the spectra were collected in methanol, the concentration of all the samples was 10^{-3} M. The base 2-fluoro-4-iodopyridine absorbs at 351 nm and iodine monobromide IBr absorbs at 317 nm and 454 nm. The new band appears at 378 nm when the two above starting materials are mixed which is not attributed to the 2-fluoro-4-iodopyridine or IBr. λ_{max} for 2-fluoro-4-iodopyridine were shifted more than 27 nm toward higher wavelength, Figure (4.8.1). Starting material and the resulting complex are also characterised by ATR-FTIR, Figures (3.8.2, 4.8.2).

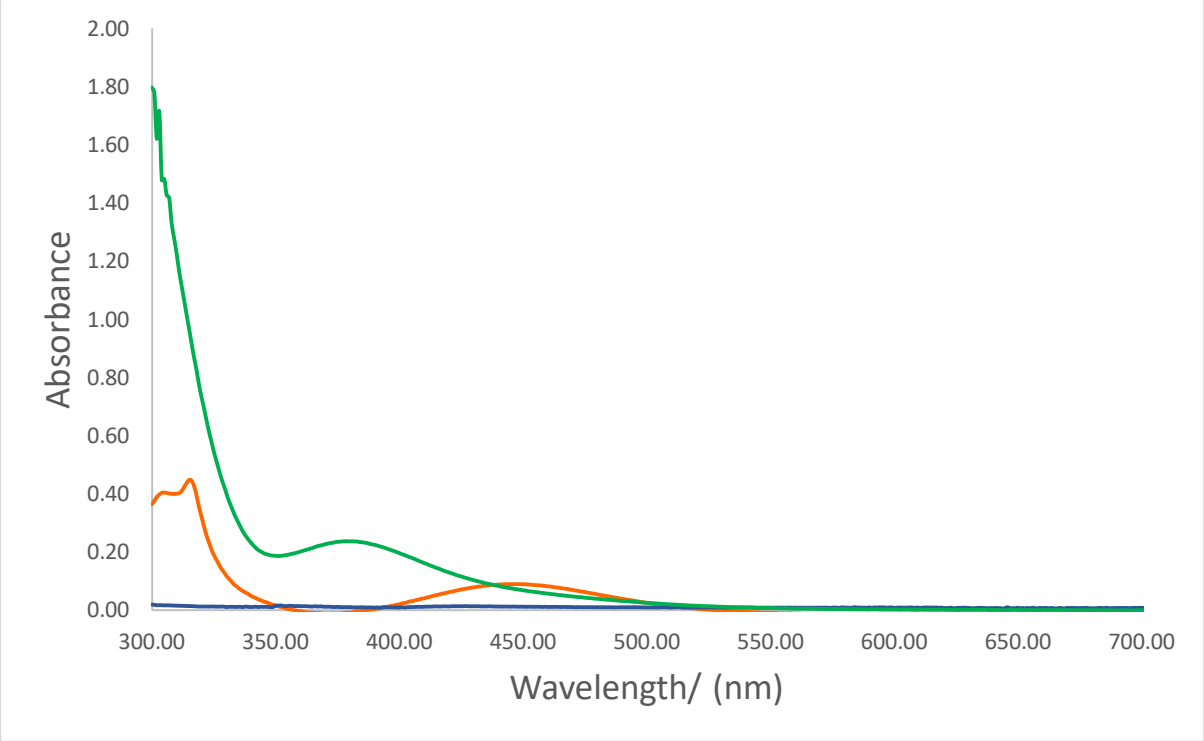

Figure (4.8.1) UV- Visible Spectra of 2-fluoro-4-iodopyridine -IBr : 2-fluoro-4-iodopyridine (Blue), IBr(Orange), 2-fluoro-4-iodopyridine - IBr (Green), the spectra were collected using methanol as the solvent, the concentration of the samples was 10^{-3} M.

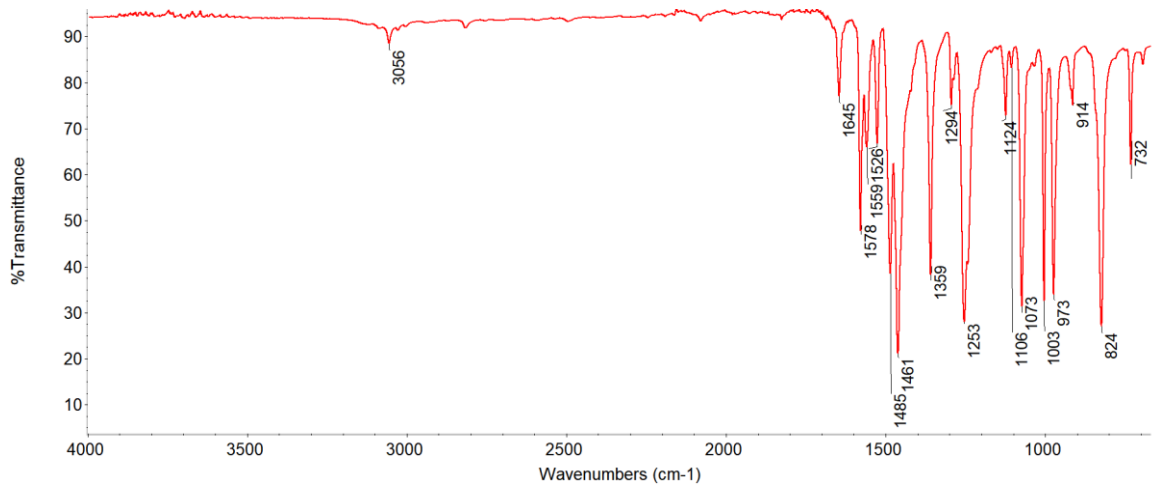

Figure (3.8.2) ATR-FTIR spectrum of 2-fluoro-4-iodopyridine

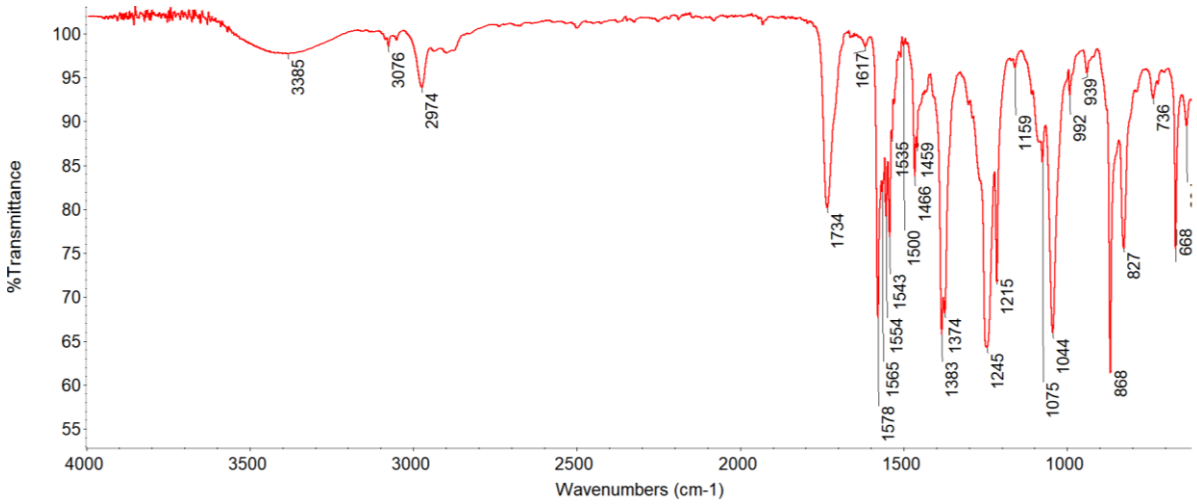

Figure (4.8.2) ATR-FTIR spectrum of 2-fluoro-4-iodopyridine –IBr

4.3.9 2-fluoro- 5-iodopyridine- IBr

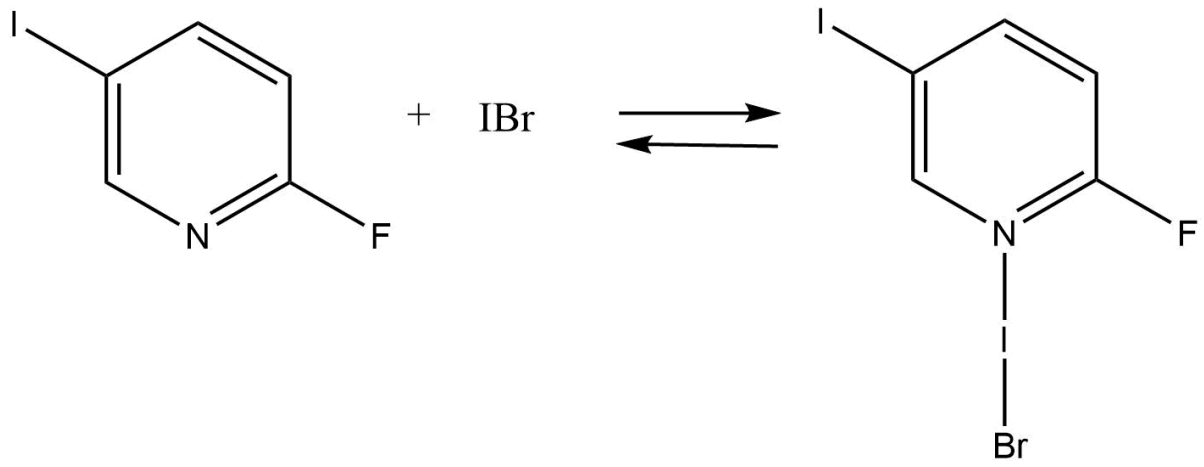

UV-Visible Spectra for 2-fluoro-5-iodopyridine -IBr solution

All the spectra were collected in methanol, the concentration of all the samples was 10^{-3} M. The base 2-fluoro-5-iodopyridine absorbs at 317 nm and iodine monobromide IBr absorbs at 317 nm and 454 nm. The new band appears at 385 nm when the two above starting materials are mixed which is not attributed to the 2-fluoro-5-iodopyridine or IBr. λ_{max} for 2-fluoro-5-iodopyridine were shifted 68 nm toward higher wavelength, Figure (4.9.1).

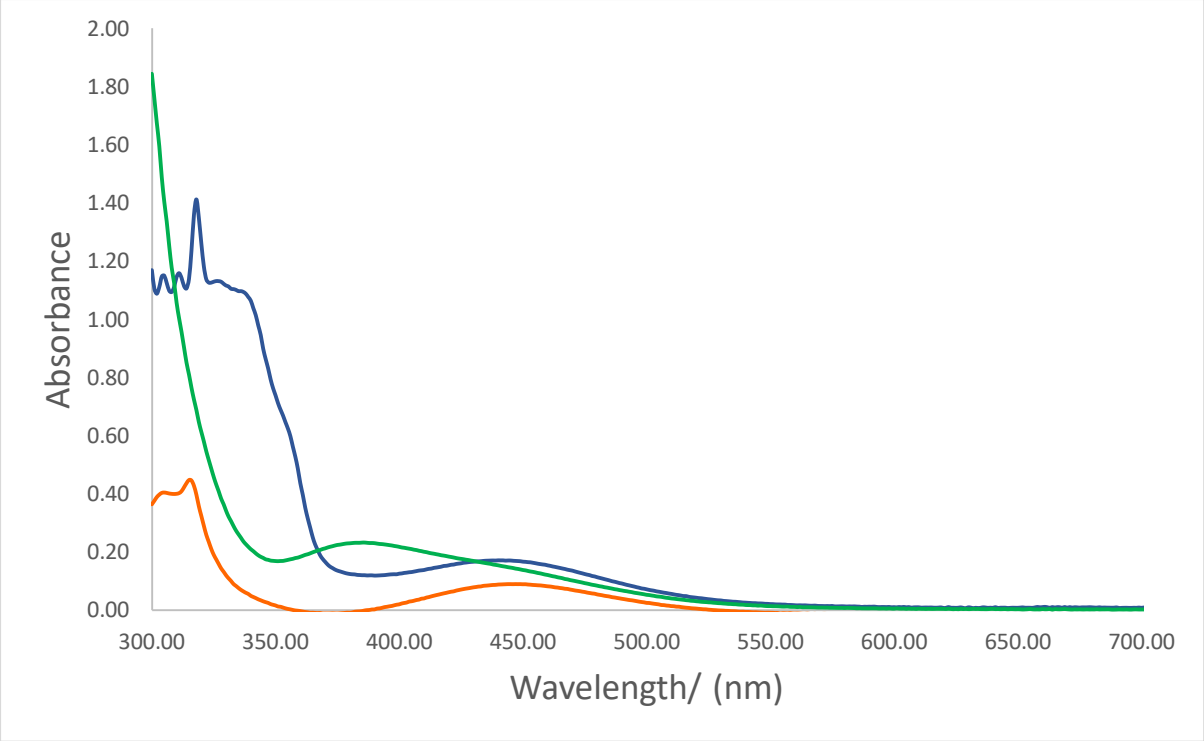

Figure (4.9.1) UV- Visible Spectra of 2-fluoro-5-iodopyridine -IBr : 2-fluoro-5-iodopyridine (Blue), IBr(Orange), 2-fluoro-5-iodopyridine - IBr (Green), the spectra were collected using methanol as the solvent, the concentration of the samples was 10^{-3} M.

4.3.10 1,10-phenanthroline-IBr

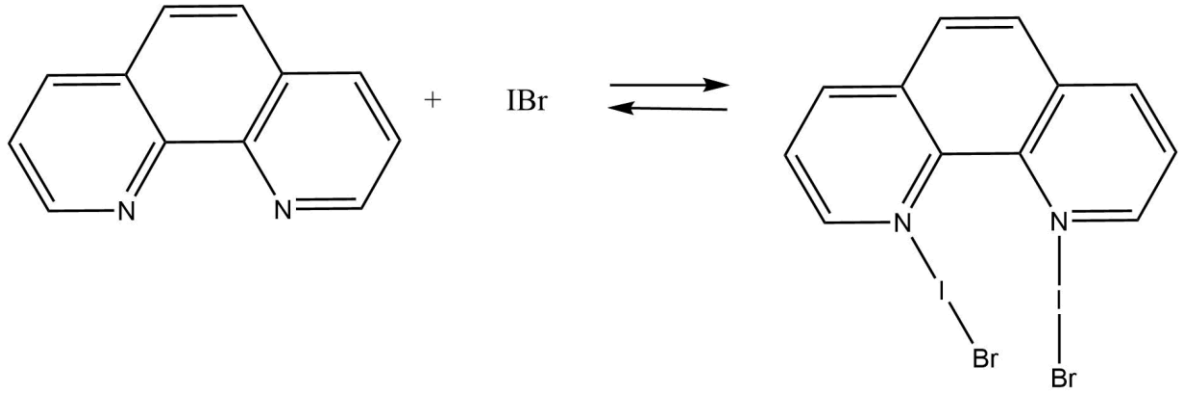

UV-Visible Spectra for 1,10-Phenanthroline -IBr solution

All the spectra were collected in methanol, the concentration of all the samples was 10^{-3} M. The base 1,10-Phenanthroline absorbs at 308 nm and iodine monobromide IBr absorbs at 317 nm and 454 nm. The new band appears at 429 nm when the two above starting materials are mixed which is not attributed to the 1,10-Phenanthroline or IBr. λ_{max} for 1,10-Phenanthroline were shifted 121 nm toward higher wavelength, Figure (4.10.1). Starting material and the resulting complex are also characterised by ATR-FTIR, Figures (3.11.2, 4.10.2).

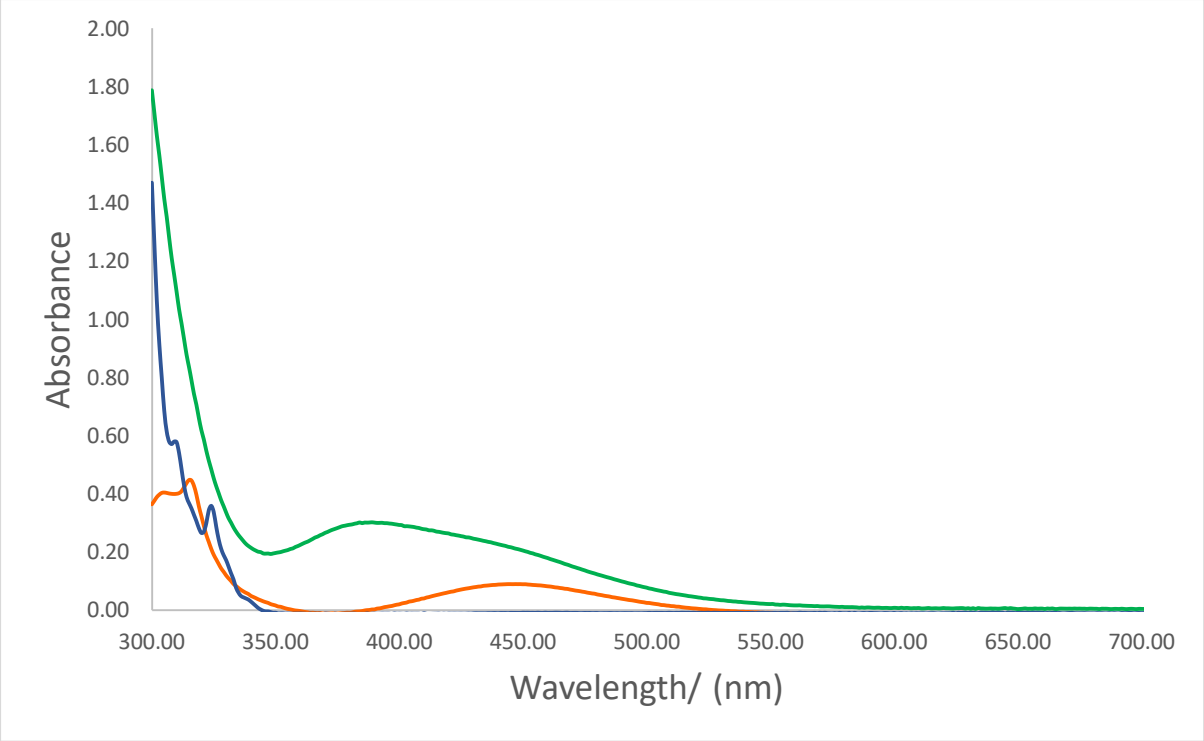

Figure (4.10.1) UV- Visible Spectra of 1,10-phenanthroline -IBr : 1,10-phenanthroline (Blue), IBr (Orange), 1,10-phenanthroline-IBr (Green), the spectra were collected using methanol as the solvent, the concentration of the samples was 10^{-3} M.

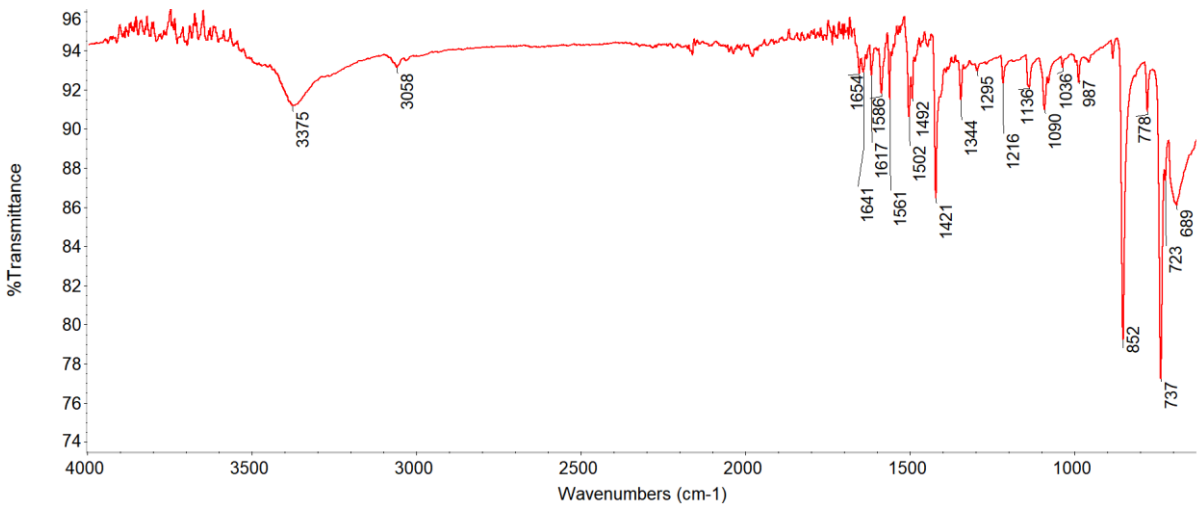

Figure (3.11.2): ATR-FTIR spectrum of 1,10-phenanthroline

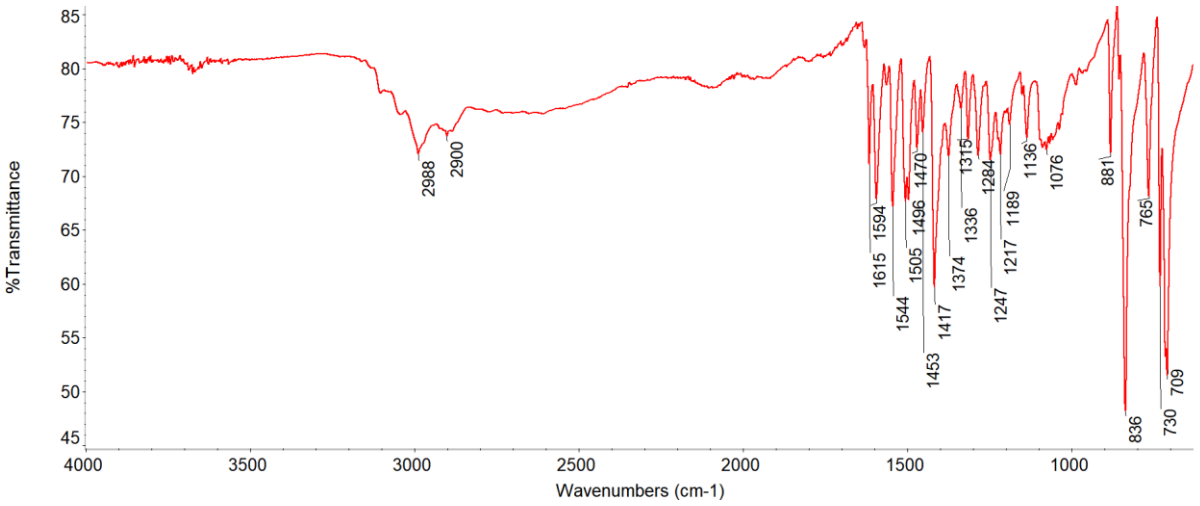

Figure (4.10.2) ATR-FTIR spectrum of 1,10-phenanthroline –IBr.

XRD measurements for 1,10-Phenanthroline –IBr

1.Crystal Structure of 1,10-Phenanthroline –IBr

Crystallographic data for 1,10-Phenanthroline –IBr are given in Table (4.3), and selected bond lengths and angles in Table (4.4). A thermal ellipsoid plot of the structure together with the numbering scheme used is given in Figure (4.10.3).

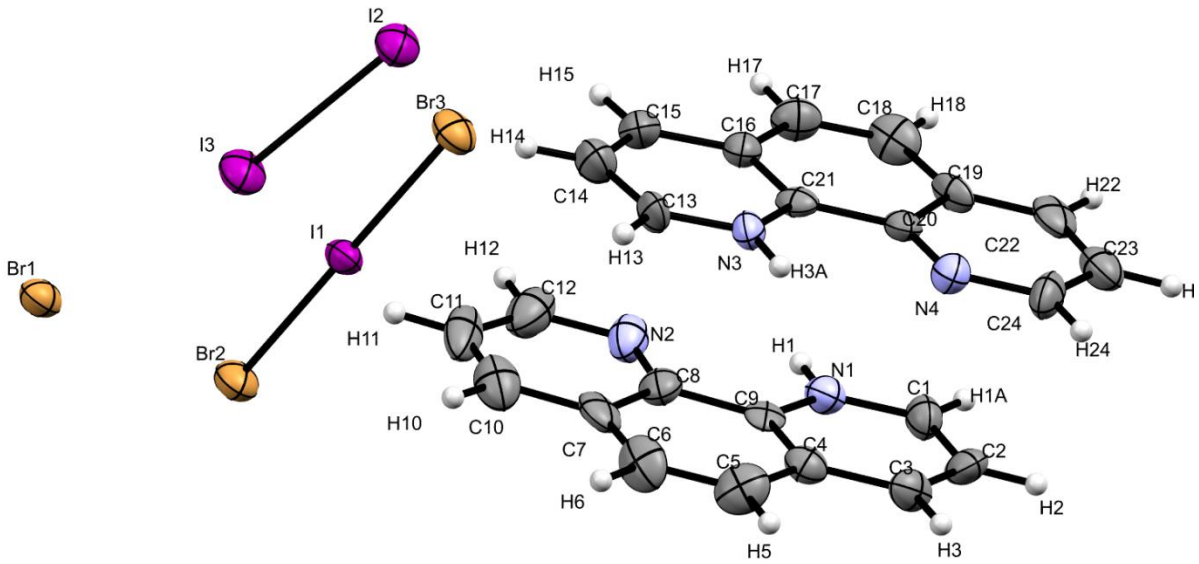

Figure (4.10.3) Thermal Ellipsoid plot for the 1,10-phenanthroline complex.

The complex crystallises in the monoclinic crystal system; space group $P2_1/c$. The asymmetric unit consists of two protonated 1,10-phenanthroline ions, one molecule of iodine, IBr_2^- and bromide ion. The possible mechanisms of polyhalogen ions formation are discussed above. The Br3-I1-Br2 angle is 178.95°, which is very close to being completely linear, but even though the bond lengths in the IBr_2^- ion are not symmetrical (I1-Br2 2.691(2) Å, I1-Br3 2.702(1) Å), it cannot be concluded that the ion is involved in any of the non-covalent interactions that could cause this length difference. The observed short contact distances (C13···Br3 3.658 Å, C23···Br3 3.814 Å, C10···Br2 3.813 Å, C5···Br2 3.721 Å, C1···Br2 3.655 Å) are significantly longer than the reported values for C-H···Br HB (3.376 Å).[138] However, the bromide ion is involved in several interactions. Firstly, the iodine molecule forms a bridging halogen bond interaction with two bromide ions, thus forming an infinite chain. The Br1···I2-I3 XB has the Br1···I2 interaction length of 3.136(1) Å, while for the Br1···I3-I2 XB, the distance between Br1 and I3 is 3.181(1). Both distances are less than the sum of Van der Walls radii (3.83 Å).[121] The I2-I3 distance is elongated, when compared to the distance of the iodine molecule in the gas phase (2.6663 Å),[27] and the corresponding angles of these halogen bonds are 171.93° and 169.88°, respectfully. (Figure 4.10.4) Moreover, there are two kinds of N-H···Br hydrogen bonds present. (Figure 4.10.5) In the N1-H1···Br1 HB, the distance between N atom and Br atom is 3.279 Å, and the N1-H1-Br1 angle is 149.84°, while for the N3-H3A···Br1, N3···Br1 distance is 3.308 Å and the N3-H3A-Br1 angle is 150.36. (Figure 4.10.5) Both distance values are close to the literature reported average range for the N-H···Br hydrogen bond, where the N···Br distance is 3.302 Å. [139]

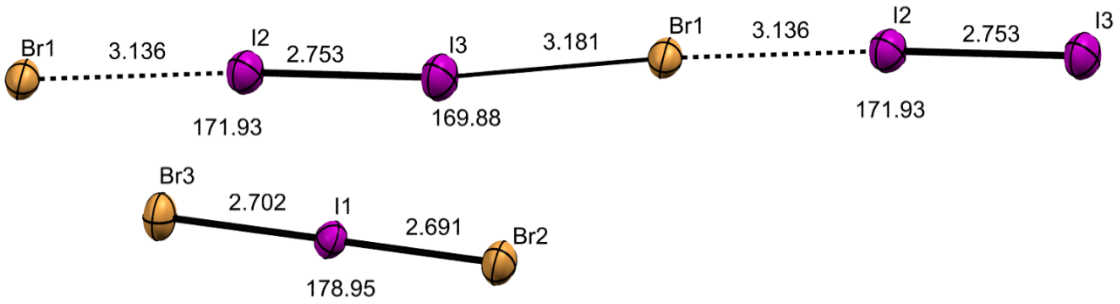

Figure (4.10.4) View showing Br1···I3-I2 and Br1···I2-I3 halogen bonds and IBr_2^- with the corresponding geometric parameters,

1,10-phenanthroline molecules are omitted for clarity

The distance between the centroids of two adjacent protonated 1,10-phenanthroline ions is 3.609 Å. (Figure 4.10.6) The mentioned non-covalent interactions cause the packing of a complex to resemble the three-fold axis formed around the Br··· I-I chain. (Figure 4.10.7)

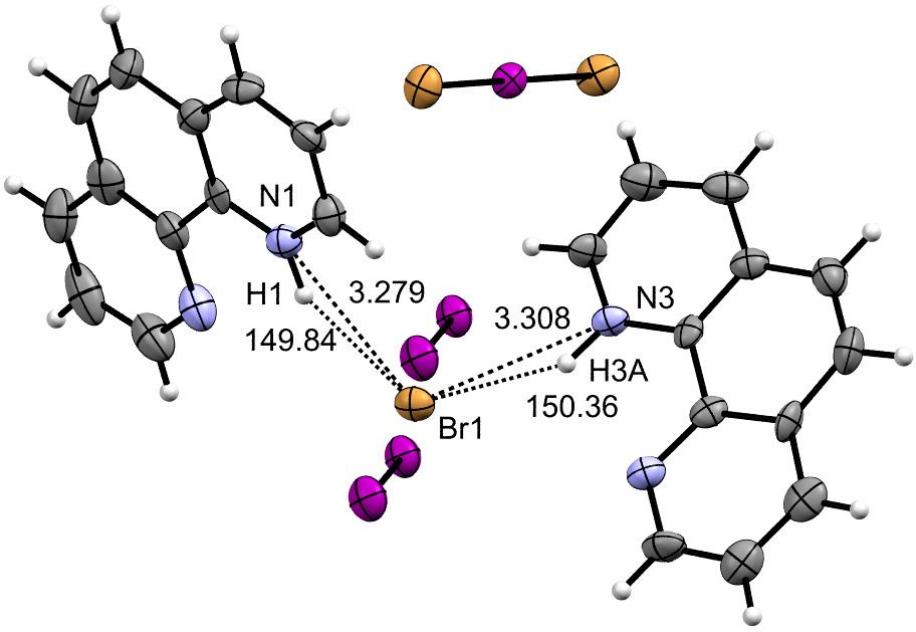

Figure (4.10.5) View showing N-H···Br hydrogen bonds 1,10-phenanthroline-IBr complex and the ponding geometric parameters

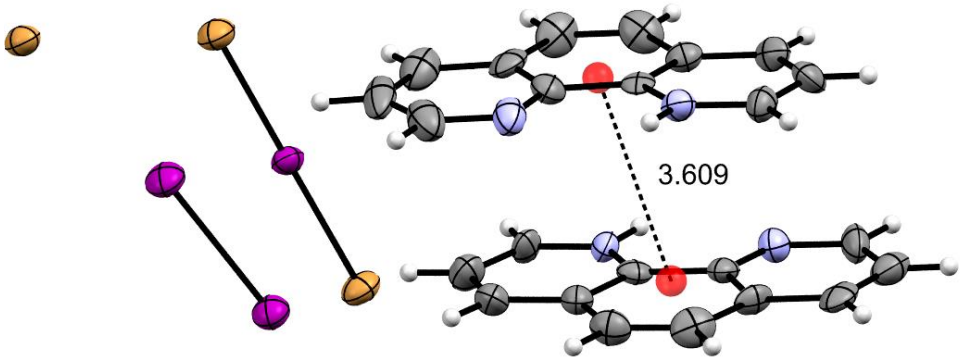

Figure (4.10.6) View showing the distance between the centroids of two 1,10-phenantrolinium ions

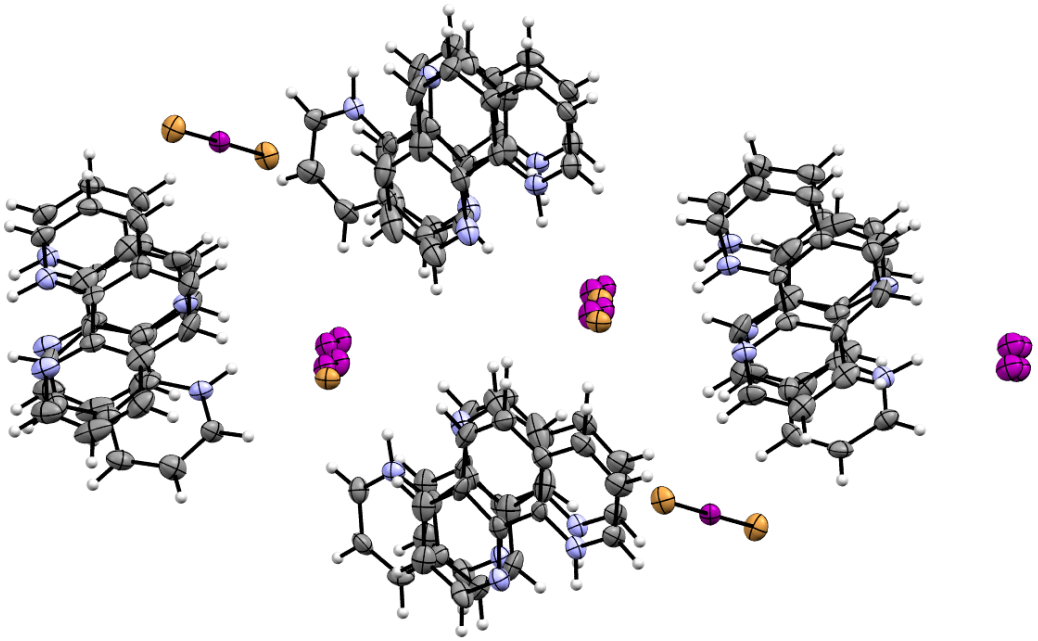

Figure (4.10.7) View showing the packing 1,10-phenanthroline-IBr complex alongside Br···I-I infinite chains

Table 4.3: Crystallographic data for the 1,10-Phenanthroline –IBr complex.

Crystal data	
Chemical formula	$Br_2I{\cdot}I_2{\cdot}Br{\cdot}2(C_{12}H_9N_2)$
M_r	982.85
Crystal system, space group	Monoclinic, $P2_1/c$
T/K	195
a, *b*, *c* (Å)	9.0428 (10), 15.9337 (17), 20.083 (2)
β (°)	99.896 (4)
V/ (Å^3)	2850.6 (5)
Z	4
Radiation type	Mo *K*α
μ/ (mm^{-1})	7.52
Crystal size/ (mm)	0.29 × 0.21 × 0.16
Data collection	
Diffractometer	Bruker *APEX*-II CCD
Absorption correction	Multi-scan *SADABS2016*/2 (Bruker,2016/2) was used for absorption correction. wR
T_{min}, T_{max}	0.463, 0.746

No. of measured, independent and observed [$I > 2\sigma(I)$] reflections	21007, 6867, 4877
R_{int}	0.056
$(\sin \theta/\lambda)_{max}$ /(Å^{-1})	0.661
Refinement	
$R[F^2 > 2\sigma(F^2)]$, $wR(F^2)$, S	0.066, 0.239, 1.03
No. of reflections	6867
No. of parameters	315
No. of restraints	20
H-atom treatment	H atoms treated by a mixture of independent and constrained refinement
	$w = 1/[\sigma^2(F_o^2) + (0.150P)^2 + 20.P]$ where $P = (F_o^2 + 2F_c^2)/3$
$\Delta\rho_{max}$, $\Delta\rho_{min}$ (e Å^{-3})	1.52, −2.40

Table 4.4: Selected interatomic contacts /Å and /^{o} for the complex 1,10-Phenanthroline –IBr

Atom1	Atom2	Length	Atom1	Atom2	Atom3	Angle
I1	Br2	2.691(2)	Br2	I1	Br3	178.95(5)
I1	Br3	2.702(1)	H1	N1	C1	114(5)
I2	I3	2.753(1)	H1	N1	C9	123(5)
N1	H1	0.96(7)	C1	N1	C9	123(1)
N1	C1	1.336(14)	C8	N2	C12	115(1)
N1	C9	1.359(14)	N1	C1	H1A	121
N2	C8	1.334(16)	N1	C1	C2	119(1)
N2	C12	1.337(17)	C1	C2	H2	119
C1	C2	1.383(17)	C1	C2	C3	121(1)
C2	C3	1.346(17)	C2	C3	H3	120
C3	C4	1.416(16)	C2	C3	C4	120(1)
C4	C5	1.405(17)	C3	C4	C5	124(1)
C4	C9	1.399(15)	C3	C4	C9	117(1)
C5	C6	1.349(19)	C5	C4	C9	119(1)
C6	C7	1.443(19)	C4	C5	H5	120
C7	C8	1.391(17)	C4	C5	C6	120(1)
C7	C10	1.409(18)	H5	C5	C6	120

C8	C9	1.434(15)	C5	C6	H6	119
C10	C11	1.36(2)	C5	C6	C7	121(1)
C11	C12	1.39(2)	H6	C6	C7	119
N3	H3A	1.0(1)	C6	C7	C8	120(1)
N3	C13	1.300(13)	C6	C7	C10	122(1)
N3	C21	1.355(14)	C8	C7	C10	118(1)
N4	C20	1.36(2)	N2	C8	C7	125(1)
N4	C24	1.315(15)	N2	C8	C9	118(1)
C13	C14	1.378(17)	C7	C8	C9	117(1)
C14	C15	1.390(18)	N1	C9	C4	120(1)
C15	C16	1.400(16)	N1	C9	C8	118(1)
C16	C17	1.416(17)	C4	C9	C8	122(1)
C16	C21	1.417(16)	C7	C10	H10	121
C17	C18	1.336(18)	C7	C10	C11	118(1)
C18	C19	1.435(17)	H10	C10	C11	121
C19	C20	1.408(14)	C10	C11	H11	120
C19	C22	1.383(16)	C10	C11	C12	120(1)
C20	C21	1.437(15)	H11	C11	C12	120
C22	C23	1.381(19)	N2	C12	C11	124(1)

C23	C24	1.377(18)	N2	C12	H12	118
			C11	C12	H12	118
			H3A	N3	C13	112(7)
			H3A	N3	C21	124(7)
			C13	N3	C21	124(1)
			C20	N4	C24	118(1)
			N3	C13	H13	120
			N3	C13	C14	120(1)
			C13	C14	H14	120
			C13	C14	C15	120(1)
			C14	C15	H15	120
			C14	C15	C16	120(1)
			C15	C16	C17	125(1)
			C15	C16	C21	118(1)
			C17	C16	C21	117(1)
			C16	C17	H17	119
			C16	C17	C18	122(1)
			H17	C17	C18	119
			C17	C18	H18	119

	C17	C18	C19	122(1)
	H18	C18	C19	119
	C18	C19	C20	118(1)
	C18	C19	C22	125(1)
	C20	C19	C22	117(1)
	N4	C20	C19	123(1)
	N4	C20	C21	118(1)
	C19	C20	C21	119(1)
	N3	C21	C16	119(1)
	N3	C21	C20	120(1)
	C16	C21	C20	121(1)
	C19	C22	H22	121
	C19	C22	C23	119(1)
	C22	C23	C24	120(1)
	N4	C24	C23	123(1)
	N4	C24	H24	118
	C23	C24	H24	119

4.3.11 2-cyanopyridine-IBr

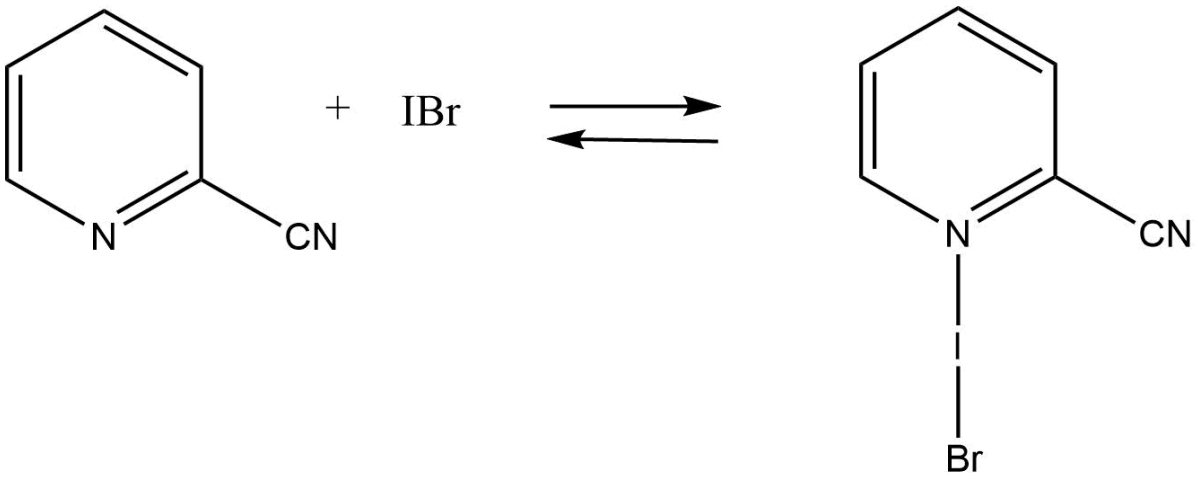

UV-Visible Spectra for 2-cyanopyridine -IBr solution

All the spectra were collected in methanol, the concentration of all the samples was 10^{-3} M. The base 2-cyanopyridine absorbs at 305 nm and iodine monobromide IBr absorbs at 317 nm and 454 nm. The new band appears at 438 nm when the two above starting materials are mixed which is not attributed to the 2-cyanopyridine or IBr. λ_{max} for 2-cyanopyridine was shifted 87 nm toward higher wavelength, Figure (4.11.1). Starting material and the resulting complex are also characterised by ATR-FTIR, Figures (3.10.2, 4.11.2).

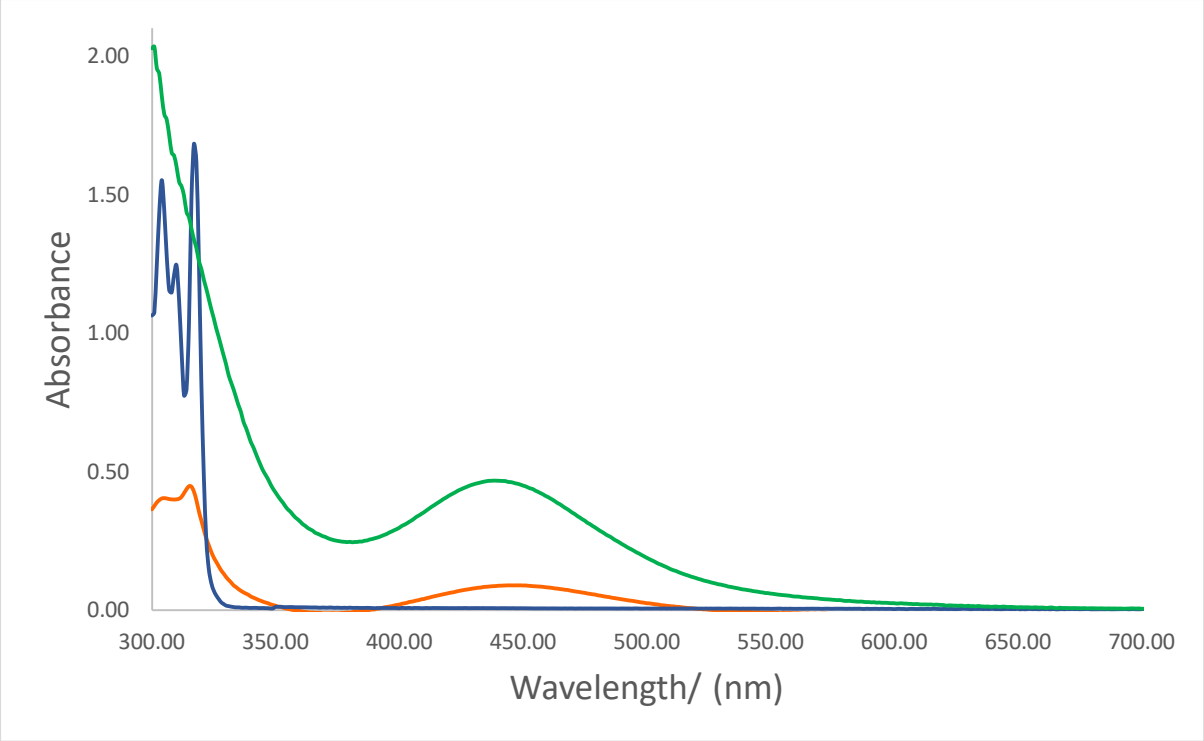

Figure (4.11.1) UV- Visible Spectra of 2-cyanopyridine-IBr: 2-cyanopyridine (Blue), IBr(Orange), 2-cyanopyridine -IBr (Green), the spectra were collected using methanol as the solvent, the concentration of the samples was 10^{-3} M.

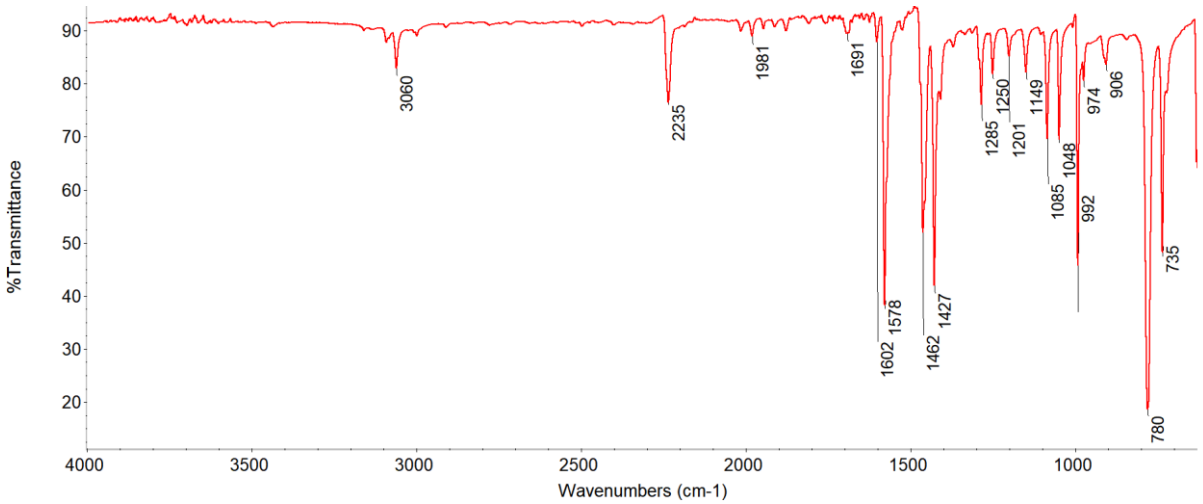

Figure (3.10.2) ATR-FTIR spectrum of 2-cyanopyridine

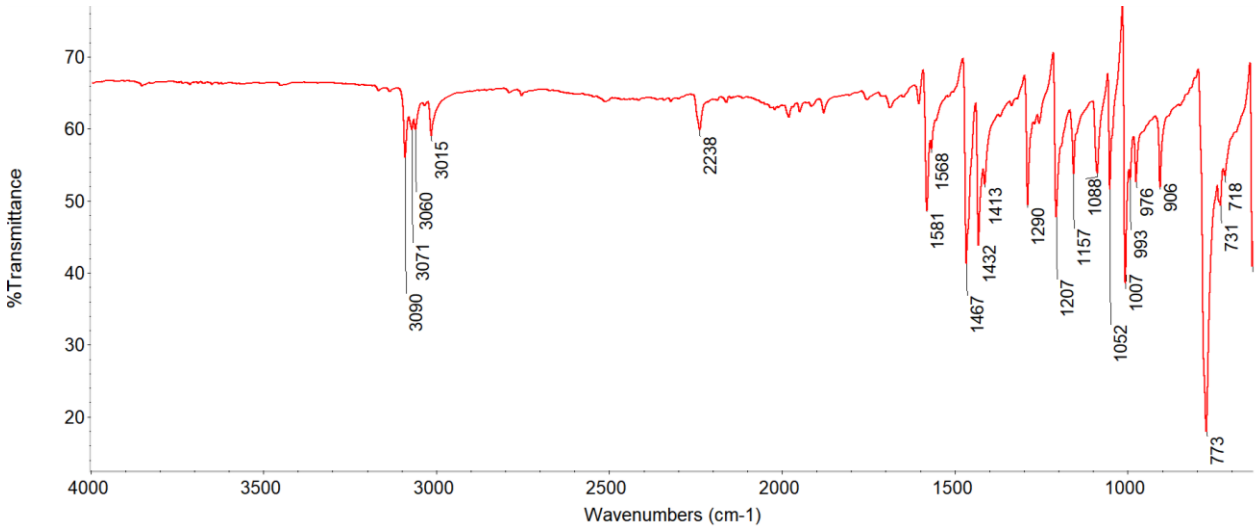

Figure (4.11.2) ATR-FTIR spectrum of 2-cyanopyridine –IBr.

XRD measurements for 2-cyanopyridine –IBr

1.Crystal Structure of 2-cyanopyridine -IBr

Crystallographic data for 2-cyanopyridine-IBr are given in Table (4.5), and selected bond lengths and angles in Table (4.6). A thermal ellipsoid plot of the structure together with the numbering scheme used is given in Figure (4.21).

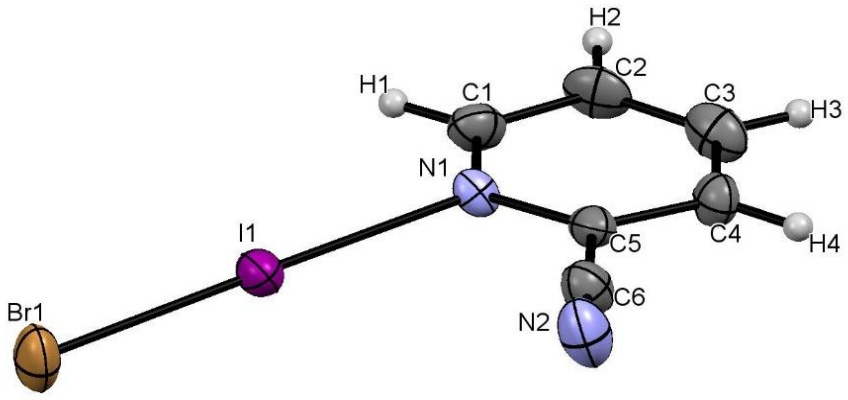

Figure (4.11.3) Thermal Ellipsoid plot for 2-cyanopyridine-IBr.

2-cyanopyridine-IBr crystallises in the Triclinic crystal system and the space group is P-1 The asymmetric unit consists of one 2-cyanopyridine and one IBr molecule. The two moieties are connected by N···I-Br halogen bond. The distance between N1 and I1 is 2.466(6) Å, which is less than the sum of Van der Walls radii of the corresponding atoms (3.53Å),[121] while the distance between the iodine atom and bromine atom is 2.566(1) Å. This is longer than the distance for the starting material (IBr) in gas phase 2.4691 Å[27] and the measured N1-I1-Br1 angle is 178.8(2)°, Figure (4.11.4). Complexes are further connected via C-H···N hydrogen bonds and Br···Br interactions to form a step-like pattern, Figures (4.11.5, 4.11.6)

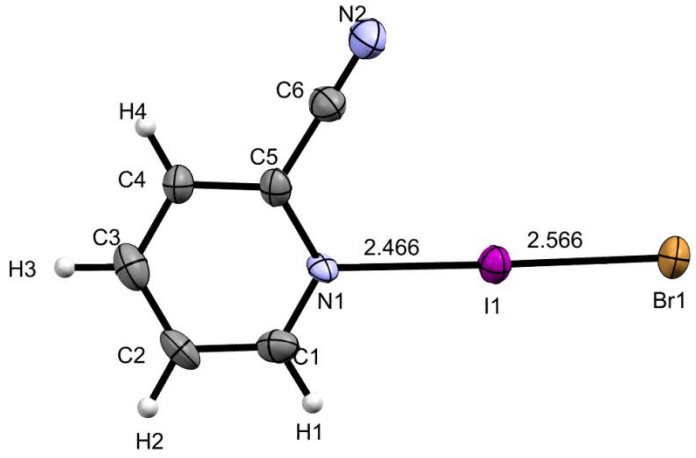

Figure (4.11.4) View showing halogen bond geometrical information

of 2-cyanopyridine-IBr complex

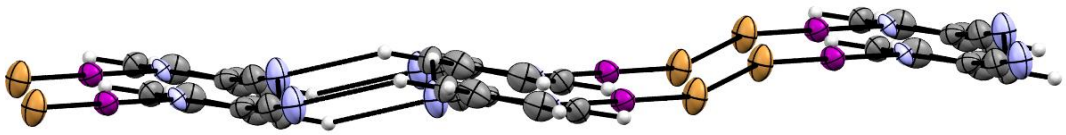

Figure (4.11.5) Side-view of the step-like packing pattern of 2-cyanopyridine-IBr complex

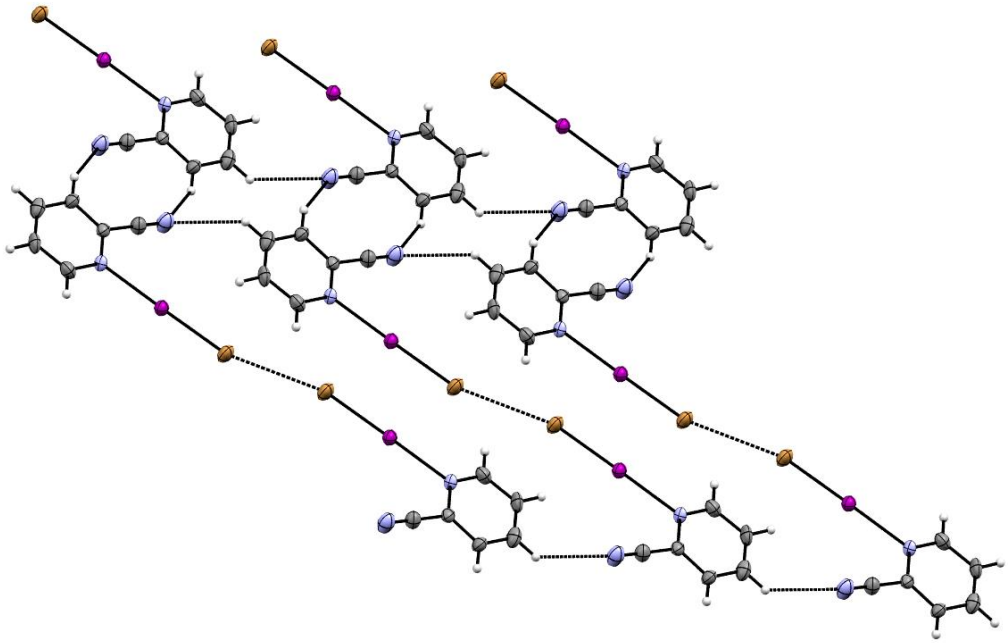

Figure (4.11.6) Top-view of the step-like packing pattern of 2-cyanopyridine-IBr complex

The cyano-group nitrogen atom is a bifurcated HB acceptor. The two types of C-H···N hydrogen bonds are C3-H3···N2 where the C3···N2 distance is 3.378 Å and the C3-H3-N2 angle is 136.78°, and C4-H4···N2 hydrogen bond, in which the C4···N2 distance is 3.454 Å and the C4-H4-N2 angle is 147.13°, Figure (4.11.7). Both distances are shorter than the reported values for C-H···N hydrogen bond in similar systems (3.521 Å)[140], while the measured angles are greater (134.41°). These halogen bonds form two types of graph-set motifs, two C4-H4···N2 are a part of $R_2^2(10)$ motif, while two C4-H4···N2 and two C4-H4···N2 HBs form a $R_4^2(10)$ motif, (Figure 4.11.7). As it was mentioned, apart from the hydrogen bonds, type I halogen interactions[1,125] between the two bromine atoms, can be observed. The Br···Br distance is 3.470 Å, which is shorter than the sum of Van der Waals radii (3.70 Å), while the I-Br···Br angles are both 165.12°, Figure (4.11.8). These are characteristic properties for this kind of short contacts which can be observed as a result of close packing of complexes. [1,125] The distance between the centroids of the pyridine rings of the adjacent molecules in the unit cell is 8.066 Å, Figure (4.11.9).

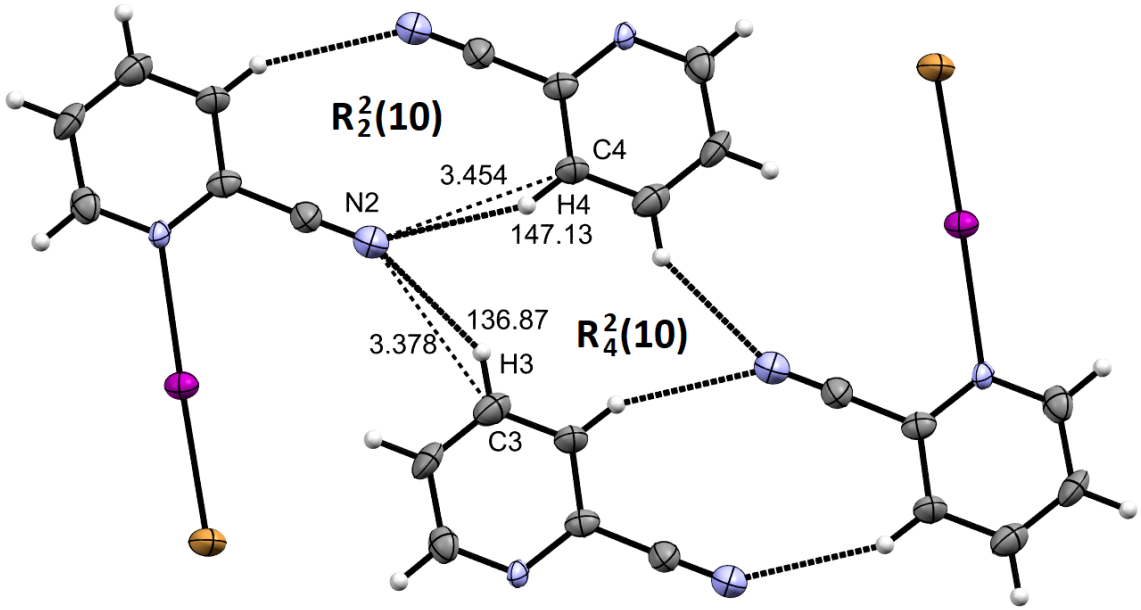

Figure (4.11.7) View of the hydrogen bonds in 2-cyanopyridine-IBr complex with the corresponding graph-set motif notation

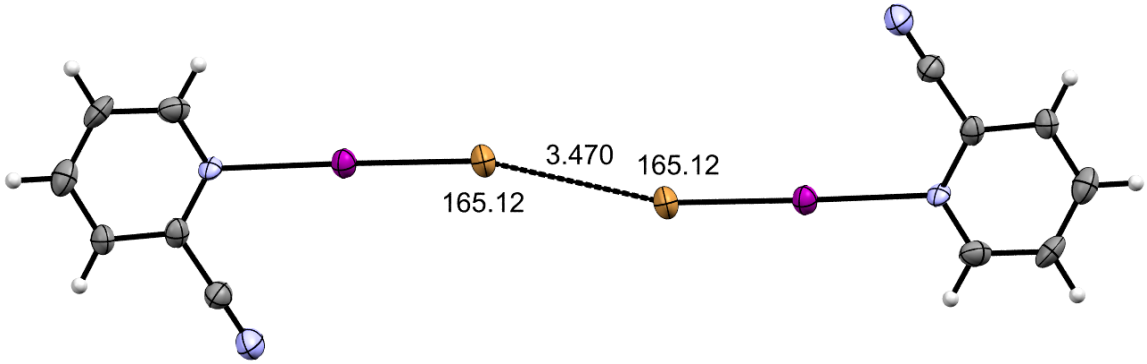

Figure (4.11.8) View of type I halogen bond in 2-cyanopyridine-IBr complex

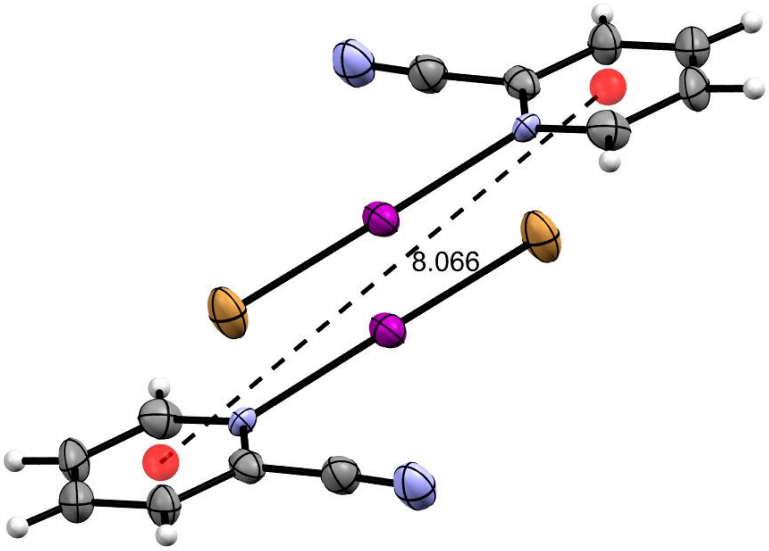

Figure (4.11.8) View showing the distance between the two centroids of 2-cyanopyridine-IBr complexes

Table 4.5: Crystallographic data for the 2-cyanopyridine –IBr complex.

Crystal data	
Chemical formula	$C_6H_4BrIN_2$
M_r	310.92
Crystal system, space group	Triclinic, P-1
T/K	195
a, *b*, *c* (Å)	7.941 (2), 7.974 (2), 8.266 (2)
α, β, γ (°)	76.275 (8), 65.978 (8), 61.910 (7)
V/ (Å^3)	421.11 (19)
Z	2
Radiation type	Mo *K*α
μ/ (mm^{-1})	8.47
Crystal size/ (mm)	0.29 × 0.21 × 0.08
Data collection	
Diffractometer	Bruker *APEX*-II CCD
Absorption correction	Multi-scan
T_{min}, T_{max}	0.322, 0.746
No. of measured, independent and observed [$I > 2\sigma(I)$] reflections	5207, 2529, 2047

R_{int}	0.042
$(\sin \theta/\lambda)_{max}$ /(Å^{-1})	0.719
Refinement	
$R[F^2 > 2\sigma(F^2)]$, $wR(F^2)$, S	0.056, 0.147, 1.17
No. of reflections	2529
No. of parameters	91
H-atom treatment	H-atom parameters constrained
$\Delta\rho_{max}$, $\Delta\rho_{min}$ (e Å^{-3})	2.98, −2.42

Table 4.6: Selected interatomic contacts /Å and /^{o} for the complex 2-cyanopyridine-IBr.

Atom1	Atom2	Length	Atom1	Atom2	Atom3	Angle
I1	Br1	2.5663(11)	Br1	I1	N1	178.8(2)
I1	N1	2.466(6)	I1	N1	C1	119.2(6)
N1	C1	1.296(10)	I1	N1	C5	119.8(5)
N1	C5	1.341(10)	C1	N1	C5	120.8(8)
N2	C6	1.126(12)	N1	C1	H1	120
C1	C2	1.391(13)	N1	C1	C2	120.9(9)
C2	C3	1.367(14)	H1	C1	C2	120
C3	H3	0.95	C1	C2	C3	119(1)
C3	C4	1.368(12)	H2	C2	C3	121

C4	H4	0.95	C2	C3	C4	120(1)
C4	C5	1.382(10)	H3	C3	C4	120
C5	C6	1.429(11)	C3	C4	C5	117.5(9)
			H4	C4	C5	121.3
			N1	C5	C4	121.6(8)
			N1	C5	C6	118.9(8)
			C4	C5	C6	119.5(8)
			N2	C6	C5	177(1)

4.3.12 quinoxaline-IBr

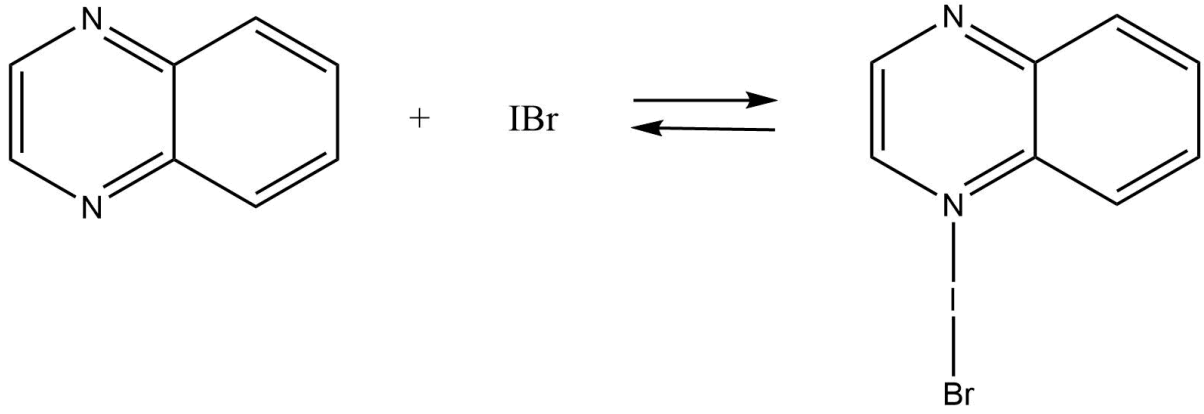

Instead of the expected halogen bonded quinoxaline-IBr complex, two other complexes are obtained (quinoxaline - IBr_2^-, quinoxaline -I_2). Since the latter one contains N···I-I halogen bond, it is discussed in the chapter (5).

UV-Visible Spectra for Quinoxaline - IBr_2^- solution

All the spectra were collected in methanol, the concentration of all the samples was 10^{-3} M. The base Quinoxaline absorbs at 323 nm and iodine monobromide IBr absorbs at 317 nm and 454 nm. A new band appears at 439 nm when the two above starting materials are mixed which is not attributed to the Quinoxaline or IBr. λ_{max} for Quinoxaline was shifted 131 nm toward higher wavelength, Figure (4.12.1). Starting material and the resulting complex are also characterised by ATR-FTIR, Figures (3.12.2, 4.12.2).

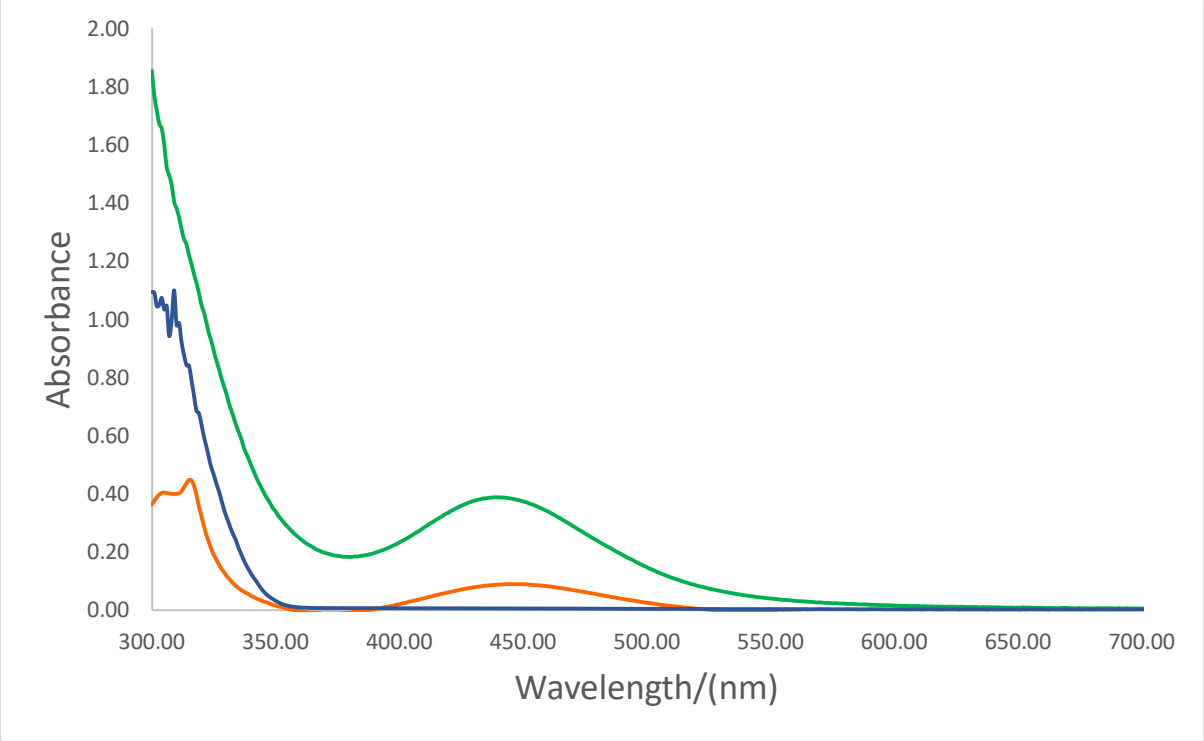

Figure (4.12.1) UV- Visible Spectra of Quinoxaline-IBr_2^-: Quinoxaline (Blue), IBr(Orange), Quinoxaline- IBr_2^- (Green), the spectra were collected using methanol as the solvent, the concentration of the samples was 10^{-3} M.

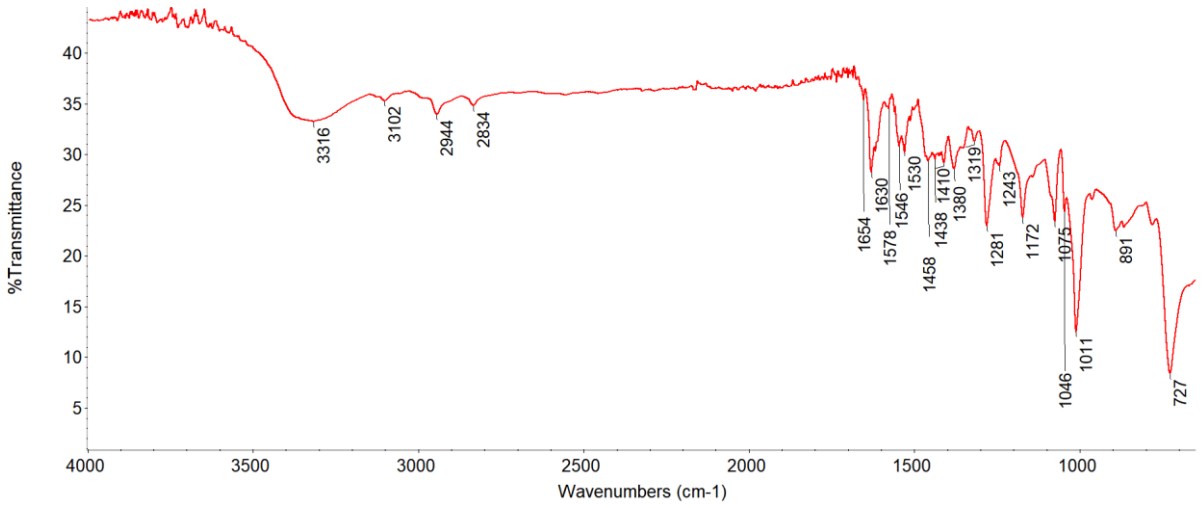

Figure (3.12.2): ATR-FTIR spectrum of quinoxaline

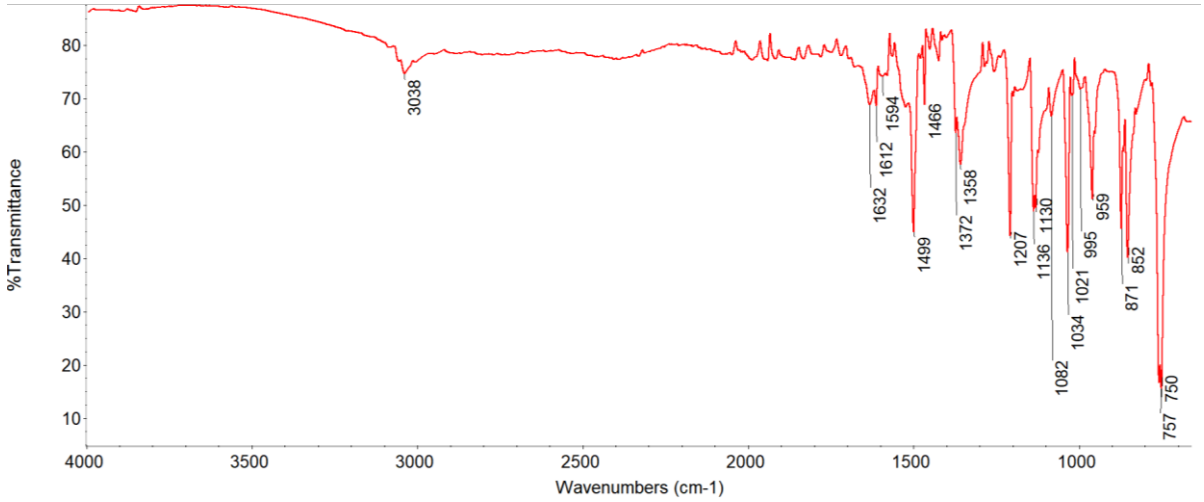

Figure (4.12.2) ATR-FTIR spectrum of Quinoxaline – IBr_2^-.

XRD measurements for Quinoxaline-IBr_2^-

Crystallographic data for quinoxaline-IBr_2^- are given in Table (4.7), and selected bond lengths and angles in Table (4.8). A thermal ellipsoid plot of the structure together with the numbering scheme used is given in Figure (4.12.3), packing diagram of Quinoxaline-IBr_2^- approximately along to the b axis is shown in Figure(4.12.4).

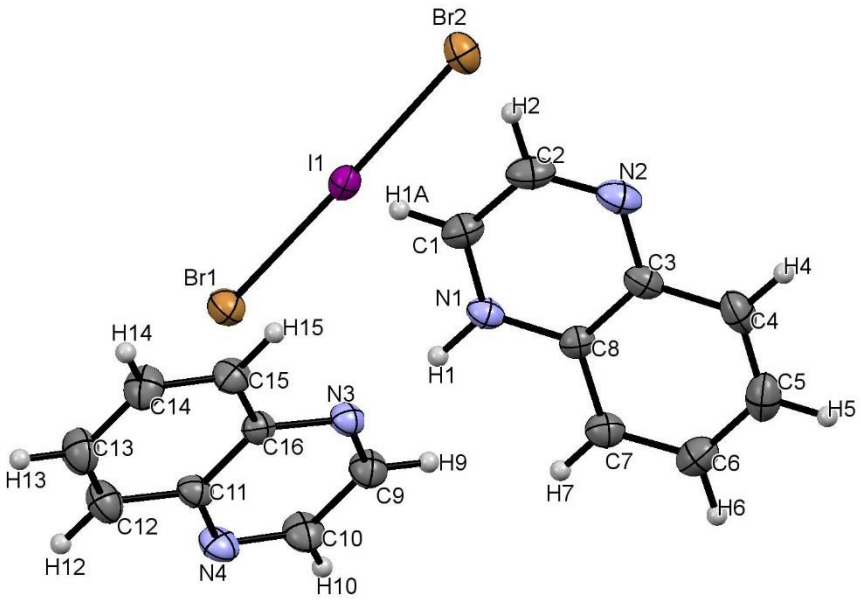

Figure (4.12.3) Thermal Ellipsoid plot for Quinoxaline (Yellow)-IBr

Quinoxaline- IBr_2^- crystallises in the Triclinic system, and the space group is P-1. The asymmetric unit consists of two molecules of quinoxaline, and IBr_2^- ion. The unit cell consists of 2 asymmetric units, Figure (4.12.4). The iodine is bonded to 2 bromine atoms to produce the IBr_2^- ion. Of the two molecules of quinoxaline is protonated, while the other is neutral. Moreover, two quinoxaline molecules are connected by an N1-H1···N3 hydrogen bond. The N···N distance is 2.704 Å, and N-H-N angle is 172.00°, Figure (4.12.5). Despite a difference in bond lengths, I-Br 2.677 Å and I-Br2 is 2.716 Å, IBr_2^- ion is not involved in a halogen bond, nor any other non-covalent interaction, but serves only for the charge compensation within the complex. The observed short contacts (C12···Br2 3.880 Å, C1···Br2 3.719 Å, C10···Br3 3.675 Å, C4···Br3 3.820 Å) are significantly longer than the reported C-H···Br hydrogen bond length (3.376 Å).[138] The distance between the two adjacent quinoxaline molecules is 4.377 Å, Figure (4.12.6).

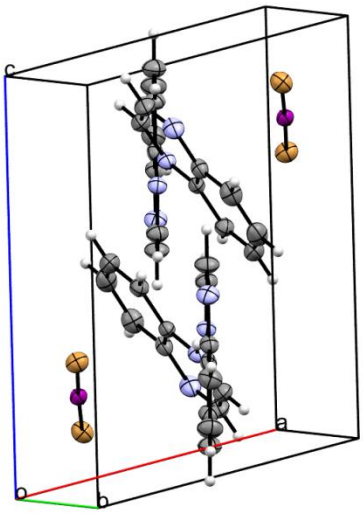

Figure (4.12.4) Packing diagram of quinoxaline-IBr_2^- approximately along to b axis

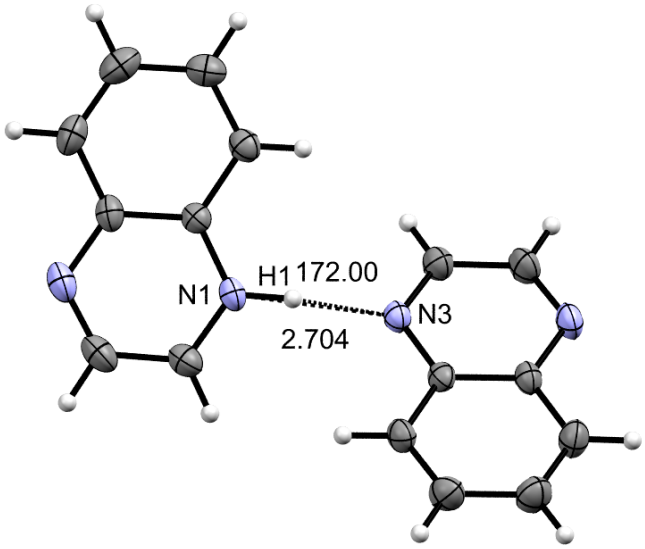

Figure (4.12.5) View showing N1-H1···N3 hydrogen bond in quinoxaline-IBr_2^- complex

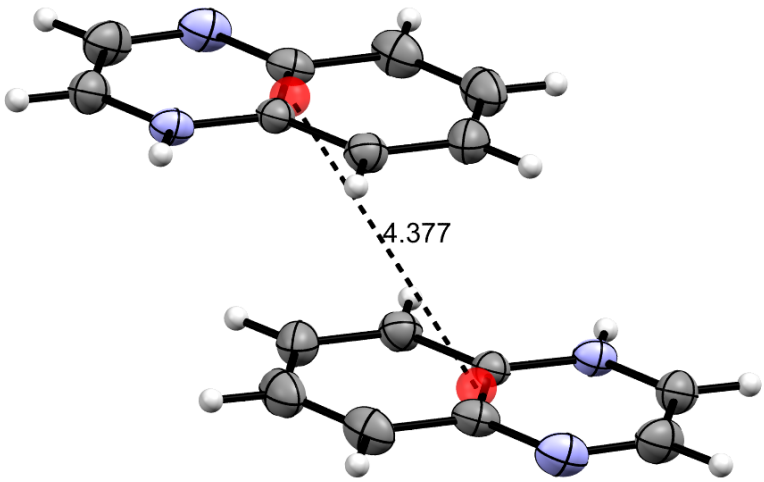

Figure (4.12.6) View showing the distance between two adjacent quinoxaline molecules in quinoxaline-IBr_2^- complex

Table 4.7: Crystallographic data for the Quinoxaline- IBr_2^- complex.

Crystal data	
Chemical formula	$Br_2I{\cdot}C_8H_7N_2{\cdot}C_8H_6N_2$
M_r	548.02
Crystal system, space group	Triclinic, *P*1
T/K	180
a, *b*, *c* (Å)	7.3002 (18), 11.243 (3), 12.079 (3)
α, β, γ (°)	72.322 (10), 75.31 (1), 73.318 (9)
V/ (Å^3)	889.7 (4)
Z	2
Radiation type	Mo *K*α
μ/ (mm^{-1})	6.30
Crystal size/ (mm)	0.29 × 0.26 × 0.07
Data collection	
Diffractometer	Bruker *APEX*-II CCD
Absorption correction	Multi-scan
T_{min}, T_{max}	0.526, 0.747
No. of measured, independent and observed [$I > 2\sigma(I)$] reflections	18917, 7843, 5211

R_{int}	0.037
$(\sin \theta/\lambda)_{max}$ /(Å^{-1})	0.817
Refinement	
$R[F^2 > 2\sigma(F^2)]$, $wR(F^2)$, S	0.043, 0.117, 1.04
No. of reflections	7843
No. of parameters	211
No. of restraints	1
H-atom treatment	H atoms treated by a mixture of independent and constrained refinement
$\Delta\rho_{max}$, $\Delta\rho_{min}$ (e Å^{-3})	1.33, −2.03

Table 4.8: Selected interatomic contacts /Å and /^{o} for the complex Quinoxaline-IBr_2^-.

Atom1	Atom2	Length	Atom1	Atom2	Atom3	Angle
I1	Br1	2.6773(9)	C1	N1	C8	113.7(7)
I1	Br2	2.7161(9)	C2	N2	C3	114.9(7)
N1	H1	0.98(2)	N1	C1	C2	124.2(8)
N1	C1	1.314(4)	H1	C1	C2	117.9
N1	C8	1.369(5)	N2	C2	C1	123.5(8)
N2	C2	1.310(5)	N2	C3	C4	119.6(7)
N2	C3	1.362(4)	N2	C3	C8	121.9(7)
C1	C2	1.405(6)	C4	C3	C8	118.5(7)
C3	C4	1.412(5)	C3	C4	C5	120.6(8)
C3	C8	1.409(4)	H4	C4	C5	119.7
C4	C5	1.366(6)	C4	C5	C6	120.7(8)
C5	C6	1.402(7)	H5	C5	C6	119.6
C6	C7	1.369(6)	C5	C6	C7	120.5(8)
C7	C8	1.413(4)	H6	C6	C7	119.6
N3	C9	1.313(5)	C6	C7	C8	119.8(8)
N3	C16	1.371(6)	H7	C7	C8	120.1
N4	C10	1.311(6)	N1	C8	C3	121.7(7)

N4	C11	1.363(5)	N1	C8	C7	118.5(7)
C9	C10	1.405(6)	C3	C8	C7	119.7(7)
C11	C12	1.407(7)				
C11	C16	1.410(4)				
C12	C13	1.361(6)				
C13	C14	1.411(6)				
C14	C15	1.365(7)				
C15	C16	1.403(5)				

4.3.13 2-ethoxyquinoline -IBr

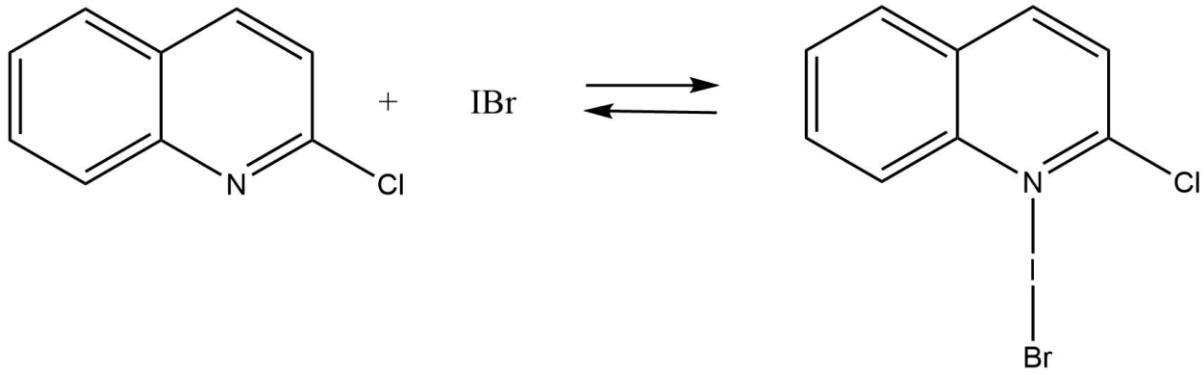

UV-Visible Spectra for 2-ethoxyquinoline -IBr_2^- solution

All the spectra were collected in methanol, the concentration of all the samples was 10^{-3} M. The base 2-chloroquinoline absorbs at 319 nm and iodine monobromide IBr absorbs at 317 nm and 454 nm. The new band appears at 436 nm when the two above starting materials are mixed which is not attributed to the 2-chloroquinoline or IBr. λ_{max} for 2-chloroquinoline were shifted 114 nm toward higher wavelength, Figure (4.13.1). Starting material and the resulting complex are also characterised by ATR-FTIR, Figures (3.13.2, 4.13.2).

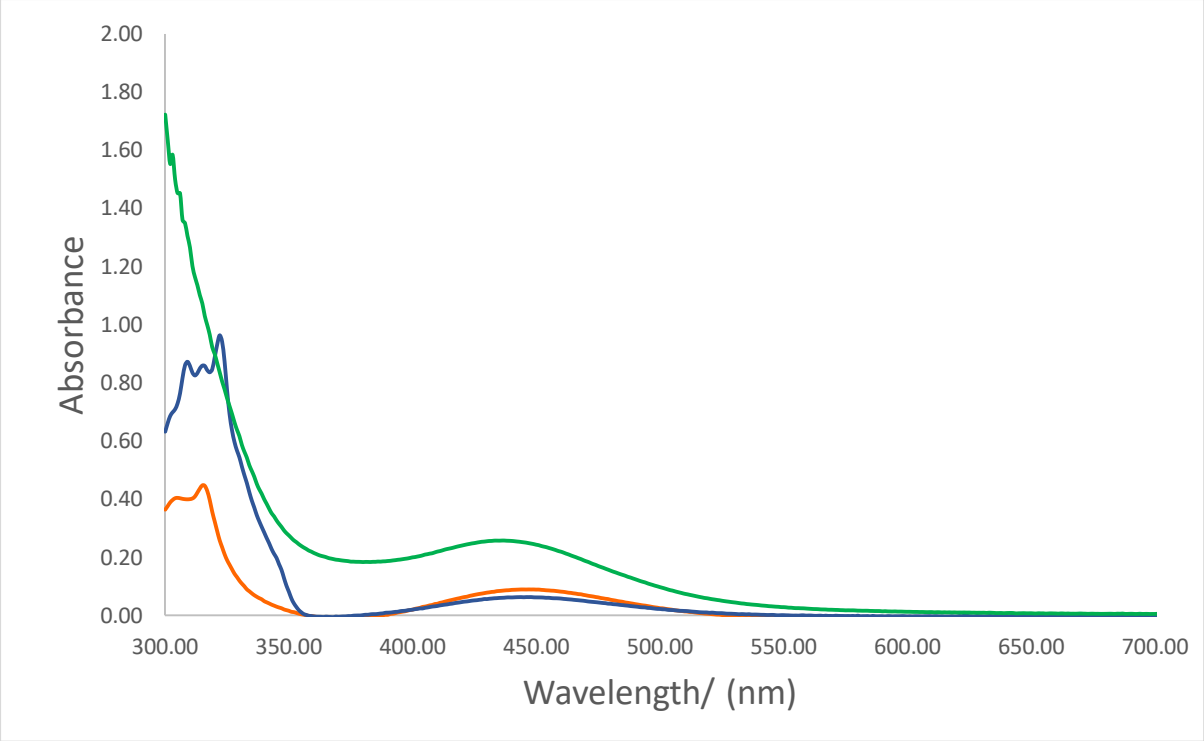

Figure (4.13.1) UV- Visible Spectra of 2-chloroquinoline -IBr : 2-chloroquinoline (Blue), IBr (Orange), 2-chloroquinoline -IBr (Green), the spectra were collected using methanol as the solvent, the concentration of the samples was 10^{-3} M.

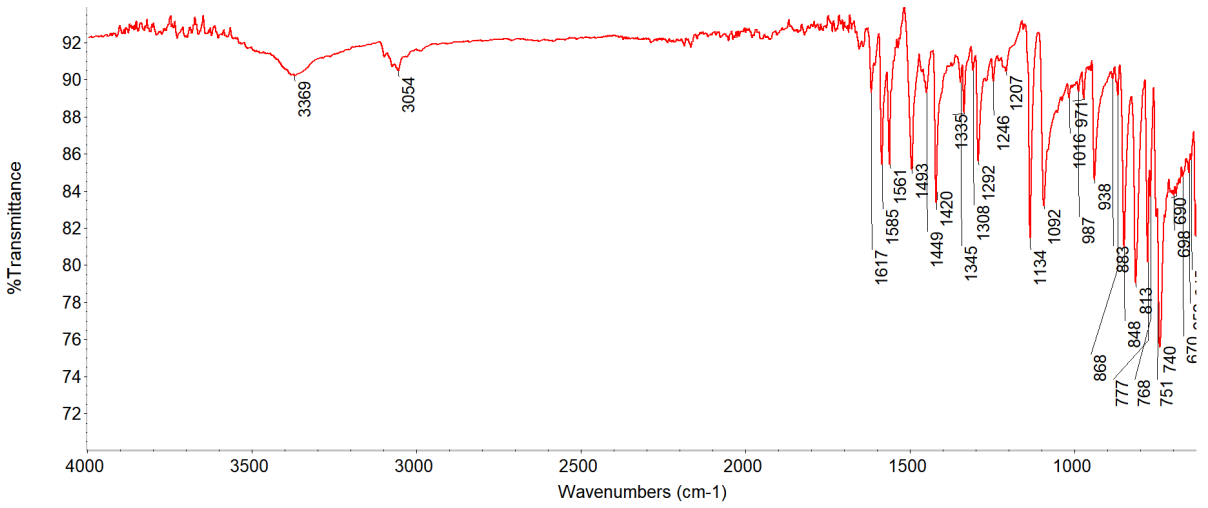

Figure (3.13.2): ATR-FTIR spectrum of 2-chloroquinoline

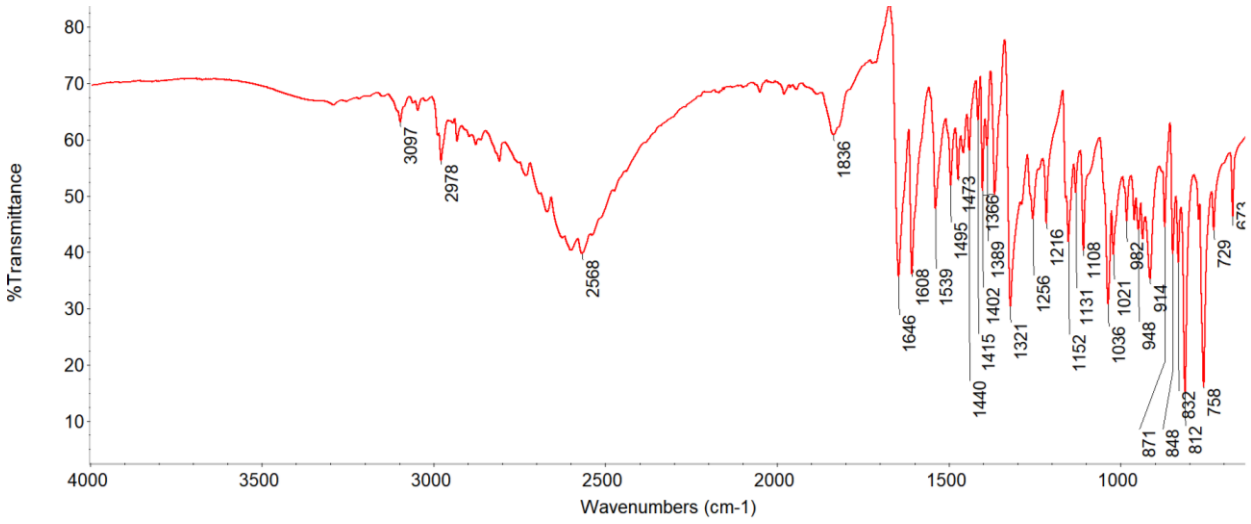

Figure (4.13.2) ATR-FTIR spectrum of 2-ethoxyquinoline - IBr_2^-

XRD measurements for 2-ethoxyquinoline –IBr_2^-

Crystallographic data for 2-ethoxyquinoline - IBr_2^- are given in Table (4.9), and selected bond lengths and angles in Table (4.10). A thermal ellipsoid plot of the structure together with the numbering scheme used is given in Figure (4.35).

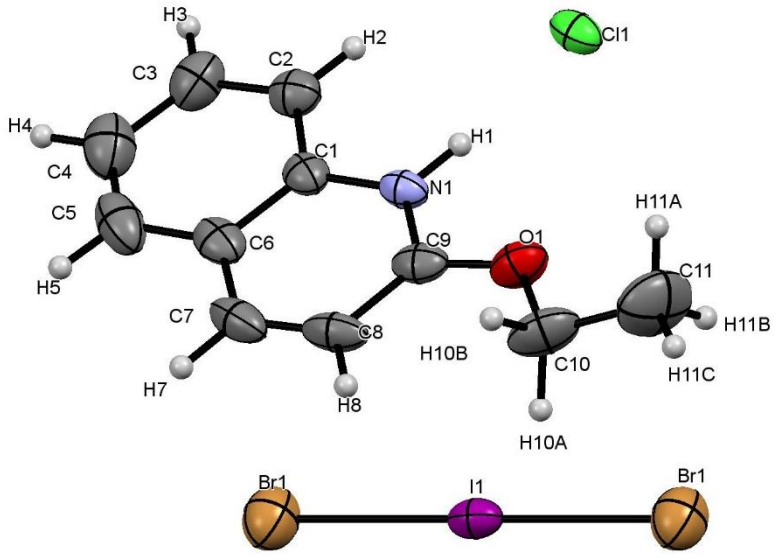

Figure (4.13.3) Thermal Ellipsoid plot for 2-ethoxyquinoline $–IBr_2^-$

Even though 2-chloroquinoline and IBr were used as starting materials, instead of the expected 2-chloroquinoline-IBr halogen bonded complex, 2-ethoxyquinoline-IBr_2^- was obtained as a crystalline product. 2-ethoxyquinoline-IBr_2^- crystallises in the monoclinic crystal system and the space group is, C 2/c. The asymmetric unit contains one molecule of protonated ethoxyquinoline, a half of IBr_2^- ion and a half of chloride ion. Packing of 2-ethoxyquinoline –IBr_2^- within the unit cell approximately along to the a-axis is shown in Figure (4.13.4). The formation of polyhalide anion could stem from one of the previously discussed mechanisms. I-Br distances in the IBr_2^- ion are equal (2.671 Å) and the measured Br-I-Br angle is 180.00° (Figure 4.13.5), which indicates that the IBr_2^- ion is not involved in any of the non-covalent interactions. There is N1-H1⋯Cl1 hydrogen bond present between the protonated 2-ethoxyquinoline and the chloride ion, Figure (4.13.5). The distance between N1 and Cl1 is 3.05(3) Å which less than the sum of Van der Waals radii (3.30 Å)[121] for these atoms, the N1-H1-Cl1 measured angle is 173.48°, as well. The distance between two adjacent protonated 2-ethoxyquinoline molecules is 5.108 Å, Figure (4.13.6)

Forming of 2-ethoxyquinoline in the resulting complex, rather than 2-chloroquinoline, which was used as a starting material could be explained by Williamson reaction, Figure (4.13.7). This kind of reaction includes the reaction of an organohalide with alkoxide (in this system coming from ethanol, which is the solvent) to produce a corresponding ether. The chloride ion, that observed in the structure, is a product of substitution between 2-chloroquinoline and ethoxy anion.

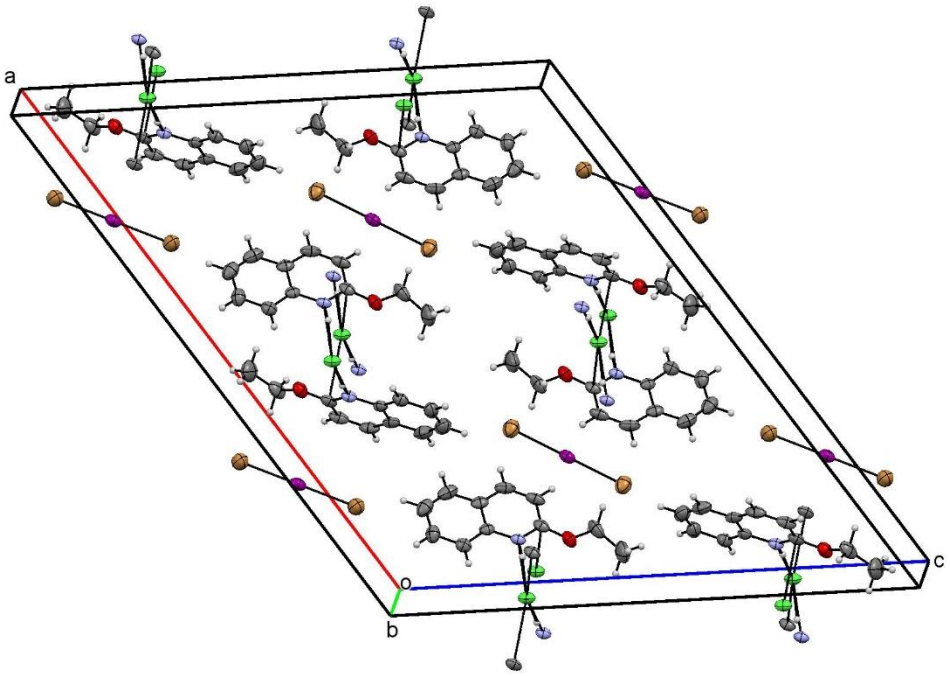

Figure (4.13.4) Packing diagram of 2-ethoxyquinoline $–IBr_2^-$ approximately along to a-axis.

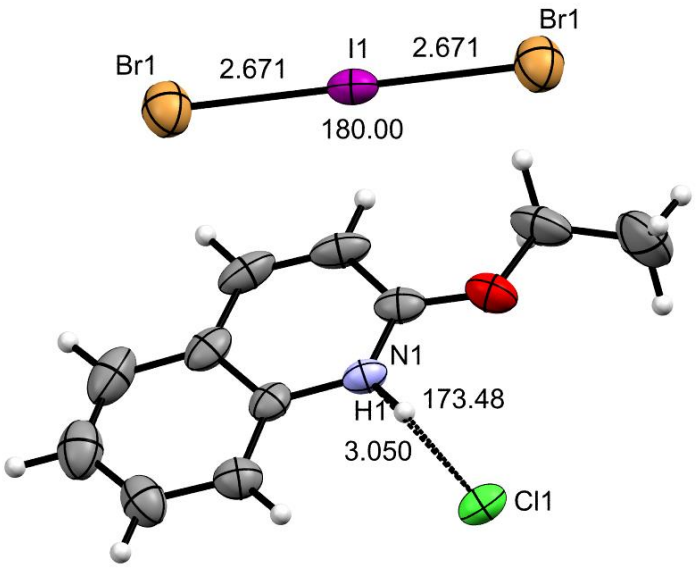

Figure (4.13.5) View showing the geometrical parameters of IBr_2^- and N1-H1⋯Cl1 hydrogen bond in 2-ethoxyquinoline $–IBr_2^-$ complex

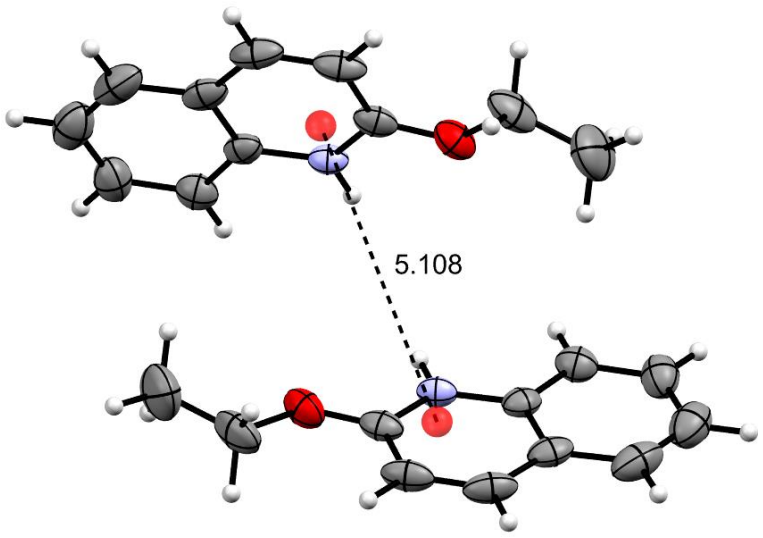

Figure (4.13.6) View showing the distance between two centroids of adjacent 2-ethoxyquinoline molecules in 2-ethoxyquinoline $-IBr_2^-$ complex

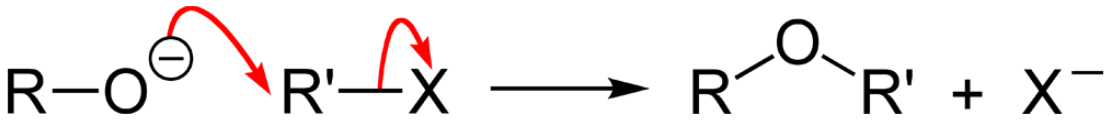

Figure (4.13.7) Scheme for the formation of ether and halide ion.

Table (4.9) Crystallographic data for the product formed for 2-ethoxyquinoline $–IBr_2^-$.

Chemical formula	$Br_2I·Cl·2(C_{11}H_{12}NO)$
M_r	670.60
Crystal system, space group	Monoclinic, *C*2/*c*
T/K	180
a, *b*, *c* (Å)	26.495 (7), 5.1241 (14), 22.276 (7)
β (°)	122.864 (8)
V/ (Å^3)	2540.2 (12)
Z	4
Radiation type	Mo *K*α
μ/ (mm^{-1})	4.53
Crystal size/ (mm)	0.22 × 0.16 × 0.1
Chemical formula	$Br_2I·Cl·2(C_{11}H_{12}NO)$
Data collection	
Diffractometer	Bruker *APEX*-II CCD
Absorption correction	Multi-scan
T_{min}, T_{max}	0.572, 0.746
No. of measured, independent and observed [$I > 2\sigma(I)$] reflections	10841, 3949, 2416
R_{int}	0.055

$(\sin \theta/\lambda)_{max}$ /(Å^{-1})	0.721
Refinement	
$R[F^2 > 2\sigma(F^2)]$, $wR(F^2)$, S	0.045, 0.091, 1.01
No. of reflections	3949
No. of parameters	143
No. of restraints	1
H-atom treatment	H atoms treated by a mixture of independent and constrained refinement
$\Delta\rho_{max}$, $\Delta\rho_{min}$ (e Å^{-3})	0.67, −1.14

Table 4.10: Selected interatomic contacts /Å and /^{o} for the complex 2-ethoxyquinoline –IBr_2^-.

Atom 1	Atom2	Length	Atom1	Atom2	Atom3	Angle
I1	Br1	2.6714	Br1	I1	Br1	180
I1	Br1	2.6714	C9	O1	C10	118.8(4)
O1	C9	1.309(7)	H1	N1	C1	117(2)
O1	C10	1.453(7)	H1	N1	C9	120(2)
N1	H1	0.92(3)	C1	N1	C9	123.3(4)
N1	C1	1.376(7)	N1	C1	C2	120.0(4)
N1	C9	1.317(5)	N1	C1	C6	118.6(4)
C1	C2	1.396(6)	C2	C1	C6	121.4(4)
C1	C6	1.401(6)	C1	C2	H2	120.9
C2	C3	1.36(1)	C1	C2	C3	118.4(4)
C3	C4	1.393(8)	C2	C3	H3	119.3
C4	C5	1.348(8)	C2	C3	C4	121.3(5)
C5	C6	1.406(9)	H3	C3	C4	119.4
C6	C7	1.407(7)	C3	C4	C5	120.2(5)
C7	C8	1.350(9)	H4	C4	C5	119.9
C8	C9	1.408(6)	C4	C5	C6	121.1(5)
C10	H10B	0.99	C1	C6	C5	117.5(4)
			C1	C6	C7	117.4(4)
			C5	C6	C7	125.1(4)
			C6	C7	C8	122.5(4)
			H7	C7	C8	118.7
			C7	C8	C9	118.2(4)

	H8	C8	C9	120.9
	O1	C9	N1	113.4(4)
	O1	C9	C8	126.5(4)
	N1	C9	C8	120.1(4)
	O1	C10	C11	106.9(5)
	H10A	C10	C11	110.3
	H10B	C10	C11	110.3

Table 4.11: Distance between atoms, measured angles, λ_{max} and melting point for IBr complexes.

Compound	N---I Å	I-Br Å	N---I-Br o	λ_{max} /nm	Mp /°C
3,5-difluoropyridine-IBr.	---	---	---	381	Mrt
3,5-dichloropyridine- IBr.	---	---	---	388	Mrt
2,6-dichloropyridine-I IBr.	---	---	---	434	77-80
2,6-dimethoxypyridine- IBr	---	---	---	440	52-55
4-methoxypyridine- IBr	---	---	---	435	38-40
3-fluoropyridine- IBr	2.369(3)	2.6222(5)	178.93(6)	387	58-61
2-fluoropyridine-3-iodopyridine- IBr	---	---	---	436	76-79
2-fluoropyridine-4-iodopyridine- IBr	---	---	---	378	88-91
2-fluoropyridine-5-iodopyridine- IBr	---	---	---	385	96-99
2-cyanopyridine-IBr	2.466(6)	2.566(1)	178.8(2)	438	94-96
1,10-phenanthroline- IBr	---	---	---	429	191-194
Quinoxaline- IBr	---	---	---	439	56-59
2-chloroquinoline- IBr	---	---	---	436	131-133

Mrt: (melt at room temperature)

4.4- Discussion

Iodine monobromide complexes can be classified into two groups, the first characterised only by UV-VIS and ATR-FTIR spectroscopy, while the second is characterised by single-crystal X-ray diffraction and UV-VIS and ATR-FTIR spectroscopy. The latter consists of two main subgroups:

(1) complexes with N···I-Br halogen bond (2-cyanopyridine-IBr and 3-fluoropyridine-IBr). Table 4.12 contains geometric properties of these two complexes, as well as the similar aromatic sp^2 N-based halogen bonds with iodine monobromide. Based on this dataset, some conclusions regarding the correlation of halogen bonds strength with the functional groups on the aromatic ring could be made. If the pyridine-IBr complex, is taken as a reference point because it does not have any functional groups attached, it can be seen that amongst the available compounds, this system has the shortest N-I distance, which indicates the strongest N···I-Br halogen bond. This is also confirmed by the biggest elongation of the I-Br bond, 2.653 Å, as compared to 2.4691 Å[27] in the starting material.

From the complexes prepared in this work, it has been observed that the N-I halogen bond distance in 2-cyanopyridine-IBr (2.466 Å) which is considerably longer than the corresponding distance in 3-fluoropyridine-IBr (2.368 Å). This difference could be correlated with the electron-withdrawing properties of the functional groups on the pyridine ring. Cyano- group is stronger electron-withdrawing group than the fluorine atom and withdraws more electrons from the N atom of the pyridine ring and reduces the electron density. As a result, there is a decrease in the interaction between N and I hence, the halogen bond formed is weaker and the N···I distance is longer. Since the fluoro- group is the weaker electron-withdrawing group, XB in 3-fluoropyridine-IBr complex is shorter than the N···I halogen

bond distance in the 2-cyanopyridine-IBr complex. The literature-reported N···I distances are between the values of the two complexes within this work, Figure (4.14.1)

Table 4.12 Geometric parameters of selected N···I-IBr halogen bonded complexes, adapted from ref.106,112, data reported in this work is marked bold.

Complex name (REFCODE)	**N···I (Å)**	**I-Br (Å)**	**N···I-Br (°)**	**C-N-C (°)**
Pyridine-IBr (PYIOBR03)[129]	2.304	2.653	178.57	119.46
3-fluoropyridine-IBr	**2.368**	**2.622**	**178.93**	**121.53**
2,5-bis(2-Pyridiniumyl)-3,6-bis(2-pyridyl) pyrazine bis IBr (TASPEJ)[136]	2.405	2.595	175.14	118.70
N, N-bis(3-pyridylmethyl)-imidazolidine-4,5-dione-2-thione (TASPEJ)[136]	2.410	2.588	173.99	118.75
2-[(4-chlorophenyl) selanyl] pyridine – IBr (ZESSAU)[135]	2.411	2.623	178.74	120.29
Cis N, N-2,2-bipyridine- IBr (TAGNIZ)[118]	2.461	2.577	175.84	120.32
2-cyanopyridine-IBr	**2.466**	**2.566**	**178.79**	**120.76**

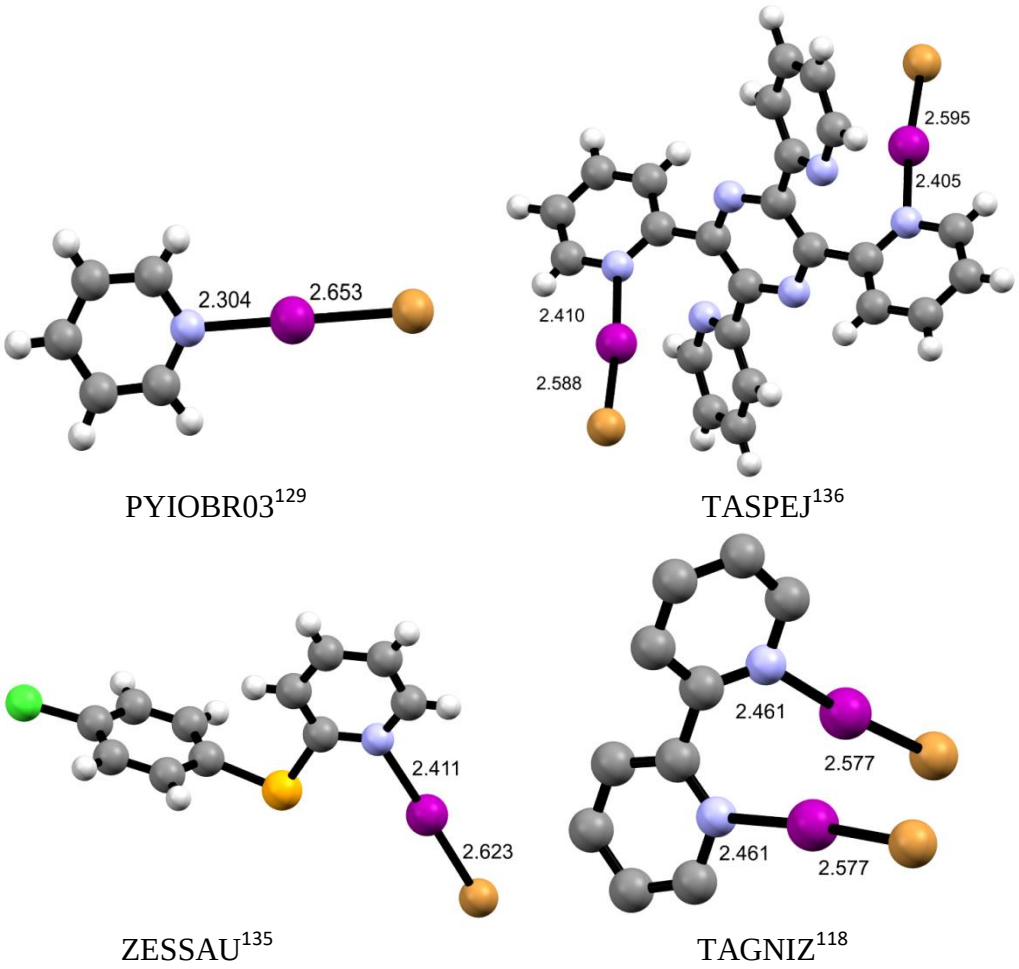

PYIOBR03[129] TASPEJ[136]

ZESSAU[135] TAGNIZ[118]

Figure (4.14.1) Thermal ellipsoid plots of selected literature complexes, Å.

(2) The second group contains ionic complexes containing polyhalogen ions, (IBr_2^-). In this chapter, three complexes of this kind are prepared (1,10-phenanthroline- IBr_2^-, quinoxaline- IBr_2^- and 2-chloroquinoline- IBr_2^-). Instead of co-crystallising the starting materials, the formation of pyridinium ions with IBr_2^- is obtained. As discussed previously, one of the mechanisms suggests that these ions could be formed due to the presence of water in the reaction system.[130] Among the complexes in this group, the main difference that can be observed is that for 1,10-phenanthroline- IBr_2^- and quinoxaline- IBr_2^- the I-Br distances are not identical, while in the 2-chloroquinoline- IBr_2^- complex, the IBr_2^- ion is symmetrical and both of the distances are equal (2.671(4) Å), Table 4.13. The difference in the I-Br bond lengths in the former two complexes should indicate that at least one side of the ion is

involved in non-covalent interactions since the I-Br bond lengthening occurs when involved in a halogen bond. However, no such contacts can be detected. Several C-H···Br short contacts are observed, but their distances are significantly longer than the literature ones, so this option is excluded. Most likely this bond length difference occurs due to the close packing of complexes.

Table (4.13) Geometrical parameters of IBr_2^- ions in 1,10-phenanthroline-IBr_2^-, quinoxaline-IBr_2^- and 2-chloroquinoline- IBr_2^- complexes.

Crystalline complexes	**I-Br1(Br3*) (Å)**	**I-Br2 (Å)**
1,10-phenanthroline-IBr_2^-	2.691	2.702
Quinoxaline- IBr_2^-	2.677	2.716
2-chloroquinoline- IBr_2^-	2.671	2.671

*In 1,10-phenanthroline-IBr_2^- because the labelling scheme is different (Br3-I-Br2)

In this chapter, the focus was put on the impact of the addition of dihalogens (IBr) to a range of organic starting materials. In cases when crystals of suitable size could not be obtained, the presence of interaction between the organic bases and iodine monobromide was determined by comparison of the pyridine ring vibrations in the IR part of the spectrum. N=C bond was of specific interest since if there is an interaction between the pyridine N atom and IBr, there should be a redistribution of electron density. If the N atom is included in a non-covalent or supramolecular interaction then part of its electron density should be transferred into that interaction, thus weakening the bonds already present in the compound. In FTIR spectrum it would mean that wavenumber corresponding to C=N bond should be moved towards lower wavenumbers (Table 4.14).

Table (4.14) Wavenumbers of selected bands in ATR-FTIR spectra correlated with specific bonds of the starting materials (St. m.) and the corresponding IBr complexes (C.)

Starting material	ν(C=N), cm^{-1}		ν(C=C), cm^{-1}		ν(C-H), cm^{-1}	
	St. m	C.	St. m	C.	St. m.	C.
3,5-difluoropyridine	1476	1461	1577	1538	3101	3065
3,5-dichloropyridine	1423	1414	1555	1551	3070	3054
2,6-dichloropyridine	1467	1414	1584	1556	3142	3087
2,6-dimethoxypyridine	1545	1457	1629	1609	3102	3003
4-methoxypyridine	1547	1560	1616	1604	3110	3097
3-fluoropyridine	1557	1537	1645	1603	3054	3063
2-fluoropyridine-4-iodopyridine	1578	1554	1645	1578	3056	2974
2-cyanopyridine	1578	1568	1602	1581	3060	3015
1,10-phenanthroline	1561	1505	1617	1594	3058	2988
Quinoxaline	1530	1499	1630	1612	3102	3038
2-chloroquinoline	1561	1539	1617	1608	3054	2978

In the complexes characterised by X-ray diffraction, interaction like halogen bond was observed, for example in the system of 3-fluoropyridine-IBr where the halogen bond is present, the band of the starting material was shifted from 1557 cm^{-1} to 1537 cm^{-1} and this shift confirms the bonding between 3-fluoropyridine and IBr. Moreover, 2-cyanopyridine - IBr where the halogen bond is present as well, the band of the starting material was shifted from 1578cm^{-1} to 1568 cm^{-1}. Also, the same shift occurs with C=C band and C-H band and these shifts confirm the bonding between 2-cyanopyridine and IBr. This shifting towards lower wavelengths (with some exception) refers to an interaction of IBr with the N atom of the pyridine ring, which leads to a decrease of the conjugated double bond features. [123,141]

Table (4.15) Wavelengths of selected bands in UV-VIS spectra of the starting materials and the corresponding IBr complexes

Starting material	$\lambda_{(Starting\ material)}$ /nm	$\lambda_{(Complex)}$ /nm
3,5-difluoropyridine	303	384
3,5-dichloropyridine	335	388
2,6-dichloropyridine	316	434
2,6-dimethoxypyridine	328	440
4-methoxypyridine	303	435
3-fluoropyridine	316,445	387
2-fluoropyridine-3-iodopyridine	351	436
2-fluoropyridine-4-iodopyridine	317,448	378
uy2-fluoropyridine-5-iodopyridine	305	385
2-cyanopyridine	308	438
1,10-phenanthroline	323, 460	383, 450
Quinoxaline	319, 460	439
2-chloroquinoline	303	436

Despite in the IUPAC list of features, where it is listed that the formation of the halogen bonds usually moves the absorption bands to lower wavelengths, for these systems, the opposite influence is noticed, i.e. λ_{max} for both starting materials were shifted towards higher wavelengths, which is called a bathochromic or a red shift. Complexes, where the structure is characterised by single crystal X-ray diffraction, have several distinctive features in their UV-VIS spectra. Halogen bonded complexes (3-fluoropyridine-IBr, 2-cyanopyridine-IBr) have a single and a more intense peak when compared to complexes containing polyhalogen ions. This peak intensity could be correlated with the charge-transfer feature of the halogen bond.

When there is a non-covalent interaction present, either halogen or a hydrogen bond, the charge transfer component is more significant than just the electrostatic interactions.[142] The position of the peak could also be correlated with observed interaction strength, in case of 3-fluoropyridine, the peak is at 387 nm, while for the 2-cyanopyridine-IBr where the XB interaction is much weaker, the peak is observed at 438 nm. For the IBr_2^- containing complexes, it has been observed that the peak is of a much lower intensity and positioned from 440-450 nm. These peak positions could be attributed to an equilibrium between IBr_2^- and iodide ions, similar to the corresponding ICl_2^- systems.[133] Also, 1,10-Phenantroline- IBr_2^- complex contains both the IBr_2^- ion and a halogen bond (Br···I-I) and in the UV-VIS spectrum, wide peak containing a shoulder can be observed, which indicates two unresolved peaks, 383 nm peak should stem from the XB and ~450 nm shoulder that corresponds to IBr_2^-. Based on peak shapes, positions and intensities in their UV-VIS spectra, it would be reasonable to assume that 3,5-difluoropyridine-IBr, 2-fluoro-4-iodopyridine-IBr and 2-fluoro-5-iodopyridine-IBr complexes are halogen-bonded, Figure (4.14.2), 3,5-dichloropyridine-IBr_2^- contains both the IBr_2^- ion and a halogen bond Figure (4.14.3), 2-ethoxyquinoline - IBr_2^-, quinoxaline- IBr_2^-, 2-fluoro-3-iodopyridine - IBr_2^-, 4-methoxypyridine- IBr_2^-, 2,6-dimethoxypyridine- IBr_2^-, 2,6-dichloropyridine- IBr_2^- contain just the IBr_2^- ion Figure (4.15).

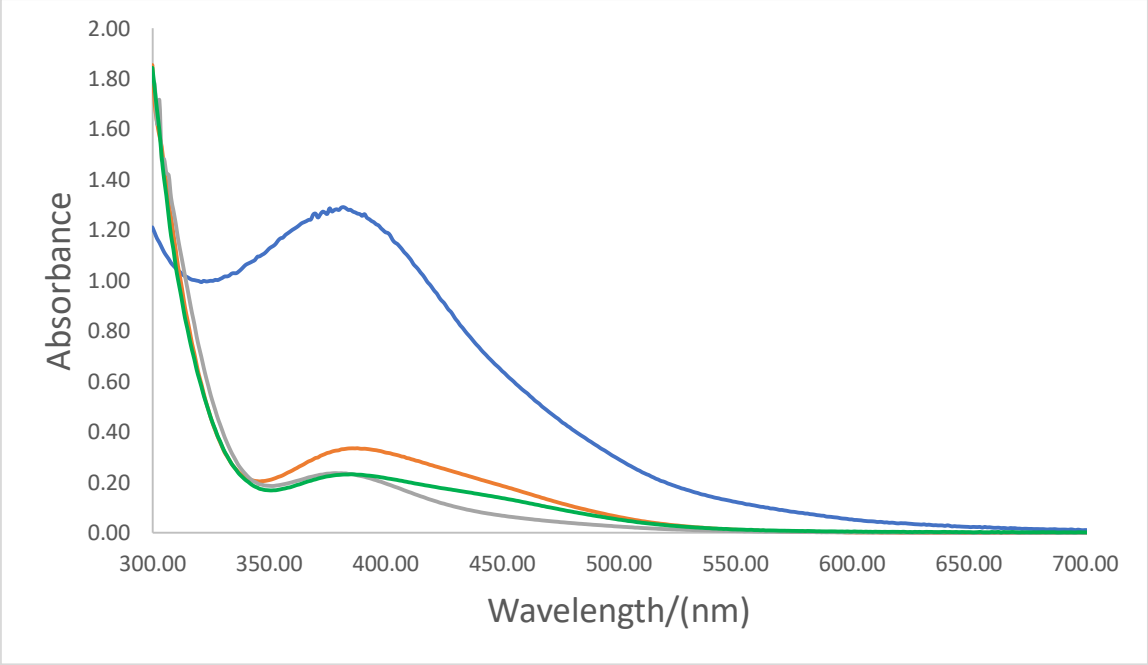

Figure (4.14.2) UV-VIS spectra of 3,5-difluoropyridine-IBr (Blue), 3-fluoropyridine-IBr (Orange), 2-fluoro-4-iodopyridine-IBr (Silver), 2-fluoro-5-iodopyridine-IBr (Green), the spectra were collected using methanol as the solvent, the concentration of the samples was 10^{-3} M.

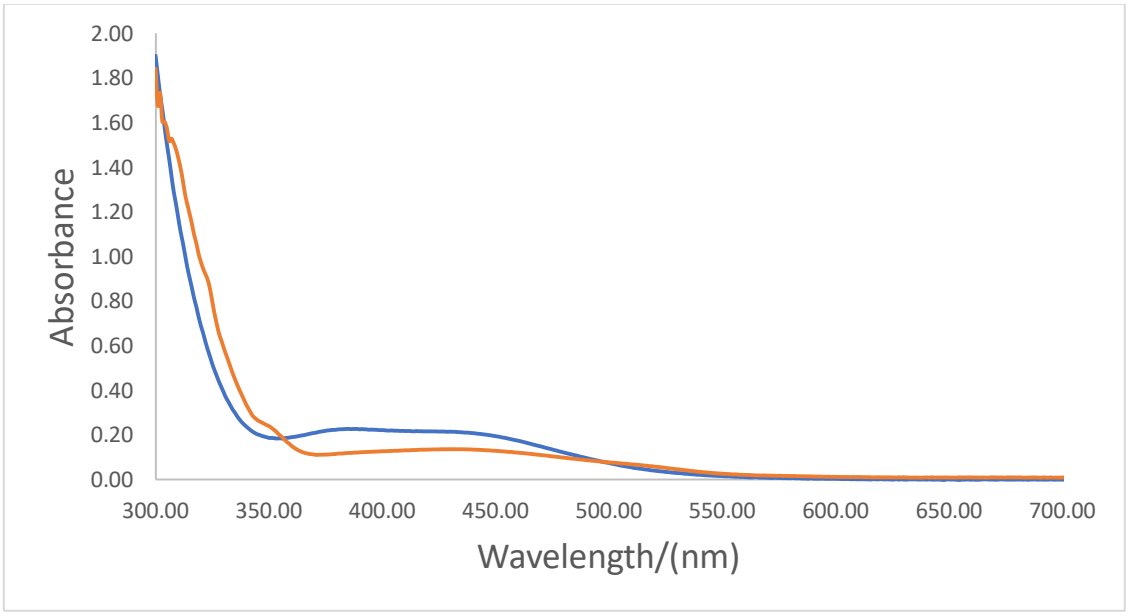

Figure (4.14.3) UV-VIS spectra of 3,5-dichloropyridine- IBr_2^- (Blue), 1,10-phenantroline- IBr_2^-(Orange), the spectra were collected using methanol as the solvent, the concentration of the samples was 10^{-3} M.

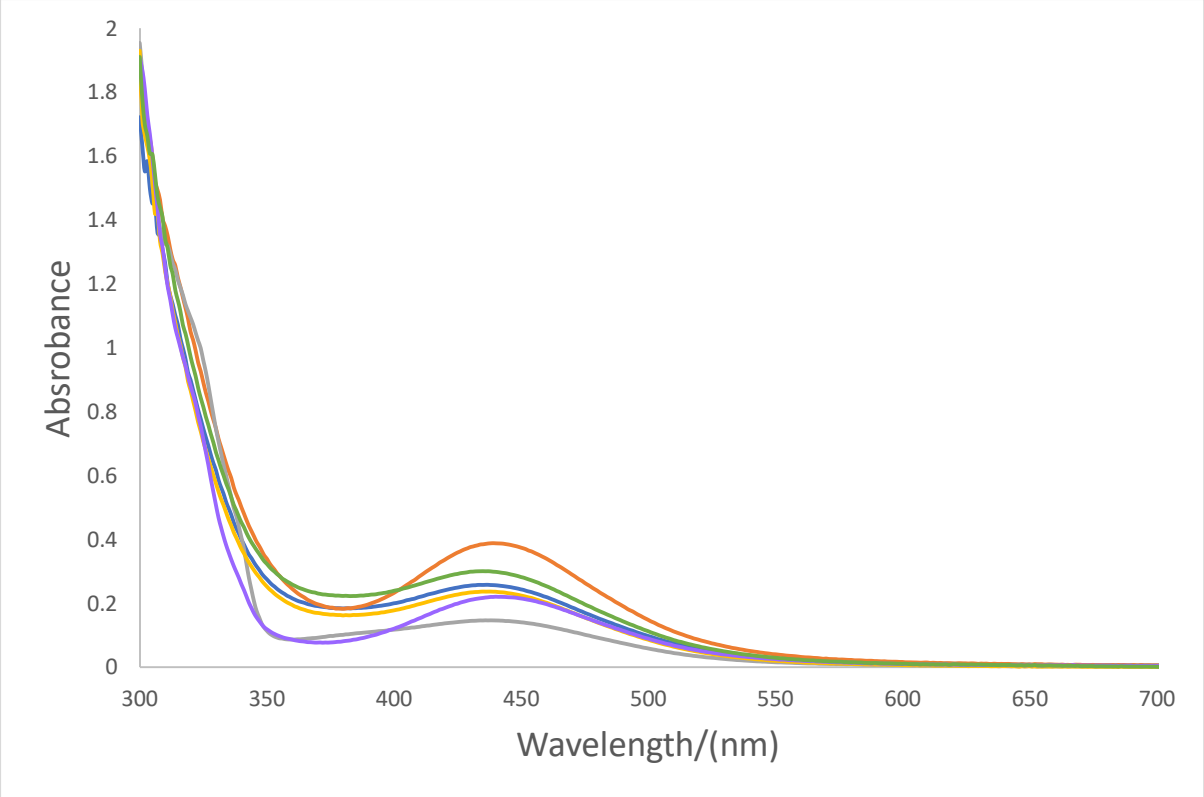

Figure (4.14.4) UV-VIS spectra of 2-ethoxyquinoline- IBr_2^- (Blue), quinoxaline- IBr_2^- (Orange), 2-fluoro-3-iodopyridine- IBr_2^- (Silver), 4-methoxypyridine- IBr_2^- (Yellow), 2,6-dimethoxypyridine- IBr_2^- (Purple), 2,6-dichloropyridine- IBr_2^- (Green), the spectra were collected using methanol as the solvent, the concentration of the samples was 10^{-3} M.

Chapter (5)
Iodine

5.1 Introduction.

Iodine is the heaviest stable halogen. At room temperature, it exists as a lustrous purple-black solid. The melting and boiling points of iodine are 144 °C and 184 °C, respectively. However, it is well known that even with the light heat, iodine sublimes easily.[126,134] In the gas phase, the I-I bond length was determined by Raman spectroscopy 2.6663 Å.[27]

Iodine as an element is of crucial importance for halogen bonding since it has the best XB donor properties. As it was mentioned in the general introduction, the molecular iodine is found in the first reported XB adduct $H_3N\cdots I_2$ [5] and the benzene$\cdots$ I_2 adduct was studied by Benesi and Hildebrand in their pioneering spectroscopic work.[9]

Nowadays, it is being discovered that halogen bonding is an important factor in many biochemical systems, but particularly in thyroid biochemistry, which is iodine dependent. Research is focused on elucidating XB interactions with thyroid enzymes[107,143] and the interaction of antithyroid drugs with molecular iodine.[108]

Depending on a variety of factors (steric effects, XB acceptor atom, other non-covalent interactions), several different structural interaction modes are observed in dihalogen XBs.[106] Electron donors which interact at only one end of the X_2 or XY molecule form discrete adducts (Figure 5.0.1, A). Except for these simple adducts, in systems with halogen bonded diiodine, bridging mode (Figure 5.0.1, B) where both iodine atoms are involved in XB interaction, is observed for diazines (pyrazine and derivatives,[144] phenazine and quinoxaline[145]), 9-chloroacridine[146] and the diiodine with hexamethylenetetramine complex.[147] Apart from the mentioned two modes, amphoteric adducts (Figure 5.0.1, AA) and amphoteric bridging mode (Figure 5.0.1, BA) are observed. In the former, polarization on the X_2 is sufficient enough to make X atom which is not interacting with XB acceptor act as a Lewis base to adjacent dihalogens, while in the latter, both the amphoteric effect and bridging modes can be observed.

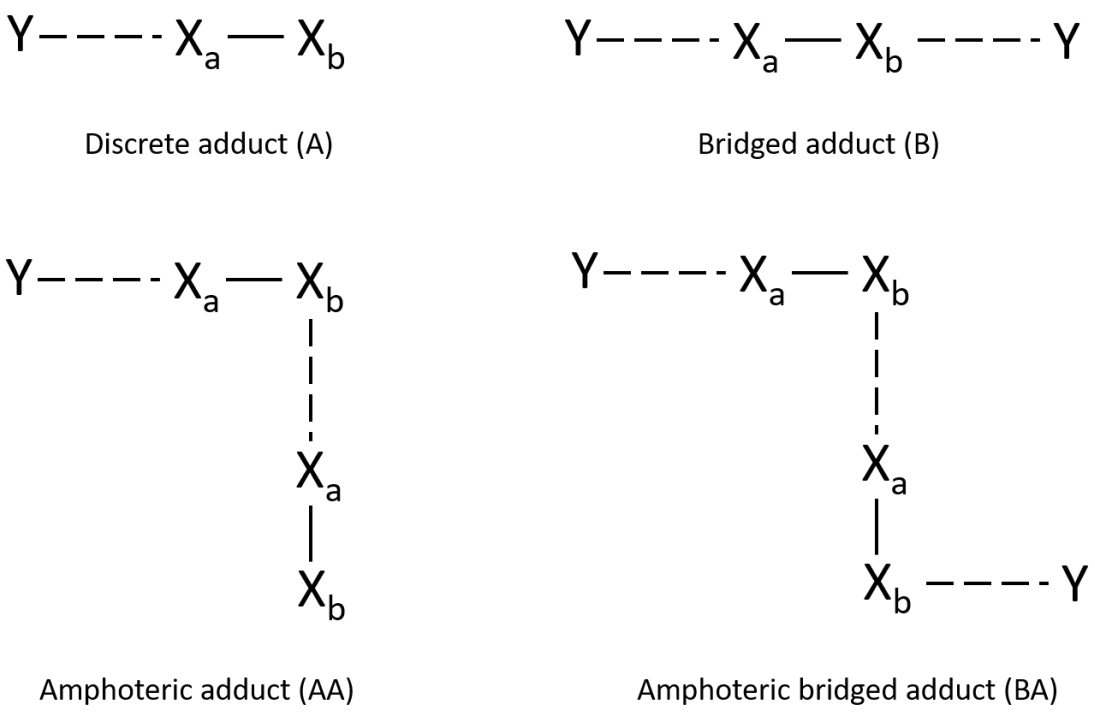

Figure 5.0.1 Dihalogen XB interaction modes, adapted from [106]

Most N···I_2 complexes, and all N···IBr, and N···ICl complexes are discrete adducts (mode A). However, from the above-mentioned modes, the bridging mode is observed in this work, as well. Since the XB iodine chemistry is abundant and with many reported complexes, only the ones containing N···I-I halogen will be presented in Table 5.0.1.

Table 5.0.1 Geometric parameters of literature reported N···I-I halogen bonded complexes, adapted from ref.[106,112]

REFCODE	Complex name	N···I (Å)	I-I (Å)	N···I-I (°)
CHXADI10[148]	9-cyclohexyladenine diiodine	2.520	2.764	177.14
GAWXEH[149]	N-iodine-2,3-diazabicyclo (2.2.2) oct-2-ene	2.431	2.807	175.49
HMCPZI[150]	Hexamethylcyclotriphosphazene diiodine	2.418	2.823	177.80
HXMIOD[147]	Hexamethylenetetramine bis (diiodine)	2.497 2.498	2.791 2.771	173.92 173.85
NULBEB[145]	2,3-bis (2-pyridyl) quinoxaline diiodine	2.530	2.759	173.80
NULBIF[145]	4-cyanopyridine diiodine	2.543 2.554	2.745 2.750	175.47 175.50
NULBOL[145]	4,4-dipyridyl bis (diiodine)	2.407	2.796	177.83
NULCEC[145]	2,3,5,6-Tetrakis (2-pyridyl) pyrazine bis (diiodine)	2.563	2.750	173.02
PICOLI[151]	4-picoline diiodine	2.322	2.823	175.51
QIHBOY[152]	1,2-Bis (4-pyridyl) ethylene bis (diiodine)	2.422	2.802	178.78
TMEAMI[153]	Trimethylamine diiodine	2.271	2.830	178.33
WEKGIC[154]	(Triphenylphosphonio(trimethylsilyl)imino) diiodine	2.432	2.833	178.93
YUYNUB[155]	1,3,5,7-Tetraazatricyclo (3.3.1.13,7) decane tris (diiodide)	2.593	2.746	177.58
HMTNTI[156]	Hexamethylenetetramine tri-iodo-nitrogen	2.475	2.808	175.41

	diiodine	3.247		178.10
HXMTDI[147]	Hexamethylenetetramine diiodine	2.439 3.482	2.830	173.07 179.75
NULBUR[145]	Quinoxaline diiodine	2.949 2.918	2.724	178.77 175.77
PHNAZI01[157]	Phenazine diiodine	2.986 3.099	2.726	180.00 180.00
QARGUL[146]	Bis (9-chloroacridine) diiodine	2.981	2.741	178.75
PEWQIT[158]	1-(Diiodane)-4-(2-(4-(octyloxy)phenyl) vinyl) pyridine	2.353	2.830	177.19
LEWKOP[159]	3,3'-(1,4-Phenylenediethyne-2,1-diyl) bis(1-(1λ3-diiodan-1-yl)-1λ5-pyridine) diiodine	2.358	2.818	176.08
VUHDIN[160]	Pyridine diiodine	2.425	2.804	176.44
YIPCEG[161]	Isonicotinamide iodine	2.439	2.790	178.04
BULJUP[162]	(E)-1,2-bis(pyridine-4-yl) diazene bis(iodine)	2.477	2.773	179.58
ZESQUM[135]	bis(2,6-bis(phenylselanyl) pyridine) di-iodine	2.936	2.722	175.76
DARZAY[163]	2,3,5,6-tetrakis(2-Pyridyl) pyrazine hexakis (di-iodine)	2.498 2.568	2.760 2.755	174.46 168.30
CECZAL[164]	2,2'-Bipyridine diiodine	2.604	2.746	179.41
ZESQOG[135]	2-[(4-chlorophenyl) selanyl] pyridine di-iodine	2.497	2.769	178.18
SUBWEU[165]	N-(diiodine)-2,2,6,6-tetramethylpiperidine	2.469	2.854	177.18

It can be observed that 28 complexes containing N···I-I have been reported. The average N···I distance is 2.610 Å, while the value for I-I bond is 2.779 Å. A complex with refcode TMEAMI[153] has the shortest N···I value (2.271 Å) that means the strongest XB, and the most elongated bond (2.833 Å) is noticed in the same system, as well. Also, it can be observed that the average value of all the N···I-I angles is 176.65° which is so close to the ideal value of 180°.

5.2 Aim

Preparation and characterisation of N···I halogen bonded crystalline complexes is the aim of this chapter. The strength of the N···I XB is going to be studied on iodine (XB donor) adducts with a series of pyridine derivatives (XB acceptor). The impact of functional groups of the nitrogen-containing organic starting materials is going to be correlated with the strength of the halogen bond interaction. All the crystalline complexes are going to be characterised by ATR-FTIR and UV-Vis spectroscopy, and single-crystal X-ray diffraction, if the suitable crystal is obtained. From the structures obtained by X-ray diffraction the halogen bond lengths and angles within the N···I unit will be determined and correlated with the electronic spectra.

5.3 Investigation of halogen bonded complexes

5.3.1 3,5-difluoropyridine- I_2

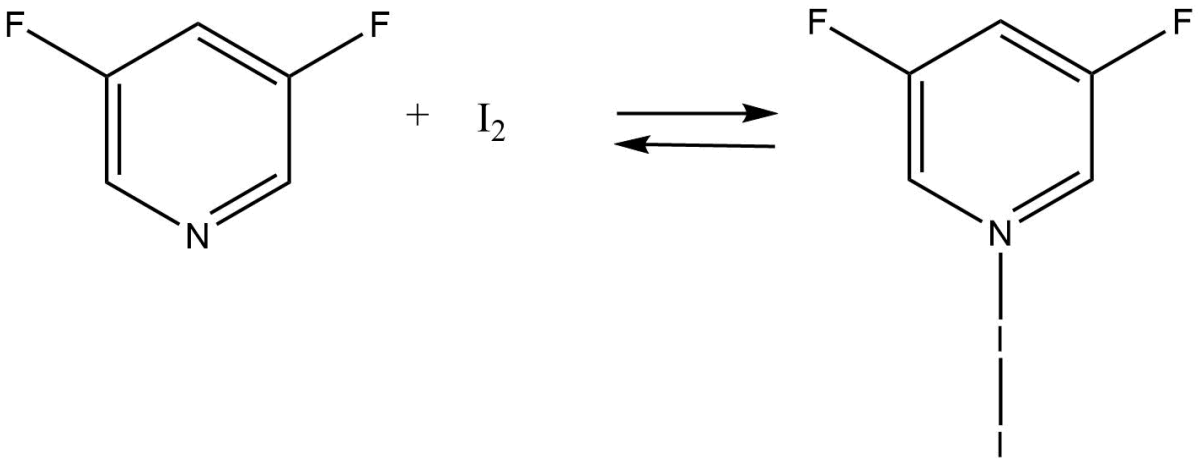

UV-Visible Spectra for 3,5-difluoropyridine –I_2 solution

All the spectra were collected in methanol, the concentration of all the samples was 10^{-3} M. The base 3,5-difluoropyridine absorbs at 303 nm and iodine absorbs at 304 nm. A new band appears at 362 nm when the two above starting materials are mixed. This band is not attributed to the 3,5-difluoropyridine or iodine. λ_{max} for 3,5-difluoropyridine was shifted 59 nm toward higher wavelength which is called bathochromic shift or redshift, Figure (5.1.1). Starting material and the resulting complex are also characterised by ATR-FTIR, Figures (3.1.2, 5.1.2).

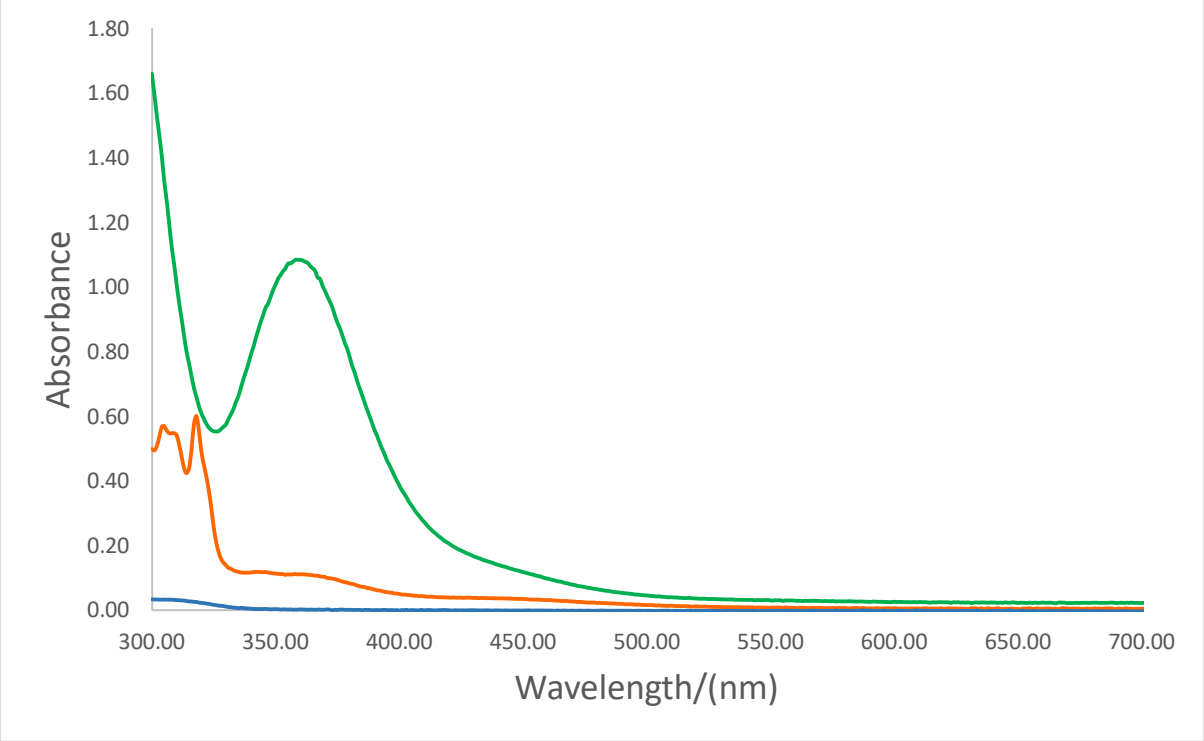

Figure (5.1.1) UV- Visible Spectra of 3,5-difluoropyridine-I_2: 3,5-difluoropyridine (Blue), I_2 (Orange), 3,5- difluoropyridine-I_2 (Green), the spectra were collected using methanol as the solvent, the concentration of the samples was 10^{-3} M.

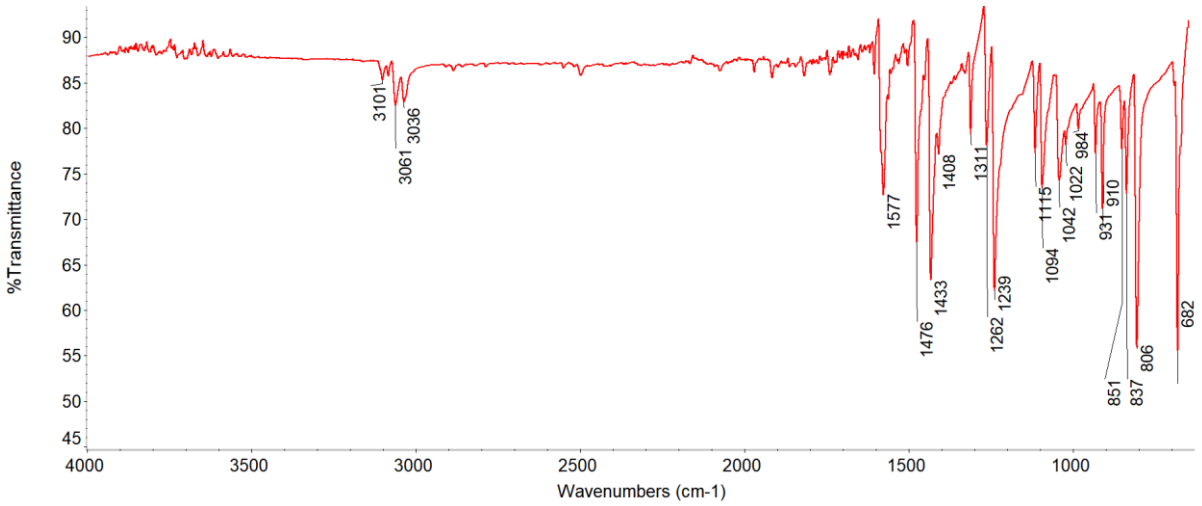

Figure (3.1.2): IR spectrum of 3,5-difluoropyridine.

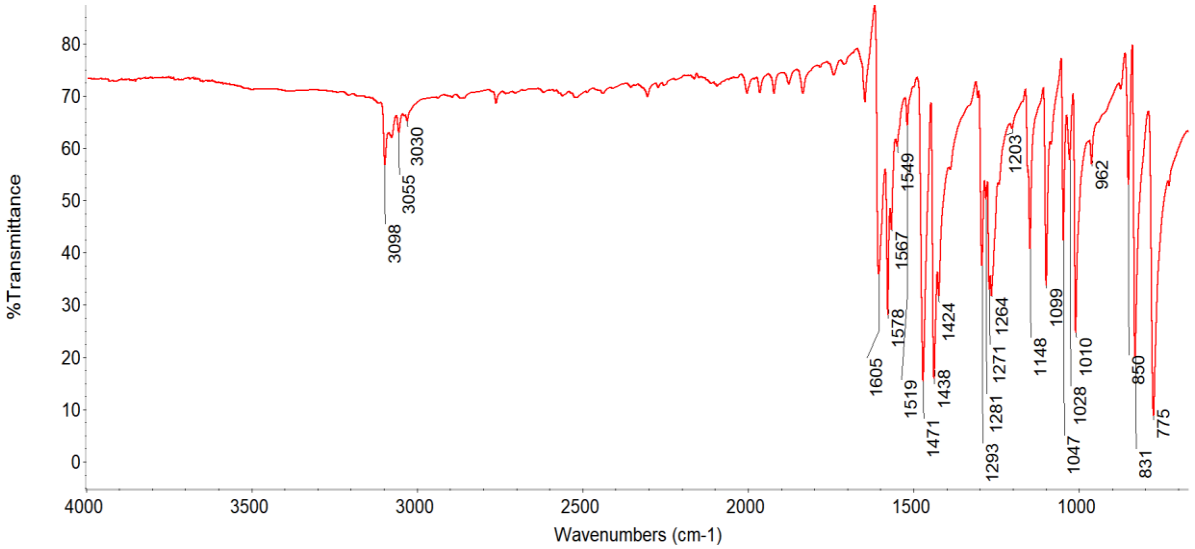

Figure (5.1.2) ATR-FTIR spectrum of 3,5-difluoropyridine-I_2.

5.3.2 3,5-dichloropyridine - I_2

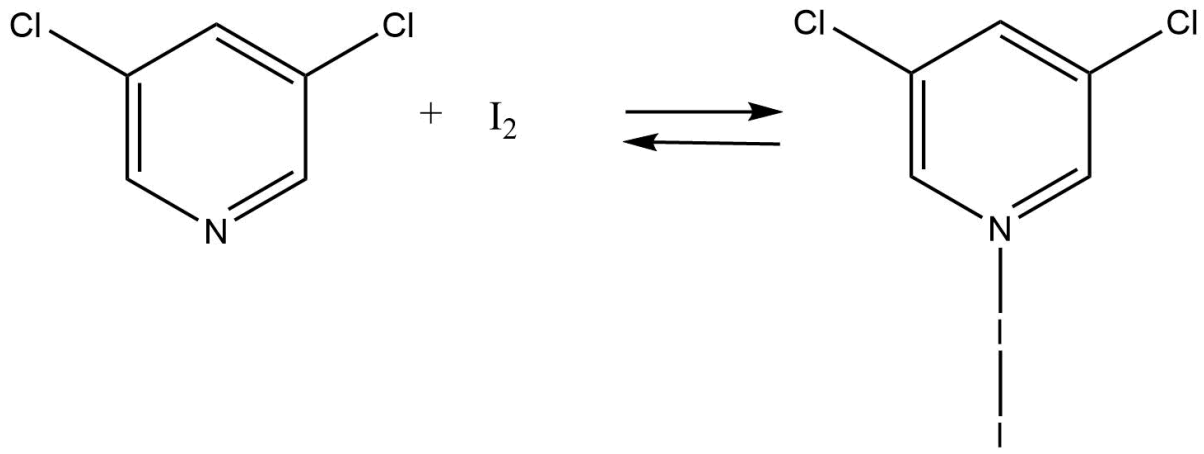

UV-Visible Spectra for 3,5-dichloropyridine –I_2 solution

All the spectra were collected in methanol, the concentration of all the samples was 10^{-3} M. The base 3,5-dichloropyridine absorbs at 335 nm and iodine absorbs at 304 nm. A new band appears at 360 nm when the two above starting materials are mixed. This new band is not attributed to the 3,5-dichloropyridine or I_2. λ_{max} for 3,5-dichloropyridine was shifted 25 nm toward higher wavelength, Figure (5.2.1). Starting material and the resulting complex are also characterised by ATR-FTIR, Figures (3.2.2, 5.2.2).

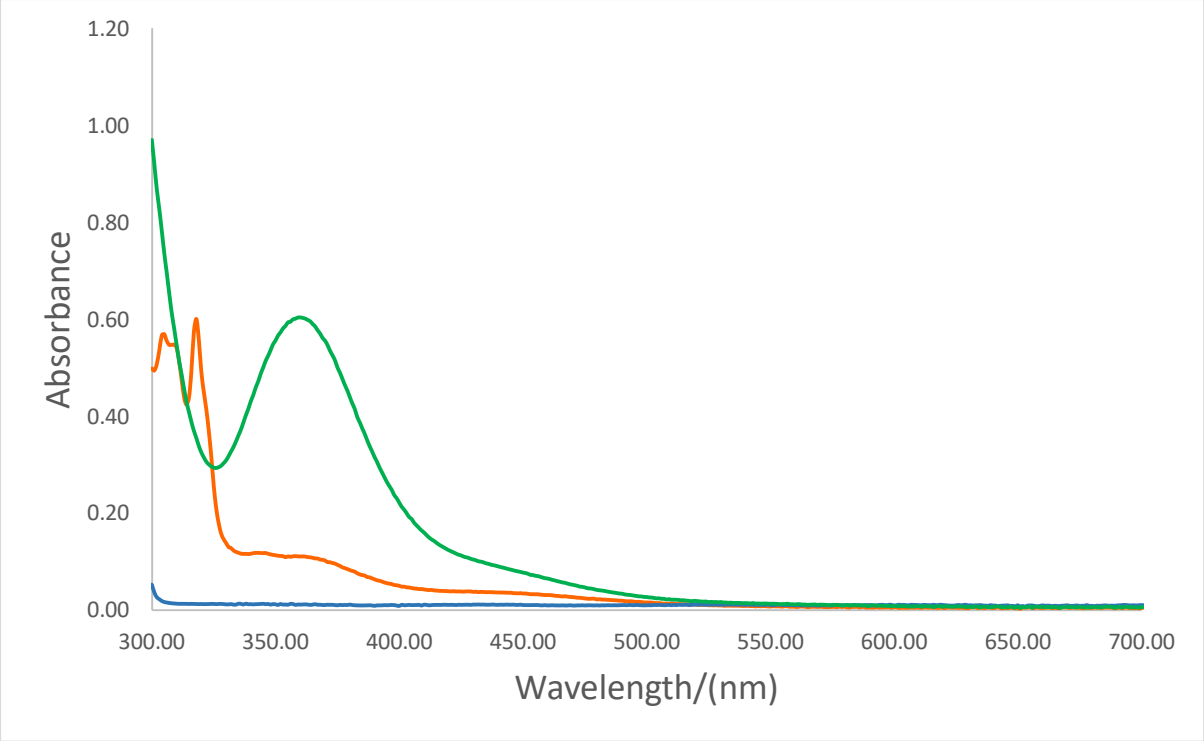

Figure (5.2.1) UV- Visible Spectra of 3,5-dichloropyridine-I_2: 3,5-dichloropyridine (Blue), I_2 (Orange), 3,5-dichloropyridine-I_2 (Green), the spectra were collected using methanol as the solvent, the concentration of the samples was 10^{-3} M.

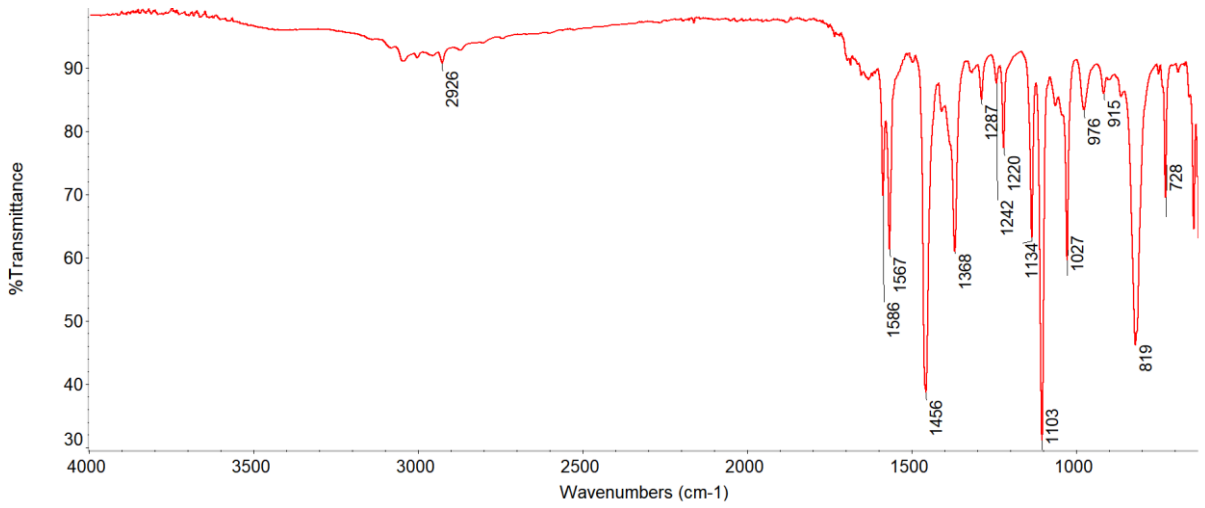

Figure (3.2.2): IR spectrum of 3,5-dichloropyridine.

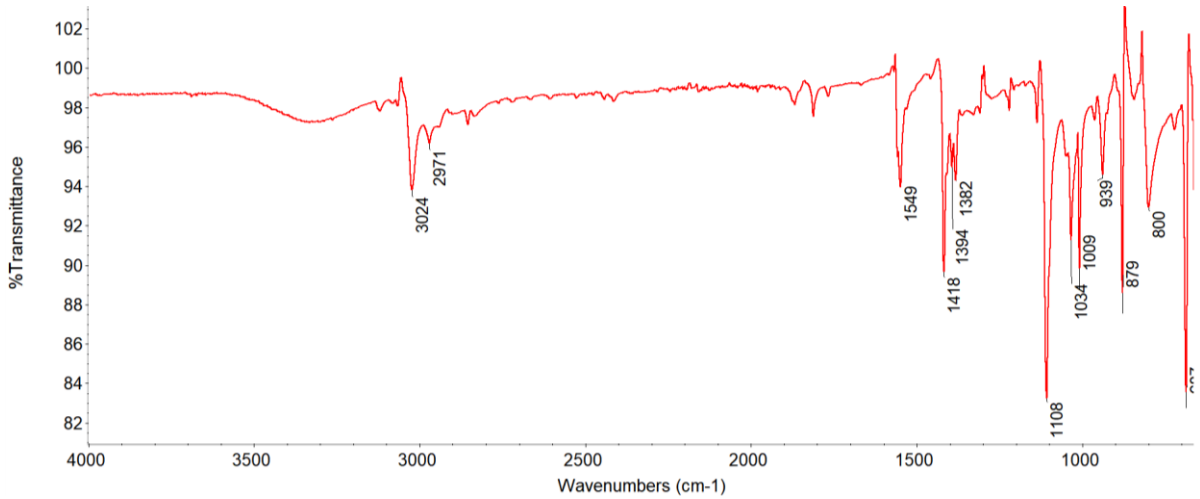

Figure (5.2.2) ATR-FTIR spectrum of 3,5-dichloropyridine-I_2

5.3.3 2,6-dichloropyridine-I_2:

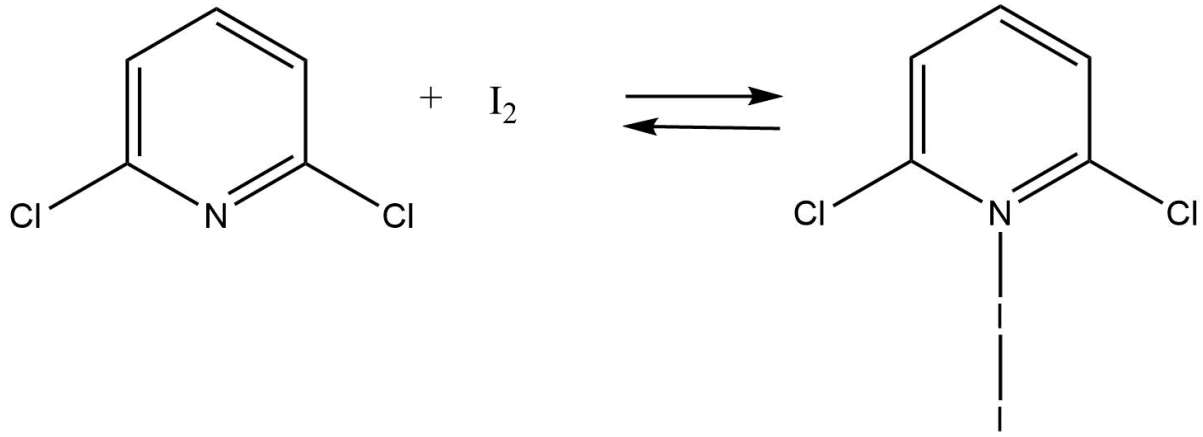

UV-Visible Spectra for 2,6-dichloropyridine –I_2 solution

All the spectra were collected in methanol, the concentration of all the samples was 10^{-3} M. The base 2,6-dichloropyridine absorbs at 335 nm and iodine absorbs at 304 nm. The new band appears at 359 nm when the two above starting materials are mixed which is not attributed to the 2,6-dichloropyridine or iodine. λ_{max} for 2,6-dichloropyridine was shifted 24 nm toward higher wavelength, Figure (5.3.1). Starting material and the resulting complex are also characterised by ATR-FTIR, Figures (3.3.1, 5.3.2).

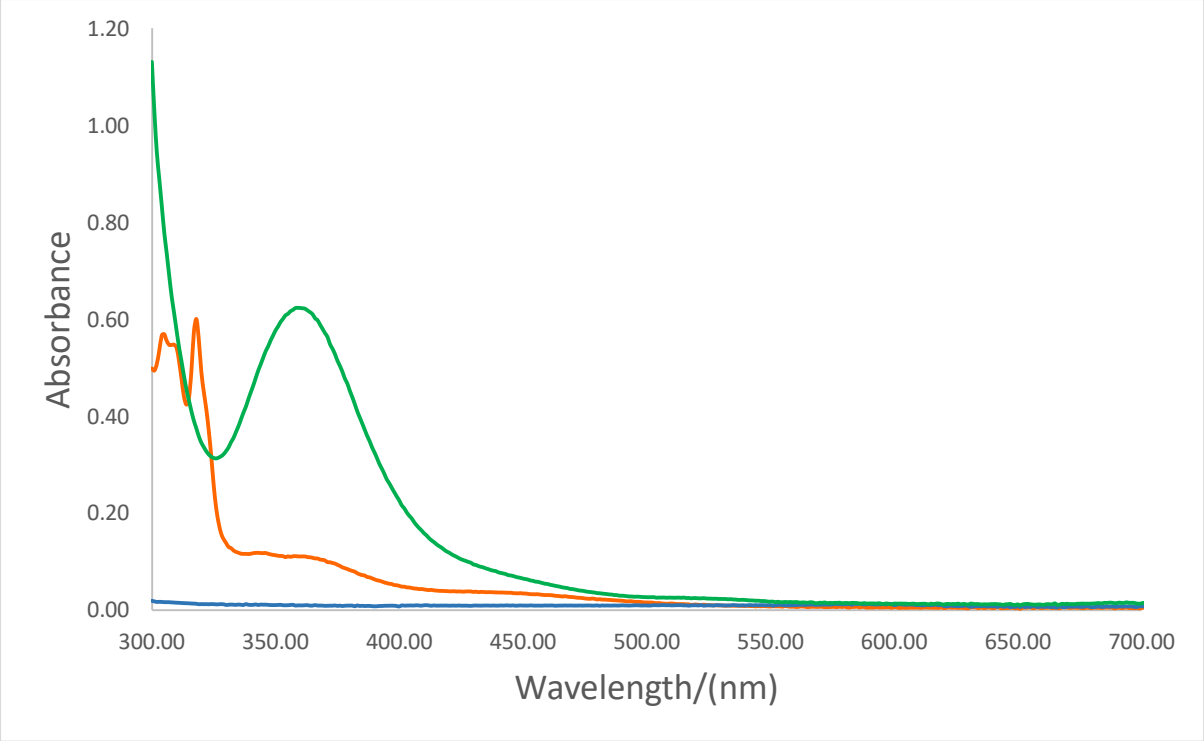

Figure (5.3.1) UV- Visible Spectra of 2,6-dichloropyridine-I_2: 2,6-dichloropyridine (Blue), I_2 (Orange), 2,6-dichloropyridine-I_2 (Green), the spectra were collected using methanol as the solvent, the concentration of the samples was 10^{-3} M.

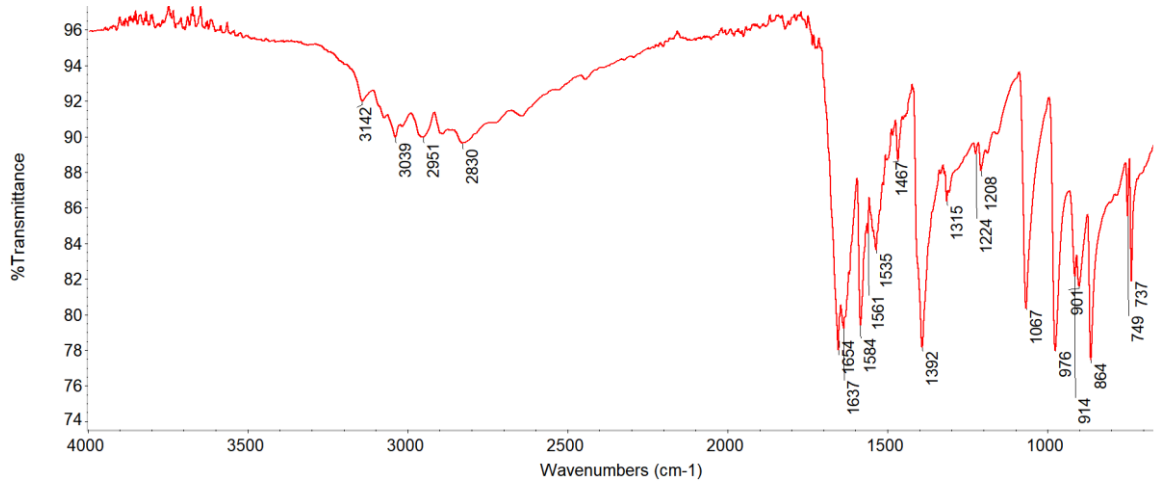

Figure (3.3.1) ATR-FTIR spectrum of 2,6-dichloropyridine

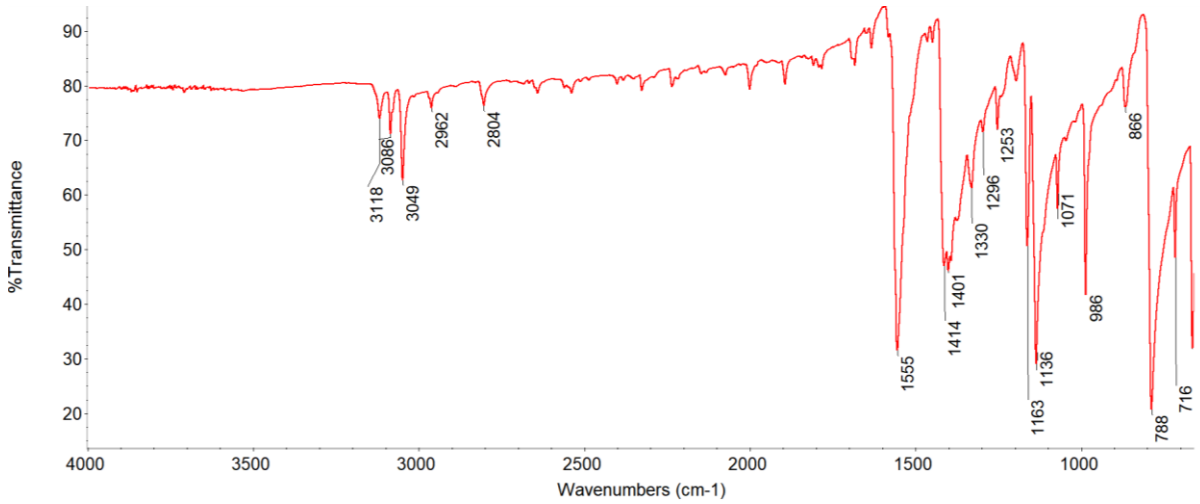

Figure (5.3.2) ATR-FTIR spectrum of 2,6-dichloropyridine-I_2.

5.3.4 2,6-dimethoxypyridine-I_2

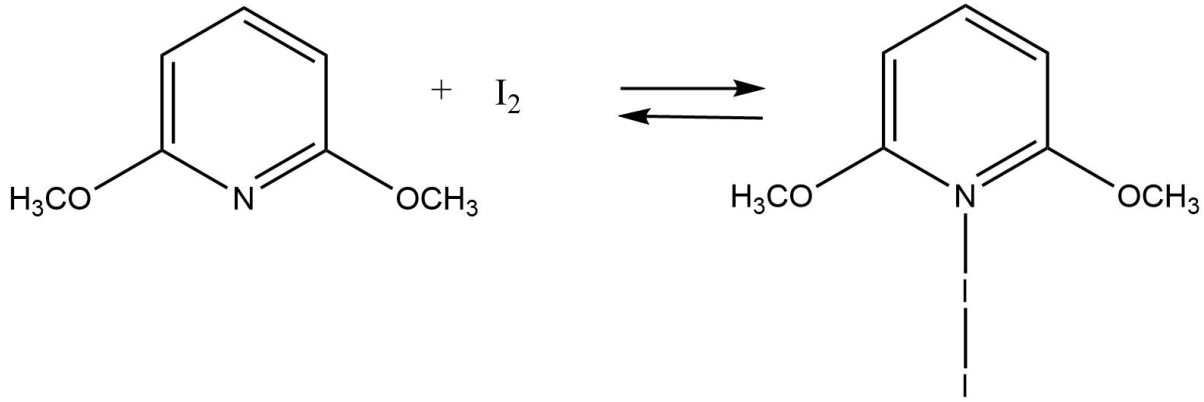

UV-Visible Spectra for 2,6-dimethoxypyridine –I_2 solution

All the spectra were collected in methanol, the concentration of all the samples was 10^{-3} M. The base 2,6-dimethoxypyridine absorbs at 316 nm and iodine absorbs at 304 nm. The new band appears at 358 nm when the two above starting materials are mixed which is not attributed to the 2,6-dimethoxypyridine or I_2. λ_{max} for 2,6-dimethoxypyridine was shifted 42 nm toward higher wavelength, Figure (5.4.1). Starting material and the resulting complex are also characterised by ATR-FTIR, Figures (3.4.2, 5.4.2).

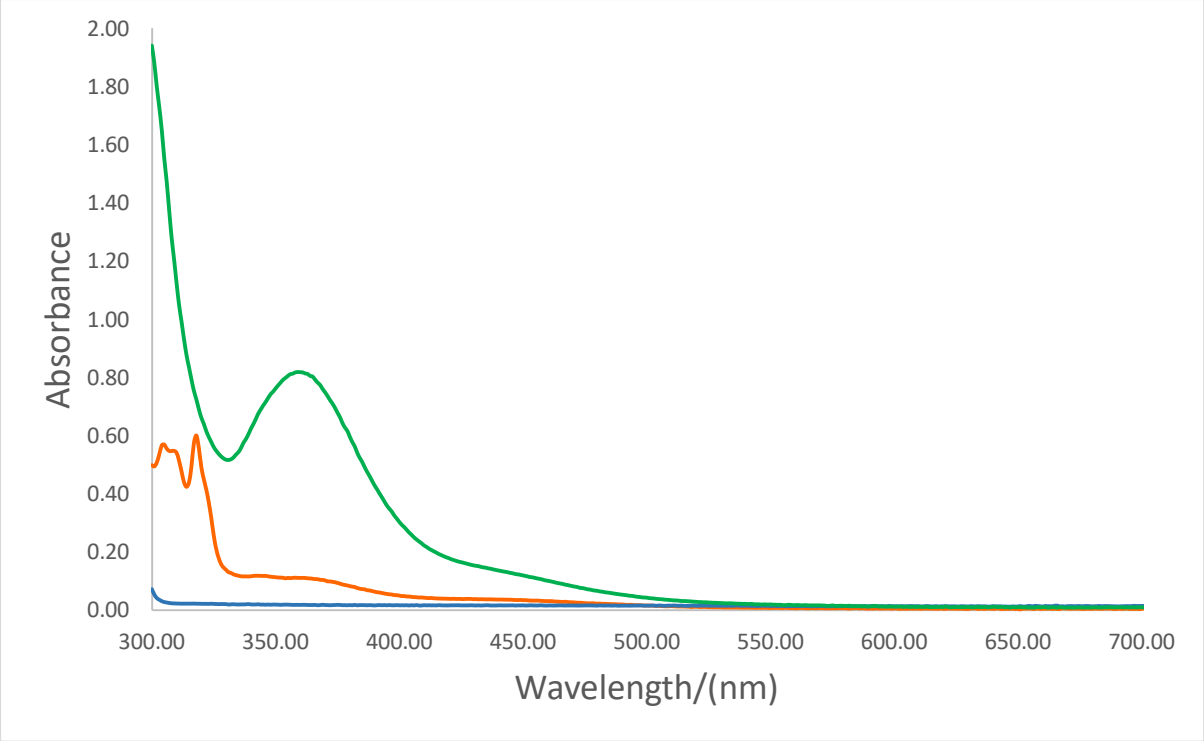

Figure (5.4.1) UV- Visible Spectra of 2,6-dimethoxypyridine -I_2: 2,6-dimethoxypyridine (Blue), I_2 (Orange), 2,6-dimethoxypyridine -I_2 (Green), the spectra were collected using methanol as the solvent, the concentration of the samples was 10^{-3} M.

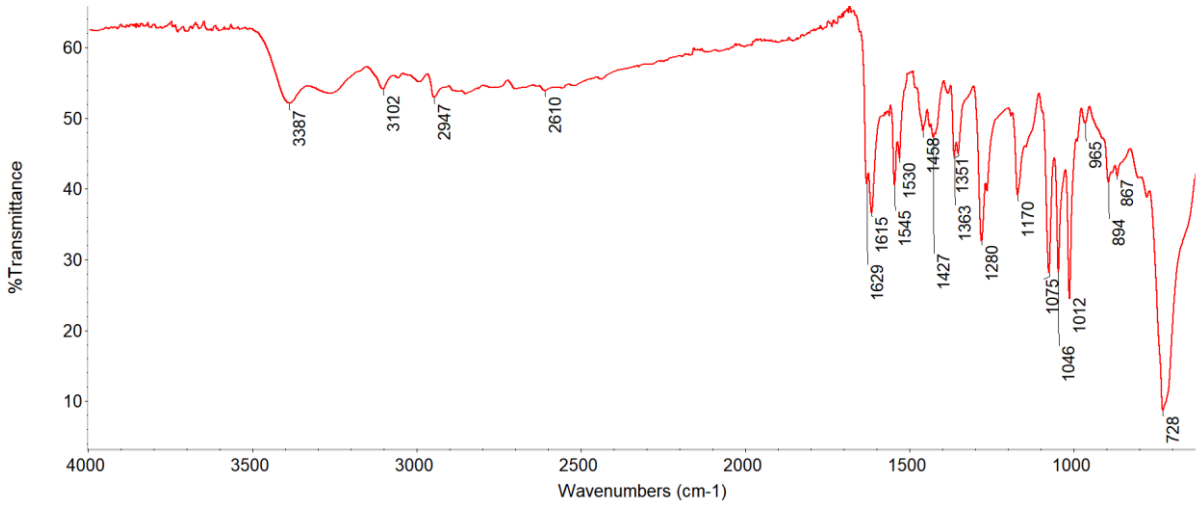

Figure (3.4.2): ATR-FTIR spectrum of 2,6-dimethoxypyridine.

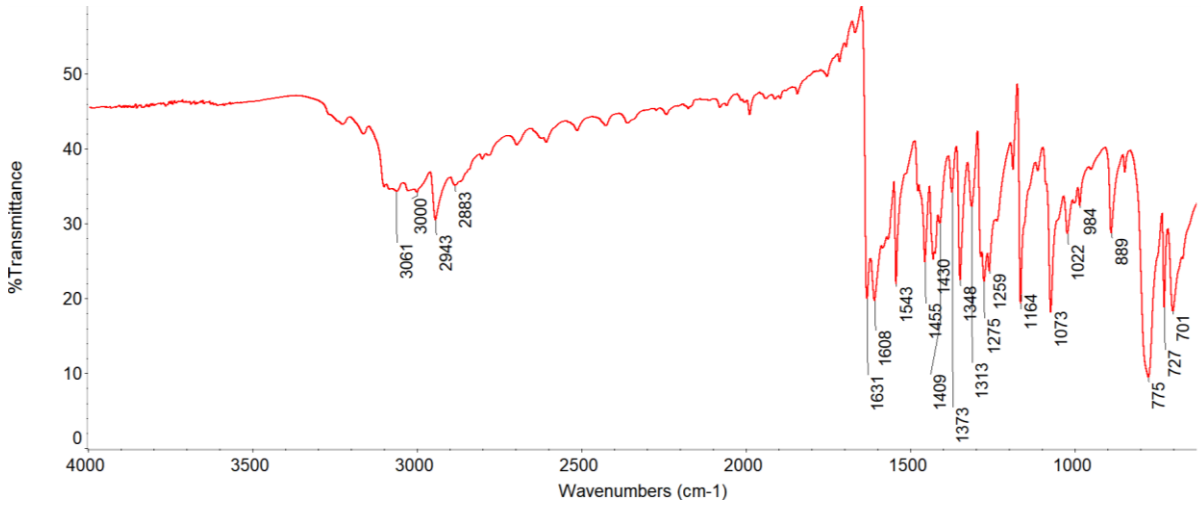

Figure (5.4.2) ATR-FTIR spectrum of 2,6-dimethoxypyridine -I_2.

5.3.5 4-methoxypyridine-I_2

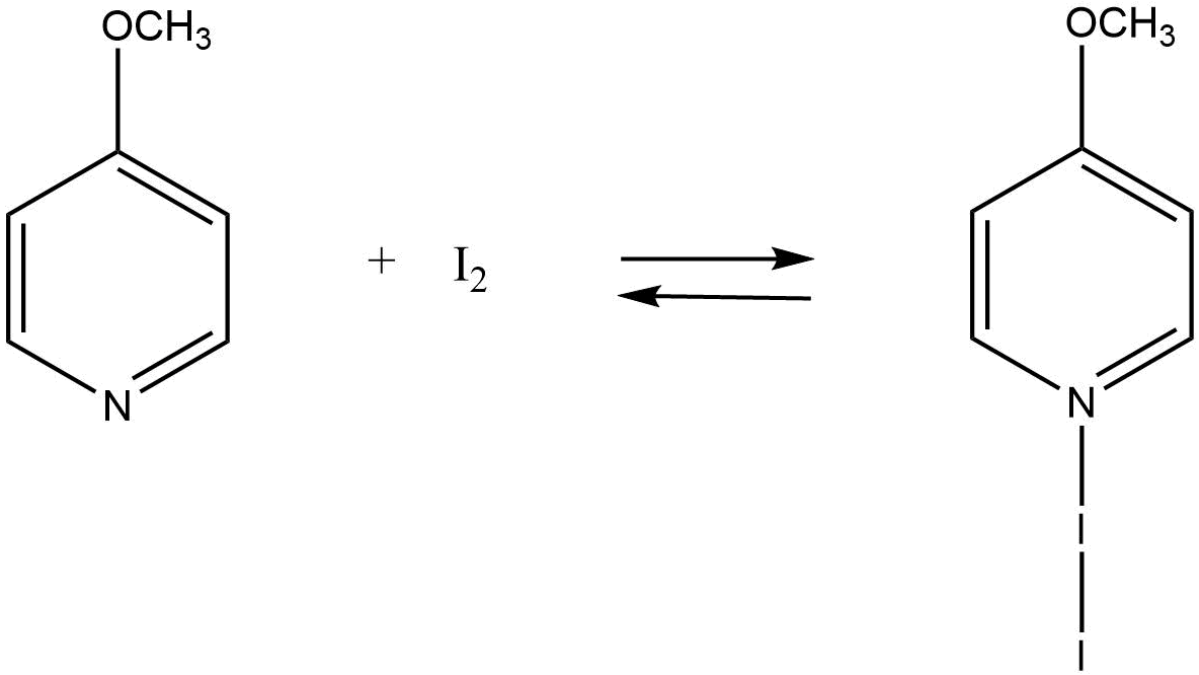

UV-Visible Spectra for 4-methoxypyridine –I_2 solution

All the spectra were collected in methanol, the concentration of all the samples was 10^{-3} M. The base 4-methoxypyridine absorbs at 328 nm and iodine absorbs at 304 nm. The new band appears at 359 nm when the two above starting materials are mixed which is not attributed to the 4-methoxypyridine or I_2. λ_{max} for 4-methoxypyridine was shifted 31 nm toward higher wavelength, Figure (5.5.1). Starting material and the resulting complex are also characterised by ATR-FTIR, Figures (3.5.2, 5.5.2).

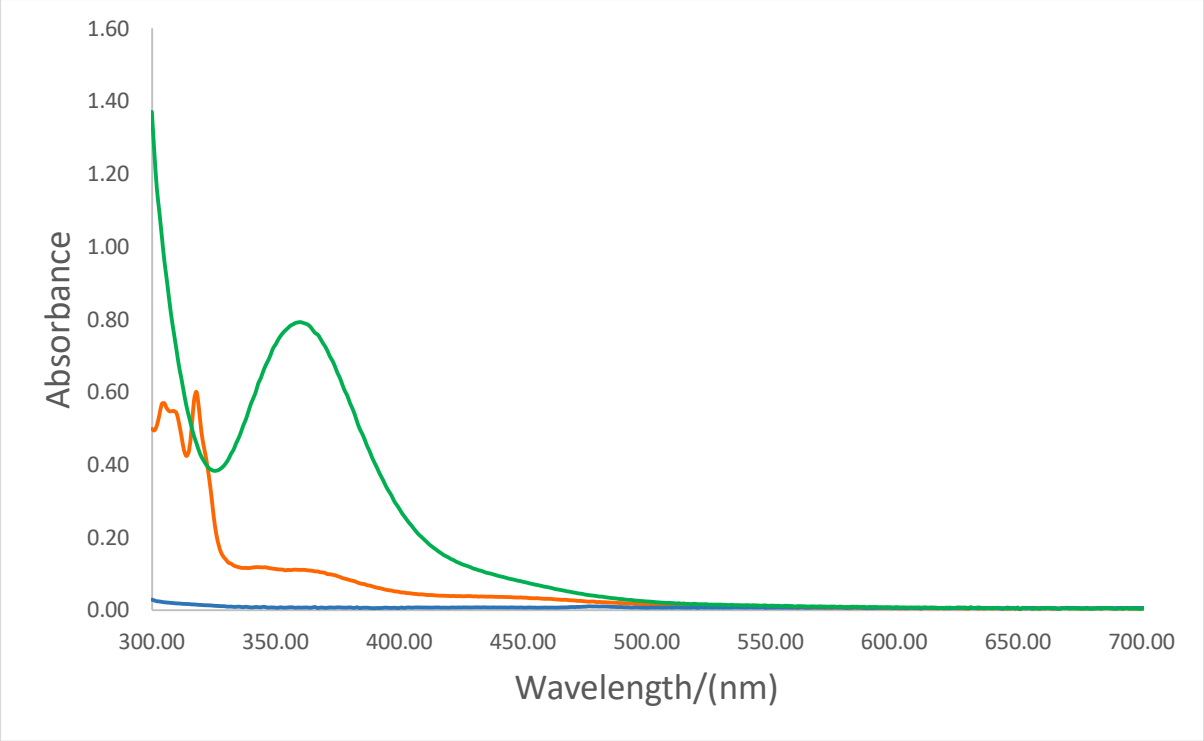

Figure (5.5.1) UV- Visible Spectra of 4-methoxypyridine-I_2: 4-methoxypyridine (Blue), I_2 (Orange), 4-methoxypyridine -I_2 (Green), the spectra were collected using methanol as the solvent, the concentration of the samples was 10^{-3} M.

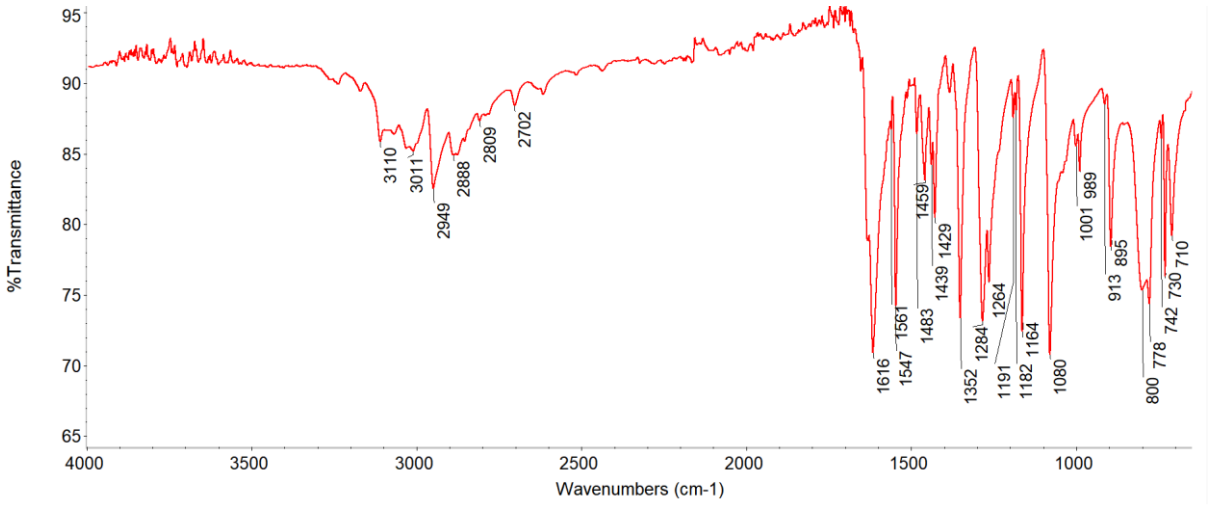

Figure (3.5.2): ATR-FTIR spectrum of 4-methoxypyiridine.

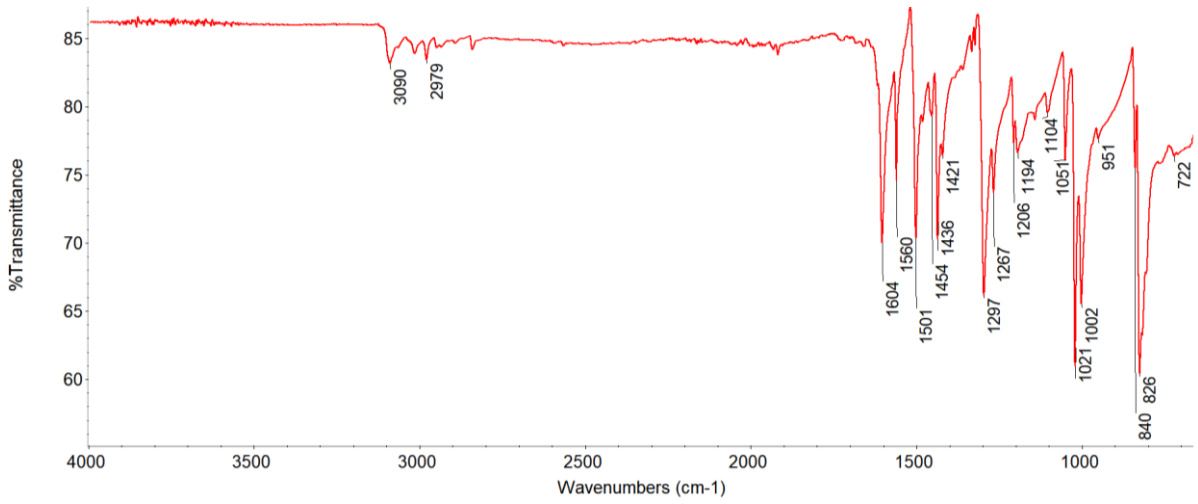

Figure (5.5.2) ATR-FTIR spectrum of 4-methoxypyridine -I_2.

5.3.6 3-fluoropyridine-I_2

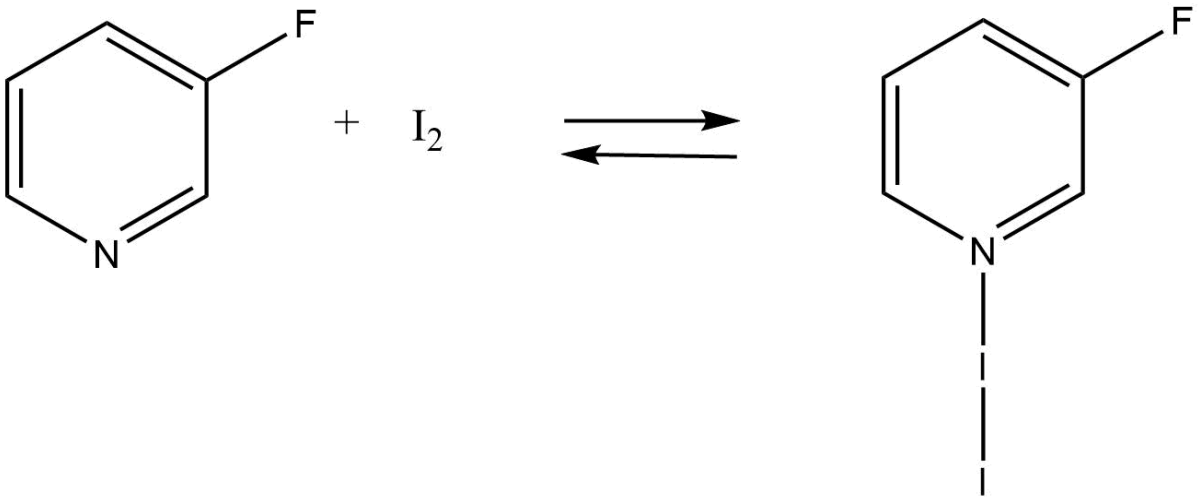

UV-Visible Spectra for 3-fluoropyridine –I_2 solution

All the spectra were collected in methanol, the concentration of all the samples was 10^{-3} M. The base 3-fluoropyridine absorbs at 303 nm and iodine absorbs at 304 nm. The new band appears at 361 nm when the two above starting materials are mixed which is not attributed to the 3-fluoropyridine or I_2. λ_{max} for 3-fluoropyridine was shifted 58 nm toward higher wavelength, Figure (5.6.1). Starting material and the resulting complex are also characterised by ATR-FTIR, Figures (3.6.2, 5.6.2).

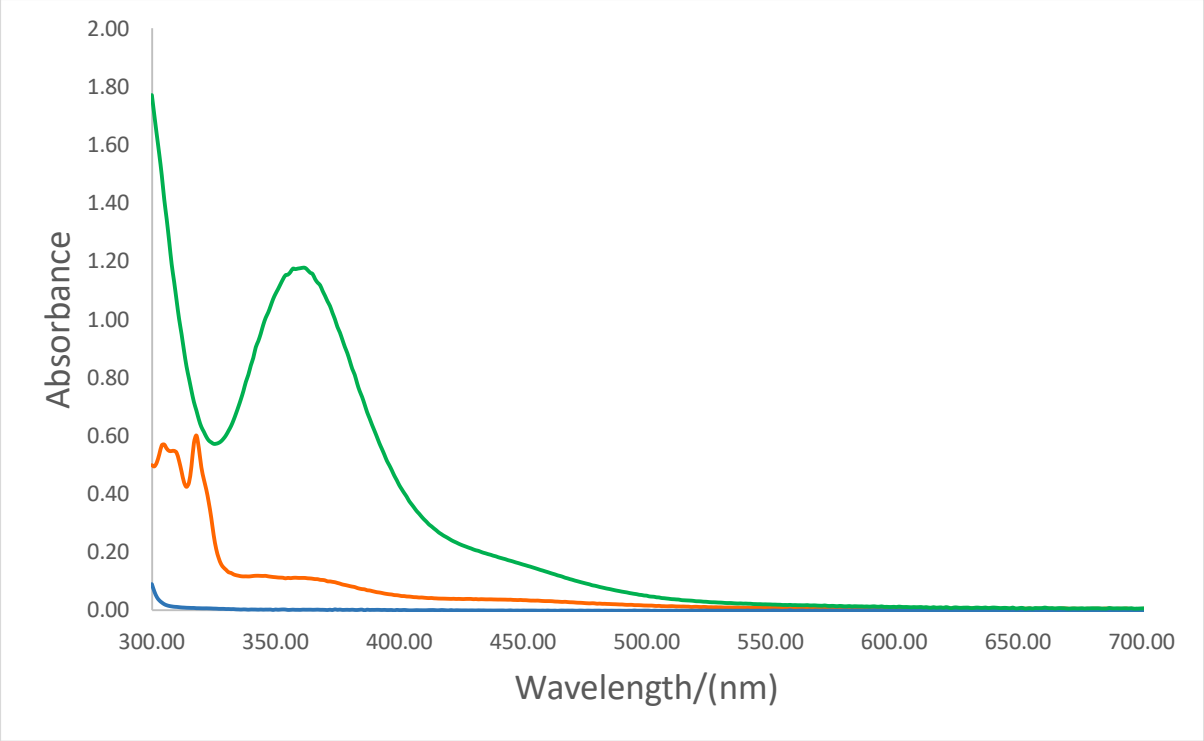

Figure (5.6.1) UV- Visible Spectra of 3-fluoropyridine -I_2: 3-fluoropyridine (Blue), I_2 (Orange), 3-fluoropyridine -I_2 (Green), the spectra were collected using methanol as the solvent, the concentration of the samples was 10^{-3} M.

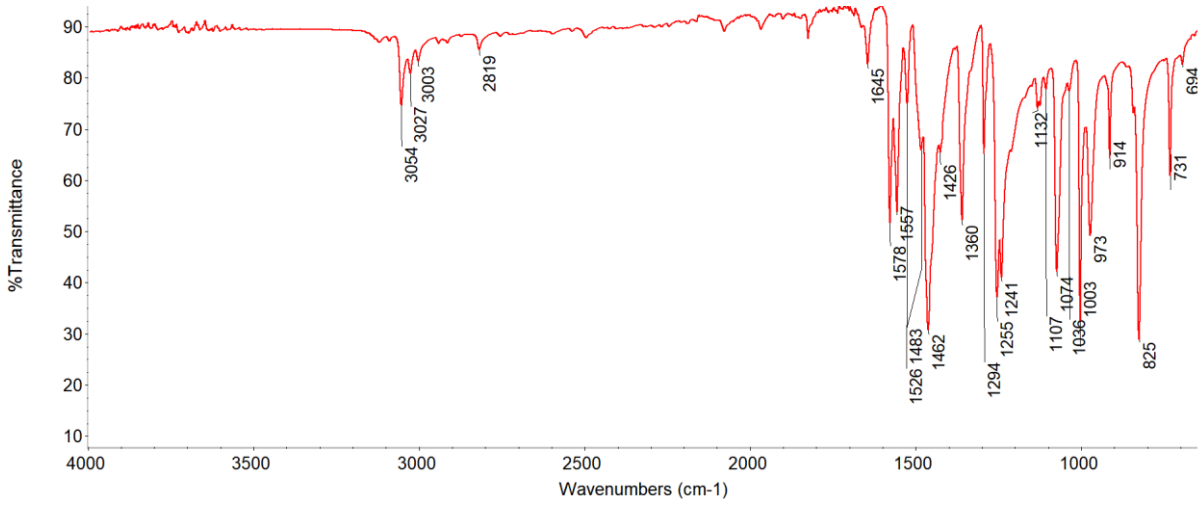

Figure 3.6.2 ATR-FTIR spectrum of 3-fluoropyridine

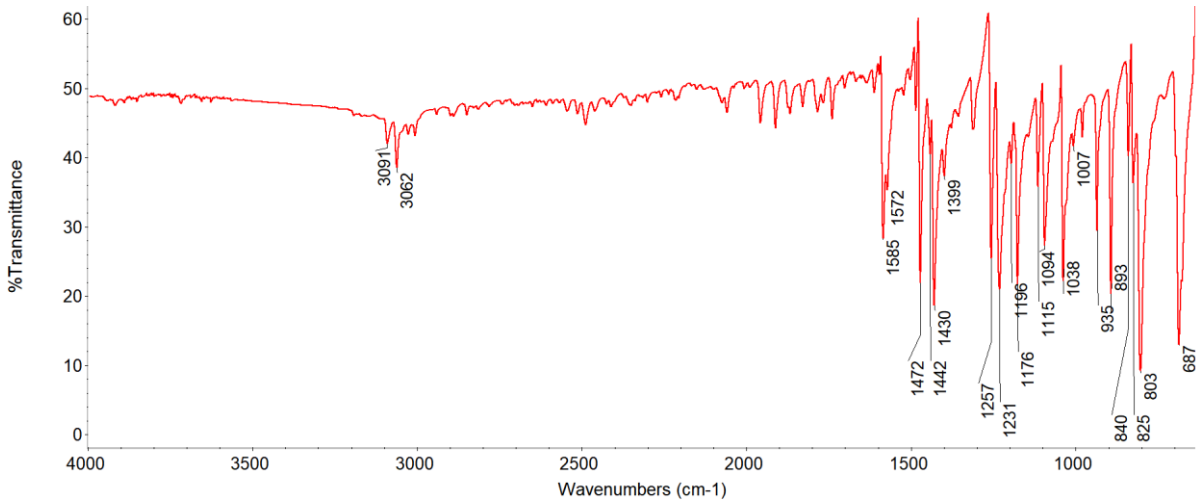

Figure (5.6.2) ATR-FTIR spectrum of 3-fluoropyridine -I_2

5.3.7 2-fluoro-3-iodopyridine-I_2

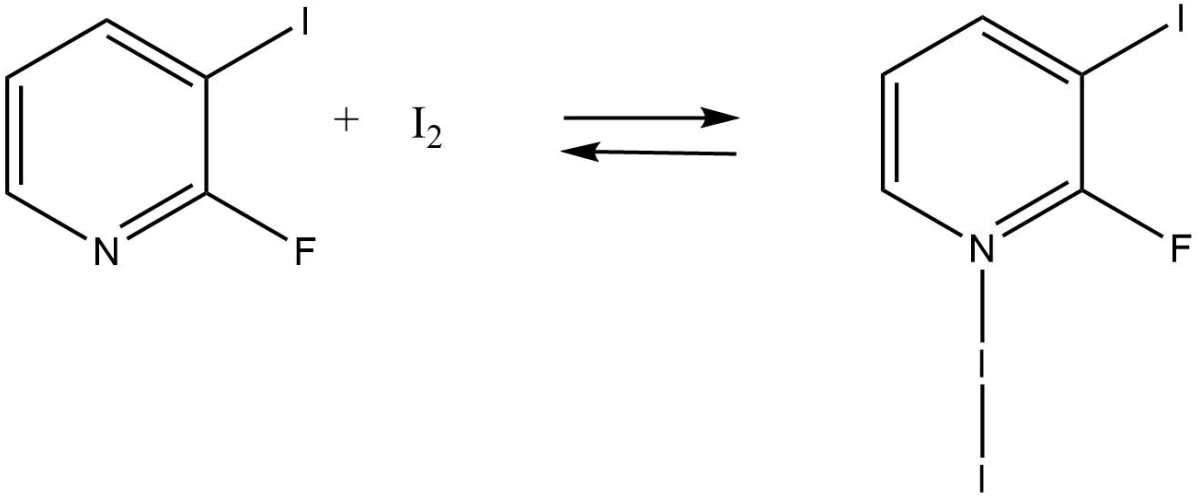

UV-Visible Spectra for 2-fluoro-3-iodopyridine –I_2 solution

All the spectra were collected in methanol, the concentration of all the samples was 10^{-3} M. The base 2-fluoro-3-iodopyridine absorbs at 316 nm and iodine absorbs at 304 nm. The new band appears at 359 nm when the two above starting materials are mixed which is not attributed to the 2-fluoro-3-iodopyridine or I_2. λ_{max} for 2-fluoro-3-iodopyridine was shifted 43 nm toward higher wavelength, Figure (5.7.1).

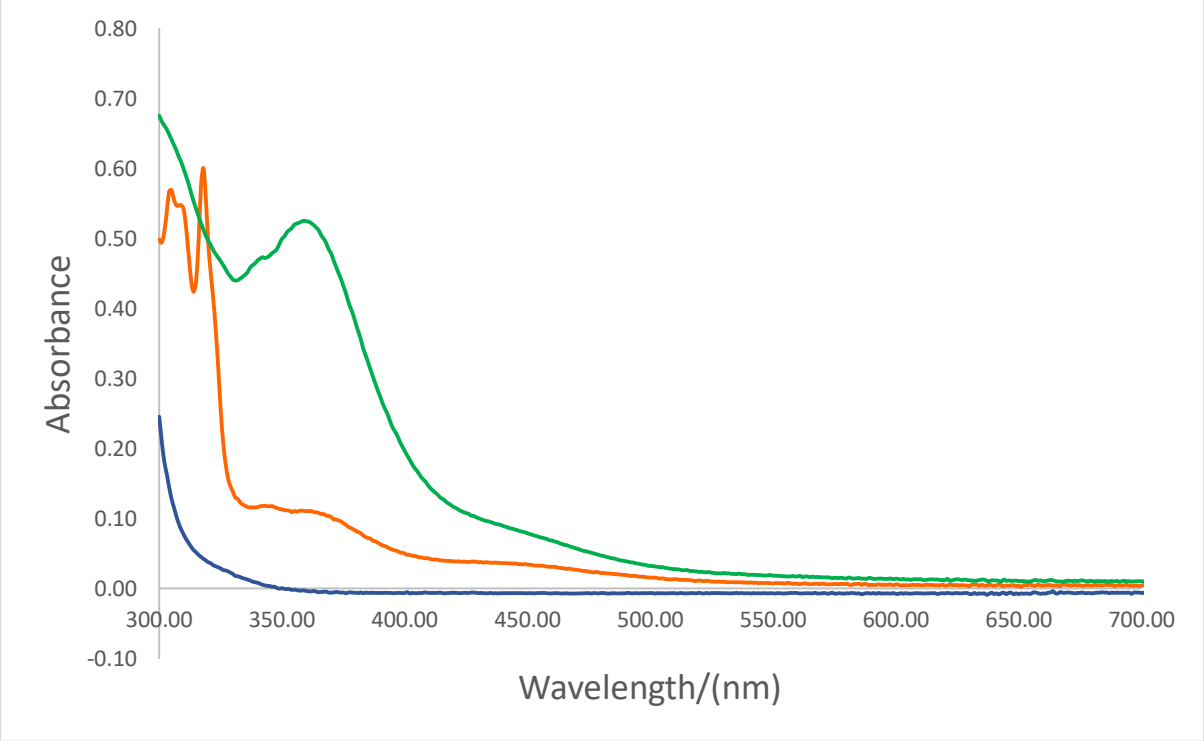

Figure (5.7.1) UV- Visible Spectra of 2-fluoro-3-iodopyridine -I_2: 2-fluoro-3-iodopyridine (Blue), I_2 (Orange), 2-fluoro-3-iodopyridine -I_2 (Green), the spectra were collected using methanol as the solvent, the concentration of the samples was 10^{-3} M.

5.3.8 2-fluoro-4-iodopyridine-I_2

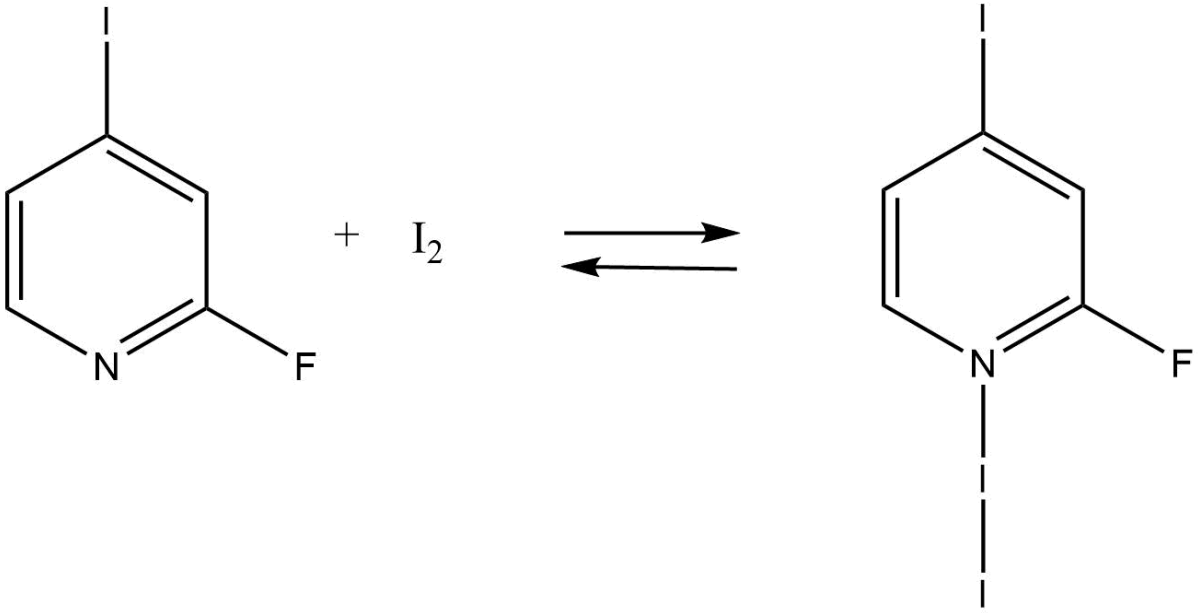

UV-Visible Spectra for 2-fluoro-4-iodopyridine –I_2 solution

All the spectra were collected in methanol, the concentration of all the samples was 10^{-3} M. The base 2-fluoro-4-iodopyridine absorbs at 351 nm and iodine absorbs at 304 nm. The new band appears at 356 nm when the two above starting materials are mixed which is not attributed to the 2-fluoro-4-iodopyridine or I_2. λ_{max} for 2-fluoro-4-iodopyridine was shifted 5 nm toward higher wavelength Figure (5.8.1). Starting material and the resulting complex are also characterised by ATR-FTIR, Figures (3.8.2, 5.8.2).

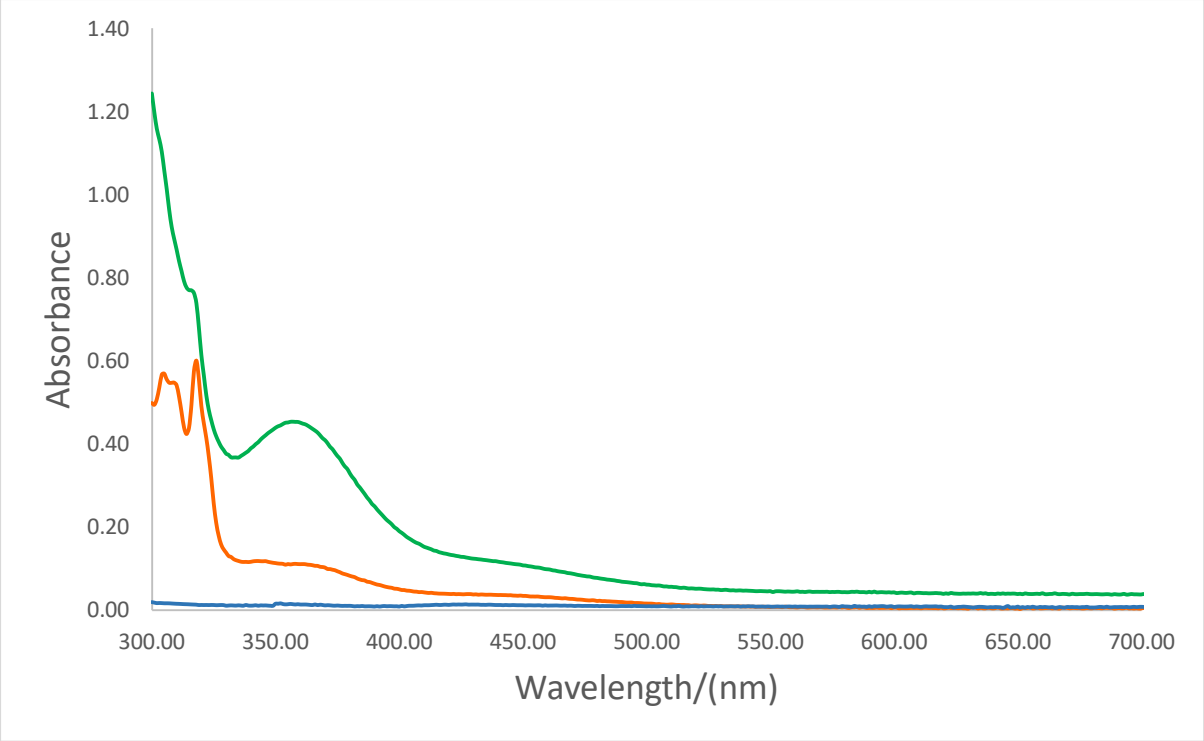

Figure (5.8.1) UV- Visible Spectra of 2-fluoro-4-iodopyridine -I_2: 2-fluoro-4-iodopyridine (Blue), I_2 (Orange), 2-fluoro-4-iodopyridine -I_2 (Green), the spectra were collected using methanol as the solvent, the concentration of the samples was 10^{-3} M.

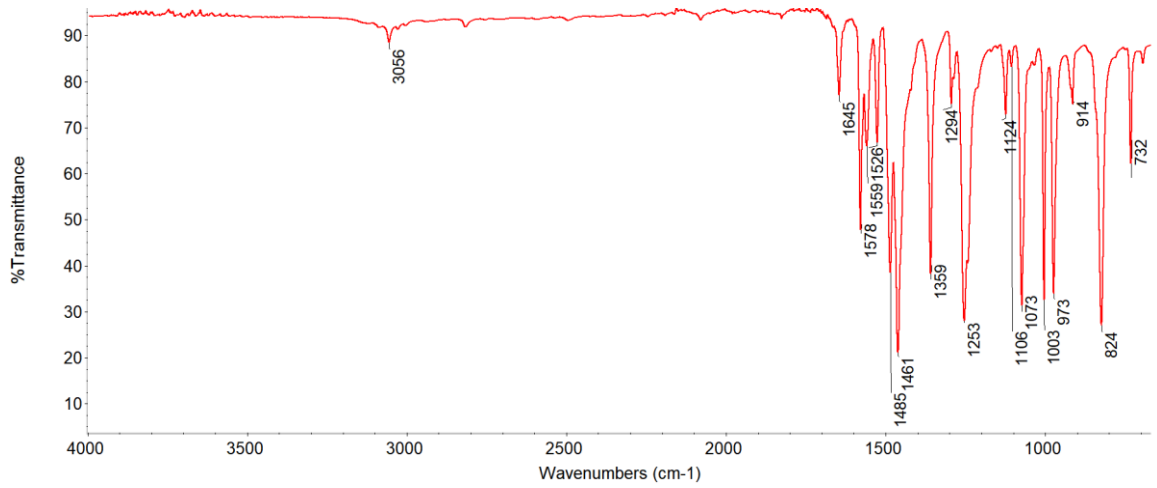

Figure (3.8.2) ATR-FTIR spectrum of 2-fluoro-4-iodopyridine

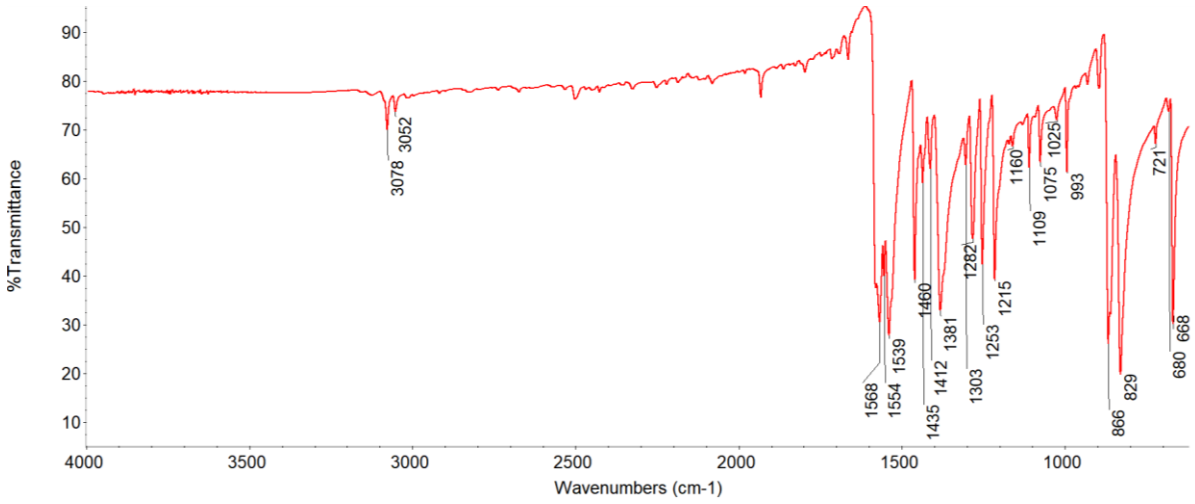

Figure (5.8.2) ATR-FTIR spectrum of 2-fluoro-4-iodopyridine -I_2

5.3.9 2-fluoro-5-iodopyridine-I_2

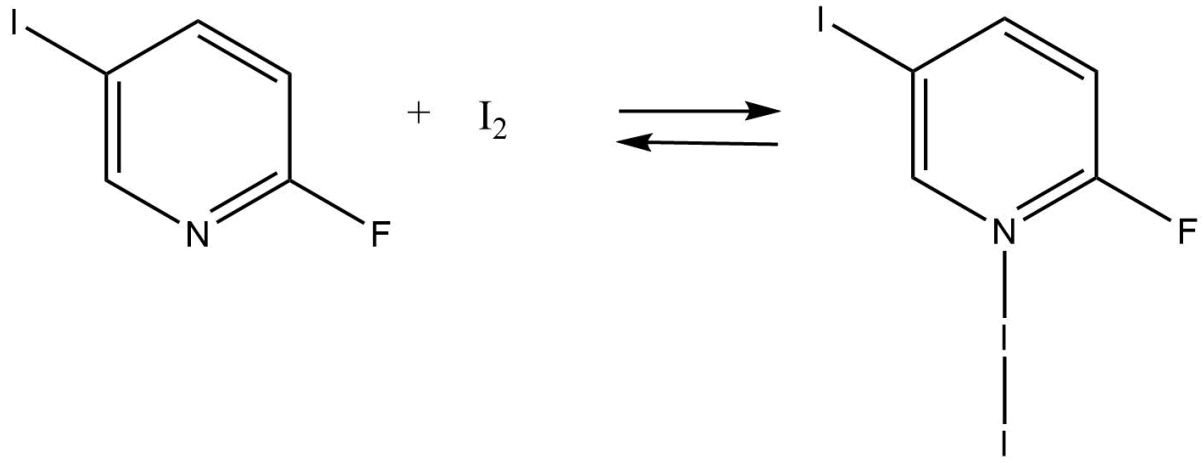

UV-Visible Spectra for 2-fluoro-5-iodopyridine –I_2 solution

All the spectra were collected in methanol, the concentration of all the samples was 10^{-3} M. The base 2-fluoro-5-iodopyridine absorbs at 317 nm and iodine absorbs at 304 nm. A new band appears at 353 nm when the two above starting materials are mixed which is not attributed to the 2-fluoro-5-iodopyridine or I_2. λ_{max} for 2-fluoro-5-iodopyridine was shifted 36 nm toward higher wavelength, Figure (5.9.1).

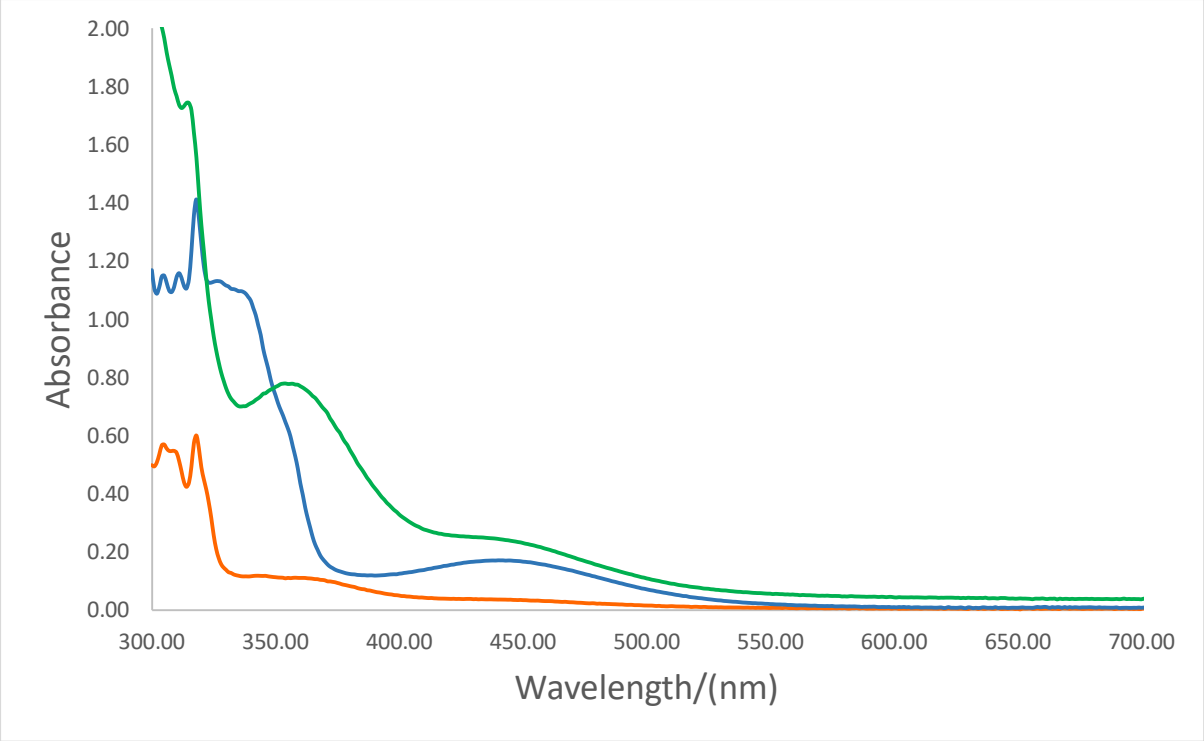

Figure (5.9.1) UV- Visible Spectra of 2-fluoro-5-iodopyridine -I_2: 2-fluoro-5-iodopyridine (Blue), I_2 (Orange), 2-fluoro-5-iodopyridine -I_2 (Green), the spectra were collected using methanol as the solvent, the concentration of the samples was 10^{-3} M.

5.3.10 2-cyanopyridine-I_2

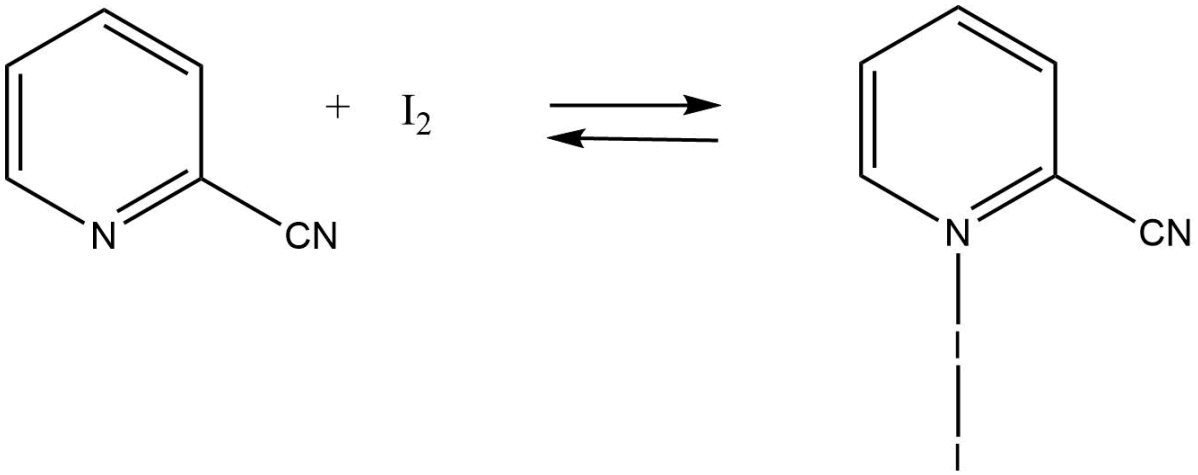

UV-Visible Spectra for 2-cyanopyridine –I_2 solution

All the spectra were collected in methanol, the concentration of all the samples was 10^{-3} M. The base 2-cyanopyridine absorbs at 305 nm and iodine absorbs at 304 nm. A new band appears at 361 nm when the two above starting materials are mixed which is not attributed to the 2-cyanopyridine or I_2. λ_{max} for 2-cyanopyridine was shifted 10 nm toward higher wavelength, Figure (5.10.1). Starting material and the resulting complex are also characterised by ATR-FTIR, Figures (3.10.2, 5.10.2).

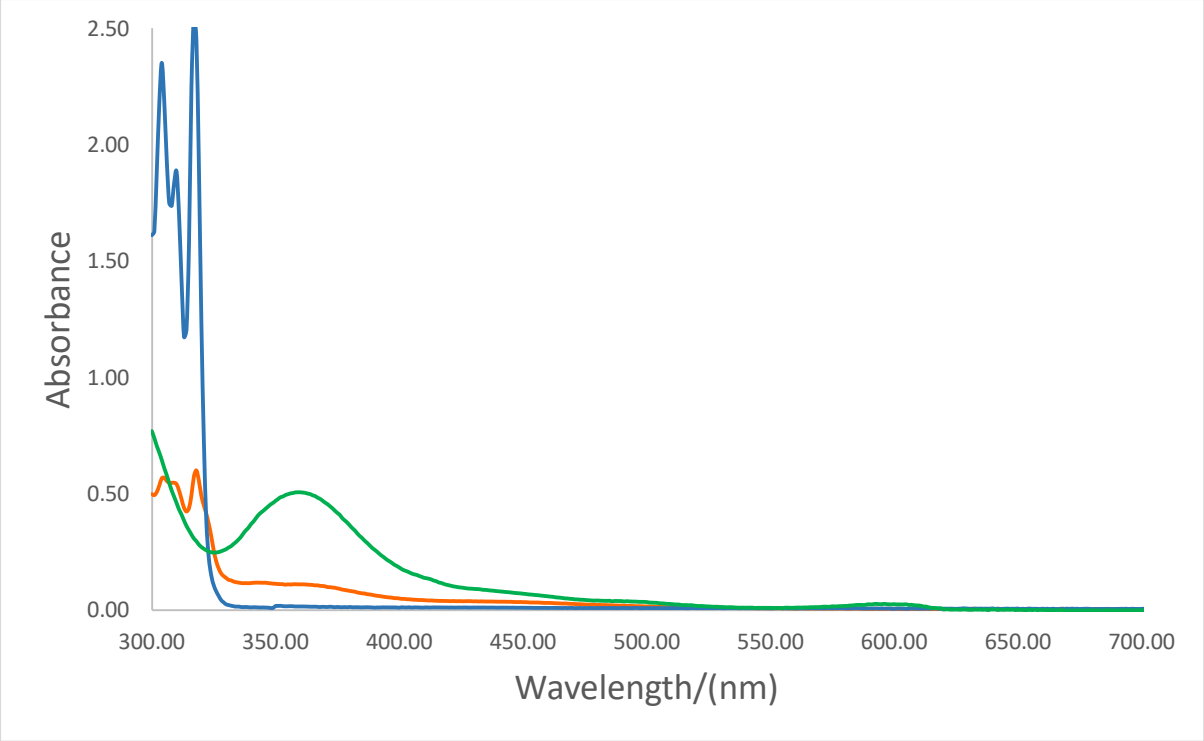

Figure (5.10.1) UV- Visible Spectra of 2-cyanopyridine -I_2: 2-cyanopyridine (Blue), I_2 (Orange), 2-cyanopyridine -I_2 (Green), the spectra were collected using methanol as the solvent, the concentration of the samples was 10^{-3} M.

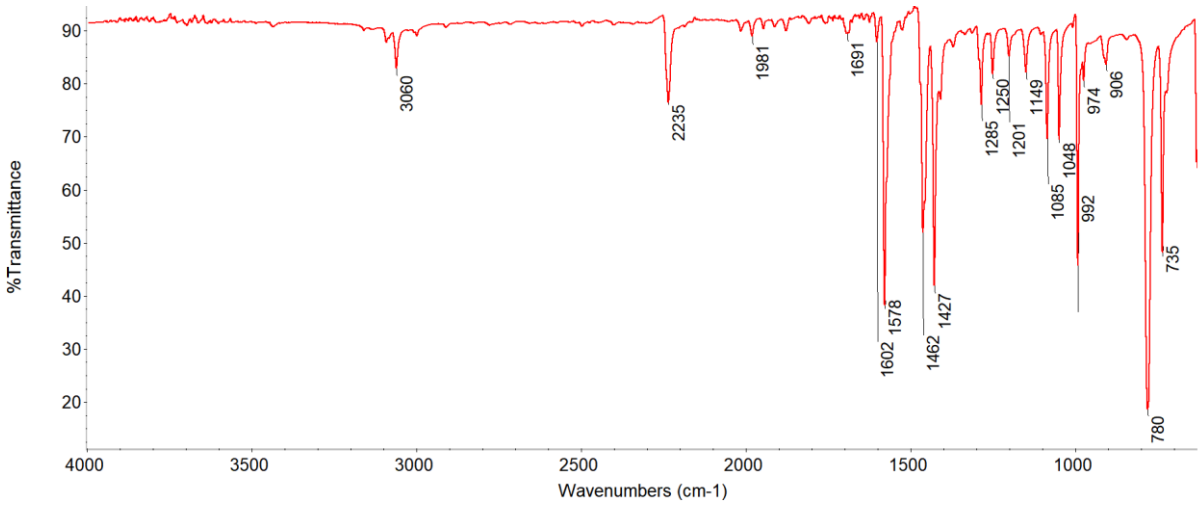

Figure (3.10.2) ATR-FTIR spectrum of 2-cyanopyridine

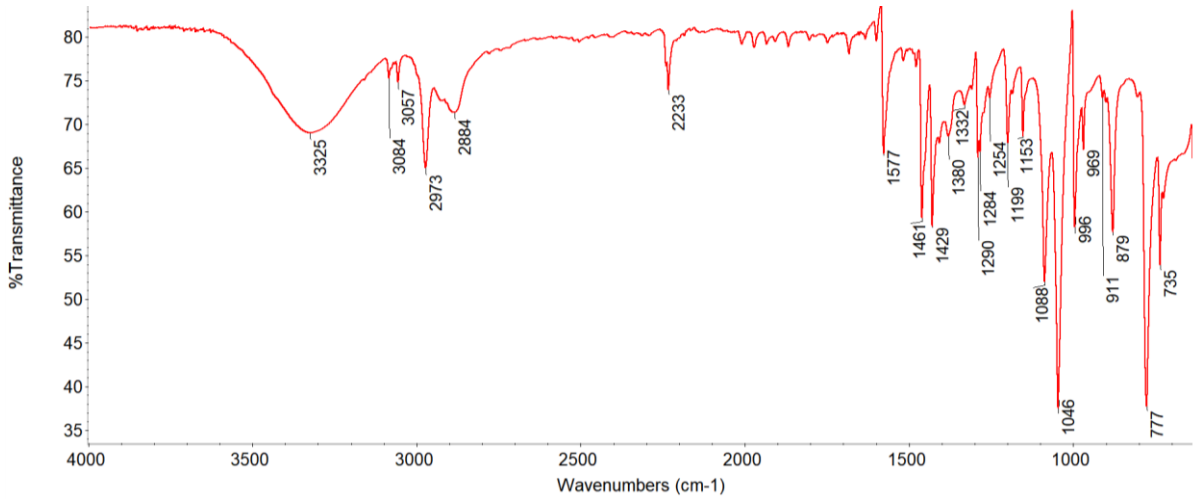

Figure (5.10.2) ATR-FTIR spectrum of 2-cyanopyridine $-I_2$

XRD measurements for 2-cyanopyridine –I_2

Crystallographic data for 2-cyanopyridine- I_2 are given in Table (5.1), and selected bond lengths and angles in Table (5.2). A thermal ellipsoid plot of the structure together with the numbering scheme used is given in Figure (5.10.3).

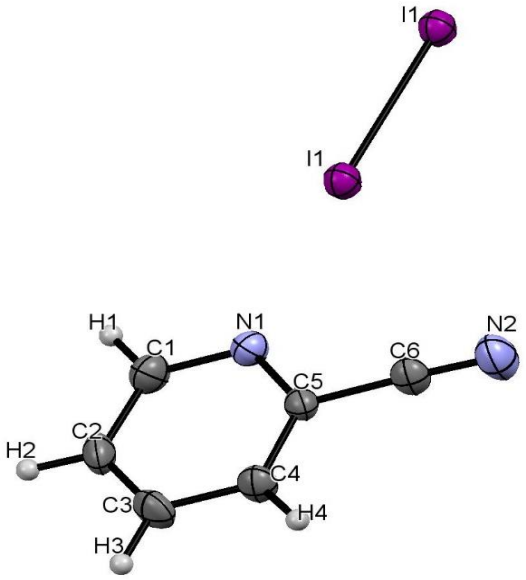

Figure (5.10.3) Thermal Ellipsoid plot for 2-Cyanopyridine- I_2.

2-cyanopyridine- I_2 crystallises in the triclinic, the space group is P-1. The asymmetric unit is one molecule of 2-cyanopyridine and one molecule of I_2. The organic base and iodine are connected via N1···I1-I1 halogen bond. N1···I1 bond length is 2.872 (4) Å, which is less than the sum of van der Waals radii of nitrogen and iodine (3.53 Å).[121] The I-I distance (2.7149 (6) Å) is longer compared to the same distance for the iodine in the gas phase (2.663 Å)[27] and the measured angle for N1-I1-I1 is 177.28 (8)°. One iodine molecule is involved in two N1···I1-I1 halogen bonds with two 2-cyanopyridine molecules. Thus, it forms a bridged adduct,[106] Figure (5.10.4). Apart from this type of interactions, the complexes are further connected by the C-H···N hydrogen bonds to form ribbons, Figure (5.10.5, 5.10.6). The nitrogen atom of the cyano-group is a bifurcated HB acceptor. The two types of C-H···N

hydrogen bonds linking the complexes are C3-H3···N2 where the C3···N2 distance is 3.397 Å and the C3-H3-N2 angle is 137.23°, and C4-H4···N2 hydrogen bond, in which the C4···N2 distance is 3.505 Å and the C4-H4-N2 angle is 154.39°, Figure (5.10.5). Both distances are shorter than the reported values for C-H···N hydrogen bond in similar systems (3.521 Å)[140], while the measured angles are greater (134.41°)[140] These halogen bonds form two types of graph-set motifs, two C4-H4···N2 are a part of $R_2^2(10)$ motif, while two C4-H4···N2 and two C3-H3···N2 HBs form a $R_4^2(10)$ motif, (Figure 5.10.5).

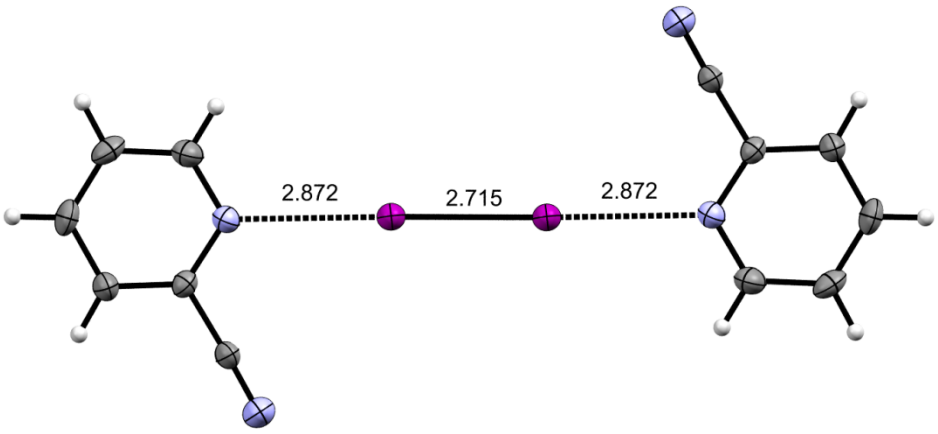

Figure (5.10.4) View showing bridged halogen bond adduct in the 2-cyanopyridine-I_2 complex.

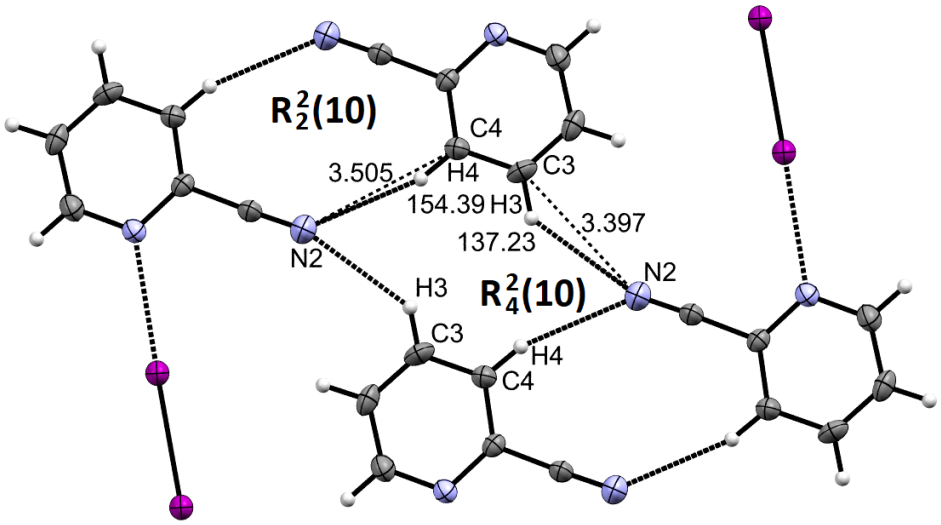

Figure (5.10.5) View showing 2-cyanopyridine $–I_2$ with the corresponding hydrogen bonds labelled according to graph set motif nomenclature.

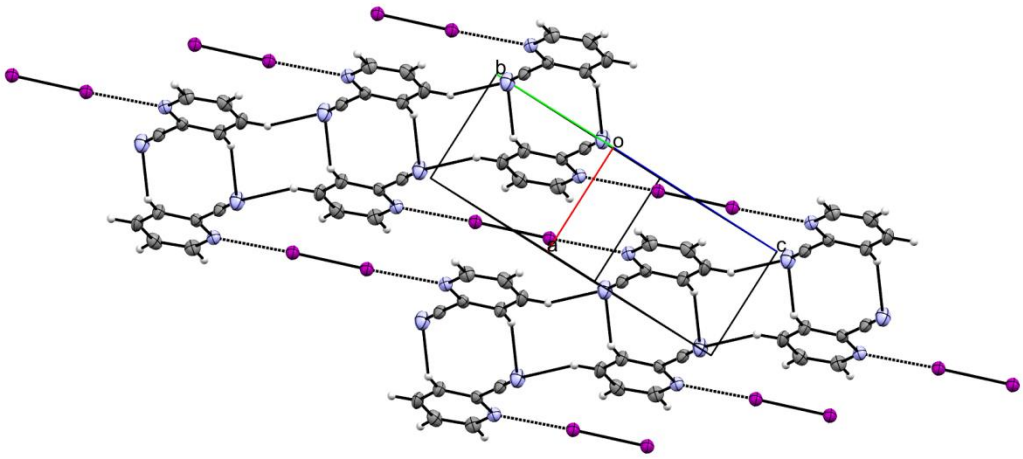

Figure (5.10.6) Packing diagram of 2-cyanopyridine $–I_2$ approximately along to b axis.

Table 5.1: Crystallographic data for the 2-cyanopyridine –I_2 complex.

Crystal data	
Chemical formula	$I_2 \cdot 2\ (C_6H_4N_2)$
M_r	462.02
Crystal system, space group	Triclinic, *P*1
T/K	160
a, *b*, *c* (Å)	4.4377 (10), 6.3823 (13), 12.689 (3)
α, β, γ (°)	83.580 (8), 83.081 (9), 84.521 (9)
V/ (Å^3)	353.32 (13)
Z	1
Radiation type	Mo *K*α
μ/ (mm^{-1})	4.44
Crystal size/ (mm)	0.17 × 0.04 × 0.04
Data collection	
Diffractometer	Bruker *APEX*-II CCD
Absorption correction	Multi-scan
T_{min}, T_{max}	0.612, 0.746
No. of measured, independent and observed [$I > 2\sigma(I)$] reflections	4287, 1912, 1570
R_{int}	0.040

$(\sin \theta/\lambda)_{max}$ /($Å^{-1}$)	0.689
Refinement	
$R[F^2 > 2\sigma(F^2)]$, $wR(F^2)$, S	0.035, 0.061, 1.03
No. of reflections	1912
No. of parameters	82
H-atom treatment	H-atom parameters constrained
$\Delta\rho_{max}$, $\Delta\rho_{min}$ (e $Å^{-3}$)	0.72, −0.73

Table (5.2): Selected interatomic contacts /Å and /^{o} for the complex 2-cyanopyridine-I_2

Atom1	Atom2	Length	Atom1	Atom2	Atom3	Angle
I1	I1	2.7149 (6)	C1	N1	C5	116.9 (4)
N1	C1	1.327 (6)	N1	C1	C2	122.8 (4)
N1	C5	1.336 (5)	C1	C2	C3	119.1 (4)
N2	C6	1.137 (6)	C2	C3	C4	119.2 (4)
C1	C2	1.387 (6)	C3	C4	C5	117.4 (4)
C2	C3	1.373 (7)	N1	C5	C4	124.6 (4)
C3	C4	1.378 (7)	N1	C5	C6	116.3 (3)
C4	C5	1.378 (5)	C4	C5	C6	119.1 (3)
C5	C6	1.447 (6)	N2	C6	C5	177.8 (4)

5.3.11 1,10-Phenanthroline –I_2

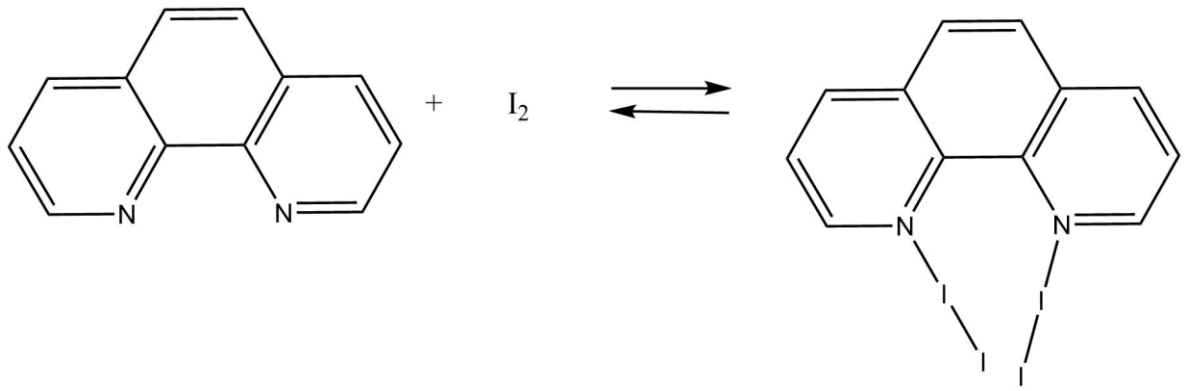

UV-Visible Spectra for 1,10-Phenanthroline –I_2 solution

All the spectra were collected in methanol, the concentration of all the samples was 10^{-3} M. The base 1,10-Phenanthroline absorbs at 308 nm and iodine absorbs at 304 nm. The new band appears at 355 nm when the two above starting materials are mixed which is not attributed to the 1,10-Phenanthroline or I_2. λ_{max} for 1,10-Phenanthroline was shifted 47 nm toward higher wavelength, Figure (5.11.1). Starting material and the resulting complex are also characterised by ATR-FTIR, Figures (3.11.2, 5.11.2).

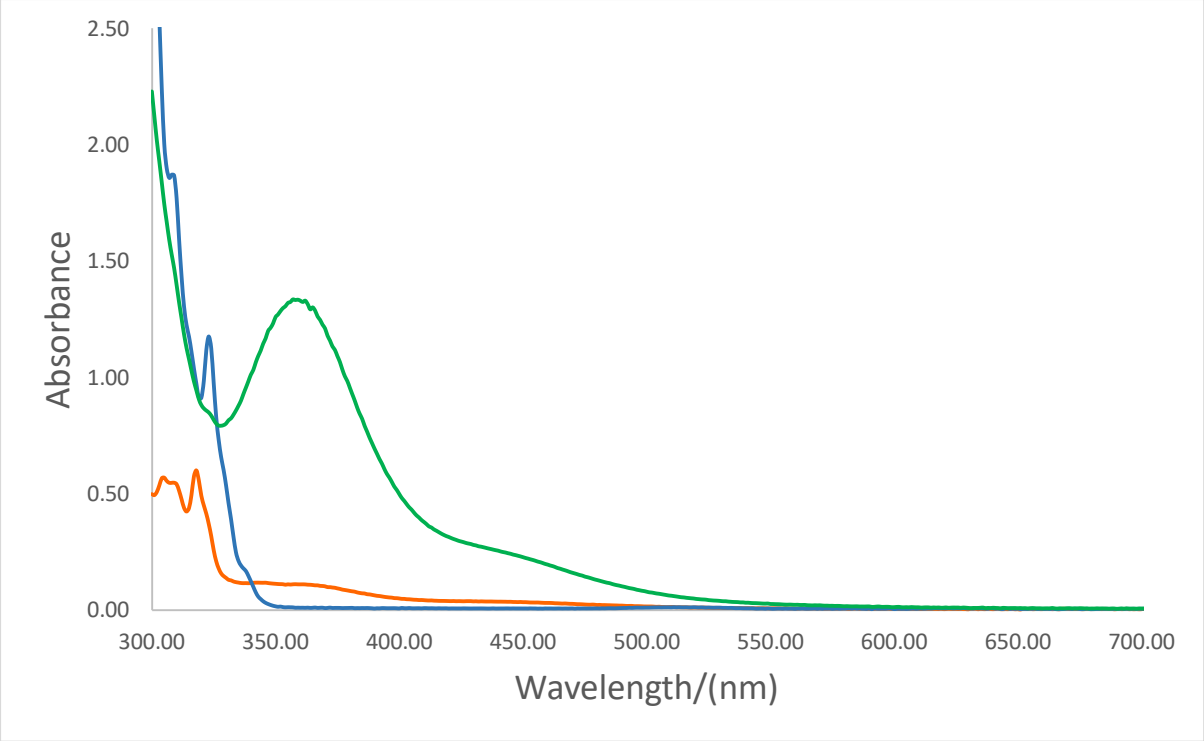

Figure (5.11.1) UV- Visible Spectra of 1,10-Phenanthroline -I_2: 1,10-Phenanthroline (Blue), I_2 (Orange), 1,10-Phenanthroline -I_2 (Green), the spectra were collected using methanol as the solvent, the concentration of the samples was 10^{-3} M.

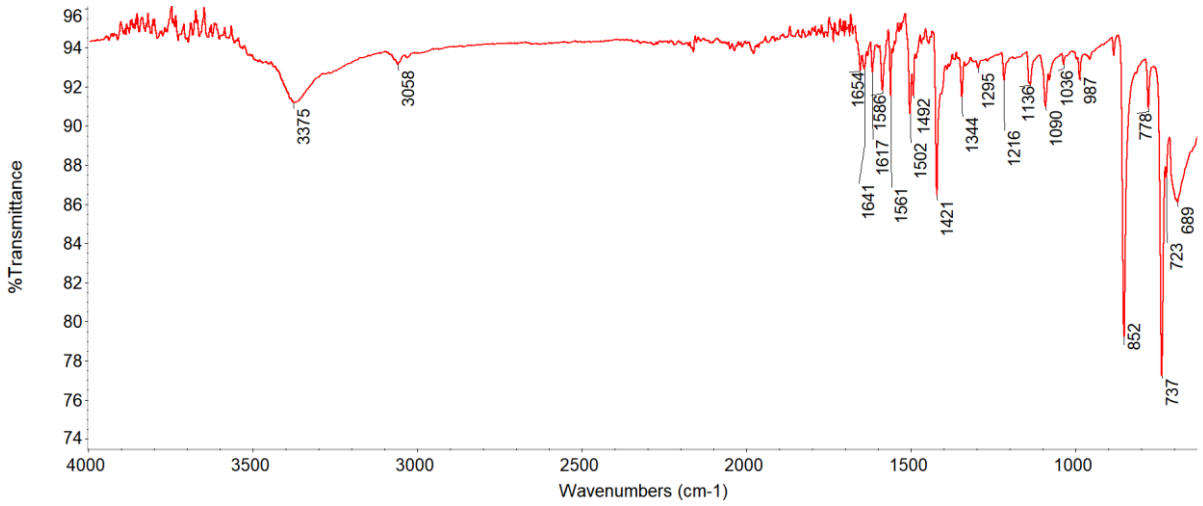

Figure (3.11.2): ATR-FTIR spectrum of 1,10-phenanthroline

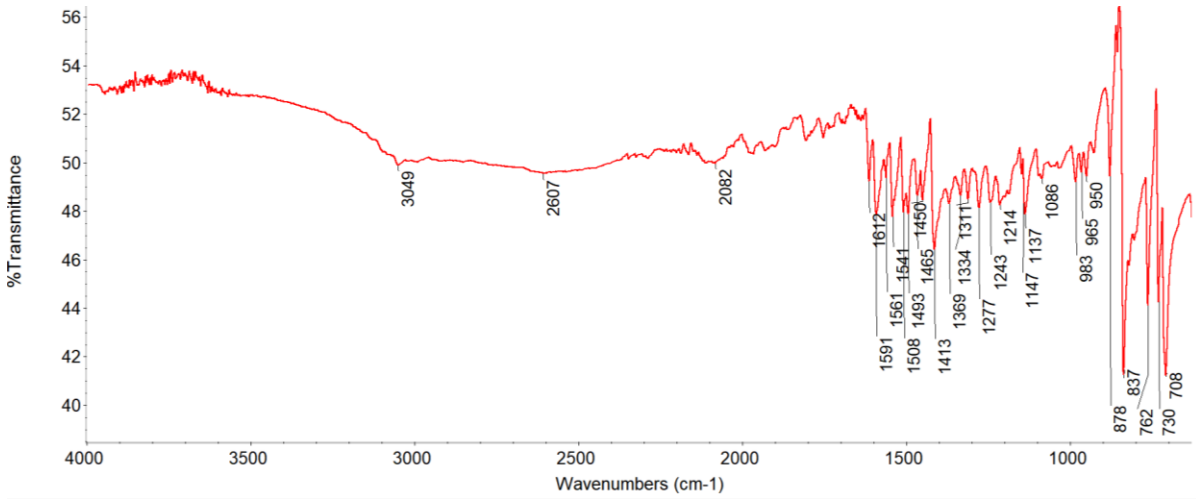

Figure (5.11.2) ATR-FTIR spectrum of 1,10-Phenanthroline -I_2

5.3.12 quinoxaline– I_2

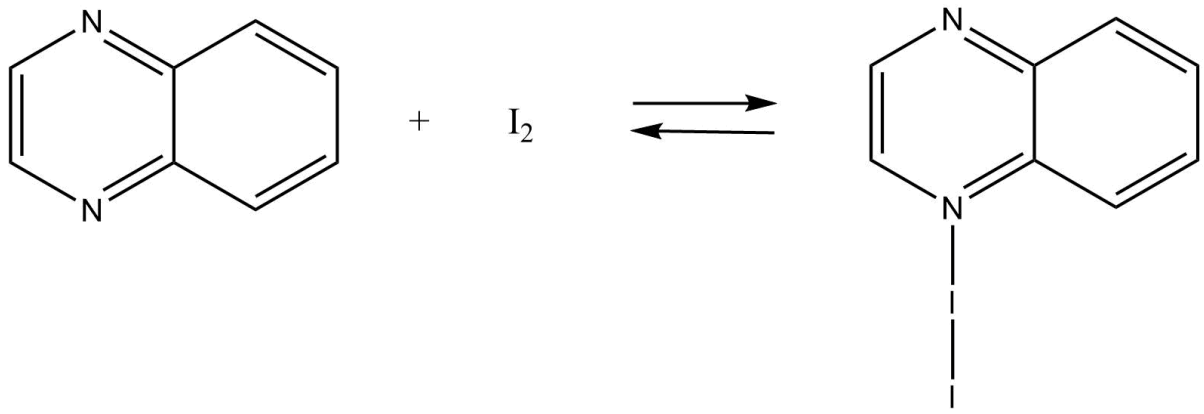

UV-Visible Spectra for quinoxaline –I_2 solution

All the spectra were collected in methanol, the concentration of all the samples was 10^{-3} M. The base quinoxaline absorbs at 323 nm and iodine absorbs at 304 nm. A new band appeared at 354 nm with the shoulder at 442 nm. When the two above starting materials are mixed which is not attributable to the quinoxaline or I_2. λ_{max} for quinoxaline was shifted toward higher wavelengths, Figure (5.12.1). Starting material and the resulting complex are also characterised by ATR-FTIR, Figures (3.12.2, 5.12.2).

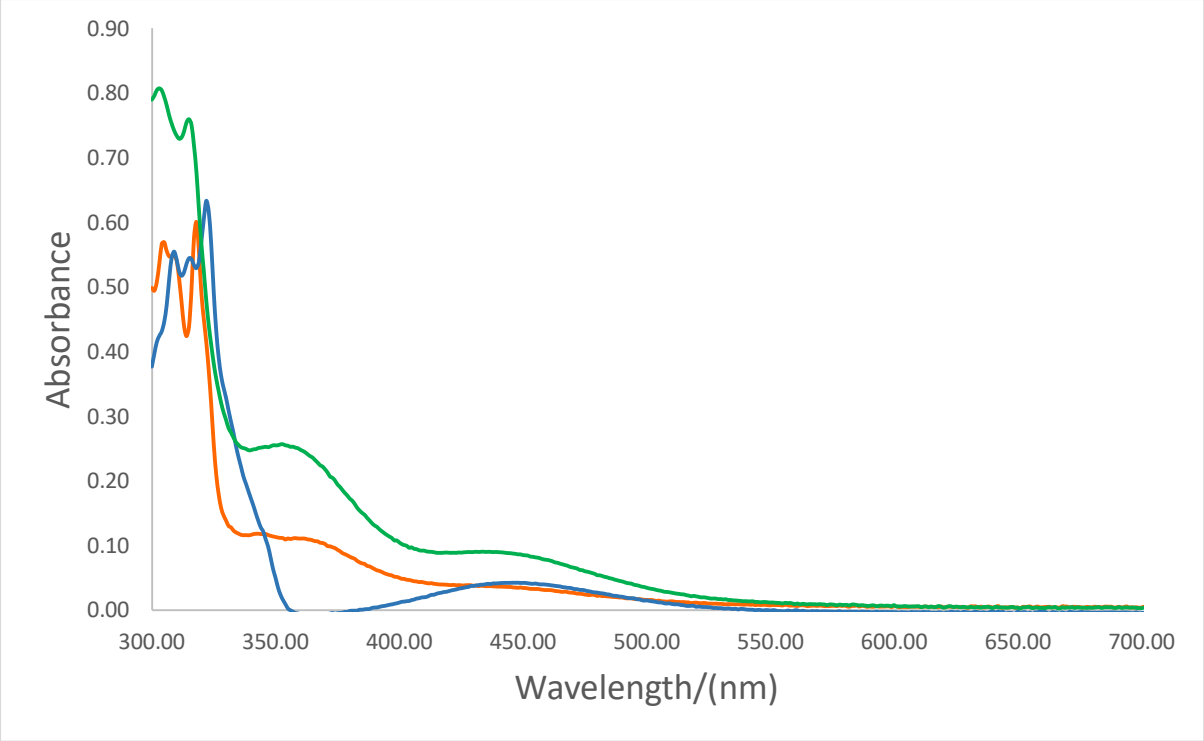

Figure (5.12.1) UV- Visible Spectra of quinoxaline -I_2: quinoxaline (Blue), I_2 (Orange), 1,10- quinoxaline -I_2 (Green), the spectra were collected using methanol as the solvent, the concentration of the samples was 10^{-3} M.

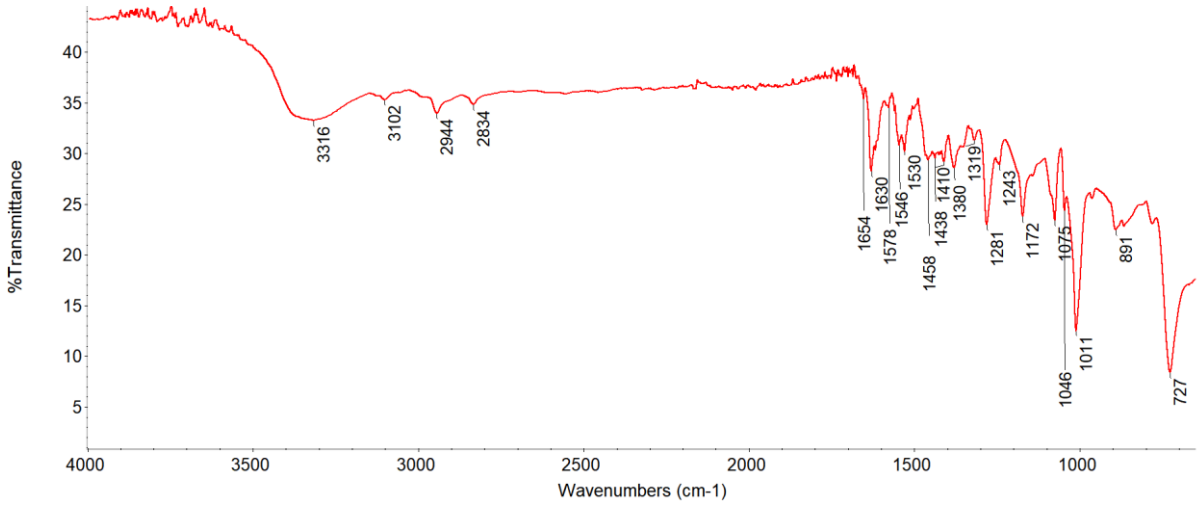

Figure (3.12.2): ATR-FTIR spectrum of quinoxaline

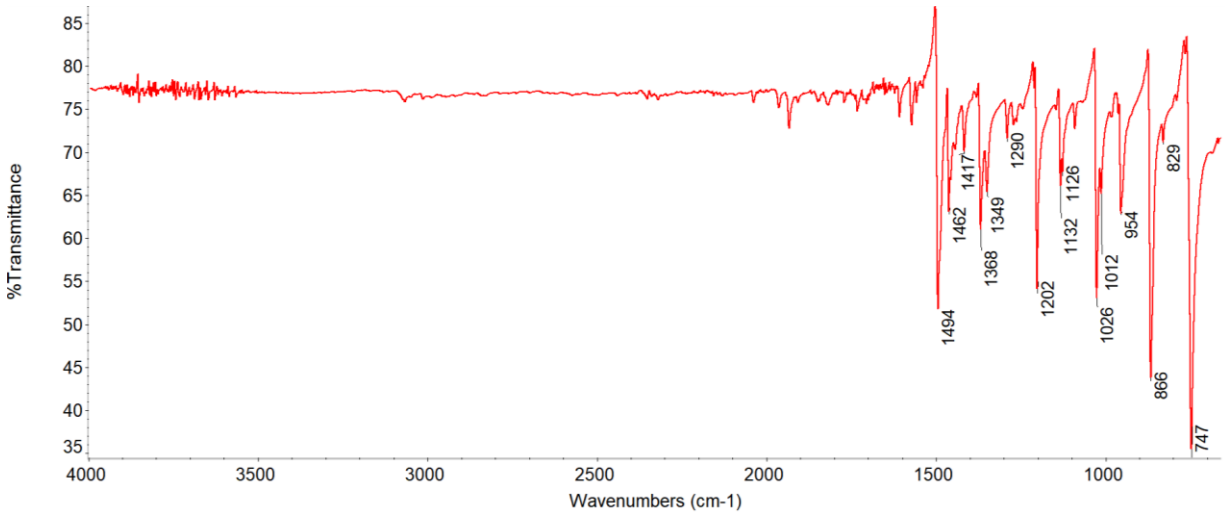

Figure (5.12.2) ATR-FTIR spectrum of quinoxaline -I_2

XRD measurements for quinoxaline –I_2

Crystallographic data for quinoxaline-I_2 are given in Table (5.3), and selected bond lengths and angles in Table (5.4). A thermal ellipsoid plot of the structure together with the numbering scheme used is given in Figure (5.12.3).

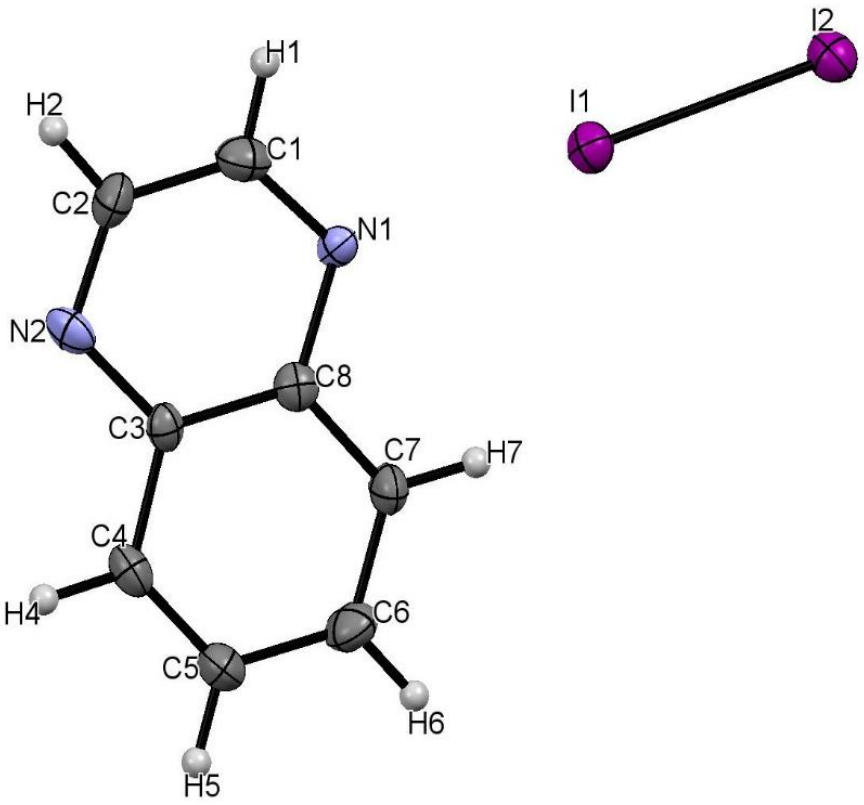

Figure (5.12.3) Thermal ellipsoid plot for quinoxaline –I_2

quinoxaline-IBr2– crystallises in the Orthorhombic, space group is Pbca. The asymmetric unit is one molecule of quinoxaline and one molecule of I_2. Even though iodine monobromide was used as a starting material, iodine is observed as an XB donor in this complex. The crystallisation of iodine instead of iodine monobromide could be explained by the previously discussed formation of polyhalogen ions. Complexes are connected in one-dimensional chains by N···I-I halogen bonds. Similar to 2-cyanopyridine-I_2 complex, bridged adduct mode is observed. However, the N···I distances are not equal, Figure (5.12.4). The

N1···I1 distance is 2.857 (7) Å and N2···I2_is 2.875 (8) Å, which are both less than the sum of van der Waals radii of nitrogen and iodine (3.53 Å),[121] Figure (5.12.4). The bond length in the molecule of iodine is 2.725 (1)Å, which is an elongation compared to the distance for the iodine in gas phase 2.6663 Å,[27] Figure (5.12.4). The N-I-I angles also are not equal, N1-I1-I2: 179.1 (1)° and N2-I2-I1: 177.0 (1)°. This difference in XB feature should indicate that there are some other non-covalent interactions present, but none could be observed. The distance between the centroids of the adjacent molecules is 4.295 Å, Figure (5.12.5)

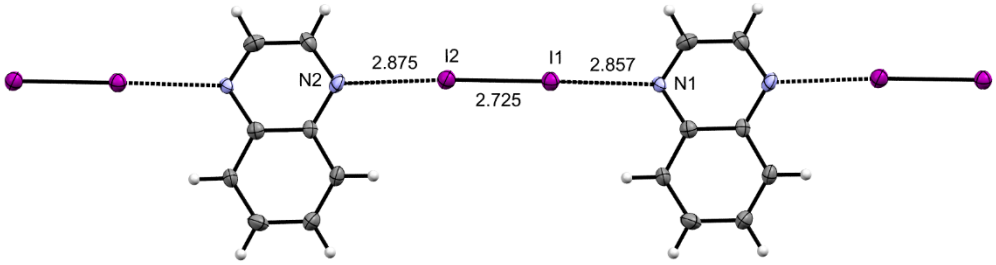

Figure (5.12.4) View showing an infinite chain of halogen bond connected complexes of quinoxaline-I_2

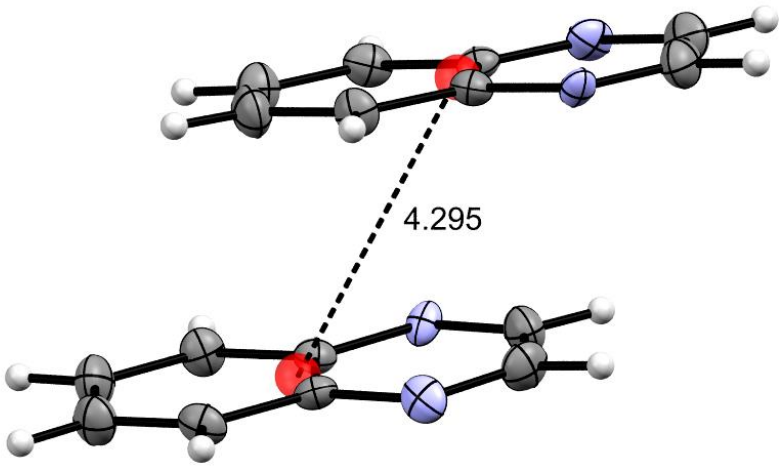

Figure (5.12.5) View showing the distance (Å) between the two centroids of quinoxaline molecules in quinoxaline-I_2 complexes

Table 5.3: Crystallographic data for the quinoxaline $–I_2$

Crystal data	
Chemical formula	$I_2 \cdot C_8H_6N_2$
M_r	383.95
Crystal system, space group	Orthorhombic, *Pbca*
T/K	180
a, *b*, *c* (Å)	21.564 (3), 11.3419 (18), 8.1360 (11)
V/ (Å^3)	1989.8 (5)
Z	8
Radiation type	Mo *K*α
μ/ (mm^{-1})	6.27
Crystal size/ (mm)	0.23 × 0.07 × 0.07
Data collection	
Diffractometer	Bruker *APEX*-II CCD
Absorption correction	Multi-scan
T_{min}, T_{max}	0.539, 0.746
No. of measured, independent and observed [$I > 2\sigma(I)$] reflections	15578, 2888, 1970

R_{int}	0.039
$(\sin \theta/\lambda)_{max}$ /(Å^{-1})	0.703
No. of measured, independent and observed [$I > 2\sigma(I)$] reflections	15578, 2888, 1970
Refinement	
$R[F^2 > 2\sigma(F^2)]$, $wR(F^2)$, S	0.048, 0.108, 1.17
No. of reflections	2888
No. of parameters	109
H-atom treatment	H-atom parameters constrained $w = 1/[\sigma^2(F_o^2) + (0.007P)^2 + 42.509P]$ where $P = (F_o^2 + 2F_c^2)/3$
$\Delta\rho_{max}$, $\Delta\rho_{min}$ (e Å^{-3})	1.56, −2.97

Table 5.4: Selected interatomic contacts /Å and /^{o} for the complex quinoxaline –I_2.

Atom1	Atom2	Length	Atom1	Atom2	Atom3	Angle
I1	I2	2.725 (1)	C1	N1	C8	113.7 (7)
N1	C1	1.33 (1)	C2	N2	C3	114.9 (7)
N1	C8	1.41 (1)	N1	C1	C2	124.2 (8)
N2	C2	1.32 (1)	N2	C2	C1	123.5 (8)
N2	C3	1.39 (1)	N2	C3	C4	119.6 (7)
C1	C2	1.42 (1)	N2	C3	C8	121.9 (7)
C3	C4	1.42 (1)	C4	C3	C8	118.5 (7)
C3	C8	1.42 (1)	C3	C4	C5	120.6 (8)
C4	C5	1.36 (1)	H4	C4	C5	119.7
C5	C6	1.41 (1)	C4	C5	C6	120.7 (8)
C6	C7	1.37 (1)	H5	C5	C6	119.6
C7	C8	1.41 (1)	C5	C6	C7	120.5 (8)
			H6	C6	C7	119.6
			C6	C7	C8	119.8 (8)
			H7	C7	C8	120.1
			N1	C8	C3	121.7 (7)
			N1	C8	C7	118.5 (7)

	C3	C8	C7	119.7 (7)

5.3.13 2-chloroquinoline - I_2:

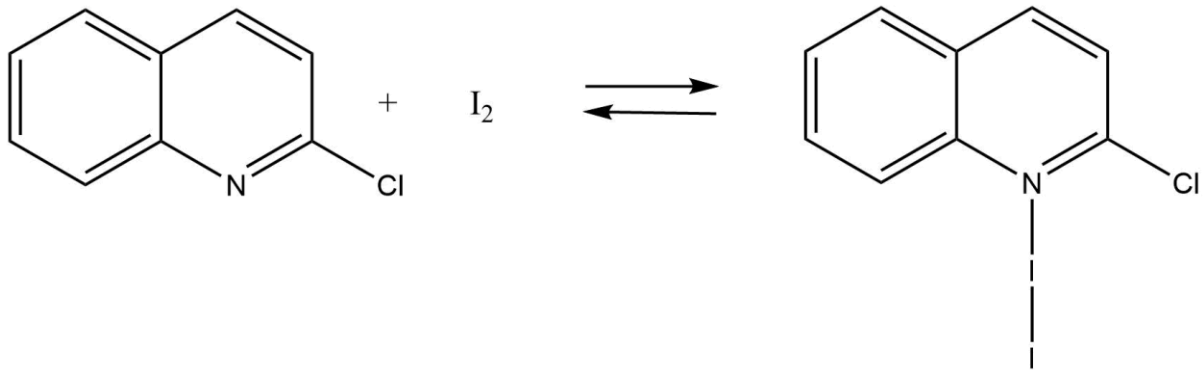

UV-Visible Spectra for 2-chloroquinoline –I_2 solution

All the spectra were collected in methanol, the concentration of all the samples was 10^{-3} M. The base 2-chloroquinoline absorbs at 319 nm and iodine absorbs at 304 nm. Two new bands appear at 364 and 443 nm when the two above starting materials are mixed which is not attributed to the 2-chloroquinoline or I_2. λ_{max} for 2-chloroquinoline was shifted toward higher wavelengths, Figure (5.13.1).Starting material and the resulting complex are also characterised by ATR-FTIR, Figures (3.13.2, 5.13.2).

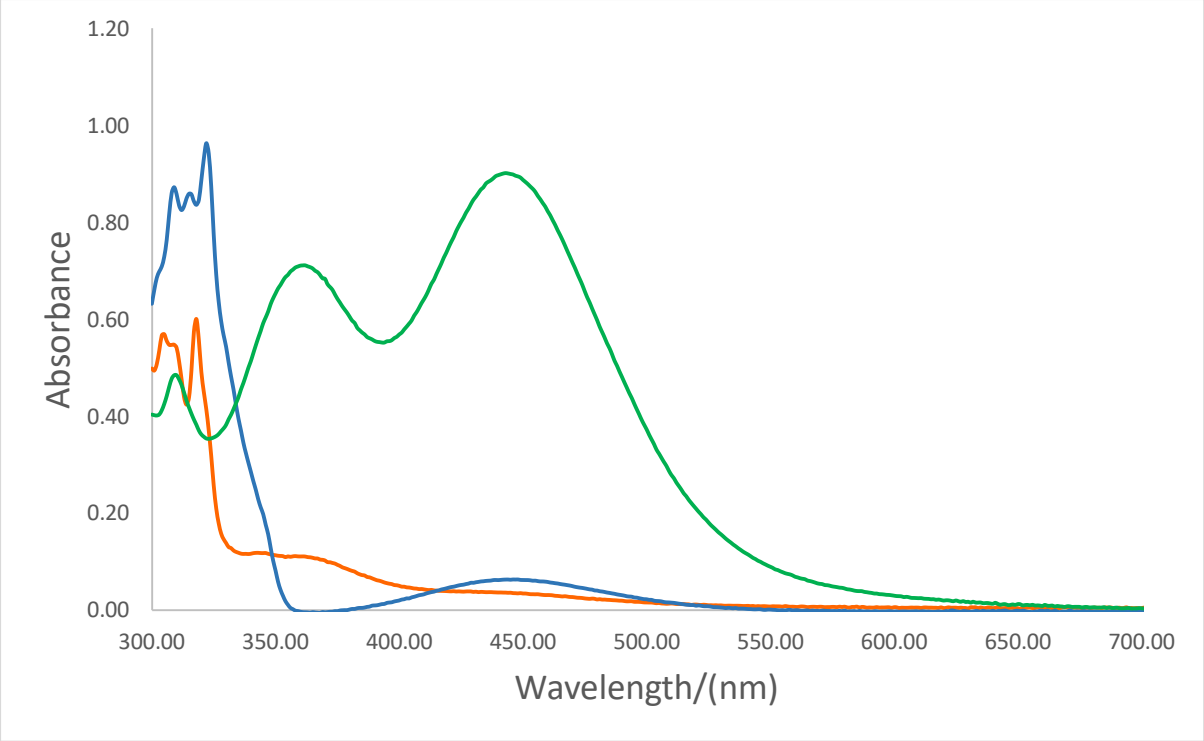

Figure (5.13.1) UV- Visible Spectra of 2-chloroquinoline-I_2: 2-chloroquinoline (Blue), I_2 (Orange), 2-chloroquinoline -I_2 (Green), the spectra were collected using methanol as the solvent, the concentration of the samples was 10^{-3} M.

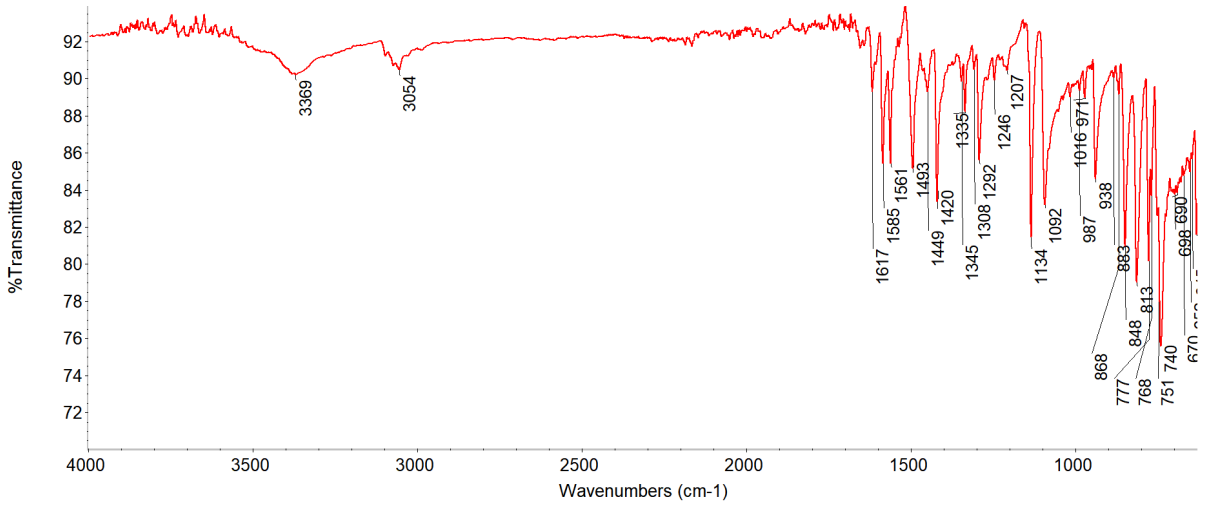

Figure (3.13.2): ATR-FTIR spectrum of 2-chloroquinoline

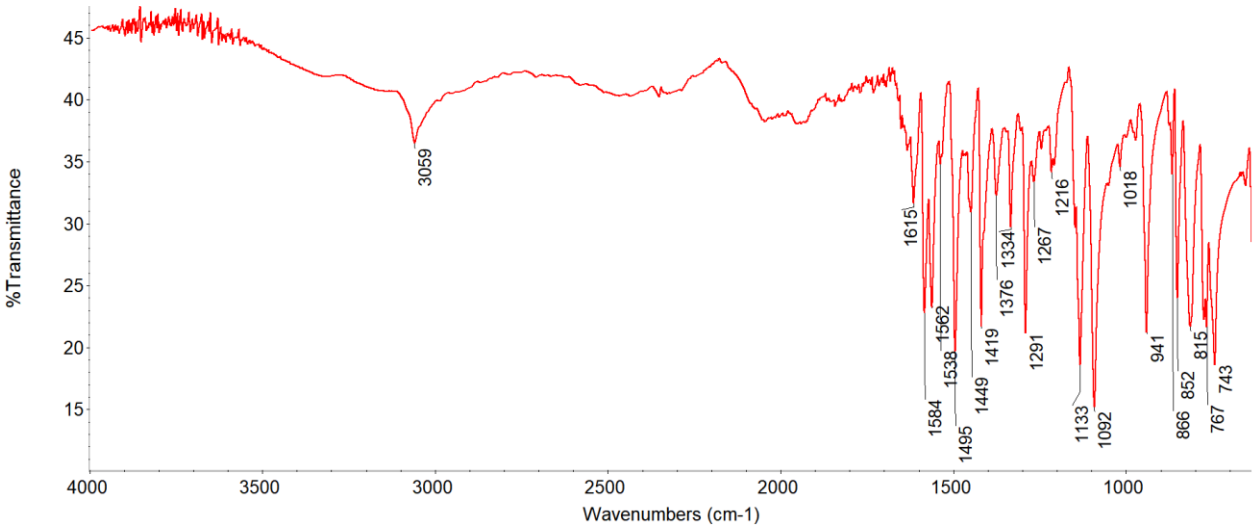

Figure (5.13.2) ATR-FTIR spectrum of 2-chloroquinoline-I_2.

5.4 Discussion

Most Iodine complexes were characterized only by UV-VIS and ATR-FTIR spectroscopy, except the 2-cyanopyridine-I_2 and quinoxaline- I_2 complexes that were characterised by single-crystal X-ray diffraction and UV-VIS and ATR-FTIR spectroscopy. Also, quinoxaline-I_2 complex resulted from adding iodine monobromide to the quinoxaline and quinoxaline-IBr was the expected product. However, halogen bonded co-crystalline quinoxaline-I_2 is obtained instead.

Because this chapter involves only two prepared halogen bond complexes (2-cyanopyridine-I_2 and quinoxaline-I_2) XB geometrical properties of these compounds are compared with the selected literature data in Table (5.5). From 28 complexes listed in Table (5.1), in 16 of them sp^2 nitrogen atom in N···I-I halogen bond is observed. In addition, the labelling scheme of the reported complexes was adapted, and ball-stick representations along with halogen bond geometric parameters are listed in Figure (5.14.1) for better clarity. Pyridine-I_2 (VUHDIN)[160] with the N···I distance of 2.425 Å and I-I bond length of 2.804 Å, can be taken as a reference point for studying the effect of functional groups to the strength of XB interactions.

Table (5.5) Geometric parameters of selected N···I-I halogen bonded complexes, adapted from ref.[106,112] Data reported in this work are marked bold.

Complex name (REFCODE)	N···I (Å)	I-I (Å)	N···I-I (°)	C-N-C (°)
4-Picoline- I_2 (PICOLI)[151]	2.322	2.823	175.51	119.24
4-(2-(4-(octyloxy)phenyl)vinyl)pyridine - I_2 (PEWQIT)[158]	2.353	2.83	177.19	116.44
3,3'-(1,4-Phenylenediethyne-2,1-diyl)bis-1λ5-pyridine - I_2 (LEWKOP)[159]	2.358	2.818	176.08	119.75
1,2-Bis (4-pyridyl) ethylene bis - I_2 (QIHBOY)[152]	2.421	2.801	178.78	118.48
Pyridine- I_2 (VUHDIN)[160]	2.425	2.804	176.44	119.83
Isonicotinamide - I_2 (YIPCEG)[161]	2.439	2.79	178.04	120.88
(E)-1,2-bis(pyridine-4-yl) diazene- I_2 (BULJUP)[162]	2.477	2.773	179.58	118.97
2-[(4-chlorophenyl) selanyl] pyridine- I_2 (ZESQOG) [135]	2.497	2.769	178.18	119.62
2,3,5,6-tetrakis(2-Pyridyl) pyrazine - I_2 (DARZAY)[163]	2.498	2.76	174.46	118.35
2,3-bis (2-pyridyl) quinoxaline-I_2	2.530	2.759	173.8	117.74

(NULBEB)[145]				
4-cyanopyridine-I_2 (NULBIF) [145]	2.543	2.745	175.47	116.02
4-cyanopyridine-I_2 (NULBIF) [145]	2.554	2.750	175.50	118.03
2,3,5,6-tetrakis(2-Pyridyl) pyrazine - I_2 (DARZAY)[163]	2.568	2.755	168.30	116.87
2,2'-Bipyridine-I_2 (CECZAL)[164]	2.604	2.746	179.41	113.58
Quinoxaline-I_2	**2.857**	**2.725**	**179.11**	**113.75**
2-cyanopyridine-I_2	**2.872**	**2.7149**	**177.28**	**116.89**
Quinoxaline-I_2	**2.875**	**2.725**	**176.99**	**114.88**
quinoxaline I_2 (NULBUR) [145]	2.918	2.724	175.77	116.00
bis(2,6-bis(phenylselanyl)pyridine)-I_2 (ZESQUM)[135]	2.936	2.722	175.76	117.68
quinoxaline I_2 (NULBUR) [145]	2.949	2.724	178.77	122.72
bis(9-Chloroacridine) iodine - I_2 (QARGUL)[146]	2.981	2.741	178.75	117.58
Phenazine-I_2 (PHNAZI01)[157]	2.986	2.726	180	117.6
Phenazine-I_2 (PHNAZI01)[157]	3.099	2.726	180	120.49

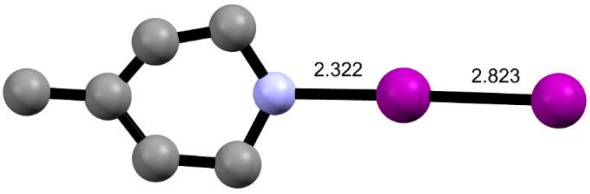

PICOLI[151]

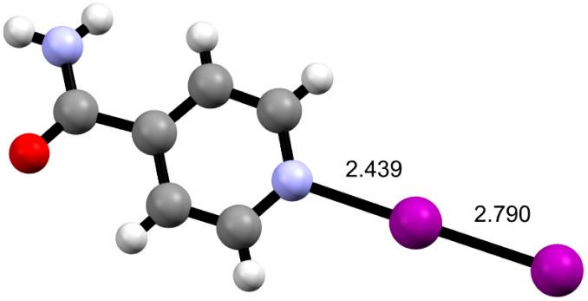

YIPCEG[161]

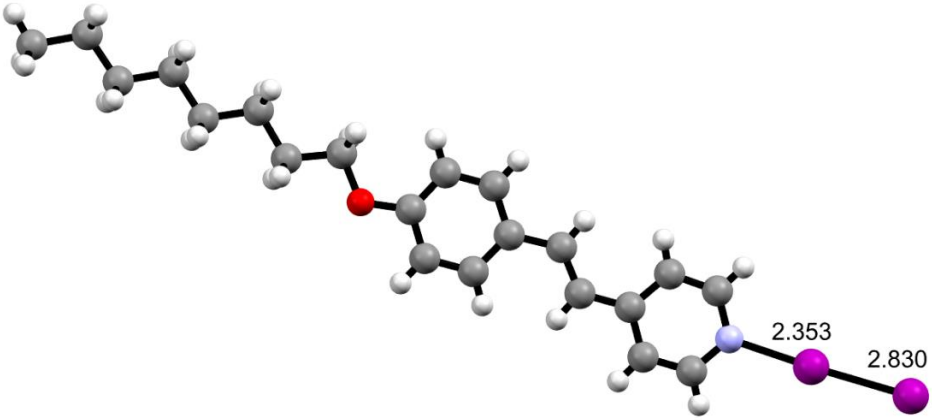

PEWQIT[158]

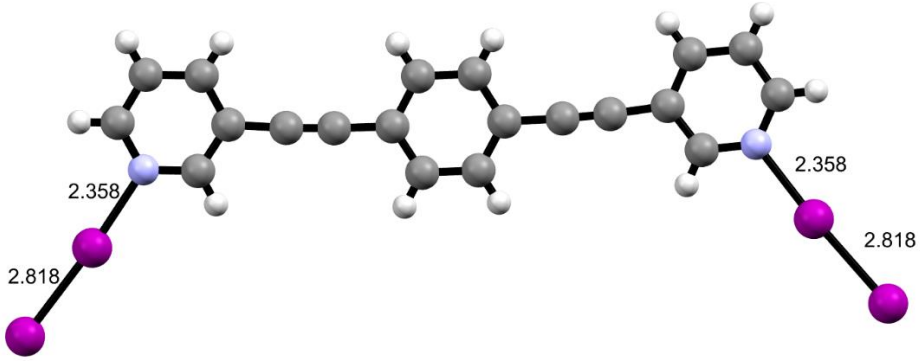

LEWKOP[159]

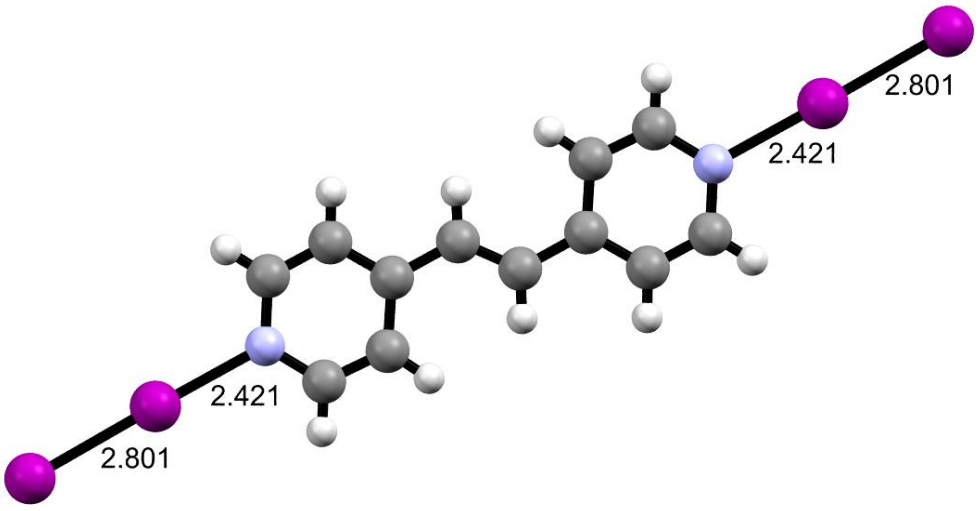

QIHBOY[152]

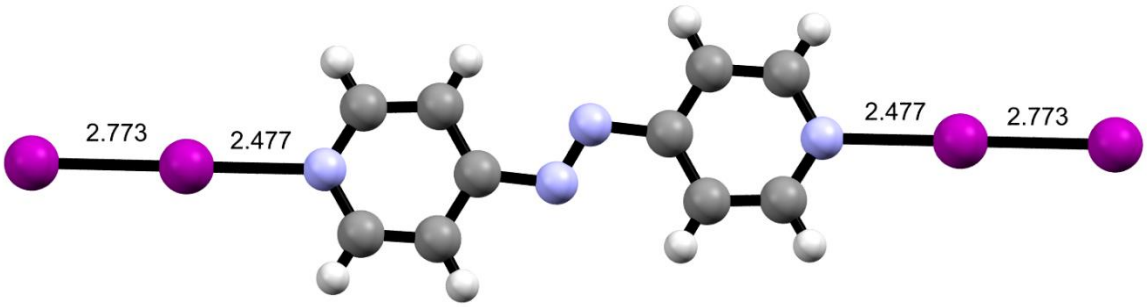

BULJUP[162]

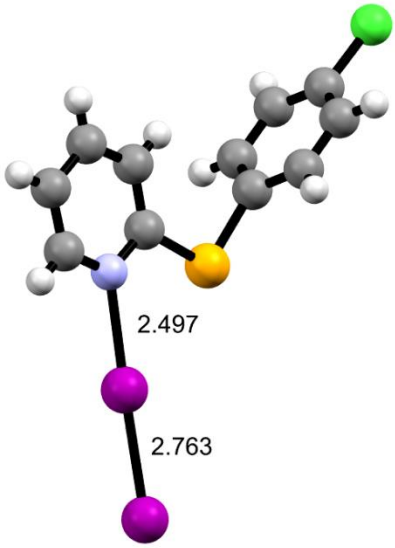

ZESQOG[135]

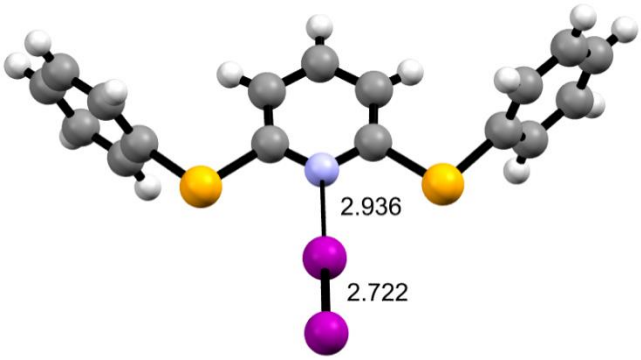

ZESQUM[135]

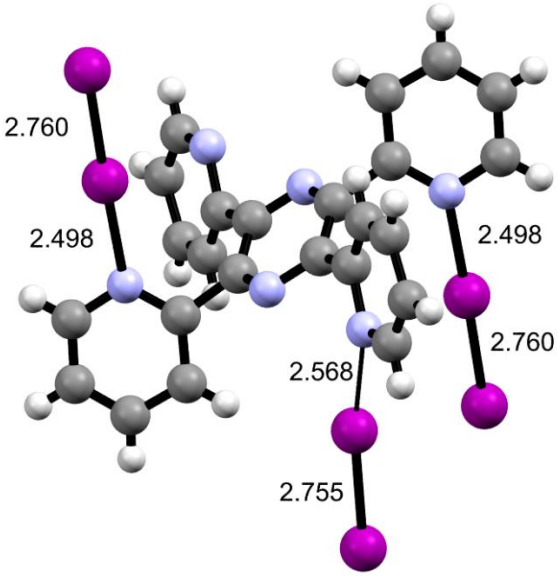

DARZAY[163]

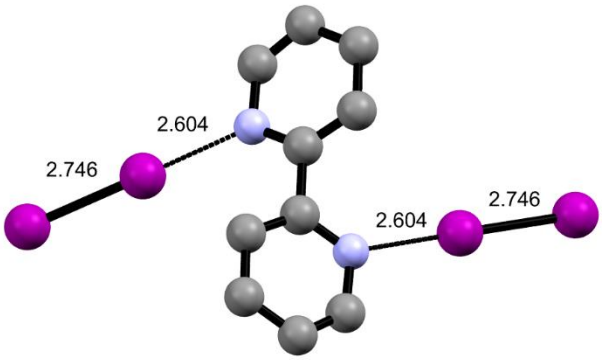

CECZAL[164]

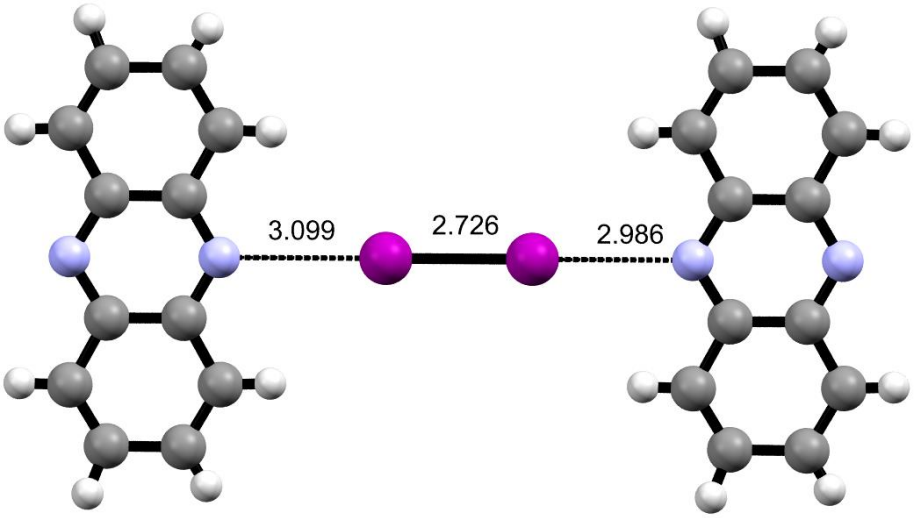

PHNAZI01[157]

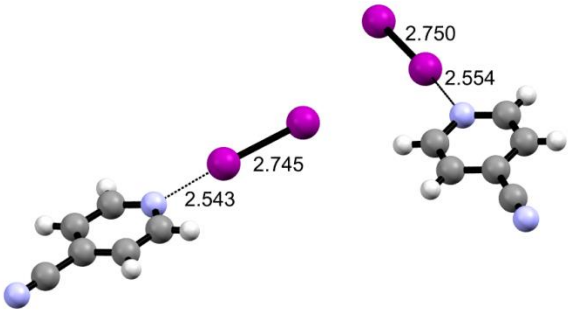

NULBIF[145]

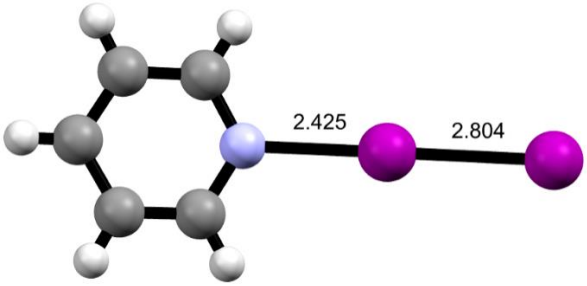

VUHDIN[160]

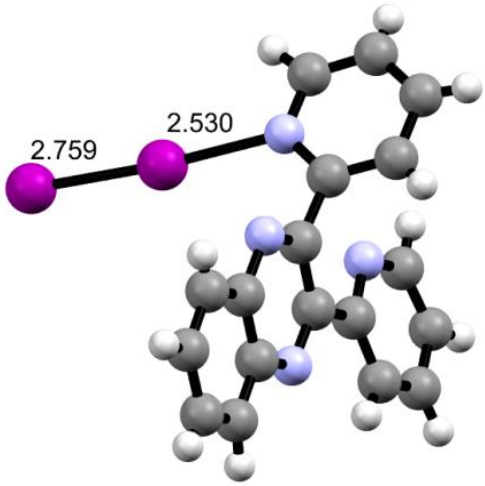

NULBEB[145]

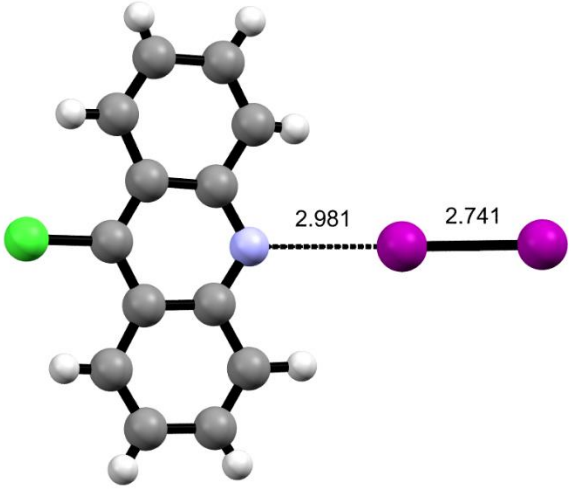

QARGUL[146]

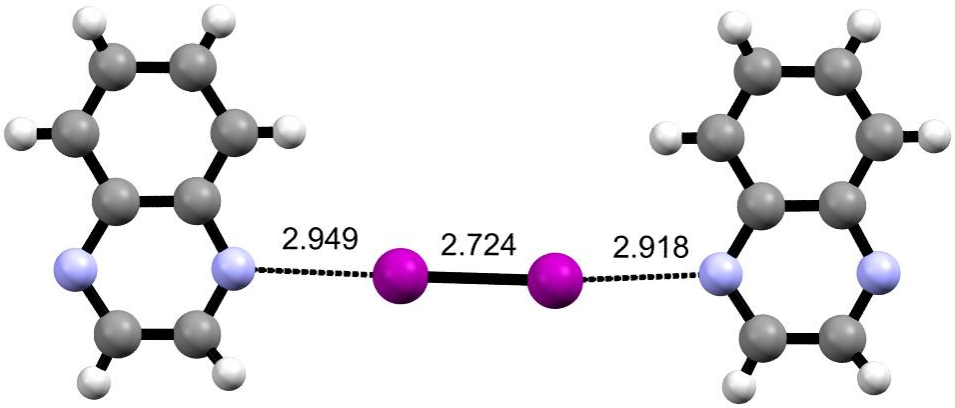

NULBUR[145]

Figure (5.14.1) Ball-stick representations of selected literature complexes.

The 4-picoline-I_2 (PICOLI)[151] complex has the shortest N···I interaction distance, indicating the strongest halogen bond among the reported compounds. All the complexes that have the N···I interaction shorter than in the Pyridine-I_2 contain electron-donating groups, thus supporting the previously stated hypothesis that the XB interaction strength is correlated with electron-donating or -withdrawing properties of the functional groups of the pyridine ring. The exception to the rule is found in isonicotinamide - I_2 (YIPCEG)[161] that has an amide group in para- position to the N atom of the pyridine ring. Since amide groups are very good electron-donating groups (better than alkyl- groups) it should be expected to have the strongest XB interaction among all the complexes in Table (5.5). However, it is falling short after the pyridine-I_2 N···I distance. A possible explanation for this discrepancy could be found in the two N-H···O hydrogen bonds that link two adjacent complexes, Figure (5.14.2). Having these two types of in non-covalent interactions should redistribute the electron density for both XB and HBs, thus decreasing the highest possible density in N···I-I halogen bond.

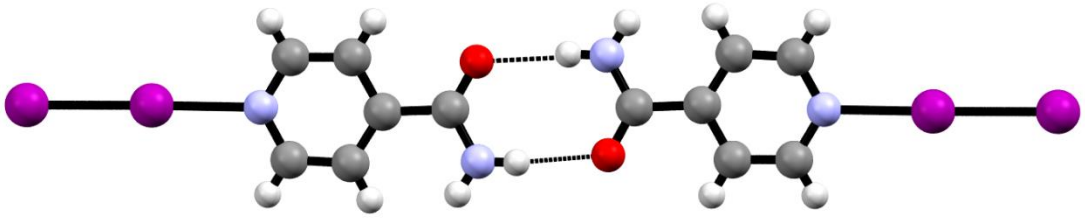

Figure (5.14.2) View showing the N-H···O hydrogen-bonded isonicotinamide - I_2 complexes

In addition to HBs in isonicotinamide - I_2 complex, the type I interaction between the two terminal iodine atoms occurs, Figure (5.14.3). This packing feature is also observed in three other complexes (QIHBOY,[152] PEWKIT,[158] BULJUP[162]), Figure (5.14.3).

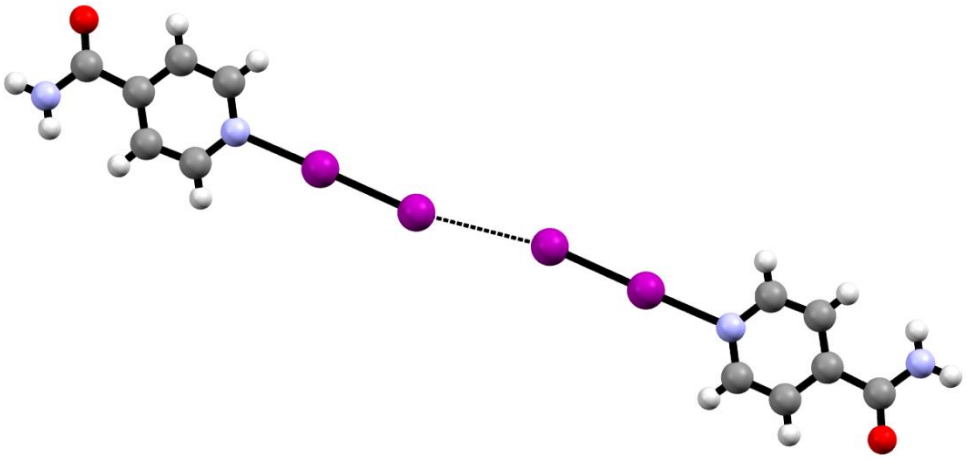

YIPCEG[161]

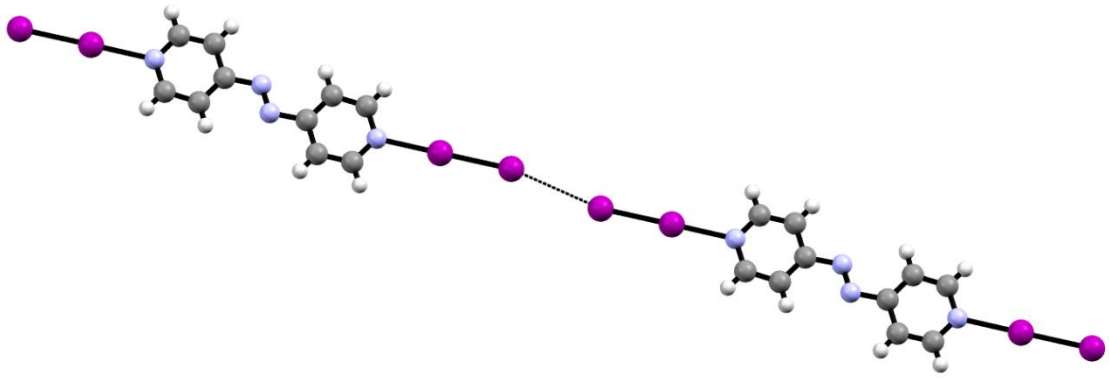

BULJUP[162]

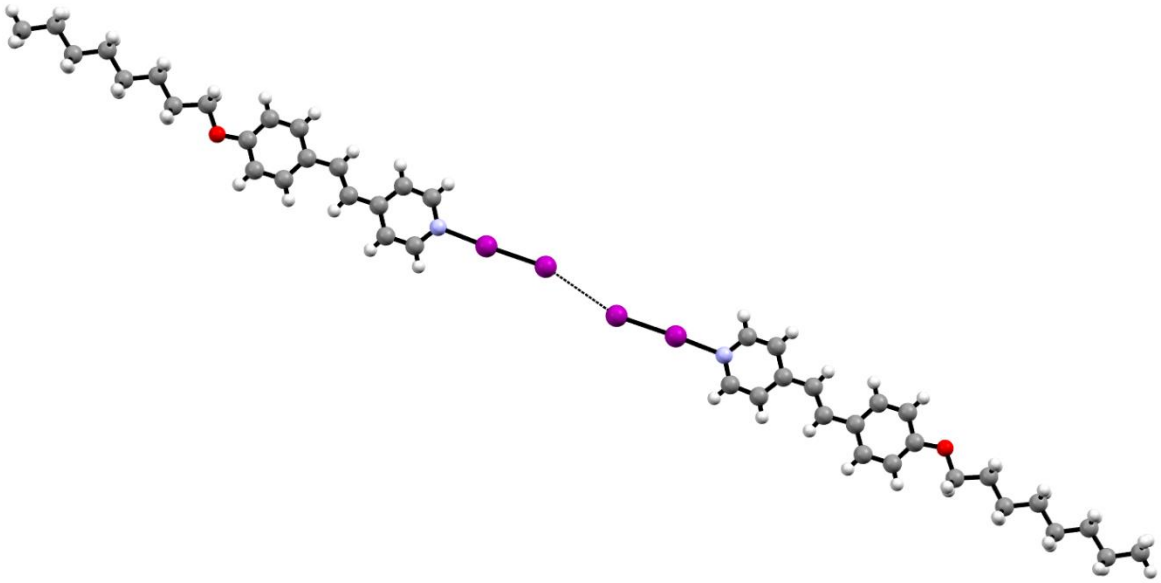

PEWKIT[158]

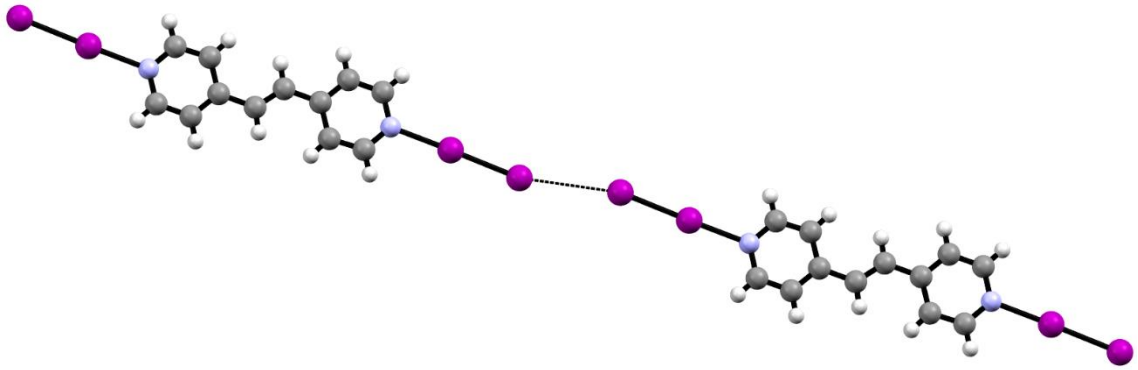

QIHBOY[152]

Figure (5.14.3) View showing type I interactions in selected literature complexes

Apart from type I interaction, bridged adducts are observed both in prepared and literature complexes. The main difference among these complexes is that they could be either just discrete adducts or linked into infinite chains via halogen bonds. It is impossible to make a general statement since only several complexes are reported, but based on the current data set, it could be concluded that in discrete adducts XB geometrical parameters are symmetrical. In the other hand, systems where they are in infinite chains, the difference between N···I distances and N-I-I angles occur, Table (5.6), Figures (5.10.4), (5.12.4), (5.14.4), (5.14.5).

Table 5.6 Geometrical parameters of halogen bonded complexes with bridged adduct patterns, complexes prepared in this work are marked bold

Complex name (REFCODE)	N···I (Å)	N···I (Å)	N···I-I (°)	N···I-I (°)
2-cyanopyridine-I_2	**2.872**	**2.872**	**177.28**	**177.28**
bis(9-Chloroacridine) iodine - I_2 (QARGUL) [146]	2.981	2.981	178.75	178.75
bis(2,6-bis(phenylselanyl)pyridine)-I_2 (ZESQUM) [135]	2.936	2.936	175.76	175.76
Quinoxaline-I_2	**2.875**	**2.857**	**176.99**	**179.11**
quinoxaline I_2 (NULBUR) [145]	2.949	2.918	178.77	175.77
Phenazine-I_2 (PHNAZI01)[157]	3.096	2.986	180.00	180.00

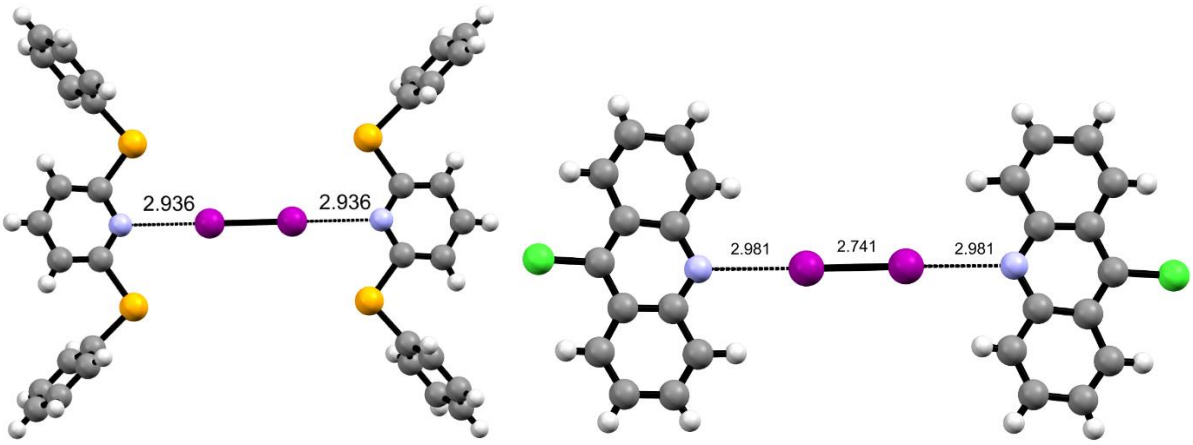

ZESQUM[135] QARGUL[146]

Figure (5.14.4) Ball-stick representations and geometrical parameters of selected literature complexes containing discrete bridged adduct mode

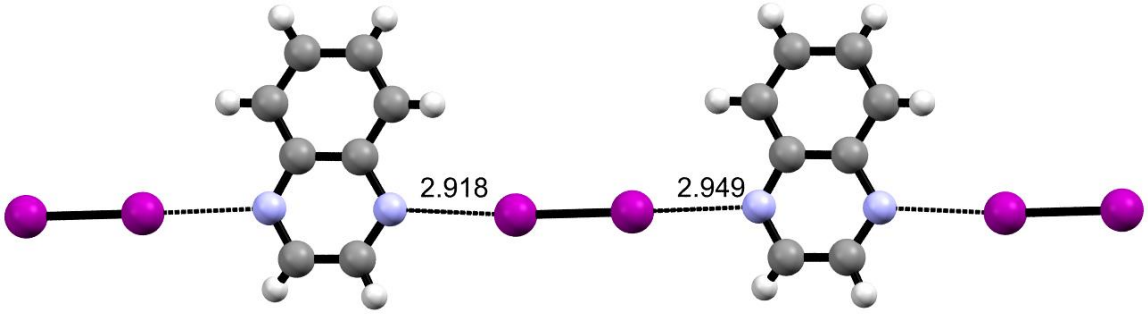

NULBUR[145]

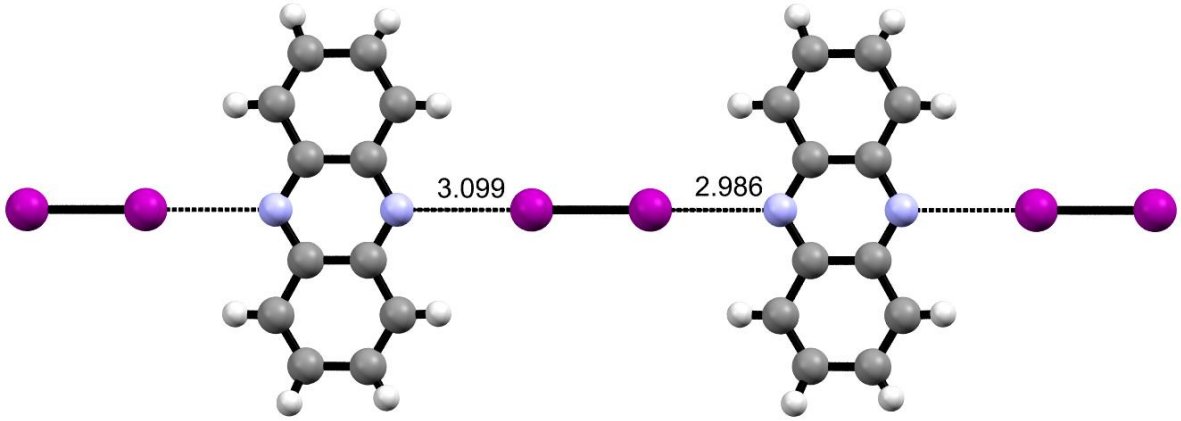

PHNAZI01[157]

Figure (5.14.5) Ball-stick representations and geometrical parameters of selected literature complexes containing infinite chain bridged adduct mode

From Table (5.5) can be observed that the N···I interaction distances in N···I-I halogen bonds that are connected only via one iodine atom of the iodine molecule are significantly shorter than the complexes where both iodine atoms are involved in XBs. A good example of this can be seen when the prepared 2-cyanopyridine-I_2 complex (2.872 Å) is compared to literature reported 4-cyanopyridine-I_2 (NULBIF),[145] 2.543 Å. Since these two complexes are constitutional isomers, some difference should be attributed to the steric hindrance effect due to the cyano- group in the ortho position, as well. A similar trend is observed in complexes with refcodes ZESQOG[135] and ZESQUM[135], where for ZESQOG, only the singly halogen bonded iodine atom N···I distance is 2.497 Å and for ZESQUM where bridged adduct occurs N···I distance is 2.936 Å. Here, the steric hindrance effect should be considered too, since the

second bulky functional group is added, but the difference of 0.439 Å seems to significant to stem only from the steric effects. On the other hand, I-I bond length for 2-cyanopyridine-I_2 is 2.714 Å that is slightly shorter than the corresponding distance for 4-cyanopyridine diiodine (NULBIF) 2.745Å.

The prepared quinoxaline-I_2 complex has stronger halogen bonds, N···I distances are 2.857 Å, 2.875 Å, which are shorter than the corresponding distances for the literature reported quinoxaline-I_2 (NULBUR),[145] 2.949Å and 2.918 Å. However, it is interesting to note that I-I bond length for prepared quinoxaline-I_2 is 2.725 Å is nearly equal to the distance for complex with refcode NULBUR 2.724 Å.

This chapter also has been focused on the influence of addition I_2 to the starting material by comparison of the pyridine ring vibrations since they could be observed on the available instrument, and N=C bond especially, to determine whether I_2 interacts with the pyridine N atom. If the N atom is involved in a non-covalent or supramolecular interaction then part of its electron density should be moved into that interaction, thus weakening the bonds already present in the compound. In FTIR spectrum it would mean that wavenumber corresponding to C=N bond should be moved toward lower wavenumbers (Table 5.7). and for UV-VIS spectroscopy that band characteristic for an organic base should be shifted towards higher wavelengths. (Table 5.8)

Table (5.7) Wavenumbers of selected bands in ATR-FTIR spectra correlated with specific bonds of the starting materials (St. m.) and the corresponding I_2 complexes (C.)

Starting material	ν (C=N), cm^{-1}		ν (C=C), cm^{-1}		ν (C-H), cm^{-1}	
	St. m	C.	St. m	C.	St. m.	C.
3,5-difluoropyridine	1476	1438	1577	1549	3101	3055
3,5-dichloropyridine	1423	1418	1555	1549	3070	3024
2,6-dichloropyridine	1467	1414	1584	1555	3142	3086
2,6-dimethoxypyridine	1545	1455	1629	1608	3102	3061
4-methoxypyridine	1547	1501	1616	1604	3110	3090
3-fluoropyridine	1557	1472	1645	1585	3054	3062
2-fluoropyridine-4-iodopyridine	1578	1539	1645	1568	3056	3052
2-cyanopyridine	1578	1461	1602	1577	3060	2973
1,10-phenanthroline	1561	1541	1617	1591	3058	3049
quinoxaline	1530	1462	1630	1580	3102	3045
2-chloroquinoline	1561	1538	1617	1584	3054	3059

Various types of interactions were observed in the complexes characterised by X-ray diffraction such as halogen bond and hydrogen bond in systems like 2-cyanopyridine-I_2 where the halogen bond is present, the band of the starting material was shifted from 1578 cm^{-1} to 1461 cm^{-1} and this shift confirms the bonding between 2-cyanopyridine and I_2. Simultaneously using the starting material such as quinoxaline, the shift was also observed (from 1530 cm^{-1} to 1462 cm^{-1}) upon the addition of iodine to the starting material. The same shift occurs with C=C band and C-H band, respectively. This shifting towards lower wavelengths refers to an interaction of the I_2 with N atom of the pyridine ring, which as result of the resonance and the conjugation on the pyridine ring and this leads to a decrease of the

double bond feature and due to the presence of the electron-withdrawing group on the ring which caused decreasing the electron density reducing bond order. [141,123]

Table (5.8) Wavelengths of selected bands in UV-VIS spectra of the starting materials and the corresponding I_2 complexes

Starting material	$\lambda_{(Starting\ material)}$ /nm	$\lambda_{(Complex)}$ /nm
3,5-difluoropyridine	303	362
3,5-dichloropyridine	335	360
2,6-dichloropyridine	316	359
2,6-dimethoxypyridine	328	358
4-methoxypyridine	303	359
3-fluoropyridine	316,445	361
2-fluoropyridine-3-iodopyridine	351	359
2-fluoropyridine-4-iodopyridine	317,448	356
2-fluoropyridine-5-iodopyridine	305	353
2-cyanopyridine	308	361
1,10-phenanthroline	323, 460	355
quinoxaline	319, 460	354, 442
2-chloroquinoline	303	364, 443

Contrary to the XB features listed by IUPAC, where it is listed that the formation of the halogen bonds usually moves the absorption bands to lower wavelengths, for these complexes, the opposite influence is noticed, i.e. λmax is shifted towards higher wavelengths, which is called a bathochromic or a redshift. Complexes that were characterised by single-crystal X-ray diffraction, have several distinctive features in their UV-VIS spectra. Similar to halogen bonded compounds observed in previous chapters, both complexes prepared in this

chapter have a single intense peak. This peak intensity could be correlated with the charge-transfer feature of the halogen bond. When there is a non-covalent interaction present, either halogen or a hydrogen bond, the charge transfer component is more significant than just the electrostatic interactions.[142] The 361 nm peak for the 2-cyanopyridine-I_2 could be attributed to N···I-I XB interaction. Peaks at similar wavelengths are observed in most of the prepared complexes in this chapter, Figures (5.14.5, 5.14.6). Spectra are split in two figures for clarity. The intensity of 2-cyanopyridine peak is the lowest among the complexes in Figure (5.14.5), which could be linked to the strongest electron-withdrawing feature of the cyano- group. However, the trend following the electron-donating or withdrawing properties of functional groups could not be observed. The possible explanation for this discrepancy could be found in possibility that there are other factors affecting the electron density involved in interactions, hydrogen bonds like in isonicotineamide-I_2 where the XB interaction is much weaker than expected, or due to different bonding patterns (discrete adducts or bridged adducts). The big exception to the trend of a single peak from 355-365 nm is found 2-chloroquinoline-I_2 complex, where two intensive peaks occur. Without the crystal structure of the complex, it is impossible to predict the XB or HB bonding features, because nothing similar is observed in known complexes. Due to the high intensity of the second peak, it could be speculated that two types of halogen bonds are present. For the quinoxaline -I_2 complex, where iodine monobromide was used as a starting material, and I_2 was formed due to dissociation of IBr, apart from the 354 nm peak associated with halogen bond formation, a characteristic low-intensity shoulder peak at 442 nm stemming from IBr_2^- can be observed[133], Figure (5.12.1)

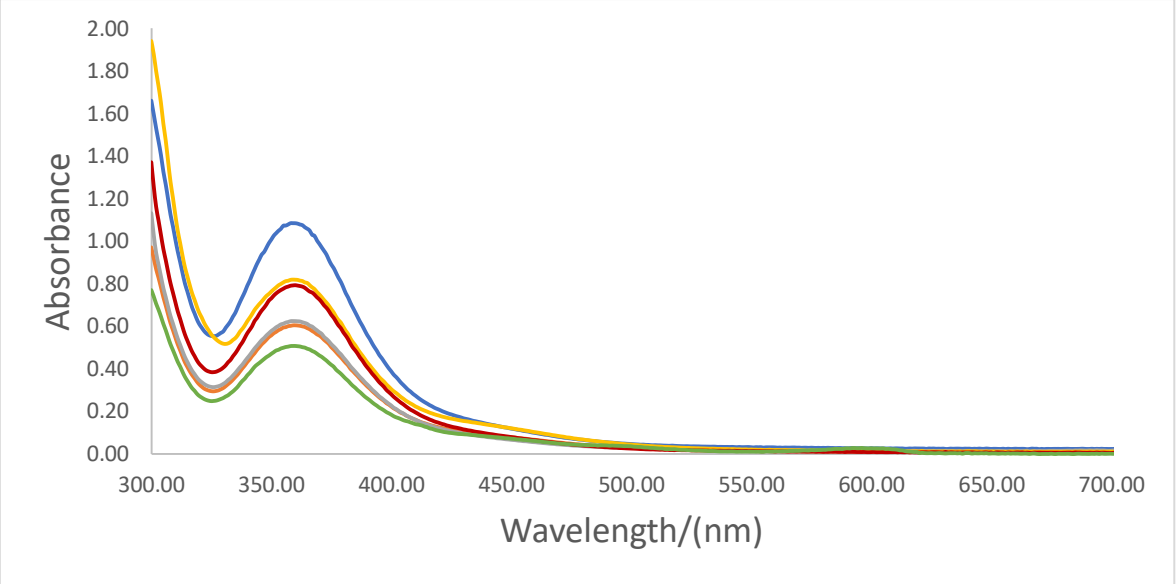

Figure (5.14.6) UV-VIS spectra of 3,5-difluoropyridine-IBr (Blue), 3,5-dichloropyridine-IBr (Orange),2,6-dichloropyridine-IBr(Silver),2,6-dimethoxypyridine-IBr(Gold),4-methoxypyridine -IBr (Red), 2-cyanopyridine-IBr (Green), the spectra were collected using methanol as the solvent, the concentration of the samples was 10^{-3} M.

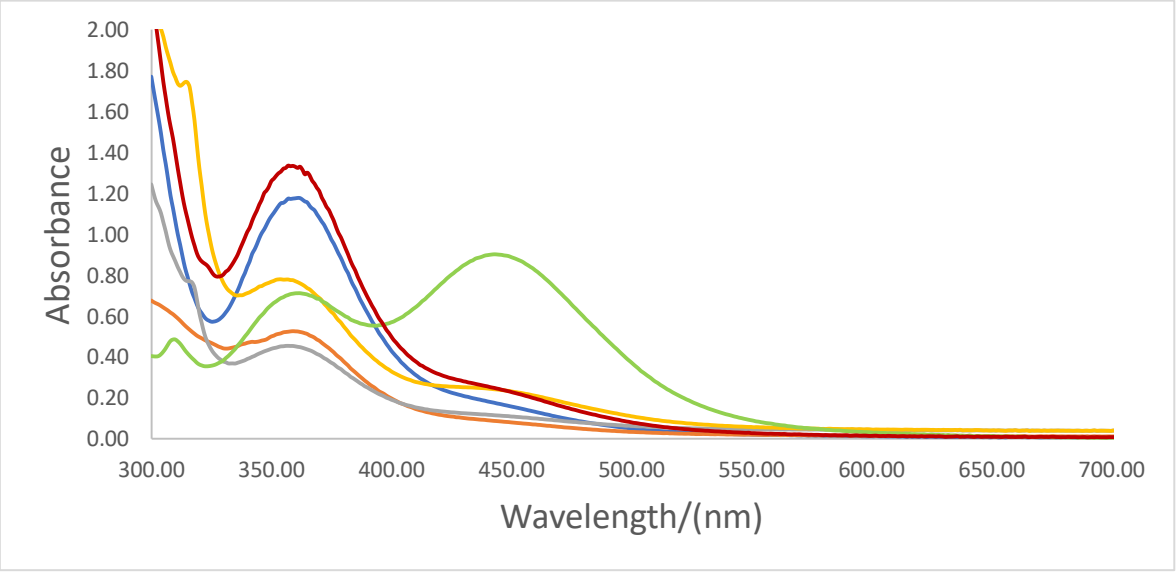

Figure (5.14.7) UV-VIS spectra of 3-fluoropyridine-IBr (Blue), 2-fluoropyridine-3-iodopyridine-IBr (Orange), 2-fluoropyridine-4-iodopyridine-IBr (Silver), 2-fluoropyridine-5-iodopyridine-IBr (Gold), 1,10-phenanthroline-IBr (Red), 2-chloroquinoline-IBr (Green), the spectra were collected using methanol as the solvent, the concentration of the samples was 10^{-3} M.

CHAPTER (6)
Discussion

Discussion

Growing crystals:

During the preparation of crystalline complexes, the following points can be noted. It was found that with the majority of ICl compounds the crystals formed immediately, with few exceptions that needed to be placed in the freezer to produce crystals (2-fluoro-3-iodopyridine-ICl, 2-fluoro-4-iodopyridine-ICl, quinoxaline-ICl). In the case of compounds formed using IBr, for most of the complexes, crystals were formed immediately as well. However, some of them needed to be placed in a freezer for more than 12 hours (3,5-difluoropyridine-IBr, 3,5-dichloropyridine-IBr, quinoxaline-IBr), but even so, the products formed more easily than for I_2, where for some of them it was necessary to cool the reaction mixture down to -75 °C or to put it in the fume hood for more than two weeks. In some cases, it was needed to add a minimum amount of suitable solvent and to cool the reaction mixture down or evaporate and leave in the fume hood for a long time. These additional steps would influence the economic cost in future practical applications.

Percentage yields:

In general, ICl products have the best yields among the prepared complexes, such as 3,5-difluoropyridine-ICl (76%). The average yields decreased from ICl (60%) over IBr complexes (45%) to I_2 containing complexes (38%). This trend could be affected by the solubility of the complexes, but also since it took a long time for IBr and I_2 containing complexes to precipitate, some side-reactions not leading to the formation of crystals could be happening in parallel and thus reducing the yield of the obtained complexes.

Crystals size and morphology

Most ICl crystals have a diamond or cubic morphologies which made the XRD investigation the samples more straightforward compared to the with IBr and I_2 samples. This was

especially pronounced for the iodine-containing products that were either needle-like or microcrystalline.

Halogen bond features

As it was mentioned in previous chapters, prepared samples could be divided in can be separated into four categories (A, B, C, D). The first three ones are characterised by single-crystal X-ray diffraction, UV-VIS and ATR-FTIR spectroscopy, while for the latter one, samples are characterised only by UV-VIS and ATR-FTIR.

A- Complexes which contain N···I-X (X= Cl, Br, I) halogen bond. In this work, seven complexes of that kind were prepared. Their geometrical features are listed in Table (6.1). Apart from the trend of increasing the N···I interaction length by using the organic bases with electron-donating groups to electron-withdrawing groups with a single dihalogen, it can be noticed that the N···I distance increase is ICl<IBr<I_2. The more electronegative the atom covalently bonded to iodine is, the more charge separation will occur. [106,112] Thus, the sigma hole on the iodine atom will be more prominent and the XB interaction stronger.[1] This trend has been observed among the literature reported complexes, as well, Table (6.2).

Table (6.1) Geometric parameters of halogen-bonded complexes prepared in this work

Compound	N···I Å	I-X Å	N···I-X ^{o}
ICl complexes			
3,5-difluoropyridine-ICl	2.358(6)	2.470(2)	178.69(1)
3,5-dichloropyridine-ICl	2.341(3)	2.4872(9)	180.00
4-methoxypyridine-ICl	2.2717(12)	2.5305(4)	177.76(3)
IBr complexes			
3-fluoropyridine-IBr	2.368	2.622	178.93
2-cyanopyridine-IBr	2.466	2.566	178.79
I_2 complexes			
2-cyanopyridine-I_2	2.872	2.7149	177.28
Quinoxaline-I_2	2.857, 2.875	2.725	179.11, 176.99

Table (6.2) Geometric parameters of selected literature complexes

Organic base	N···I, ICl Å	N···I, IBr Å	N···I, I_2 Å
Pyridine[160]	2.284	2.304	2.425
2,2-bipyridine[164]	2.336, 2.343	2.461	2.604
2,3,5,6-tetrakis(2-Pyridyl) pyrazine[163]	-	2.405, 2.410	2.498, 2.568
2-[(4-chlorophenyl) selanyl] pyridine[135]	-	2.411	2.497
2-cyanopyridine	-	2.466	2.566

Among the analogous compounds similar packing and non-covalent bonding patterns can be observed, Figures (4.11.6), (5.10.6), (6.0.1). In both IBr and I_2 complexes the same hydrogen bonds (C-H···N) and motifs can be observed, Figures (4.11.7), (5.10.5). The HB C-N lengths are slightly longer in iodine complex than in the iodine monobromide one (3.505 Å, 3.397 Å for I_2 complex and 3.454 Å, 3.378 Å for IBr complex, respectively). Even though two IBr complexes are linked via type I halogen interactions, while in the iodine-containing system, the bridged adduct is present, both complexes are packed in a similar stepwise manner, Figure (6.0.1). This indicates that the corresponding ICl complex, whose structure is still not elucidated, should have the same structural features.

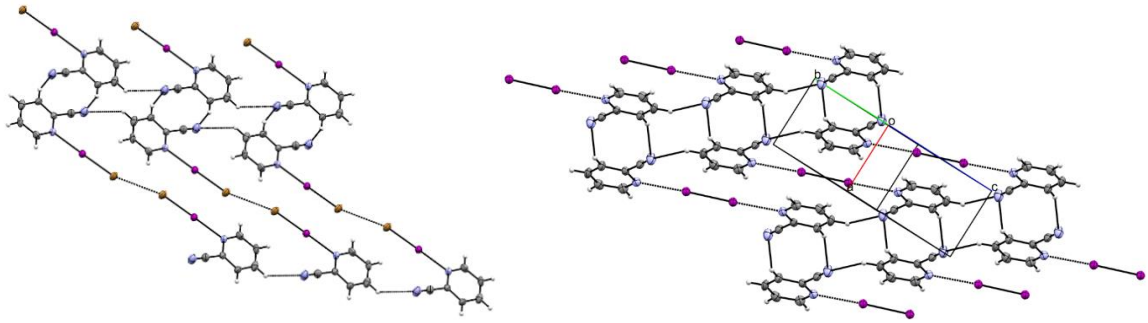

Figure (6.0.1) View showing non-covalent interactions of
2-cyanopyridine-IBr (left) and 2-cyanopyridine I_2 (right)

In addition to the impact of the position of the group on the ring relative to the pyridine N atom, electron-donating act to activate N atom of the pyridine ring. However, these groups become more activating when are substituted in ortho- and para- positions on pyridine ring and less activating when are substituted in meta- position. The opposite is observed for electron-withdrawing groups.[128]

In all cases, the halogen bond should be located along the axis of a free electron pair.[106,112] The great advantage of dihalogens or interhalogens for studying this feature is their compact size, having no steric hindrance. In the definition of halogen bond, where this type of

interactions is described by R-X···Y, for dihalogens or interhalogens, when iodine atom acts as XB donor (X), the one possible variability for the R group is the type of the atom bonded. Thus, the nature of XB interactions can be studied at an elementary level, where donors are not affected by any other effect except the polarisation of the bond due to the change in atoms bonded to XB donor.[116]

Pennington et al.[106] and Ouvrard et al.[112] reported that the hybridisation of the halogen bond acceptor atom affects the XB length. Also, sp^3 hybridised atoms should have longer N···I distance than sp^2 and sp hybridised, respectively. In this work, nor the literature, sp nitrogen atom involved in the halogen bond has not been prepared. In addition, there are only several cases of sp^3 nitrogen atoms (Trimethylamine-ICl (TMEICL) [119], 2,2,6,6-tetramethylpiperidine-I_2 (SUBWEU)[165]). In Table (6.3) and Figure (6.0.2) are shown geometrical features of these compounds compared to pyridine-I-X (X=Cl, I), which could be considered as a representative sample of dihalogen or interhalogen complexes containing sp^2 hybridised nitrogen atom. While the N-I-X (X=Cl, I) angles are all very similar, both the N···I distances, and I-X bond lengths are shorter for sp^2- than in sp^3 nitrogen containing halogen bond complexes.

Table (6.2) Geometric parameters of selected literature complexes

Compound	N···I Å	I-X Å	N···I-X ^{o}
ICl complexes			
Trimethylamine -ICl (TMEICL)[119]	2.303	2.524	176.88
Pyridine-ICl (PYRIIC10)[116]	2.290	2.510	178.72
I_2 complexes			
2,2,6,6-tetramethylpiperidine-I_2 (SUBWEU)[165]	2.469	2.854	177.18
Pyridine-I_2 (VUHDIN) [160]	2.425	2.804	176.44

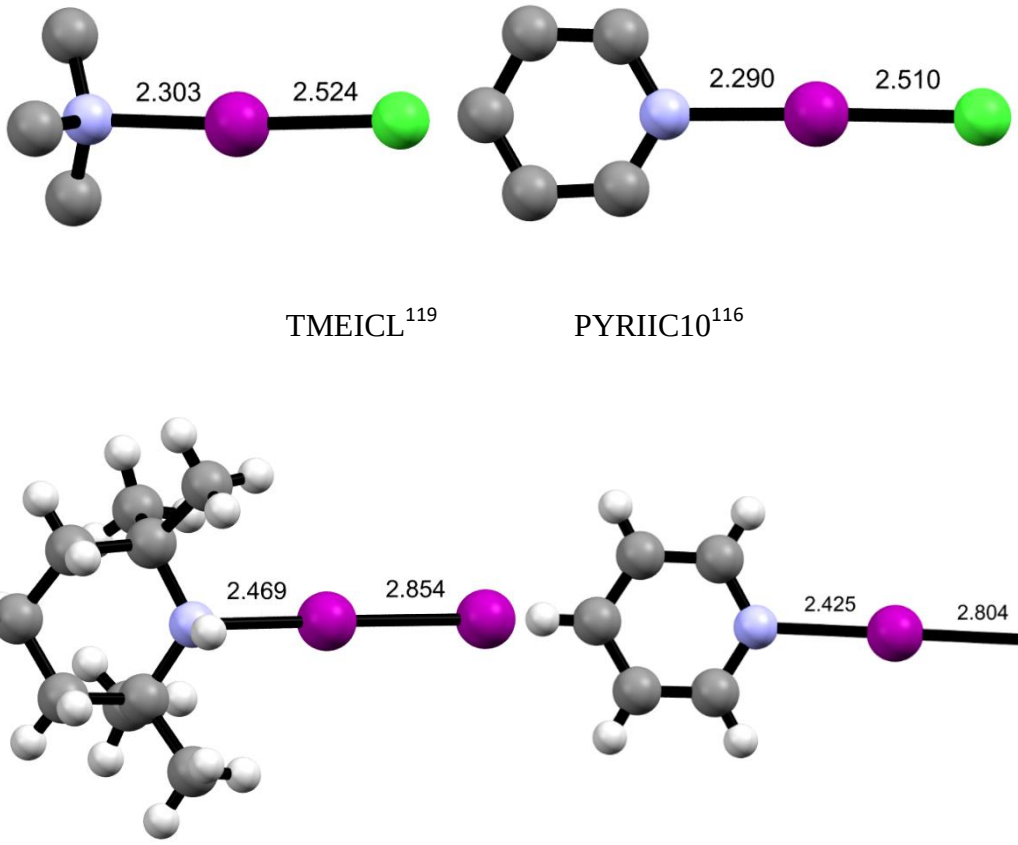

TMEICL[119] PYRIIC10[116]

SUBWEU[165] VUHDIN[160]

Figure (6.0.2) Ball-stick representations of selected literature complexes

B- Second group comprises ionic complexes containing polyhalogen ions (2,6-dimethoxypyridine-ICl_2^-, 2-cyanopyridine- ICl_2^-, 1,10-phenanthroline- IBr_2^-, quinoxaline- IBr_2^- and 2-ethoxyquinoline- IBr_2^-). Instead of co-crystallising the starting materials, the formation of pyridinium ions with ICl_2^- and IBr_2^-, respectively, could be obtained. In 2,6-dimethoxypyridinium-ICl_2^-, quinoxaline- IBr_2^- and 1,10-phenanthroline- IBr_2^- the polyhalogen ions are not symmetrical. While for the 2,6-dimethoxypyridinium-ICl_2^- there is a hydrogen bond between the pyridinium cation and the polyhalogen anion, for the IBr_2^- containing complexes, the distances that are significantly longer than the literature reported values. On the other hand, the bond distance between iodine and both of chlorine atoms in 2-cyanopyridinium-ICl_2^- and iodine and both of bromine atoms in quinoxaline- IBr_2^- is nearly

equal. This is because ICl_2^-, IBr_2^- are not included in any type of supramolecular interactions, rather an N-H···N hydrogen bond links two organic bases, from which, one is positively charged and the other is neutral. (Table 6.3)

Table (6.3) Geometrical parameters for both of ICl_2^- and IBr_2^- crystalline complexes.

Crystalline complexes	I-Cl1	I-Cl2
2,6-dimethoxypyridine-ICl_2^-	2.6041(5)	2.5177(6)
2-cyanopyridine-ICl_2^-	2.5531(6)	2.5540(6)
Crystalline complexes	I-Br1(Br3*)	I-Br2
1,10-phenanthroline-IBr_2^-	2.702	2.691
Quinoxaline- IBr_2^-	2.677	2.716
2-ethoxyquinoline- IBr_2^-	2.671	2.671

C- The third group has only one sample. Instead of 2,6-dichloropyridine-ICl halogen-bonded complex, just the organic starting material crystallised from the reaction solution. However, the structure of 2,6-dichloropyridine was still not reported in Cambridge Structural database. As possible reasons for not obtaining the XB complex, the electron-withdrawing property of chlorine atoms in 2,6-dichloropyridine that reduce the electron density on N atom of the pyridine ring, as well as the ortho- positions on the pyridine ring act to prevent N atom of the pyridine ring from interacting with iodine monochloride by the steric hindrance.

The product of adding IBr to 2-chloroquinoline should be 2-chloroquinoline –IBr. However, 2-ethoxyquinoline-IBr_2^- is observed instead of the expected complex. Due to Williamson reaction, 2-ethoxyquinoline was formed from the 2-chloroquinoline, that was used as an organic starting material and ethoxy species stemming from ethanol used as a solvent, Figure

(6.0.3). Furthermore, the formation of polyhalide anions in this and the other mentioned samples was observed.

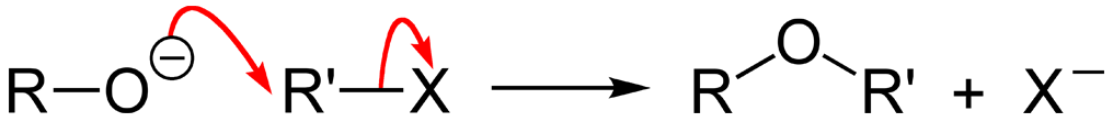

Figure (6.0.3) - Scheme for the formation of ether and halide ion.

Because these products were observed in crystalline materials, as well as quinoxaline-I_2 complex, where iodine monobromide was used as starting material, it was difficult to predict the structural properties of complexes where crystals were not of a suitable size for single-crystal X-ray diffraction. Therefore, based on known features from the structure of elucidated structures and linking them to peak positions and intensities observed in FTIR and UV-VIS spectra the unknown structures were predicted.

D-Complexes in which no suitable crystalline material was obtained could be characterised by other techniques like UV-VIS and ATR-FTIR spectroscopy to determine the presence of the halogen bond or polyhalogen ions in the complex. Since the spectrometer with a range wide enough to observe N···I and I-X (X=Cl, Br, I) was not available, FTIR spectrum analysis has been focused on the impact of addition ICl, IBr and I_2 to the starting material. XB interactions were studied through comparison of the pyridine ring vibrations generally, and N=C bond specifically, to determine whether interhalogens or dihalogens interact with the pyridine N atom. If there is an interaction between the organic base and a dihalogen, the wavenumber corresponding to the C=N bond should be moved toward lower wavenumbers. Tables (3.14.3), (4.14.3), (5.7).

In FTIR the big difference in a characteristic band wavenumber between the starting material and the complex indicates that the interaction is strong, and the halogen bond is short. For example, in the 4-methoxypyridine-ICl complex that has the shortest N···I interaction distance (2.227 Å), the C=N band is moved toward lower wavenumbers, from 1547 cm^{-1} for the organic starting material to 1500 cm^{-1} for the complex, as shown in Table (3.14.3). In contrary, 2-cyanopyridine-I_2 complex, where N···I halogen bond distance is 2.872 Å which is the longest among the prepared complexes, the difference in wavenumbers between the starting material and the complex is almost negligible, the wavenumbers for the starting material and the I_2 complex are 1578 cm^{-1} and 1577 cm^{-1} respectively.

For UV-VIS spectra, based on peak intensities observed in spectra of structures characterized by single-crystal X-ray diffraction, structural properties can be predicted. Peaks of higher intensity are attributed either to halogen or hydrogen bonds since they have a strong charge-transfer component in the interaction, which should be visible in this part of the electromagnetic spectrum. On the other hand, peaks of low intensity are associated with the presence of equilibrium between halogen (I^-) and polyhalogen ions (ICl_2^-, IBr_2^-) in the sample solution,[133] Table (6.4). Complexes, where the structure was characterized by single-crystal X-ray diffraction, are marked bold. Complexes that should have halogen-bonded structures are marked with an asterisk (*), while the structures where the polyhalogen ion and ionic complex is expected, are marked with an octothorpe ($^{\#}$). Correlation of peak positions and intensities among the same dihalogen or interhalogen used, with the electron-donating or withdrawing properties has not been observed. Since multiple non-covalent interactions in the structure could be present and interfere with the halogen bond strength. As a general trend, it could be observed that the peaks attributed to halogen bonded complexes move from 340-390 nm, 440-460 nm for ICl complexes, 380-390 nm for IBr complexes to 350-360 nm for I_2 complexes.

Table (6.4) Wavelengths of selected bands in UV-VIS spectra of the starting materials (St.m.) and the corresponding interhalogen or dihalogen complexes (C.), Complexes that should have halogen-bonded structures are marked with an asterisk (*), while the structures where the polyhalogen ion and ionic complex is expected, are marked with an octothorpe ($^{\#}$).

Starting material	$\lambda_{(St.\ m.)}$ /nm	$\lambda_{(ICl\ C.)}$ /nm	$\lambda_{(IBr\ C.)}$ /nm	$\lambda_{(I2\ C.)}$ /nm
3,5-difluoropyridine	303	451*	384*	362*
3,5-dichloropyridine	335	458*	388, 441*,#	360*
2,6-dichloropyridine	316	-	434#	359*
2,6-dimethoxypyridine	328	442#	440#	358*
4-methoxypyridine	303	386*	435#	359*
3-fluoropyridine	316,445	369, 469*	387*	361*
2-fluoropyridine-3-iodopyridine	351	326, 438*	436#	359*
2-fluoropyridine-4-iodopyridine	317,448	434*	378*	356*
2-fluoropyridine-5-iodopyridine	305	346, 440*	385*	353*
2-cyanopyridine	308	343, 435#	438*	361*
1,10-phenanthroline	323, 460	440#	383, 450#	355*
Quinoxaline	319, 460	439*	439#	354, 442*,#
2-chloroquinoline	303	444#	436#	364, 443*

CHAPTER (7)
Conclusion

Conclusion

In this work, the aim was to prepare crystalline halogen-bonded complexes of dihalogens (iodine monochloride, iodine monochloride and iodine) with a range of aromatic nitrogen-containing compounds. Dihalogens as a class of compounds have an advantage over other XB donors for studying halogen bonds. Due to their compact size, no steric hindrance is present and except the polarisation of the bond that is dependent on the atom that bonded to an XB donor, there are no other effects presents.

Complexes were prepared by dissolving the appropriate organic starting material and dihalogen or interhalogen in 1:1 molar ratio. The minimum amount of ethanol used as a solvent. In total 13 organic nitrogen-containing compounds and three dihalogens were used. The crystalline material was prepared in all cases. However, due to the size and morphology of the crystals, only 13 complexes were suitable for characterisation by single-crystal X-ray diffraction. For all the complexes crystal size, colour, yield percentage and melting points are noted, as well as they have been characterised FTIR and UV-VIS spectra.

The products formed by iodine monochloride were generally well-formed clear crystals that formed easily and in high yields which aid in their characterisation.

Iodine monobromide products have similar properties to iodine monochloride products, however, they were more difficult to crystalize and required cooling. Also, several of these complexes have melting points below room temperature, which made them more difficult to handle.

The products formed with iodine were even more difficult to crystalize than IBr ones, with cooling down to -75 °C required in some cases. The crystal colours were between brown to dark brown.

Based on the X-ray diffraction characterisation of the products from this work, they can be divided into four types:

A- Well-formed halogen-bonded crystalline complexes:

3,5-difluoropyridine-ICl,

3,5-dichloropyridine-ICl,

4-methoxypyridine-ICl,

3-fluoropyridine-IBr,

2-cyanopyridine-IBr,

2-cyanopyridine-I_2,

Quinoxaline-I_2.

In this class of complexes, the halogen bond strength with the single dihalogen or interhalogen compound could be tuned by changing the electron-withdrawing and electron-donating properties of functional groups of nitrogen-containing aromatic compounds. The more electron-donating the group is, the stronger the interaction will be. The opposite correlation is observed when increasing the electron-withdrawing properties of the functional group. The position regarding the nitrogen atom of the pyridine ring plays an important role, as well. The ortho- and para- positions enhance the effect of the donating groups, while the meta- positions favour the electron-withdrawing properties. The hybridisation of the XB acceptor atom, nitrogen in these systems, affects the halogen bond strength as well. The longest and weakest bonds are for sp^3, followed by sp^2 and sp hybridised acceptor atoms. Additionally, the XB interaction strength is increasing as an effect of changing the XB donor used (I_2> IBr> ICl). Finally, other non-covalent interactions, like hydrogen bonds affect the XB strength through possible charge redistribution.

B- Polyhalogen containing products:

2,6-dimethoxypyridine-ICl_2^-,

2-cyanopyridine- ICl_2^-,

1,10-phenanthroline- IBr_2^-,

Quinoxaline- IBr_2^-,

2-ethoxyquinoline- IBr_2^-.

Contrary to the formation of expected halogen-bond connected samples, the ionic complexes containing protonated organic starting materials and polyhalogens ions are obtained in five cases. In 2-cyanopyridine-ICl_2^- and 2-ethoxyquinoline- IBr_2^- complexes, polyhalogen ions are symmetrical, while for the other three samples, a difference between the bond lengths form the central to the terminal atoms is present. This difference indicates that at least one terminal atom of the ion is involved in non-covalent interactions. Also, 2-ethoxyquinoline-IBr_2^- complex resulted from the addition of 2-chloroquinoline and iodine monobromide. This substitution could be explained by the Williamson ether synthesis mechanism.

C -Recrystallised starting materials:

2,6-dichloropyridine

The product that should have crystallised from the reaction between ICl with 2,6-dichloropyridine should have been 2,6-dichloropyridine-ICl. Rather than that complex, only 2,6-dichloropyridine, which was the starting material, formed crystals.

D- Complexes characterised only by FTIR and UV-VIS spectroscopy:

All the samples were characterised using FTIR spectrometer from 600 to 4000 cm^{-1} and UV-VIS spectrometer from 300 to 900 nm. Due to the limitation of the FTIR instrument, complexes were studied indirectly. The bonds of the pyridine ring adjacent to the point of XB

interaction (C=N, C=C, C-H) were compared with the corresponding bands in the starting material. Due to the redistribution of electron density from the pyridine ring, these bands should be shifted toward lower wavenumbers. UV-VIS spectra were interpreted based on peak intensities observed in spectra of structures characterized by single-crystal X-ray diffraction. Peaks of higher intensity were attributed either to halogen or hydrogen bonds since they have a strong charge-transfer component in the interaction. On the other hand, peaks of low intensity were associated with the presence of equilibrium between halogen (I^-) and polyhalogen ions (ICl_2^-, IBr_2^-) in the sample solution.

Goals and recommendations for further work:

- To obtain the crystals of the suitable size for single-crystal X-ray diffraction, of complexes where no such crystals are obtained, by changing the reaction conditions. For example, to choose another solvent or solvent mixtures, or to conduct a reaction on higher temperatures, or utilising mechanochemistry followed by recrystallisation in a solvent.

- To obtain halogen bonded crystals of systems where ionic complexes and unexpected products are obtained.

-To study the conditions of polyhalogen ions formation. For example, by conducting reactions in conditions of controlled humidity or with distilled and dried solvents. Also, to study systems where a fixed amount of water is added, to possibly discover the threshold percentage, after which ions are preferred over XB adducts.

-To use iodine monobromide or iodine monochloride as sources of iodine for samples, where there are difficulties for obtaining iodine-containing complexes. This method was observed with quinoxaline and IBr were mixed, but iodine crystallised in the complex.

- To use the aliphatic nitrogen compounds (e.g. piperidine derivatives) to compare the properties with the aromatic nitrogen compounds.

-To prepare polymorphs with different bonding modes (discrete adducts, bridged adducts…) to study this effect on halogen bond interaction strengths.

-To conduct computational calculations of systems containing halogen bonded dihalogens or interhalogens to elucidate interaction features and to provide a better insight in FTIR spectra interpretation.

-To study potential real-life applications of these systems. For example, to utilise the colossal anisotropic negative thermal expansion of Pyridine-IBr complex, observed by Jones et al.[129]

References

[1] Cavallo, G.; Metrangolo, P.; Milani, R.; Pilati, T.; Priimagi, A,; Resnati, G.; Terraneo, G., *Chemical Reviews*. **2016,** *116* (4), 2478-601.

[2] Hantzsch, A., *Ber. Dtsch. Chem. Ges*. **1915,** *48*, 797−816.

[3] Rhoussopoulos, O., *Ber. Dtsch. Chem. Ges*. **1883,** *16*, 202−203.

[4] Politzer, P.; Lane, P.; Concha, M.C.; Ma, Y.; Murray, J.S., *J. mol. model.* **2007,** *13*(2), 305-311.

[5] Colin, M. M.; Gaultier de Claubry, *H., Ann. Chim*. **1814,** *90*, 87−100.

[6] Guthrie, F., *J. Chem. Soc*. **1863,** *16*, 239−244.

[7] Remsen, I.; Norris, J. F., *Am. Chem. J*. **1896,** *18*, 90−95.

[8] Metrangolo, P.; Meyer, F.; Pilati, T.; Resnati, G.; Terraneo, G., *Angew. Chem., Int. Ed*. **2008,** *47*, 6114−6127.

[9] Benesi, H. A.; Hildebrand, J. H., *J. Am. Chem. Soc*. **1949,** *71*, 2703−2707.

[10]Mulliken, R. S., *J. Phys. Chem*. **1952,** *56*, 801−822.

[11] Hassel, O.; Rømming, C., *Quarterly Reviews, Chemical Society*. **1962,** *16*(1), 1-8.

[12] Bent, H.A., *Chemical Reviews*. **1968,** *68*(5), 587-648.

[13] Ramasubbu, N.; Parthasarathy, R.; Murray-Rust, P., *J. Am. Chem. Soc*. **1986,** *108*, 4308−4314.

[14] Murray, J. S.; Paulsen, K.; Politzer, P., *Proc. Indian Acad. Sci., Chem. Sci*. **1994,** *106*, 267−275

[15] Metrangolo, P.; Resnati, G., eds. *Halogen bonding: fundamentals and applications*. Springer, **2008** Apr 12.

[16] Desiraju, G.R.; Ho, P.S.; Kloo, L.; Legon, A.C.; Marquardt, R.; Metrangolo, P.; Politzer, P.; Resnati, G.; Rissanen, K., *Pure Appl. Chem*. **2013,** *85*(8),1711-1713.

[17] Metrangolo, P.; Resnati, G., *Chem. - Eur. J.* **2001,** *7*, 2511−2519.

[18] Metrangolo, P.; Neukirch, H.; Pilati, T.; Resnati, G., *Acc. Chem. Res*. **2005,** *38*, 386−395.

[19] Erdelyi, M., *Nat. Chem*. **2014,** *6*, 762−764.

[20] Auffinger, P.; Hays, F.A.; Westhof, E.; Shing, Ho, P., *Proc Nat Acad Sci* **2004,** *101,* 16789–16794.

[21] Valadares, N. F.; Salum, L. B.; Polikarpov, I.; Andricopulo, A.D.; Garratt, R. C.; *J. Chem. Inf. Model*. **2009,** *49,* 2606–2616.

[22] Zingaro, R.A.; Hedges, M., *J. Phys. Chem*. **1961,** *65*, 1132−1138.

[23] Martire, D. E.; Sheridan, J. P.; King, J. W.; O'Donnell, S. E., *J. Am. Chem. Soc*. **1976,** *98,* 3101−3106.

[24]Dumas, J.-M.; Gomel, M.; Guerin, M. *Molecular Interactions Involving Organic Halides. In Halides, Pseudo-Halides and Azides: Volume 2*; John Wiley & Sons, Ltd.: Chichester, U.K., **1983,** 985− 1020.

[25] Desiraju, G. R.; Steiner, T., *The Weak Hydrogen Bond in Structural Chemistry and Biology*; Oxford University Press: Oxford, U.K., **1999.**

[26] Alkorta, I.; Elguero, J., *Chem. Soc. Rev*. **1998,** *27*, 163−170.

[27] Haynes, W. M.; Lide, D. R.; Bruno, T. J., *CRC handbook of chemistry and physics: a ready-reference book of chemical and physical data.* 2016-2017, 97th Edition / Boca Raton, Florida: CRC Press, **2016.**

[28] Politzer, P.; Murray, J. S.; Clark, T., *Phys. Chem. Chem. Phys*. **2010,** *12*, 7748−7757.

[29] El Kerdawy, A.; Murray, J.S.; Politzer, P.; Bleiziffer, P.; Heßelmann, A.; Görling, A.; Clark, T., *J. Chem. Theory. Comput.* **2013,** *9,* 2264–2275.

[30] Nyburg, S. C.; Faerman, C. H., *Acta Crystallogr., Sect. B: Struct. Sci.* **1985,** *B41*, 274−279

[31] Metrangolo, P.; Murray, J. S.; Pilati, T.; Politzer, P.; Resnati, G.; Terraneo, G., *Cryst. Growth Des.* **2011,** *11*, 4238−4246.

[32] Metrangolo, P.; Murray, J. S.; Pilati, T.; Politzer, P.; Resnati, G.; Terraneo, G., *Cryst. Eng. Comm.* **2011,** *13*, 6593−6896.

[33] Hathwar, V. R.; Chopra, D.; Panini, P.; Row, T. N. G., *Cryst. Growth Des*. **2014,** *14*, 5366−5369.

[34] Lu, Y.X.; Zou, J.W.; Wang, Y.H.; Zhang, H.X.; Yu, Q.S.; Jiang, Y.J., *J. Mol. Struct.: THEOCHEM* **2006,** *766(2-3*), 119-124.

[35] Loehr, H.G.; Engel, A.; Josel, H.P.; Voegtle, F.; Schuh, W.; Puff, H., *J. Org. Chem.* **1984**, *49*(9), 1621-1627.

[36] Clark, T.; Hennemann, M.; Murray, J. S.; Politzer, P., *J. Mol. Model*. **2007,** *13*, 291−296.

[37] Lommerse, J. P. M.; Stone, A. J.; Taylor, R.; Allen, F. H., *J. Am. Chem. Soc*. **1996,** *118*, 3108−3116.

[38] Awwadi, F.F.; Willett, R.D.; Peterson, K.A.; Twamley, B., *Chem. - Eur. J.* **2006**, *12*(35), 8952-8960.

[39] Cavallotti, C.; Metrangolo, P.; Meyer, F.; Recupero, F.; Resnati, G., *J. Phys. Chem. A.* **2008**, *112*(40), 9911-9918.

[40] Weiss, R.; Schwab, O.; Hampel, F., *Chem. - Eur. J.* **1999**,*5*(3), 968-974.

[41] Huber, S. M.; Jimenez-Izal, E.; Ugalde, J. M.; Infante, I., *Chem. Commun*. **2012,** *48*, 7708−7710.

[42] Rosokha, S. V.; Vinakos, M. K., *Cryst. Growth Des*. **2012,** *12*, 4149−4156.

[43] Kozuch, S.; Martin, J. M. L., *J. Chem. Theory Comput*. **2013,** *9*, 1918−1931.

[44] Syzgantseva, O. A.; Tognetti, V.; Joubert, L., *J. Phys. Chem*. *A.* **2013,** *117*, 8969−8980.

[45] Chudzinski, M. G.; Taylor, M. S., *J. Org. Chem*. **2012,** *77*, 3483−3491.

[46] Řezáč, J.; Riley, K.E.; Hobza, P., *J. Chem. Theory Comput*. **2012,** *8*, 4285−4292.

[47] Politzer, P.; Murray, J. S., *Chem. Phys. Chem*. **2013,** *14*, 278−294.

[48] Palusiak, M., *J. Mol. Struct.: THEOCHEM* **2010,** *945*, 89−92.

[49] Wolters, L. P.; Schyman, P.; Pavan, M. J.; Jorgensen, W. L.; Bickelhaupt, F. M.; Kozuch, S., *Wiley Interdiscip. Rev. Comput. Mol. Sci*. **2014,** *4*, 523−540.

[50] Riley, K. E.; Hobza, P., *J. Chem. Theory Comput*. **2008,** *4*, 232−242.

[51] Wang, C.; Danovich, D.; Mo, Y.; Shaik, S., *J. Chem. Theory Comput*. **2014,** *10*, 3726−3737.

[52] Clark, T.; Hennemann, M.; Murray, J.S.; Politzer, P.; *Mol. J. Model*. **2007,** *13*, 291 – 296.

[53] Messina, M.T.; Metrangolo, P.; Panzeri, W.; Ragg, E.; Resnati, G.; *Tetrahedron lett*. **1998,** *39* (49), 9069-9072.

[54] Metrangolo, P.; Panzeri, W.; Recupero, F.; Resnati, G., *J. Fluorine Chem.* **2002,** *114* (1), 27-33.

[55] Zhu, S.; He, P., *Tetrahedron* **2005,** *61*, 5679.

[56] Zhu, S.; Xu, B.; Qin, C.; Xu, G., *Inorg Chem* **1997,** *36*, 4909.

[57] Messina, T.; Metrangolo, P.; Panzeri, W.; Ragg, E.; Resnati, G., *Tetrahedron Lett*. **1998,** *39*, 9069 – 9072.

[58] Metrangolo, P.; Panzeri, W.; Recupero, F.; Resnati, G., *J. Fluorine Chem.* **2002,** *114*, 27 – 33.

[59] Sutton, L., ed., *Interatomic distances, Supplement*, Special publication No. 11, The Chemical Society, London, **1965.**

[60] Xie, Y.; Ge, Y.; Peng, Q.; Li, C.; Li, Q.; Li, Z., *Advanced Materials* **2017,** *29*(17), 1606829.

[61] Gilday, L.C.; Robinson, S.W.; Barendt, T.A.; Langton, M.J.; Mullaney, B.R.; Beer, P.D., *Chem. rev*. **2015,** *115* (15), 7118-95.

[62] Metrangolo, P.; Pilati, T.; Resnati, G., *Cryst. Eng. Comm*. **2006,** *8*(12), 946-947.

[63] Ananthavel, S.P.; Manoharan, M.; *Chem. Phys.* **2001**, *269*(1-3), 49-57.

[64] Landrum, G.A.; Goldberg, N.; Hoffmann, R., *J. Chem. Soc. Dalton Trans.* **1997** (*19*), 3605-3613.

[65] Biella, S., *Halogen Bonding: Fundamentals and Applications*, *126*, **2008,** 105-136. ; Trudeau, G.; Cole, K.C.; Massuda, R.; Sandorfy, C.; *Can. J. Chem*. **1978,** *56*, 1681 – 1686.

[66] di Paolo, T.; Sandorfy, C., *Nature.* **1974,** *252* (5), 471-483.

[67] Trudeau, G.; Cole, K.C.; Massuda, R.; Sandorfy, C., *Can. J. Chem*. **1978**, *56* (12), 1681-1686.

[68] Massuda, R.; Sandorfy, C.; *Can. J. Chem*. **1977,** *55*, 3211-3217.

[69] Syssa-Magalé, J.L.; Boubekeur, K.; Palvadeau, P.; Meerschaut, A.; Schöllhorn, B., *Cryst. Eng. Comm*. **2005,** *7*(50), 302-8.

[70] Vasilyev, A.V.; Lindeman, S.V.; Kochi, J.K.; *New J. Chem*. **2002,** *26,* 582 – 592.

[71] Corradi, E.; Meille, S.V.; Messina, M.T.; Metrangolo, P.; Resnati, G.; Angew. Chem. 2000, 112, 1852 – 1856; *Angew. Chem. Int. Ed*. **2000,** *39*, 1782 – 1786.

[72] Dunstan, S.; Henbest, H.B.; *J. Chem. Soc*. **1957,** 4905 – 4908.

[73] Mulliken, R.S.; *J. Phys. Chem.* **1952,** *56*(7), 801-822.

[74] McAlpine, R.K., *J. Am. Chem. Soc*. **1952,** *74*(3), 725-727.

[75] Lenoir, D.; Chiappe, C., *Chem.-Eur. J.* **2003,** *9*(5), 1036-1044.

[76] Chen, Q.Y.; Li, Z.T.; Zhou, C.M., *J. Chem. Soc. Perkin Trans 1*. **1993**, *20*, 2457-2462.

[77] Liantonio, R.; Luzzati, S.; Metrangolo, P.; Pilati, T.; Resnati, G., *Tetrahedron*. **2002,** *58*(20), 4023-4029.

[78] Neukirch, H.; Guido, E.; Liantonio, R.; Metrangolo, P.; Pilati, T.; Resnati, G., *Chem. Commun.* **2005,** *12*, 1534-1536.

[79] De Santis, A.; Forni, A.; Liantonio, R.; Metrangolo, P.; Pilati, T.; Resnati, G., *Chem. - Eur. J.* **2003**, *9*(16), 3974-3983.

[80] Zou, J.W.; Jiang, Y.J.; Guo, M.; Hu, G.X.; Zhang, B.; Liu, H.C.; Yu, Q.S.; *Chem.-Eur. J.* **2005,** *11*(2), 740-751.

[81] Valerio, G.; Raos, G.; Meille, S.V.; Metrangolo, P.; Resnati, G., *J. Phys. Chem. A.* **2000**, *104*(8), 1617-1620.

[82] Riley, K.E.; Murray, J.S.; Fanfrlík, J.; Řezáč, J.; Solá, R.J.; Concha, M.C.; Ramos, F.M.; Politzer, P., *J. Mol. Model*. **2011**, *17*, 3309-3318.

[83] Yamamoto, H.M.; Maeda, R.; Yamaura J.I.; Kato, R.; *J. Mater. Chem*. **2001**, *11*, 1034-1041.

[84] Yamamoto, H.M.; Yamaura, J.I.; Kato, R., *J. Mater. Chem*. **1998**, *8*, 15 – 16.

[85] Metrangolo, P.; Meyer, F.; Resnati, G.; Ursini, M., *Haloperfluorocarbons: versatile tectons in halogen bonding based crystal engineering.* Soloshonok, V.A., ed., *In Fluorine-containing synthon*. Oxford University Press, Washington, **2005,** 513.

[86] Blatov, V.A.; Shevchenko, A.P.; Proserpio, D.M., *Cryst. Growth Des.* **2014**, *14*(7), 3576-3586.

[87] Gao, K.; Goroff, N.S., *J. Am. Chem. Soc*. **2000,** *122*(38), 9320-9321.

[88] Kuhn, N.; Abu-Rayyan, A.; Eichele, K.; Schwarz, S.; Steimann, M., *Inorg. Chim. acta* **2004**, *357*(6), 1799-1804.

[89] Pinter, B.; Nagels, N.; Herrebout, W. A.; De Proft, F., *Chem. - Eur. J.* **2013,** *19*, 519−530.

[90] Politzer, P.; Riley, K. E.; Bulat, F. A.; Murray, J. S., *Comput. Theor. Chem*. **2012,** *998*, 2-8.

[91] Politzer, P.; Murray, J. S.; Clark, T., *σ-Hole Bonding: A Physical Interpretation. In Halogen Bonding I: Impact on Materials Chemistry and Life Science*; Metrangolo, P., Resnati, G., Eds.; Springer International Publishing: Cham, Switzerland, **2015,** 19-42.

[92] Clark, T., *Wiley Interdiscip. Rev. Comput. Mol. Sci.* **2013,** *3*, 13−20.

[93] Thallapally, P.K.; Desiraju, G.R.; Bagien-Bencher, M.; Masse, R.; Bourgogne, C.; Nicoud J.F., *Chem. Commun.* **2002,** 1052–1053.

[94] Imakubo, T.; Tajima, N.; Tamura, M.; Kato, R.; Nishio, Y.; Kajita, K., *Synth. Met.* **2003**, 133–134, 181–183.

[95] De Moliner, E.; Brown, N.R.; Johnson, L.N., *Eur. J. Biochem.* **2003,** *270*, 3174-3181.

[96] Metrangolo, P.; Pilati, T.; Resnati, G.; Stevenazzi, A., *Curr Opin Colloid Interface Sci* **2003,** *8*, 215–222.

[97] IUPAC, *Compendium of Chemical Terminology*, 2nd ed. (the "Gold Book"), Oxford **1997.**

[98] Etter, M.C.; Macdonald, J.C.; Bernstein. J., *Acta crystal*. **1990,** B*46*, 256-262.

[99] Pavia, D. L.; Lampman, G. M.; Kriz, G. S., *Introduction to Spectroscopy. A Guide for Students of Organic Chemistry*, Thompson Learning, New York **2001.**

[100] Skoog, D.A.; West, D.M.; Holler, F.J.; Crouch, S.R.; *Fundamentals of Analytical chemistry*, 9th ed, Cengage Learning, New York, **2013.**

[101] Clegg, W., *X-Ray Crystallography*, 2nd ed., Oxford University Press, Oxford, **2015**.

[102] Putnis, A., *Introduction to Mineral Sciences*, Cambridge University Press, Cambridge **1992**.

[103] Bond, A.D., *Single-Crystal X-ray Diffraction*, in: Müllertz, A.; Perrie, Y.; Rades, T., (eds) *Analytical Techniques in the Pharmaceutical Sciences. Advances in Delivery Science and Technology*, Springer, New York, **2016.**

[104] Altomare, A.; Cascarano, G.; Giacovazzo, C.; Guagliardi, A.; *J. Appl. Cryst.* **1994,** *27*, 435.

[105] Palatinus, L.; Chapuis, G.; *J. Appl. Cryst*. **2007,** *40*, 786–790.

[106] Pennington, W.T.; Hanks, T.W.; Arman, H.D.; *Halogen Bonding with Dihalogens and Interhalogens*, Metrangolo, P.; Resnati, G., editors. *Halogen bonding: fundamentals and applications.* Springer, New York, **2008**.

[107] Lagorce, J.F.; Comby, F.; Rousseau, A.; Buxeraud, J., Raby, C., *Chem. Pharm. Bull*. **1993,** *41*, 1258

[108] Corban, C.J.; Hadjikakou, S.K.; Hadjiliadis, N.; Kubicki, M.; Tiekink, E.R.T.; Butler, I.S.; Drougas, E.; Kosmas, A.M., *Inorg. Chem.* **2005,** *44*, 8617.

[109] Rissanen, K.; Haukka, M.; *Top. Curr. Chem*. **2015,** *359*, 77–90.

[110] Maharramov, A.M.; Mahmudov, K.T.; Kopylovich, M.N.; Pombeiro, A.J.L., Eds.; Haukka, M.; Hirva, P.; Rissanen, K.; *Non-Covalent Interactions in the Synthesis and Design of New Compounds*, John Wiley & Sons, New York, **2016.**

[111] Brisbois, R.G.; Wanke, R.A.; Stubbs, K.A.; Stick, R.V.; *"Iodine Monochloride" Encyclopedia of Reagents for Organic Synthesis*, John Wiley & Sons, New York **2004,**

[112] Ouvrard, C.; Le Questel, J.Y.; Berthelot, M.; Laurence, C., *Acta Crystallogr B* **2003,** *59*, 512-538.

[113] Bernardinelli, G.; Gerdil, R., *Acta Crystallogr. B: Stru.* **1976**, *32*, 1906.

[114] Batsanov, A.S.; Howard, J.A.K.; Lightfoot, A.P.; Twiddle, S.J.R.; Whiting, A.; *Eur. J. Org. Chem.* **2005**, 1876.

[115] Baenziger, N.C.; Nelson, A.D.; Tulinsky, A.; Bloor, J.H.; Popov, A.I., *J. Am. Chem. Soc*., **1967,** *89*, 6463.

[116] Romming, C.; *Acta Chem. Scand.* **1972,** *26*, 1555.

[117] Grebe, J.; Weller, F.; Dehnicke, K., *Z. Naturforsch.* **1996,** *51b*, 1739.

[118] Soled. S.; Carpenter, G.B., *Acta Crystallogr. B Stru.* **1974,** *30*, 910.

[119] Hassel, O.; Hope, H., *Acta Chem. Scand.* **1960,** *14*, 391.

[120] Harms, G.K.; Weller, F.; Dehnicke, K., *Z. Anorg. Allg. Chem*, **1995,** *621*, 1489.

[121] Batsanov, S.S., Inorganic Materials **2001,** *37*(9), 871–885.

[122] Howard, J.A.K.; Hoy, V.J.; Hagan, D.O'.; Smith, G.T., *Tetrahedron* **1996,** *52*(38), 12613-12622.

[123] Domenicano, A.; Vaciago, A.; Coulson, C.A., *Acta Crystallogr. Sect. B-Struct. Sci.* **1975**, *31*, 221-234.

[124] Crawford, S.; Kirchner, M.T.; Blaeser, D.; Boese, R.; David, W.I.F.; Dawson, A.; Gehrke, A.; Ibberson, R.M.; Marshall, W.G.; Parson, S.; Yamamuro, O., *Angew. Chem. –Int. Edit.* **2009,** *48*, 755-757.

[125]Desiraju, G.R.; Parthasarathy, R., *J. Am. Chem. Soc.* **1989**, *111*, 8725-8726.

[126] Greenwood, N.N.; Earnshaw, A., *Chemistry of the Elements*, Pergamon press, Oxford, **1984**.

[127] Allen, F.H.; Kennard, O.; Watson, D.G.; Brammer, L.; Orpen, A.G.; Taylor, R., *J. Chem. Soc. Perkin Trans II 12*, 1-19

[128] Clayden, J.; Greeves, N.; Warren, S.G., *Organic chemistry*. Oxford: Oxford University Press, **2012.**

[129] Jones, R. H.; Knight, K.S.; Marshall, W. G.; Clews, J.; Darton, R. J.; Pyatt, D.; Colesc S. J.; Horton P. N., *Cryst. Eng. Comm*., **2014,** *16*, 237.

[130] Philbrick, S., *J. Chem. Soc*. **1932,** 64, 620.

[131] Al-allaf, T.A.K.; Omer, A.O.; Mohammed, A.T.; *J. Res. stud*. **1996,** *11*,19.

[132] Dayagi, S.; Degani, Y.; *The chemistry of the carbon – nitrogen double bond*, ed. Putai, S., John Wiley &sons Int., New York **1970**.

[133] Kazantseva, N.N.; Ernepesova, A.; Khodjamamedov, A.; Geldyev, O.A.; Krumgalz, B.S., *Anal. Chim. Acta* **2002,** *456*, 105–119.

[134] King, R.B., ed, Encyclopaedia of inorganic chemistry, 2nd ed., New York, Wiley

[135] Montis, R.; Arca, M.; Aragoni, M.C.; Blake, A.J.; Castellano, C.; Demartin, F.; Isaia, F.; Lippolis, V.; Pintus, A.; Lenardão, E.J.; Perin, G.; O'Connor, A.E.; Thurow, S., *New J. Chem.* **2018,** *42*, 10592.

[136] Aragoni, M.C.; Arca, M.; Devillanova, F.A.; Hursthouse, M.B.; Huth, S.L.; Isaia, F.; Lippolis, V.; Mancini, A.; Ogilvie, H.R.; Verani, G., *J. Organomet. Chem.* **2005,** *690*, 1923.

[137] d'Agostino, S.; Braga, D.; Grepioni, F.; Taddei, P., *Cryst. Growth Des.* **2014,** *14*, 821.

[138] Li, F.; Ma, Z.; Fang, W.; Wang, S.; Li, T.; Sun, C.; Men, Z., *Optik* **2016,** *127*, 5347–5350.

[139]Wang, A.; Englert, U., *Acta Cryst*. **2017,** *73*, 803–809.

[140] Spada, L.; Gou, Q.; Vallejo-Lopez, M.; Lesarri, A.; Cocinero, E.J.; Camianti, W., *Phys. Chem. Chem. Phys.* **2014,** *16*, 2149-2153.

[141] Housecroft, C.; Sharpe, A.G., "*Inorganic Chemistry*", Prentice Hall, 3rd Ed., Dec **2007**

[142] Rosokha, S.; Kochi, J., *X-Ray Structures and Electronic Spectra of the π-Halogen Complexes between Halogen Donors and Acceptors with π-Receptors. In Halogen Bonding. Fundamentals and Applications*; Metrangolo, P.; Resnati, G., Eds.; Springer-Verlag: Berlin, Heidelberg, **2008,** *126*, 137−160.

[143] Lagorce, J.F.; Thomes, J.C; Catanzano, G.; Buxeraud, J.; Raby, M.; Raby, C., *Biochem. Pharm.* **1991,** *42*, 89.

[144] Bailey, R.D.; Buchanan, M.L.; Pennington W.T., *Acta Crystallogr C* **1992,** *48*, 2259.

[145] Bailey, R.D.; Drake, G.W.; Grabarczyk, M.; Hanks, T.W.; Pennington, W.T., *J. Chem. Soc. Perkin Trans. II*, **1997,** 2773.

[146] Rimmer, E.L.; Bailey, R.D.; Hanks, T.W.; Pennington, W.T., *Chem. Eur. J.* **2000,** *6*, 4071.

[147] Pritzkow. H., *Acta Crystallogr B* **1975**, *31*, 1589.

[148] van der Helm, D., *J. Cryst. Mol. Struct.* **1973,** *3*, 249.

[149] Engel, P.S.; Duan, S.; Whitmire, K.H., *J. Org. Chem.* **1998,** *63*, 5666.

[150] Markila, P.L.; Trotter, J., *Can. J. Chem*, **1974,** *52*, 2197.

[151] Hassel, O.; Romming, C.; Tufte, T., *Acta Chem. Scand.* **1961,** *15*, 967.

[152] Walsh, R.B.; Padgett, C.W.; Metrangolo, P.; Resnati, G.; Hanks, T.W.; Pennington, W.T., *Cryst. Growth Des.* **2001,** *1*, 165.

[153] Strømme, K.O., *Acta Chem. Scand.* **1959,** *13*, 268.

[154] Nusshar, D.; Weller, F.; Dehnicke, K., *Z. Anorg. Allg. Chem.* **1994,** *620*, 329.

[155] Tebbe, K.F.; Nagel, K., *Acta Crystallogr. C*, **1995**, *51*, 1388.

[156] Pritzkow, H., *Z. Anorg. Allg. Chem* **1974,** *409*, 237.

[157] Uchida, T.; Kimura, K., *Acta Crystallogr. C*, **1984,** *40*, 139

[158] McAllister, L.J.; Präsang, C.; Wong, J.P.W.; Thatcher, R.J.; Whitwood, A.C.; Donnio, B.; P. O'Brien, P.; Karadakov, P.B.; Bruce, D.W., *Chem. Commun.* **2013,** *49*, 3946.

[159] Aragoni, M.C.; Arca, M.; Coles, S.J.; Devillanova, F.A.; Hursthouse, M.B.; Coles, S.L.; Isaia, F.; Lippolis, V.; Mancini, A., *Cryst. Eng. Comm.* **2011,** *13*, 6319.

[160] Tuikka, M.; Haukka, M., *Acta Crystallogr. E***, 2015,** *71*, 463.

[161] Aakeroy, C.B.; Desper, J.; Helfrich, B.A.; Metrangolo, P.; Pilati, T.; Resnati, G.; Stevenazzi, A., *Chem. Commun.* **2007,** 4236-4238.

[162] Ravat, P.; Seetha Lekshmi, S.; Nandy Biswas, S.; Nandy, P.; Varughese, S., *Cryst. Growth Des.* **2015,** *15*, 2389.

[163] Padgett, C.W.; Walsh, R.D.; Drake, G.W.; Hanks, T.W.; Pennington, W.T., *Cryst. Growth Des.* **2005,** *5*, 745.

[164] Pohl, S., *Z. Naturforsch*, **1983,** *38b*, 1535.

[165] Skakuj, K.; Bujold, K.E.; Mirkin, C.A., *J. Am. Chem. Soc*. **2019,** *141*, 20171.